Aggresomes Inhibit Multiple Functions of the Centrosome

Anila Iqbal

School of Biological Sciences

Royal Holloway University of London

Research thesis submitted for the degree of Doctor of Philosophy

Declaration of Authorship

I, Anila Iqbal, hereby declare that this thesis and the work presented in it is entirely my own. Where I have consulted the work of others, this is always clearly stated

Signed: A.Iqbal

Date: 14/06/2019

Abstract

A hallmark of Parkinson's disease is the presence of Lewy bodies in the neurons of patients. These are large intracellular aggregates of many proteins but the largest constituent is α- synuclein. Aggresomes are closely related to Lewy bodies; it is believed that Lewy bodies form in an aggresome related process. The cellular localisation of the aggresome coincides with that of the centrosome, the microtubule oragnising centre of the cell. Since the aggresome is positioned in close proximity to and shares componenets with the centrosome, it is possible that it hinders centrosomal function. Many disease symptoms suggest the centrosme function could be compromised in Parkinson's, including the loss of smell, that may precede other symptoms that lead to diagnosis. I assessed the effects of aggresomes on centrosome function, using cell-based models. Aggresomes were formed by treating cells with MG-132 or overexpressing GFP expression constructs encoding α- synuclein wild-type and familial mutants, confirmed by aggresome markers. In the presence of aggresomes, the centrosome is no longer able to nucleate and maintain the microtubule network, cell polarity is also affected as the rate of cell migration is reduced. In cell-based models and using zebrafish larvae as a model, I show that ciliogenesis is inhibited in the presence of aggresomes. Similarly, when α- synuclein wild-type and familial mutant forms were overexpressed in zebrafish larvae, the cilia at the olfactory pit were reduced in length and in numbers. The loss of centrosome and cilium function could contribute to the loss of neuronal function and neuronal cell death seen in Parkinson's. This is the first report showing cilia are affected in the presence of aggressomes, with further investigation this could be potentially developed as a molecular diagnostic tool for Parkinson's.

Acknowledgments

I would like to take this opportunity to thank several people who made this thesis possible. Firstly, I would like to express my thanks and gratitude to my supervisor Chris Wilkinson for giving me this opportunity. Thank you for your support , guidance, and encouragement throughout the past 4 years. Working with you has helped me grow as a scientist. I would also like to thank my secondary supervisor Jenny Murdoch. Thank you for your advice, support and always being there.

I would like to thank my advisor Philip Chen, for your advice, encouragement and always having a story for when it was worse. Thanks also goes to Angleen Flemming, thank you for your advice and support on the project, but also for the resources provided, the zebrafish work would not have been possible.

I would like to thank all members of lab 302a (Jade, Ilda, Amninder, Al, Paul, Kayvan and Marc). Thank you for your help and support, for making me laugh and making this experience enjoyable. Special thanks to my singing partner aka Jade Marsh, thank you for the motivation, the morning coffees and being a great lab partner. I would also like to thank my gym buddy Ilda, for keeping me physically fit, and being a dependable friend. Al and Amninder, thank you for being supportive, fun and a pleasure to be around.

I would like to thank my friends Amina, Anisa and Tasha for the support and ensuring I had a social life. Finally, I would like to thank my amazing family , especially my mum. Thank you for your continuous support, food and understanding my non-existence for the past few years, I'm sure you're glad I'm back.

Table of Contents

Table of Figures

Table of Tables

1.Introduction

1.1 Parkinson's Disease

Parkinson's disease (PD) is an age-related progressive neurodegenerative disease (Olanow et al. 2004). It is the second most prevalent neurodegenerative disease affecting 1 in 500 of the population (von Campenhausen et al. 2005; Van Den Eeden et al. 2003; Schrag et al. 2000). It was first medically characterised by James Parkinson which it was then named after (Parkinson 1817; Pearce 1989). The pathological hallmark of Parkinson's is the presence of intracellular aggregates known as Lewy Bodies (LB) found in the substantia nigra pars compacta (SNpc) region of the brain (Trétiakoff 1919; Lewy 1912). Lewy bodies are known to be predominantly found within dopaminergic neurons within this region (Forno 1996). One of the theories proposes the presence of these Lewy bodies are toxic which are believed to cause neuronal death (Trojanowski et al. 1998). As a result, a number of clinical symptoms are manifested affecting both the peripheral and central nervous systems including; resting tremor, bradykinesia, muscular rigidity, sensory dysfunction; including loss of smell and, in later stages of disease progression, dementia (Sveinbjornsdottir 2016).

1.1.2 Parkinson's Disease aetiology

Parkinson's is considered to be a multisystem disorder with both genetic and environmental influences. Increasing evidence from familial cases of Parkinson's have found several genetic mutations that are recognised as genetic risk factors. Key genes including *SNCA* (encoding α-synuclein), Parkin, PINK-1 and LRRK2 are some of the genes that have been identified to be instrumental in the pathogenesis of both familial and sporadic Parkinson's (Tan & Skipper 2007) . Epidemiological studies have shown familial Parkinson's counts for 15% of overall cases whereas sporadic Parkinson's account's for 85% of the cases (Thomas & Beal 2007). While familial and sporadic Parkinson's have different etiological backgrounds no differences in the clinical manifestation of the disease have been found (Baba et al. 2006; Papapetropoulos et al. 2007). The heritability of Parkinson's can be autosomal recessive or autosomal dominant dependent on the gene affected. For example, mutations in α-synuclein have an autosomal dominant

inheritance pattern whereas mutations in Parkin result in autosomal recessive inheritance (Polymeropoulos et al. 1997; Shimizu et al. 1998). Other risk factors include gender, were males have a higher inclination to women by a ratio of 3:2 (de Lau & Breteler 2006).

It is likely that environmental factors also influence the penetrance of familial Parkinson's. Although Parkinson's has a worldwide distribution, demographic studies have shown increased Parkinson's prevalence in Europe, North and South America in comparison to Africa, Asia and Middle eastern countries (von Campenhausen et al. 2005; Strickland & Bertoni 2004; Bauso et al. 2012; Okubadejo et al. 2006; Muangpaisan et al. 2009; Benamer 2014). Some environmental factors contribute to the risk of developing Parkinson's however, other environmental factors decrease the risk of developing Parkinson's including; caffeine intake, smoking and use of non-steroidal anti-inflammatory drugs (Hancock et al. 2007). While some of the environmental factors that increase the risk include pesticide exposure, previous head injury and exposure to rural setting (Noyce et al. 2012). The greatest risk factor is considered to be age, as there is strong association between increase in age and increased prevalence in Parkinson's (Pringsheim et al. 2014; Kalia & Lang 2015).

Several staging systems have been developed to both clinically and pathologically categorise Parkinson's and by doing so elucidating the advancement of this disease. The first staging system was established by Hoehn & Yahr and is known as Hoehn and Yahr Scale, it broadly defines categories of motor impairment in Parkinson's progression (Hoehn & Yahr 1967). A more recent and up to date tool is the Unified Parkinson's Rating Scale (UPDRS), unlike the Hoehn and Yahr scale, it also accommodates non motor symptoms including mental functioning, mood and social interactions (Fahn & S. 1987). These staging systems as well as others are extensively used by clinicians in the diagnosis and monitoring the progression of the disease.

Similarly Braak et al developed a staging system for the pathological progression of Parkinson's (Braak et al. 2003). Essentially, they developed the staging system based on α-synuclein neurite pathology from which they established a 6-stage scheme. In brief,

the pathology first begins at the olfactory bulb which follows an ascending route, with α-synuclein pathology becoming more widespread. It is at stage 3 of this scheme, the substantia nigra is affected (Braak et al. 2003). Stages 1-3 are considered pre-clinical, it is only at Braak PD stage 4-6 symptoms appear and worsen as the disease progresses.

1.2.1 Lewy Bodies

The presence of Lewy bodies and Lewy neurites (LNs) are known to be the pathological hallmark of Parkinson's. These protein inclusions were first described by Lewy (1912) over 100 years ago (Lewy 1912) however, their formation and relevance is still poorly understood. Trétiakoff (1919) later confirmed the presence of these Lewy bodies in individuals with Parkinson's and also accredited Lewy's initial observations and named the intraneuronal proteinaceous bodies after him (Trétiakoff 1919) . The presence of Lewy bodies is not restricted to the pathogenesis of Parkinson's , a group of diseases known as Lewy body diseases (LBD) have been also clinically classified , such as dementia with Lewy Bodies (DLB). The clinical manifestation is dependent on the neurological distrtibution of these Lewy bodies where there is a strong association between other neurological disorders including Parkinson's.

The relevance of Lewy bodies is still debatable as to whether their presence is the cause of neuronal dysfunction or their formation is a protective measure. Not all patients with Parkinson's have Lewy bodies as seen in the majority of autosomal recessive juvenile parkinsonism cases (Shimura et al. 1999). Similarly, Lewy bodies have been found in some elderly patients who have displayed no neurological dysfunction (Frigerio et al. 2011; Savica et al. 2013); such cases are clincally termed 'incidental Lewy body disease' (iLDB) . Interestingly the distribution of Lewy bodies in iLDB is similar to that seen in Parkinson's (Dickson et al. 2008) even though the frequency and distribution of Lewy bodies is proportional to the severity in Parkinson's (Braak et al. 2002). It remains unknown why patients with iDLB do not develop the neurological symtpoms seen in Parkinson's.

The increased manifestation of Lewy bodies is associated with increase in age (Jellinger 2004). The anatomical distribution of Lewy bodies in the brain would go on to determine the different clinical symptoms displayed. In Parkinson's, Lewy bodies are predominantly

found at the brain stem whereas in DLB a more widespread global distribution is observed. Lewy bodies are comprised of many different proteins. By identifying the composition of Lewy bodies and the different proteins involved, it is possible to identify the pathways involved in the development of Lewy bodies. Over 76 proteins have been described as constituents of Lewy bodies (Wakabayashi et al. 2007). The main constituent of these Lewy bodies is α-synuclein (Spillantini et al. 1997) , and so it is thought the aggregation of this protein is a key pathogenic event in the development of Parkinson's. These proteins have been categorised into several groups including; ubiquitin proteasome system, cytoskeletal components and autophagy pathway (Beyer et al. 2009; Wakabayashi et al. 2007).

1.3.1 α-synuclein

α-synuclein was first identified in Torpedo electric organs and was named synuclein due to its localised expression at synaptic vesicles and the nuclear envelope (Maroteaux et al. 1988). Soon after it was also found to be part of the non-amyloid-β component (NAC) found in amyloid plaques in patients with Alzheimer's disease (Uéda et al. 1993). α-synuclein belongs to a family of synuclein proteins that were discovered soon after α-synuclein including, γ-synuclein and β-synuclein which have so far been found only in vertebrates (Nakajo et al. 1990; Jakes et al. 1994; Lavedan et al. 1998). Synuclein genes have been implicated in human diseases including α-synuclein involved in the pathogenesis of Parkinson's (Polymeropoulos et al. 1997), whereas in breast cancer increased γ-synuclein expression is seen (Ji et al. 1997; Lavedan et al. 1998). The normal function of synucleins is unknown, although we do know that they have localised expression at the synapse (Totterdell et al. 2004). All three synucleins have a common domain at the N terminus which categorises them into the synuclein family whereas differences at the C-terminus distinguishes their individuality (Ducas & Rhoades 2014).

α-synuclein has been shown to be involved in the pathogenesis of many diseases including DLB, multiple system atrophy and one of the major proteins implicated in the pathology of Parkinson's (Spillantini et al. 1998; Hamilton 2006). It is primarily expressed in the brain with a ubiquitous expression, but more intensely throughout the neocortex,

hippocampus, olfactory bulb, striatum, thalamus and cerebellum of the rat brain (Jakes et al. 1994).

The first evidence of α-synuclein involvement in the pathogenesis of the disease was by Polymeropoulos et al. (1997) who identified the first genetic defect linked to Parkinson's in large Italian and Greek familial cases. The mutation localised to the *SNCA* gene encoding α-synuclein, resulting in a A53T amino acid change with a autosomal dominant inheritance pattern (Polymeropoulos et al. 1997). α-synuclein and later was found to be one of the main proteins abundantly found in Lewy bodies (Spillantini et al. 1997) .

The functional role of α-synuclein is still poorly understood, as for now its function is associated with presynaptic termini of neurons and is believed to have a role in vesicle pool refilling and trafficking. The expression of α-synuclein is developmentally regulated. During human fetal development it is expressed in various peripheral tissues including heart, kidney, liver, lung, adrenal glands, skeletal muscle and pancreas (Hashimoto & Masliah 1999; Lücking & Brice 2000; Ltic et al. 2004) whereas in adults it is predominantly expressed in the brain more specifically localised at the nerve termini in a subset of neuronal groups. It is also found in non-neuronal tissue including red blood cells and platelets (Barbour et al. 2008).

1.3.2 α-synuclein structure and function

α-synuclein is a 14 kDa cytosolic protein, it is encoded by the *SNCA* gene which consists of 6 exons ranging from 42 to 110 bp (McLean et al. 2000). Its structure has been divided into three distinct domains: a positively charged N-terminal region that interacts with lipid membranes, a central hydrophobic region that has increased predisposition to aggregate and a highly acidic C-terminal domain assumed to repress aggregation (Lashuel et al. 2013). At the presynaptic terminals α-synuclein exists in an equilibrium between a soluble and membrane bound state (Burré 2015). In general it is thought in physiological conditions α-synuclein takes an unfolded monomer conformation however, it has been also shown to adopt tetrameric and octameric structures after non-denaturing purification from mammalian cells (Bartels et al. 2011). These findings created

controversy which lead to further extensive investigation that go onto confirm α-synuclein predominantly exists in a monomeric form in the central nervous system, but cannot discard the presence of other forms of α-synuclein (Waudby et al. 2013; Theillet et al. 2016). When anchored to synaptic vesicles it adopts a metastable α-helical multimeric conformation, this conformation is believed to assist in protection against aggregation (Bartels et al. 2011). It is considered the aggregation of α-synuclein is pathological contribution to Parkinson's.

Since α-synuclein can adopt these dynamic structures at different cellular locations this suggests it has multiple functions. This conformation plasticity is regulated by the 3 structural domains. Firstly, the N terminal domain which, spans from residue 1-87 that is made up of seven 11- amino acid (AA) repeats (Bussell & Eliezer 2003). Each of these 11-AA repeats contains a highly conserved KTKEGV hexameric motif; interestingly, this hexameric motif is also found in the α-helical domains of apolipoproteins (Illustrated in Figure 1.1) (Sode et al. 2006). The 11-AA repeats at the N-terminal are thought to direct the ability of α-synuclein to disrupt lipid bilayers as well as reduce the susceptibility of forming β- sheet structures through their ability to induce α-synuclein helical structures (Sode et al. 2006). As one of the associated functions of α-synuclein is to induce lipid binding and helix folding, this may modulate the fusion of synaptic vesicles at the presynaptic membrane and result in neurotransmitter release. This domain is also believed to confer toxicity to the protein, and deleting a portion of the N-terminal domain was shown to relieve this toxicity (Vamvaca et al. 2009). More recently it was shown the N-terminal domain is also acetylated which is believed to increase helical folding, increase affinity for membranes and give resistance to aggregation (Kang et al. 2012; Dikiy & Eliezer 2014). One study showed by removing the gene responsible for N-terminal acetylation of α-synuclein, its localisation changed from plasma membrane to a diffused cytosolic localisation (Zabrocki et al. 2008). While binding at the membrane induces α-synuclein helical conformation and is said to decrease predisposition for α-synuclein aggregation which is facilitated through the N-terminal domain (Zhu & Fink 2003). Secondly, the central region of α-synuclein spanning from residues 61-95 which is also

known as NAC, is involved in fibril formation and aggregation that can form β- sheet structures (Giasson et al. 2001).

Finally, the C-terminal domain spans residues 96-140 that forms a highly acidic tail of 43 –AA containing 10 Glutamic acid (Glu) and 5 Aspartic acid (Asp) residues. Structurally the C-terminal domain adopts a random coil structure as a result of its low hydrophobicity and high net negative charge (Ahn et al. 2006). By interacting with NAC region of α-synuclein it is thought to inhibit α-synuclein aggregation (Emamzadeh 2016). Some studies have shown induction of α- synuclein aggregation by lowering the pH which neutralises the negative charge of the C-terminal (Hoyer et al. 2002). Similarly, truncation of this protein by deleting the C-terminal domain increased aggregation (Liu et al. 2005).

Each domain is shown to facilitate in a particular function that are also interchangeable but ultimately elicit its role by interacting as a single unit. However, it can be assumed each domain has its own contribution to the pathogenesis of Parkinson's independently of each other. The conformational plasticity also reflects the diversity and heterogeneity of the toxic structures of α-synuclein while, the oligomeric form is thought to be the most toxic species, amyloid fibril structures are the most abundant α-synuclein confirmation found in Lewy bodies (Spillantini et al. 1997).

As a result of the different conformations α-synuclein can adopt it could explain the multifunctional aspects of this protein. However, many of the associated functions including regulation of neurotransmitter release have not been yet linked to a particular structure of α-synuclein such as whether it is monomers or smaller oligomers that facilitate this action. α-synuclein is enriched at the presynaptic membrane where it appears to assist in SNARE-complex assembly (Burre et al. 2010). It co-localises with other presynaptic proteins including synapsin1, synapsin III, synaptotagmin and synaptophysin (Withers et al. 1997; Lee et al. 2008; Lautenschläger et al. 2018). Presynaptic proteins regulate events that result in neurotransmitter release into the synaptic cleft including docking, vesicle fusion and vesicle pool refilling, proposing α-synuclein also contributes to these functions (Denker & Rizzoli 2010).

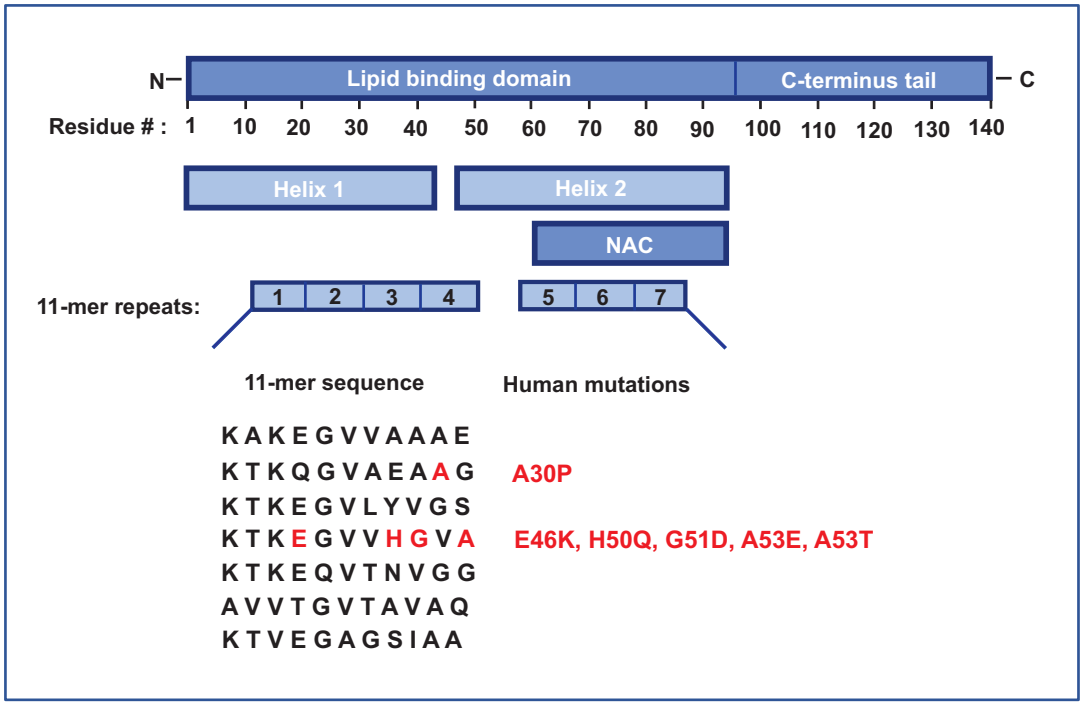

Figure 1.1 α-synuclein domain structure.

A schematic illustration of domain structures of α-synuclein. A 14 kDa protein that can be divided into 3 domains. The N-terminal is divided into seven 11-mer repeats, that facilitates in lipid binding, that folds into two amphipathic helices. Helix 2 contains the aggregation prone NAC domain; this domain is thought to confer toxicity and aggregation. Of the 6 point mutations associated with familial Parkinson's, they all localise within this domain, at the second and fourth 11-mer. The C-terminal domain is highly acidic that adopts a random coil structure. The C-terminal truncation's induce α-synuclein aggregation, suggesting modifications to the C-terminal might be involved in the aggregation of α-synuclein.

1.3.3 α-synuclein Genetic Implication

The first evidence of α-synuclein involvement in Parkinson's was through a genetic screen which found the first Parkinson disease associated mutation (*A53T)* which was later supported by being one of the predominant proteins found in Lewy bodies (Polymeropoulos et al. 1997). Confirmation comes from, multiplications and 6 coding region point mutations (A53T, A30P, E46K, A53E, G51D, H50Q) of the α-synuclein gene (*SNCA*) that have been identified in familial forms of Parkinson's (Polymeropoulos et al. 1997; Krüger et al. 1998; Zarranz et al. 2004; Kiely et al. 2013; Appel-Cresswell et al. 2013; Pasanen et al. 2014). Majority of Parkinson's cases are sporadic accounting for 90 % of the cases while only 10% have a familial inheritance (Klein & Westenberger 2012).

The penetrance of the missense mutations appears to be high, it is thought to be around 85% for the p.A53T mutation (Polymeropoulos et al. 1997). However, the penetrance of

gene multiplication is reduced to 33% (Nishioka et al. 2006) . Clinical symptoms are thought to be dependent on gene dosage as increased number of the *SNCA* gene including duplication or triplication are associated with early onset (Fuchs et al. 2007). Disease progression is thought to be faster with more severe clinical symptoms (Fuchs et al. 2007). Duplications of *SNCA* gene result in 1.5 fold increase in α-synuclein protein whereas triplications result in two fold increase, suggesting increase of wild-type α-synuclein is toxic to neurons (Farrer et al. 2004)

In general, α-synuclein is a natively unfolded monomer, when it binds to phospholipid membranes it adopts α-helical rich structures. Interestingly the two point mutations p.A53T and p.A30P tend to form stable β sheets, that exacerbate the formation of toxic oligomers, protofibrils and fibrils (Bertoncini et al. 2005; Conway et al. 2000). It is assumed, the missense mutations result in toxic gain of function that cause Parkinson's, where Lewy body formation may be a way of protecting the cell from toxic α-synuclein (Bertoncini et al. 2005). Of the six mutations identified so far, all six maps to the amino terminal domain of α-synuclein, it is thought these mutations impair the amino terminal domain. As well as point mutations and gene amplification, variation in the promotor region of the *SNCA* gene, specifically the dinucleotide repeat polymorphism known as Rep1, has been reported to increase the risk of Parkinson's (Krüger et al. 1999). Two domains that flank the Rep1site appear to interact with each other to increase expression of *SNCA*, while Rep1 is shown to act as a negative regulator (Chiba-Falek et al. 2005). Variation at the 3'region of the *SNCA* gene has also been associated as a risk for the development of Parkinson's (Mueller et al. 2005). In familial Parkinson's, mutations of the SNCA gene including the A53T and E46K can result in early onset of Parkinson's (Hill-Burns et al. 2016; Zarranz et al. 2004; Kasten & Klein 2013).

The different mutations across the *SNCA* gene exhibit different severity of clinical symptoms, including the classical Parkinson's symptoms to sensitivity to levodopa therapy (Si et al. 2017). For example, patients with the A53T mutation usually have an earlier onset, increased disease progression and lower prevalence of tremor compared with sporadic Parkinson disease patients (Kasten & Klein 2013). Patients with the A30P mutation, usually present a later onset with less progressive clinical symptoms whereas,

patients with the E46K mutation usually present more severe symptoms with early onset dementia (Zarranz et al. 2004).

1.3.4 α-synuclein Pathogenesis

α-synuclein undergoes structural modifications resulting in the formation of toxic species. Under pathological conditions α-synuclein misfolds and aggregates into multiple soluble oligomeric species and eventually insoluble amorphous or fibrillary amyloid –like assemblies (Calo et al. 2016). Accumulating evidence suggests the oligomeric or prefibrillar species confers toxicity rather than the amyloid fibril deposits found in Lewy bodies (Lambert et al. 1998; Winner et al. 2011). These oligomers have also shown to impair other functions including protein degradation as well as functions of other organelles where increased levels of these oligomers have been found in diseased brains (Emmanouilidou et al. 2010; Hansson et al. 2014). It is assumed disease progression of Parkinson's is assisted by toxic species of α-synuclein being secreted, and taken up by nearby cells (Lee et al. 2002; Rochet et al. 2004).

To model the role of α-synuclein in the development of Parkinson's, several models have been developed (Chesselet 2008). This increases the expression of *SNCA*, reflecting gene amplification and assisting in the accumulation of α-synuclein in forming protein inclusions similar to that of Lewy bodies (Chesselet 2008) . α-synuclein is selectively transported to the lysosomes for degradation (Cuervo et al. 2004). Lysosomal inhibition results in the accumulation of α-synuclein, the autophagy/lysosomal pathway is involved in the clearance of oligomeric and fibril conformations of α-synuclein (Lee et al. 2004). Since α-synuclein is considered to drive the pathogenesis in Parkinson's, elucidating its interacting partners would aid the mechanism of α-synuclein pathology. One of the proteins found to interact/associate with α-synuclein is tubulin, where α-synuclein was co-purified with microtubules (Alim et al. 2002). This interaction was confirmed by tubulin co-localising with α-synuclein positive protein inclusions including Lewy bodies (Alim et al. 2002). Microtubules are cytoskeletal polymers that form an integral component of the neuronal cytoskeleton. In neurons, normal microtubule functioning is important in axonal transport, as axonal degeneration is considered to be an early

dominant feature of Parkinson's (Li et al. 2009). Axonal transport is essential for neuronal function and survival while, failure in axonal transport is thought to contribute to the early stages of Parkinson's (Hunn et al. 2015). The dopaminergic neurons of the substantia nigra are known to have long projections, with an average arborisation of 4.6 m in humans, these neurons become particularly dependent on axonal transport (Pissadaki & Bolam 2013). The loss of dopaminergic neurons at the nigrostriatal pathway, display a 'dying back' degeneration mechanism, a pathway that starts at the axonal terminal and proceeds towards the soma (Campenot 1982). It is thought alterations of axonal transport or microtubules initiates this pathway, which could be due to the association between α-synuclein and microtubules (Cartelli et al. 2010). α-synuclein is also shown to facilitate in the development in dopaminergic neurons, as in its absence in mice, the number of dopaminergic neurons in the substantia nigra reduce (Garcia-Reitboeck et al. 2013). A study by Esteves et al (2010) biochemically investigated a Parkinson patient derived cell line and found elevated levels of free tubulin to polymerised tubulin and an increase in α-synuclein oligomeric accumulation. They showed by treating cells with Taxol known to stabilise microtubules, normalised the levels of free tubulin and polymerised tubulin and reduced α-synuclein oligomerisation, they show microtubule depolymerisation potentiates α-synuclein oligomerisation (Esteves et al. 2010). Similarly, another study also showed that α-synuclein induces polymerisation of tubulin, where this function was associated with the C-terminal domain of α-synuclein. Interestingly the mutant forms of α-synuclein were not able to do the same (Alim et al. 2004). Overexpression of α-synuclein is shown to disrupt the microtubule network in neuronal cells, impairing neurite morphology (Prots et al. 2013).

1.4 Current treatments

Like other neurodegenerative diseases Parkinson's does not have a conclusive test which could definitively test for the disease. Diagnosis is made on clinical symptoms presented including the most prevalent; resting tremor, bradykinesia and rigidity and the response to medication (Mollenhauer et al. 2013) . A number of rating scales have been developed to assist in the prognosis of Parkinson's. The Hoehn and Yahr scale and the Unified Parkinson's rating scale (UPDRS) are the two most widely used (Goetz et al. 2004). There

is no cure for Parkinson's, treatments usually involve delaying the progression of the disease and elevating the symptoms.

The presence of Lewy bodies is the most definitive diagnosis however this can only be done on post-mortem brains. The examination of different reflexes and limb movements are used as tests in the diagnosis of Parkinson's. For example, bradykinesia is tested for by measuring the ability to clamp the finger and thumb together (Goetz et al. 2004) Several symptomatic treatments have been developed for treating Parkinson's, but they are not effective in delaying the progression of the disease. The current treatments can be divided into two groups, dopaminergic and non- dopaminergic drugs. Dopaminergic drugs consist of: Levodopa (L-DOPA), MAO-B inhibitors, COMT inhibitors and dopamine agonists and non-dopaminergic drugs include: anticholinergic drugs, these treatment plans are usually administered with other drugs (Fox 2013; DeMaagd & Philip 2015).

In recent years there is increasing interest in non-motor symptoms (NMS), such as rapid eye movement (REM), sleep behaviour disorder (RBD), constipation, hyposmia as well as cognitive symptoms. Non-motor symptoms appear earlier than motor symptoms, supporting the idea of earlier clinical diagnosis (Plouvier et al. 2014).

1.5 Dopaminergic system

There are around 100 billion neurons that populate the brain (Herculano-Houzel 2009) of which 400,000 to 600,000 are dopaminergic neurons, this is less than 1 % of the total neuronal population (Chinta & Andersen 2005; Björklund & Dunnett 2007). Dopamine is a catecholamine neurotransmitter which serves as a chemical messenger. Its association with neurological diseases including Parkinson's and Schizophrenia means it is one of the most extensively studied neurotransmitters (Bogerts et al. 1983).

Dopamine was originally thought to be a precursor of noradrenaline (NA) and was not considered to have any signally properties of its own. A study by Carlsson et al (1958) showed the first evidence of dopamine as a neurotransmitter. When they administered reserpine in rabbits both dopamine and noradrenaline almost completely disappeared,

interestingly when they administered L-DOPA a precursor of dopamine it reversed the effects of reserpine but more specifically increased levels of dopamine were observed but not for noradrenaline (Carlsson et al. 1958). Follow on work by Bertler and Rosengren showed majority of dopamine localised to the basal ganglia (Bertler & Rosengren 1959). Mapping of the dopaminergic network followed identifying several distinct pathways (Fuxe 1965; Ungerstedt 1971). Dopamine has a non- uniformed distribution in the brain, with several regions where dopaminergic neurons are concentrated localising at the diencephalon, mesencephalon, olfactory bulb and the retina (Chiodo 1988). Over 70% of these neurons are found to be concentrated at the midbrain including the substantia nigra and the ventral tegmental area (VTA) (Björklund & Dunnett 2007).

Four distinct dopaminergic pathways have been identified which carry dopamine from neuronal centres across axonal projections to other brain regions. The largest being the nigrostriatal pathway which stretches its projections from the substantia nigra to the striatum (Prensa et al. 2009). Secondly, we have the mesolimbic pathway which stretches from the VTA to the nucleus accumbens (Fiorino et al. 1993). The third pathway is the mesocortical pathway that stretches from the VTA throughout the cerebral cortex and the fourth the tuberoinfundibular pathway which originates from the hypothalamus to the pituitary (Björklund et al. 1973; Deniau et al. 1980). The different anatomical distribution of these neurons reflects the wide range of cellular functions brought about by dopamine. Each pathway has shown to control specific functions with some overlap (Arias-Carrión et al. 2010).

Dopaminergic neurons of the nigrostriatal pathway are involved in controlling voluntary movement and more recently cognitive function, the pathway affected in Parkinson's individuals (Arias-Carrión et al. 2010). The mesolimbic and mesocoritcal pathway are associated with emotion based behaviour including motivation and reward . Both pathways have a considerable overlap due to projections originating from the VTA but have different end points. As a result, the pathways are collectively referred to as the mesocorticolimbic system (Yamaguchi et al. 2011).

Dopamine is synthesised by the body by specific cell types including neurons and cells of the adrenal glands. The biosynthesis of dopamine is dependent on the conversion of tyrosine through a series of enzymatic processes (Molinoff & Axelrod 1971). Tyrosine is a non- essential amino acid which can be obtained through the diet or the conversion of phenylalanine by phenylalanine hydroxylase at the liver , this conversion is brought about by tyrosine hydroxylase (TH) (Litwack & Litwack 2018). Tyrosine hydroxylase is considered to be the rate limiting enzyme in biosynthesis of dopamine. Tyrosine is converted to L-DOPA by tyrosine hydroxylase which is then further processed by L-DOPA decarboxylase to dopamine (Daubner et al. 2011). Dopamine can also by further processed to form nor-adrenaline and adrenaline . Dopamine modulates either inhibitory or excitatory synaptic transmission through binding to dopamine receptors (Keefe & Gerfen 1995). There are known to be five dopamine receptors subtypes that have been categorised into two groups based on their functional properties, D_1 and D_2 receptors. The D_1 class has been divided into D_1 and D_5. these receptors are associated with excitatory G proteins. Activation of these receptors increases adenylyl-cyclase activity, which in turn induces protein kinase A (PKA) activation resulting in increasing cyclic AMP (cAMP) levels (Beaulieu & Gainetdinov 2011). The D_2 subgroup includes receptors D_2, D_3 and D_4 that are associated with inhibitory G (Gi) proteins that inhibit adenylyl-cyclase activity resulting in decrease in cAMP levels (Obadiah et al. 1999). In Parkinson's reduced levels of dopamine in post-mortem brains has been observed. Around 50% of the nigrostriatal dopamine cells have degenerated before symptoms are observed (Cheng et al. 2010). Oxidative stress is known to play an important role in the degeneration dopaminergic neurons. The mitochondrial toxin 1-methyl-4-phenyl-1,2,3,6-tetrahydropyridine (MPTP) has been extensively studied in the mouse model MPTP, as MPTP is known to cause oxidative stress resulting in the death of neurons within the nigrostriatal pathway (Sonsalla & Heikkila 1986; Yazdani et al. 2006). Dopamine levels need to be tightly regulated as either loss or increased concentrations are implicated in Parkinson's and Schizophrenia (Dragicevic et al. 2015).

1.6 Ubiquitin proteasome system

Protein turnover is a fundamental cellular process, regulating cellular metabolism in response to the requirement of a cell. In eukaryotic cells the ubiquitin proteasome system

(UPS) is one of the two systems that manages protein degradation, regulating 80-90% of cytoplasmic protein degradation (Lilienbaum 2013). Proteasomal degradation regulates denatured, misfolded and damaged proteins which are involved in cell cycle progression, oxidative stress, gene expression and overall homeostatic functions of the cell. Impairment of the ubiquitin proteasome has been associated with many diseases ranging from neurodegenerative disease, genetic diseases and cancer (Paul 2008).

Initially it was thought the main protein degradation pathway was the autophagy and lysosomal pathway due to its high content of proteases and lysosomal involvement in the degradation of endocytosed proteins. In 1970's Alfred Goldberg and Joseph Etlinger showed another cell compartment also demonstrated protease activity which was driven by ATP. By using cell free extracts with no lysosomal traces protein degradation was observed with similar activity seen in live cells (Etlinger & Goldberg 1977).

The fundamental process of regulated protein degradation is a universal mechanism with the proteasome being highly conserved in eukaryotes. The ubiquitin proteasome system is a multi-pathway system that regulates degradation in several steps including; covalently tagging ubiquitin to the target protein which is then degraded by the 26S proteasome an ATP-dependent multi-subunit protease (Ciechanover et al. 1984; Xie & Varshavsky 2000). Ubiquitin is an 8.5 kDa protein which exists freely in the cytosol of cells. Key structural features include seven Lysine residues throughout the protein sequence all of which can be ubiquitinated resulting in a poly-ubiquitinated chain (Peng et al. 2003). Recognised as post-translational modification, ubiquitination changes the stability, localisation or activity of the target protein. Originally associated with protein degradation there is now growing evidence ubiquitin has more diverse roles than previously anticipated, it has been shown to be involved in DNA repair, apoptosis and protein trafficking (Chen et al. 2005; Donaldson et al. 2003; Sun et al. 2004). In general, a substrate protein can either be mono-ubiquitinated, polyubiquitylated or multi-monoubiquitylated, the extent of ubiquitination serves as a regulatory modification influencing different physiological roles though a certain level of overlap is seen. For example, polyubiquitination is associated with proteasomal degradation and

neurodegeneration, whereas monoubiquitylation is linked to endocytosis and signal transduction (Akutsu et al. 2016)

Ubiquitination of the target protein essentially flags the protein to be degraded by the proteasome. Tagging of ubiquitin to the substrate protein involves a 3-step cascade mechanism including several enzymatic reactions (Illustrated in Figure 1.2) (Swatek & Komander 2016).Firstly, ubiquitin is activated by ubiquitin activating enzyme E1 in a ATP dependent reaction resulting in a high-energy thiol ester intermediate. This is followed by the transfer of the activated ubiquitin moiety to the ubiquitin conjugation enzyme E2 in a transesterification reaction manner (Varshavsky 2001) whereby the ubiquitin molecule is transferred over to a specific cysteine residue of the E2 enzyme . Similarly, the final step involves the transfer of ubiquitin to a lysine residue of the target protein. This process is mediated through ubiquitin protein ligase, E3 also known as recognin, important in identifying the target protein by interacting with the protein's degradation signal (Ardley & Robinson 2005).Multiple cycles of ubiquitin conjugation will result in a polyubiquitin chain (Chau et al. 1989).

The human genome encodes two E1s, ~38 E2s and over 600 E3s (Jin et al. 2007; Buetow & Huang 2016). One of the ways by which the ubiquitin proteasome system regulates its specificity for targeting the correct protein to be degraded is through the diversity of the E3 enzyme. The ubiquitinated protein is translocated to the 26S proteasome. The 26S proteasome is a dynamic multi-subunit proteolytic complex with a molecular weight of 700 kDa. It consists of a central catalytic core known as 20S and two terminal regulatory particles 19S that are attached in opposite orientations to either end of the 20S unit, collectively this forms the enzymatically active proteasome (Chen et al. 2016). The 20S proteasome is able to degrade unfolded or loosely folded proteins in an ATP-dependent manner however they cannot degrade ubiquitin tagged proteins (Asher et al. 2006). The 20S core particle is a barrel-shaped structure that is made up of four stacked rings; two outer α-rings and two inner β-rings, each ring is formed of seven subunits. The proteolytic active site of the 20S unit is buried within the lumen of this complex at the two β-ring domains (Unno et al. 2002), a mechanism thought to avoid non-specific degradation of cytoplasmic proteins (Heinemeyer et al. 1997). The 19S component is

associated with regulatory functions, it is made up of several subunits that direct diverse functions including ATPase, ubiquitin binding and deubiquitinating (Ehlinger & Walters 2013). A 19S compartment is known as the regulatory terminal as it has key functions in facilitating the delivery of the substrate protein. One of the first steps of the 19S domain is in recognising the ubiquitinated protein, where a binding site for ubiquitinated protein has been identified at this structure. The 19S compartment is also involved in forming a route of entry at the α-ring, allowing the entry of target protein to the proteolytic site (Liu & Jacobson 2013). Since many target proteins aggregate, it is also involved in unfolding the protein which can then enter the 20S site. This process is highly energy dependent, enabled by the six ATPase subunits at the 19S domain (Glickman et al. 1999).

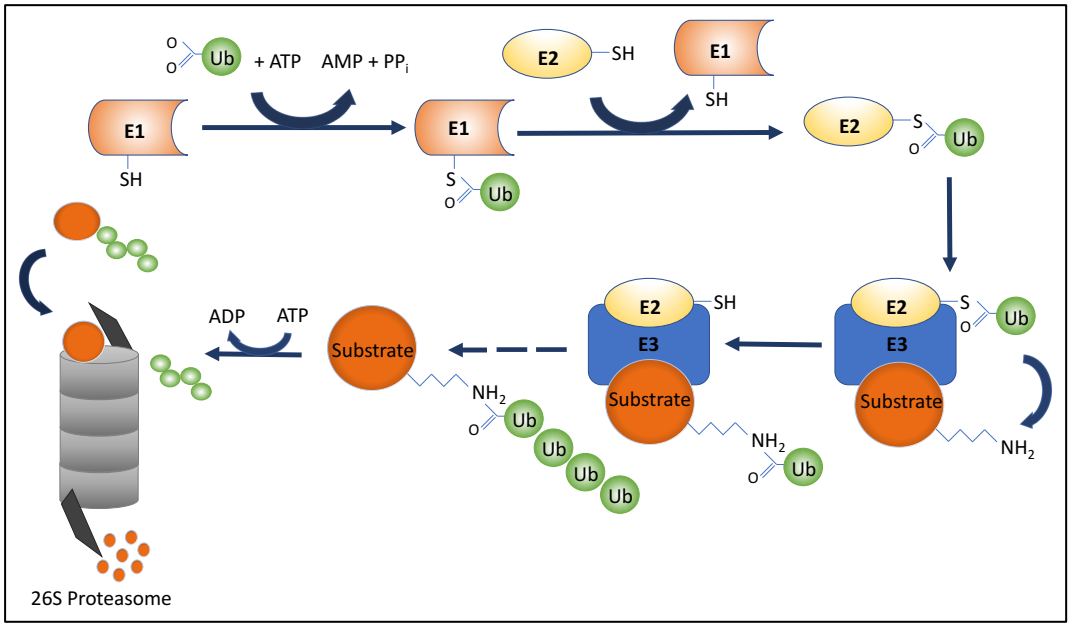

Figure 1.2 Schematic of attaching ubiquitin to mis-folded proteins.

Mis-folded or toxic proteins get degraded by the ubiquitin proteasome system. Proteins destined for degradation get tagged by ubiquitin chains that are recognised and degraded by the ubiquitin proteasome machinery. Attaching ubiquitin to the target protein can be divided into three key steps. Firstly, ubiquitin is activated by ubiquitin activating enzyme E1, in a ATP dependent reaction resulting in a high-energy thiol ester intermediate. This is followed by the transfer of the activated ubiquitin moiety to the ubiquitin conjugation enzyme E2 in a transesterification reaction manner whereby the ubiquitin molecule is transferred over to a specific cysteine residue of the E2 enzyme . Similarly, the final step involves the transfer of ubiquitin to a lysine residue of the target protein. This process is mediated through ubiquitin protein ligase, E3 also known as recognin, important in identifying the target protein by interacting with the protein's degradation signal. Multiple cycles of ubiquitin conjugation will result in a polyubiquitin chain. Ubiquitinated proteins are then translocated to the 26S proteasome where it is degraded by the proteolytic active site of the proteasome machinery.

1.6.1 Role of Ubiquitin Proteasome System in disease processes

Protein degradation by the ubiquitin proteasome system is a highly regulated mechanism and like many other systems, malfunction can occur. Ubiquitin proteasome system has been implicated in the pathogenesis of many diseases including neurodegenerative diseases, genetic diseases and cancer (Adams 2003; Chen et al. 2008). A growing amount of evidence suggests the ubiquitin proteasome machinery has the potential to be a therapeutic target in the treatment of these diseases. Predictably, a dysfunctional ubiquitin proteasome would be thought to result in the accumulation of misfolded proteins and harmful peptides. The accumulation of aggregated ubiquitinated proteins can directly impair the ubiquitin proteasome (Bence et al. 2001).

1.6.2 Parkinson's and UPS

The ubiquitin proteasome system has been implicated in the pathogenesis of Parkinson's, as ubiquitin was immunocytochemically shown to be a component of Lewy bodies (Lowe et al. 1988; Kuzuhara et al. 1988; Halliwell & Jenner 1998). Mutations resulting in the failure of ubiquitin proteasome system have been identified in familial Parkinson's, proposing impairment of the proteasome system to contribute to disease progression. Similarly, in sporadic Parkinson's, increased occurrences of protein aggregation and impaired proteolysis is observed in the substantia nigra of patients, consistent with the idea of impaired protein clearance contributes to the pathogenesis of Parkinson's (McNaught & Jenner 2001). Post-mortem brains from sporadic Parkinson patients more specifically showed loss of 20S core α-subunits and decrease expression of the 19S subunit (McNaught, et al. 2002; McNaught et al. 2003),

Of the several genes identified in familial Parkinson's, two of them have a direct role in the ubiquitin proteasome pathway. Mutations in the gene *PARK2* (Parkin) were identified as the genetic cause of autosomal-recessive juvenile parkinsonism (ARJP) (Shimizu et al. 1998). Parkin codes for the protein Parkin RBR E3 ubiquitin-protein ligase (*PARK2*), it is a ubiquitin ligase that covalently attaches ubiquitin to target proteins (Shimura et al. 2000). Similarly, mutations in the gene ubiquitin carboxyl-terminal hydroxylase L1 (UCH-L1) also causes familial Parkinson's (Leroy et al. 1998; Maraganore et al. 2004). UCH-L1 makes up

2% of total protein expressed in the human brain, which is also present in Lewy bodies. UCHL1 plays an important role in ubiquitin dependent proteolysis by recycling polymeric chains of ubiquitin to monomeric ubiquitin. Mutations associated with UCH-L1, are reported to have roughly 50% reduction in proteasome catalytic activity (Leroy et al. 1998). UCH-L1 is therefore important in recycling and providing monomeric ubiquitin for labelling abnormal proteins destined for proteasomal degradation. Cellular proteins are targeted for degradation by conjugation to a ubiquitin chain. Ubiquitin consists of seven lysine residues; each residue can be linked to the C-terminus of another ubiquitin molecule through isopeptide bond (Chau et al. 1989). When the ubiquitin chain is formed, where ubiquitin's are covalently linked by their K48 or K11 residues results in the degradation via the 26S proteasome whereas, attachments through the K63 residues to membrane associated proteins target them for lysosomal degradation (Reyes-Turcu & Wilkinson 2009). A fraction of aggregated α-synuclein protein present in Lewy bodies is also ubiquitinated, (Tofaris et al. 2003), interestingly it was shown that the ubiquitin chains found in Lewy bodies form via the K63 residue. However the accumulation of K63 linked ubiquitin in Lewy bodies was found to be partly caused by an increase of Usp8 a deubiquitinating enzyme, that deubiquitinates K63 linked chains on α-synuclein and so decreasing its degradation by the lysosomal pathway (Alexopoulou et al. 2016).

Ageing is considered to one of the main risk factors for developing Parkinson's, comparably it also affects the proteasome structure and function (Saez & Vilchez 2014). Similarly, environmental factors such as pesticide exposure known to be a high-risk factor in the development of Parkinson's is also shown to affect the proteasome machinery. Chronic exposure of the pesticide rotenone resulted in proteasomal impairment (Betarbet et al. 2006). The mitochondrial toxin 1-methyl-4-phenyl-1,2,3,6-tetrahydropyridine (MPTP) is known to impair mitochondrial function, which depletes ATP, in turn resulting in proteasomal impairment as protein degradation via the ubiquitin proteasome pathway is a ATP dependent process (Zeng et al. 2006). There is also evidence α-synuclein binds to the proteasome particularly the mutated and the aggregated form, reducing proteasomal function (Stefanis et al. 2001; Emmanouilidou et al. 2010). In a study by Linersson et al. (2004) showed that, increase accumulation of α-

synuclein led to the formation of oligomeric α-synuclein. This conformation of α-synuclein led to proteasomal inhibition, with α-synuclein binding more readily to the 20S proteasome complex (Lindersson et al. 2004) As there is strong evidence impaired proteasomal activity could contribute to the pathogenesis of Parkinson's, animal models where the proteasome is inhibited have been developed. With the aim of elucidating the mechanism by which disrupting protein homeostasis results in dopaminergic neurodegeneration in the substantia nigra.

1.6.3 Ubiquitin proteasome and Aggresomes

It is estimated that up to 30% of newly synthesised proteins are not folded properly (Schubert et al. 2000). Though misfolded proteins are considered non-functional, they can aggregate, these aggregates can have a toxic gain of function (Gloeckner et al. 2006). The ubiquitin proteasome system is involved in regulating protein homeostasis. When protein degradation via the proteasome is disturbed, it results in aberrant protein aggregation, a dominant pathological feature of many neurodegenerative diseases (McNaught, Shashidharan, et al. 2002). Protein aggregates cannot be properly unfolded to pass through the proteolytic barrel of the proteasome which further inhibits proteasome activity. Resulting in further accumulation and aggregation of misfolded proteins. These aggregates get concentrated by a microtubule dependent process driven by dynein motors forming a perinuclear inclusion body, where they are known as aggresomes (Johnston et al. 1998; Ahmad et al. 1998). As the aggregated protein cannot be properly unfolded to pass through to the enzymatic active site, while the aggregated protein cannot get cleared by the proteolytic machinery, it can actually, impair proteasomal activity. In turn further processing of proteins is inhibited resulting in the accumulation of aggregated proteins. Aggresomes are thought to be cytoprotective as they sequester toxic proteins and a mechanism to retain toxic proteins in a central location. Aggresome formation requires several ubiquitin- binding proteins, including parkin, that is known to be a genetic risk factor for familial and late onset sporadic Parkinson's (Zhao et al. 2003). Previously mentioned parkin encodes E3 Ub- protein ligase, usually when ubiquitin is covalently attached to the target protein, the attachment is through K48 residue forming a polyubiquitinated chain. Parkin is shown to attach

ubiquitin also at the K63 residue of some proteins. Attachment at this site, directs the protein to the aggresome which are then degraded by autophagy (Chin et al. 2010). As parkin is able to direct attachments of ubiquitin at different residues that in turn determine the route of degradation suggests the ubiquitin proteasome is able to regulate proteins that are directed to form the aggresome and then destroyed by autophagy.

1.7 Aggresomes

Aggresomes were first described by Johnston et al (1998), they showed misfolded proteins can accumulate at a distinct juxtanuclear location, which they called an aggresomes (Johnston et al. 1998). Aggresomes are thought to be the precursors of Lewy bodies, as both have a similarities in protein composition including, heat shock proteins, components of the ubiquitin proteasome system and cytoskeletal proteins (Kopito 2000; McNaught et al. 2002). The formation of both protein inclusions is contributed by the impairment of protein homeostasis. Aggresome formation is a multi-step process. This includes, recognising misfolded proteins that are transported on dynein motors via retrograde transport. Aggresome formation is dependent on an intact microtubule network, where dynein motors cargo the aggregated protein towards the microtubule organising centre of the cell (Illustrated in Figure 1.3) (Johnston et al. 1998; Ahmad et al. 1998). Disruption of either the microtubule network or the dynein motor complex prevents aggresome formation (Johnston et al. 1998; Johnston et al. 2002).

Formation of these protein inclusions is believed to be an approach to locate toxic proteins to a single location, that are then degraded via autophagy (Wong et al. 2008). In support of its protective role, a study by Taylor et al. (2003) showed that by blocking the formation of aggresomes, either by the inhibition of microtubule polymerisation or disrupting dynein motor function led to decreased viability in cells expressing disease proteins (Taylor et al. 2003). Protein misfolding is not an uncommon phenomenon, misfolded proteins can result from a number of different processes, including incomplete protein synthesis, missense mutations or proteins expressed at high levels (Lee et al. 2006; De Baets et al. 2015; Burré et al. 2015). It is thought misfolded and aggregated proteins can disrupt cellular functions through a number of mechanisms, including pore formation, sequestering important cellular factors and impairing the proteasome

(Emmanouilidou et al. 2010; Tsigelny et al. 2012; Woerner et al. 2016). Reflecting the importance of protein homeostasis. Protein homeostasis is particularly important in neuronal function and survival. As neurons are post-mitotic, they are unable to dilute the toxic proteins by cell division (Rich et al. 1999).

Aggresome formation is accompanied by the redistribution of intermediate filaments, which cages around the aggregated protein (Johnston et al. 1998). Vimentin which is an intermediate filament is widely used as a marker for aggresomes . The caging of the aggresome is thought to promote aggresome stability or assist in preventing non-specific interactions (Mayer et al. 1989). Other proteins that get recruited to the aggresome include heat shock proteins and centrosomal proteins, this includes Hsp70 and γ-tubulin (Johnston et al. 1998; Junn et al. 2002). In a study by Boeddrich et al. (2003) showed that overexpressing the mutant form of Huntington protein formed aggresomes. (Boeddrich et al. 2003). Similarly, in Parkinson's, a number of genes recognised as genetic risk factors have shown to form aggresomes. When either Parkin or UCH-L1 was overexpressed, aggresomes inclusions were observed (Junn et al. 2002; Ardley et al. 2004).

Though the ubiquitin proteasome does not directly degrade aggresomes, it is involved in activating the autophagy pathway. One study showed that the proteasome is involved in removing ubiquitin chains from the polyubiquitinated protein aggregates by the deubiquitinating enzyme Poh1. Poh1 cleaves ubiquitinated proteins, which release ubiquitin chains. These ubiquitin chains bind and activate deacetylase HDAC6, activation of HDAC6 in turn promotes autophagy. In cells that were Poh1 deficient, aggresome clearance was inhibited (Hao et al. 2013).

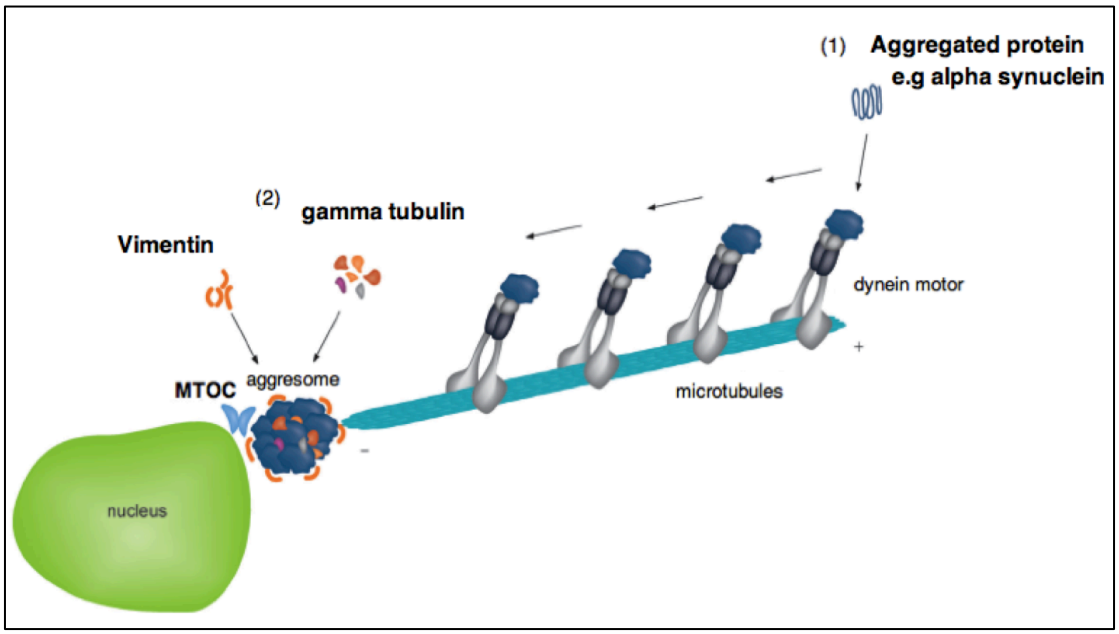

Figure 1. 3 A schematic of aggresome formation.
The centrosome nucleates microtubules that are used as tracks for microtubule based motor transport, such as dynein motors. The microtubule-based dynein motor cargos aggregated protein from the cell periphery along microtubules to the MTOC . Dynein motors cargo protein via retrograde transport. Once at the MTOC, the aggregated proteins are caged by cytoskeletal proteins including vimentin. Other proteins also get recruited to the aggresomes, such as γ-tubulin a centrosomal protein and Hsp70 a heat-shock protein.

1.8 Autophagy

Autophagy is an evolutionary conserved catabolic process that regulates the degradation of long lived proteins and dysfunctional organelles at the lysosome. Autophagy can mediate nonselective degradation or substrate specific degradation (Fujiwara et al. 2016). Depending on the different ways by which the target protein is delivered to the lysosome, autophagy can be divided into three main types: macro-autophagy, micro-autophagy and chaperone-mediated autophagy. In brief macro-autophagy delivers cytoplasmic cargo to the lysosomes once portions of the cytoplasm are engulfed by a double membrane that expands into a cytosolic vesicle called an autophagosome. The autophagosome then fuses with the lysosome to form an autolysosome, the contents are released and degraded (Ravikumar et al. 2009). In micro-autophagy, cytosolic proteins are directly taken up at lysosome, by invagination of the lysosome membrane (Li et al. 2012). In chaperone-mediated autophagy, proteins targeted for degradation form a complex with chaperone proteins such as Hsp-70. This complex translocates, and is recognised by the lysosomal-associated membrane protein 2A (LAMP-2A), where the

protein unfolds and gets degraded (Majeski & Fred Dice 2004). Macro-autophagy has been reported to be involved in different diseases, particularly neurodegenerative diseases.

In Parkinson's, a number of processes are thought to contribute to the pathogenesis of this disease including, oxidative stress, mitochondrial dysfunction and protein aggregation (Bosco et al. 2006; Narendra et al. 2008). In all of these pathways there is strong association with autophagy (Lee et al. 2012). Increasing evidence suggests the accumulation of toxic proteins that form the protein inclusions a hallmark of many neurodegenerative diseases, is a result of autophagy dysfunction (Menzies et al. 2017). In familial Parkinson's, many of the associated genes have shown to be linked to the autophagy pathway. For example, the native form α-synuclein, is degraded by the chaperone mediated autophagy (CMA) pathway (Cuervo et al. 2004). The chaperone protein Hsc70 binds to α-synuclein, which is recognised by the LAMP2A protein on the lysosomal membrane (Cuervo et al. 2004). Interestingly the mutant form of α-synuclein is not degraded by this pathway, which results in the accumulation of the mutant protein (Martinez-Vicente et al. 2008). When the wild-type α-synuclein is overexpressed the expression of LAMP2A also increases. However, the overexpression of α-synuclein led to the formation of the oligomeric form of α-synuclein which cannot be degraded via chaperone meditated autophagy (Vogiatzi et al. 2008; Xilouri et al. 2009). Inhibition of chaperone mediated autophagy by the accumulation of wild-type α-synuclein or α-synuclein point mutations A53T and A30P leads to an overall increase in autophagy. This increase in autophagy is believed to be a compensatory response that can lead to autophagic cell death. This was shown in a study by Xilouri et al. (2009), where they inhibited autophagy in cells expressing the A53T α-synuclein mutant, they found it rescued the cells from autophagic cell death (Xilouri et al. 2009). In general, the inhibition of basal autophagy results in the accumulation of cytoplasmic protein inclusion bodies that cause neurodegenerative diseases (Hara et al. 2006). In a study by Plowey et al. (2008) showed that overexpression of mutant leucine rich repeat kinase 2 (LRRK2) known to be an associate genetic risk factor for familial Parkinson's increased autophagy, this increase in autophagy led to neurite degeneration (Plowey et al. 2008). As previously

mentioned mitochondrial dysfunction is associated in Parkinson's progression. Dysfunctional mitochondria are removed by mitophagy and autophagy related process (Lemasters 2005). The *PARK2* gene that encodes Parkin is an associated genetic risk factor for Parkinson's (Shimura et al. 2000). Mutations in this gene causes autosomal recessive Parkinson's. Parkin is primarily a cytosolic ubiquitin E3 protein ligase (Shimura et al. 2000). Parkin is involved in mitophagy, where it is recruited to impaired mitochondria and promotes it degradation via autophagy (Narendra et al. 2008). Additionally, the PTEN-induced kinase 1 (PINK1) is also involved in the removal of mitochondria through autophagy. Mutations at this gene are known to cause familial Parkinson's (Valente et al. 2001). PINK1 localises to the mitochondria, though its role in mitochondria function is unclear. It has been shown that both Parkin and PINK1 work in the same regulatory pathway of mitophagy. PINK1 recruits Parkin to the mitochondria, where they coordinate the removal of dysfunctional mitochondria (Matsuda et al. 2010).

Aggresomes have also been shown to be degraded by an autophagy degradative process (Wong et al. 2008). A study by Ravikumar et al (2002) showed that when aggresome inclusion bodies were formed by overexpressing the mutated aggregation prone Huntington protein, the number of inclusion bodies decreased when autophagy was upregulated by treating cells with rapamycin (Ravikumar et al. 2002). Similarly, in another study by Sarkar et al.(2007) showed that when aggresomes were formed by overexpressing mutant α-synuclein A53T and A30P, the aggresomes were cleared when they increased autophagic activity, by treating cells with rapamycin (Sarkar et al. 2007). Interestingly, Wong et al. (2008) showed aggresome clearance by autophagy is not a universal process. More specifically they showed that the protein composition of the aggresome regulates whether it is degraded via autophagy. When mutant tau or α-synuclein was overexpressed, they were cleared by increase in autophagic activity. However, when Aminoacyl TRNA Synthetase Complex Interacting Multifunctional Protein 2 (AIMP2) was overexpressed to form aggresomes upregulating autophagy did not remove these aggresome inclusion bodies. They go onto show that by changing the composition of the aggresome by forming aggresomes by co-expressing mutant α-synuclein and AIMP2 these aggresomes can be cleared by autophagy. This change in

aggresome composition enabled the recruitment of the autophagy/lysosome system to the aggresome (Wong et al. 2008).

1.9 Cytoskeleton

Found in all three domains of life the cytoskeleton is a complex structure made up of; tubulin, actin, and intermediate filaments (IFs), that are embedded within the cytoplasm of cells. It facilitates in a number of key functions including; providing cells with mechanical strength and integrity, facilitating movement of cells, intracellular transport including of vesicles and organelles (Huber et al. 2015). The three cytoskeletal subsystems that have unique structural and physical properties which enable specific cellular functions but also interact directly for functions such as cell migration (Gotlieb et al. 1981; Gardel et al. 2010; Akhshi et al. 2014). The cytoskeletal organisation is dynamic and adaptive that is largely dependent on the requirement of the cell. Essentially it is the architecture of the cytoskeleton that controls the physical properties of the cell. This dynamic and adaptive characteristic of the cytoskeleton is reflective of the diverse functions.

1.9.1 Actin cytoskeleton

Actin is the most abundant intracellular protein in an animal cell. Actin filaments concentrate around the periphery of the cell cortex underlying the plasma membrane and in bundles known as stress fibres that are anchored to the plasma membrane at adhesions sites (Dominguez & Holmes 2011). Actin assembly can generate a variety of structures that mediate the diverse array of cellular functions. The three basic structures that are formed include; branched filament networks, parallel or mixed-polarity filament bundle arrays (Bartles 2000; Taylor et al. 2000; Vinzenz et al. 2012). Actin exists as a globular monomer known as G-actin and as a filamentous polymer, referred to as F-actin , which is a linear chain of G-actin subunits (Spudich et al. 1972). Actin polymerisation is regulated by a number of factors controlling actin assembly and the inhibition of spontaneous polymerisation. Thymosin and profilin are two actin binding proteins that play a key role in this process. Thymosin blocks filament assembly by sequestering actin monomers while, profilin inhibits spontaneous nucleation by binding to actin monomers

(Pantaloni & Carlier 1993). Actin polymerisation is driven by ATP, polymerisation of actin filaments generates force for cellular movement (Korn et al. 1987; Footer et al. 2007). The actin network plays a major role in cell motility, which is highly dependent on the formation of key actin structures lamellipodium and filopodium. The lamellipodium is characterised by the formation of a dense branches array of filaments at the leading edge of a motile cell, as these structures continue to grow and extend they form parallel filament bundles that appear finger like protrusions known as filopodia (Mallavarapu & Mitchison 1999; Vinzenz et al. 2012).

Actin is found throughout the neuronal cytoskeleton. Neurons contain a rich cortical layer of actin under the plasma membrane. This actin layer extends into the distal region of the growing axon, which assists in the formation of the growth cone. Actin is concentrated at pre-synaptic terminals, dendritic spines and growth cones (Papandréou & Leterrier 2018). The G-actin monomer can bind to additional monomers, that enable head-to-tail interactions, they polymerise to form F-actin filaments. As the actin monomers are arranged in the same direction the actin filaments are polarised filaments, as they have distinguishable plus and minus ends (Korn et al. 1987). Actin filaments are arranged in ordered structures that differ depending on the neuronal compartment. At the somatodendritic compartment the actin filaments form actin patches that are localised at the dendritic spine (Cohen et al. 1985). At the axon and dendrites, they form actin rings and actin trails that are short actin filaments (Xu et al. 2013). The short actin filaments are thought to be transported along the axon to the pre-synaptic terminal (Ganguly et al. 2015). At the growth cone, both lamellipodia and filopodia actin structures are observed (Spillane et al. 2011). The disruption of the actin cytoskeleton results in decreased dendritic spine density that results in synaptic loss (Zhang & Benson 2001). The actin cytoskeleton is regulated by many pathways, particularly by the Rho GTPase signalling pathway (Nobes & Hall 1995). Dysregulation of this pathway has been observed in a number of neurodegenerative diseases. In a mouse model of Parkinson's inhibition of Rho GTPase signalling results in increased neurite extension (Zhou et al. 2011).

1.9.2 Intermediate Filaments

Intermediate filaments (IFs) is another filamentous system of the cytoskeleton. It forms a complex network concentrated in the perinuclear region. IFs are not found in all eukaryotes, while plant and fungi do not have them, they are unique to the metazoan kingdom (Chang et al. 2009). IFs extend through the cells cytoplasm as well as lining the inner nuclear envelope in interphase cells providing the mechanical support for the internal cytoplasm and cell surface. They are also involved in shaping the cells and regulating signal transduction (Margiotta & Bucci 2016). Unlike actin and microtubule filaments, IF are very stable. The name intermediate filaments were derived from their structural size of 10 nm diameter, smaller than microtubules (24 nm) but larger then actin (7nm) (Franke et al. 1978). They are different to microtubules and actin in structure and biochemistry; as actin and microtubules filaments are polarised and their assembly is based on enzymatic activity, whereas IFs are formed by the association of monomers, they form extended dimers that overlap to form unpolarised filaments (Steinert & Parry 1985). The defining feature of IF proteins is the presence of the conserved α-helical rod domain of about 310 residues. It has a sequence feature of a coiled-coiled motif, that are flanked by two non-α-helical domains. The variability arises from the amino-terminal head and the carboxy-terminal domain. IFs are α- helical rods that assemble into rope like structures. The internal structure of IFs is not well known as compared to the other two cytoskeletal networks, however, the primary building block of IFs is the presence of a dimer that is held together by the rod domain. The two α-helical rods associate in parallel forming a dimer, that in turns associates with another dimer with an antiparallel orientation giving rise to a tetramer. These tetramers quickly assemble laterally to generate protofilaments, in turn four protofilaments associate into a protofibril, and four protofibrils associate laterally generating a 10nm filament (Premchandar et al. 2016). IFs filaments extend by joining ends of shorter filaments. The dimers associated with the subunits of IFs constitute a superfamily of highly α-helical proteins. They are tissue specific filamentous structures, often expressed in a tissue specific manner. IFs are encoded by 70 different genes that can be divided into 6 subsets (Szeverenyi et al. 2008). In addition, multiple splice variants are derived from the same gene and so increasing the diversity of IF proteins (Titeux et al. 2001). Vimentin is an intermediate filament which

belongs to the class 'type III', it is the most widely distribute protein from all intermediate filaments. Vimentin filaments support cellular membranes and is also thought to help keep the nucleus and other organelles in a place. It is also known to be a marker for aggresomes as its distribution changes from an extended cytoplasmic distribution to caging around the aggregated protein (Lowery et al. 2015).

IFs are the largest family of cytoskeleton proteins. In neurons, 5 classes of IFs are expressed, that are mainly located at the axon (Shaw & Weber 1982; Troy et al. 1990; Fliegner et al. 1994). IFs regulate axonal diameter, neuronal differentiation and axon outgrowth (Zhu et al. 1997). Accumulation of aggregated IFs is a pathological hallmark of many neurodegenerative diseases (Perrot et al. 2008). A study by Lavedan et al (2002) found a mutation at an IF gene from a Parkinson's patient (Lavedan et al. 2002). Implicating IF dysfunction in Parkinson's.

1.9.3 Microtubule Network

The microtubule network is the largest of the three cytoskeleton networks. It contributes to cell morphology, the positioning of organelles, providing tracks for transport and establishing cell polarity (Kapitein & Hoogenraad 2011). Each function relies on a specific arrangement of the microtubules, microtubules are therefore required to assemble and disassemble as the cell requires. Microtubules are made up of protofilaments through the polymerisation of heterodimers of the GTP-bound α and β tubulin subunits (Roychowdhury et al. 1999). They associate laterally forming a hollow microtubule tube with a diameter of 25nm. This arrangement defines a polarity whereby α-tubulin is exposed at the minus end and β-tubulin at the plus end, organising themselves in a head to tail manner (Bergen & Borisy 1980). Microtubules are known to be dynamically unstable, as they can switch from stably growing or rapidly shrinking depending on the demands of the cell (Mitchison & Kirschner 1984a). The plus end is the preferred site of microtubule assembly and disassembly, while the minus end is considered more stable in cells. The minus end of microtubules are usually attached and stabilised at the γ-tubulin ring complex of the centrosome. The γ-tubulin complex caps the microtubule minus end,

regulating microtubule growth only at the plus end (Keating & Borisy 2000; Wiese & Zheng 2000). In most vertebrate cells, microtubules are nucleated by the primary microtubule organising centre, the centrosome however, this is dependent on the cell type where nucleation is also associated with other sites. The dynamic rearrangement of the microtubule is reflective of the function bought about by this network. This includes, assembling an array of microtubule network during the interphase of the cell cycle where the cell is preparing for cell division, these radial arrays function as routes for intracellular movement driven by motor proteins (Schulze & Kirschner 1986). Relatedly this network changes in mitosis where the microtubules rearrange to form mitotic spindles. The dynamic assembly of microtubules enables them to mediate their function. Microtubule assembly requires nucleating factors to initiate polymerisation, thought to be typically restricted to microtubule organising centre (MTOC) (Mitchison & Kirschner 1984b).

Neurons are highly polarised cells made up of two key functional compartments, the axon and the somatodendritic compartment. The axon is instrumental in carrying forward the electrical signal to neighbouring cells whereas the somatodendritic is made up of the cell body and dendrites which receive the signals. Most protein synthesis and organelle biogenesis takes place within the soma, which reflects the need for a sophisticated mechanism that can actively transport the specific requirement of the cell. This polarity is highly dependent on the microtubule cytoskeleton (Kapitein & Hoogenraad 2015). The microtubules are orientated differently at the axon and dendritic department that contributes to neuronal polarity. In axons, the microtubules have a uniformed orientation, with microtubule plus ends orientated towards the synapses. While in the dendrites, the microtubule orientation is mixed, with their plus ends orientated towards or away from the cell soma. The difference in orientation regulates the selective transport routes of cargo either to the axons or dendrites (Baas et al. 1988).

The dynamic organisation of microtubules is governed by a number of regulatory factors, such as tubulin isoforms, posttranslational modifications (PTMs) and microtubule associated proteins (MAPs). MAPs are a diverse family of cytoskeletal proteins. Classical MAPs bind directly to the microtubule filaments, which go onto regulate microtubule stabilisation, polymerisation and microtubule bundling (Takemura et al. 1992). MAPs

were first identified when microtubules purified from the brain were found to consist of tubulin and MAPs. In neurons, the most prominent MAPs include MAP1a, MAP1b, MAP2 and tau. The distribution of MAPs in neurons are spatially heterogeneous (Tucker 1990). As the distribution of MAPs differ in axons and dendrites. Along with differences in microtubule orientations, the distribution of MAPs also regulates selective transport. For example, MAP2 is largely associated with dendritic microtubules, while tau is predominantly associated with axonal microtubules (Bernhardt & Matus 1984; Binder et al. 1985). The tau protein has been extensively studied in relation to Alzheimer's disease. In Alzheimer's disease, hyperphosphorylation of tau results in the formation Neurofibrillary tangles (NFTs), which are a pathological hallmark of Alzheimer's disease (Grundke-Iqbal et al. 1986). When tau was overexpressed in neurons, it destabilised axonal microtubules resulting in microtubules reorienting. This reorientation of microtubules induced transport defects, more specifically due to selective loss of transport (Shemesh et al. 2008).

Axonal and dendritic microtubules also differ in their stability, as axonal microtubules have been demonstrated to be more stable than dendritic microtubules. This stability is contributed by PTMs. PTMs are known to assist in specific cellular functions. For example, neurons contain a sub-population of stable microtubules more so than other cell types. This increase in microtubule stability is thought to assist in specific neuronal functions, such as long distant axonal transport, essential for neuronal function and survival. Well known PTMs include, detyrosination/ tyrosination, polyglutamylation, phosphorylation and acetylation (L'Hernault & Rosenbaum 1985; Cambray-Deakin & Burgoyne 1987; Eddé et al. 1990). These modifications increase the complexity of microtubules that are spatially and temporally organised, as well as increasing the number of proteins binding to microtubules. A study by Peris et. (2006) showed that the p150 Glued subunit of the dynein/dynactin complex, which is known to cargo retrograde transport, binds more efficiently to tyrosinated microtubules than detyrosinated microtubules (Peris et al. 2006). When the p150 glued subunit of the dynein/dynactin complex was depleted by RNAi in non-polarised cells, microtubule dynamics were not affected however, when this subunit was depleted in neurons, this lead to a dramatic increase in microtubule catastrophe (Lazarus et al. 2013). This reinforces that the

regulation and arrangement of the neuronal microtubule cytoskeleton through different regulatory pathways is necessary for neuronal function.

Microtubule stability has been implicated in many neurodegenerative diseases including Parkinson's. Lewy bodies have been found to contain cytoskeletal proteins, such as tubulin and IFs (Goldman et al. 1983; Galloway et al. 1992; Olanow et al. 2004). Additionally Parkinson's associated proteins, such as α-synuclein , LRRK2 and Parkin have been shown to modify microtubule stability (Alim et al. 2004; Yang et al. 2005; Law et al. 2014). α-synuclein was shown to polymerise tubulin into microtubule filaments, however the mutated forms of α-synuclein (A30P and A53T) were not able to do so (Alim et al. 2004). Similarly, Parkin and LRRK2 have been shown to bind to microtubules and increase microtubule stability. Comparable to the effects of α-synuclein familial mutants, mutated forms of Parkin and LRRK2 also diminish the potential of increased microtubule stability (Ren et al. 2003; Cartelli et al. 2012; Ren et al. 2015). When mutant LRRK2 mutations were overexpressed in rat cortical neurons, mitochondrial transport was inhibited. The mutated form of LRRK2 favourably associates with deacetylated microtubules. Increasing microtubule acetylation by using deacetylase inhibitors restored axonal transport (Godena et al. 2014). Though α-synuclein has shown to polymerise tubulin into microtubule filaments this remains controversial, as other studies have shown α-synuclein (wild-type) to destabilise microtubules *in vitro*, while similar effects of α-synuclein mutants were observed (Chen et al. 2007; Cartelli et al. 2016). Environmental factors including toxin exposure, is thought to induce Parkinson's. Two well studied toxins are rotenone and MPTP, both these toxins have shown to reduce microtubule assembly *in vitro* (Marshall & Himes 1978; Cappelletti et al. 2001). Reinforcing microtubule stability in the pathogenesis of Parkinson's.

I have described above the functional role of the microtubules in the neuronal cytoskeleton. Microtubules contribute to the polarised neuronal cytoskeleton structure, forming functional neuronal compartments, as well as regulating selective transport. In neurons, a number of regulatory pathways aid microtubule stability and function. That ultimately facilitates axonal integrity and transport. I have also described microtubule stability in relation to Parkinson's. As proteins associated with the pathogenesis of

Parkinson's, are shown to affect microtubule stability. Microtubules are also known to regulate autophagy, and autophagic dysfunction is known to contribute to the development of Parkinson's (Hara et al. 2006). Microtubules have been shown to regulate autophagosome formation. The first connection, between microtubules and autophagy was when the protein, microtubule-associated protein1 light chain 2 (LC3) known to be specifically involved in autophagy and belongs to the protein family of MAPs. LC3 forms a complex by binding to MAP1a/b which binds to microtubules, and regulates microtubule shape (Mann & Hammarback 1994). Under basal autophagy, treating cells with Taxol or nocodazole, cells were still able to form autophagosomes (Aplin et al. 1992). However, in nutrient deprived conditions treating cells with high doses of either Taxol or nocodazole, inhibited autophagosome formation (Köchl et al. 2006). Interestingly , at lower doses of either treatment showed a delay in autophagosome formation (Köchl et al. 2006).This suggests the dynamic instability of microtubules is important in forming autophagosomes.

1.10 Centrosomes

Centrosomes are highly conserved organelles within the metazoan kingdom. First described by cell biologists Theodor Boveri and wan in the 1900's. The name centrosome was derived from the observation of its localisation at the centre of the cell. The centrosome is a non-membranous organelle made up of two centrioles, that have a perpendicular orientation to one another (Illustrated in Figure 1.4) (Marshall 2001). The centrioles are surrounded by an electron dense matrix known as the pericentriolar material (PMC) (Robbins et al. 1968). Electron microscopy studies have revealed the centrioles are structurally composed of nine triplets of microtubules (Lyser 1968). The older of the two centrioles is known as the mother centriole, which is distinguished from the daughter centriole by the presence of distal and sub-distal appendages (Piel et al. 2000). The centrioles are about 0.5 μm long and 0.2 μm in diameter (Bettencourt-Dias et al. 2011). The centrosome is involved in many functions including, cell division, cell polarity, ciliogenesis and is known as the main microtubule organising centre (MTOC) of the cell (Yanishevsky & Stein 1981; Hong et al. 2010). The location of the centrosome within the cell is synchronised with the cell cycle. At the interphase stage of the cell cycle the centrosome is located next to the nucleus, while during cell division the centrosome

migrates to opposite ends of the cell where they organise the mitotic spindle poles (Robbins et al. 1968). In differentiated cells the centrioles of the centrosome form the basal body, acting as a template for the microtubule based axoneme (Tilney 1971; Nigg & Raff 2009).The diverse function of the centrosome is reflected by the amplitude of centrosomal genes. So far 383 human centrosomal genes have been identified, where 100 of these proteins are involved in the functioning of the centrosome. Additionally, over 466 proteins have been shown to localise to the centrosome, highlighting the complexity in the different functions that are undertaken by the centrosome (Alves-Cruzeiro et al. 2014).

In animal cells, the centrosome is the main microtubule organising centre (Joshi et al. 1992). The centrosome nucleates microtubules that form the routes for transport of cargo within the cell (Utton et al. 2005; Ahmad et al. 1998). As well as regulating cell polarity together with other cytoskeletal networks such as actin (Akhshi et al. 2014). The centrosomes role in microtubule organisation involves, nucleation, anchoring and release (Delgehyr et al. 2005). Nucleation of microtubules is initiated by the γ-tubulin ring complex (γ-TuRC) . The γ-TuRC complex provides spatial and temporal control of the initiation of microtubule polymerisation (Keating & Borisy 2000). This complex consists of γ-tubulin and γ-tubulin complex proteins (GCPs). The GCP family of proteins consist of five GCPs 2-6, that are characterised by an N-terminal Grip1 and a C-terminal Grip2 motif (Murphy et al. 1998; Gunawardane et al. 2000; Murphy et al. 2001). γ-TuRCs contain several other proteins namely, MOZART1, MOZART2a/b, NEDD1, CDK5RAP2 and NME7 (Haren et al. 2006; Fong et al. 2008; Liu et al. 2014). These proteins are not essential for the assembly of γ-TuRCs , they are thought to activate their nucleation activity (Sulimenko et al. 2017). CDK5RAP2 is a well characterised activator for γ-TuRC. It contains an activating γ- tubulin complex binding domain, depletion of CDK5RAP2 by RNAi, impaired microtubule nucleation, while γ-TuRC assembly was unaffected (Choi et al. 2010). Electron micrograph studies revealed the γ-TuRC complex forms a ring-like structure (Zheng et al. 1995) . The ring-like structure, acts as template which mimics microtubule geometry to which the α-tubulin subunit binds to, which is exposed at the microtubule minus end. This enables the formation of polarised microtubule filaments, as

microtubule minus ends are anchored at the γ-TuRC complex. The minus ends of microtubules are capped by the γ-TuRC complex, inhibiting microtubule growth at the minus, which also contributes to microtubule stability (Wiese & Zheng 2000). The plus ends of microtubules extend into the cytoplasm.

Once microtubule nucleation has been initiated the microtubules are then anchored to the centrosome (Quintyne et al. 1999; Bornens 2002; Ibi et al. 2011). Ninein recaptures minus-ends of microtubules after their release (Baird et al. 2004). Ninein, is a component of the subdistal appendages is shown to localise to centrioles , where it interacts with γ-tubulin containing complexes. Overexpression of ninein displaces endogenous ninein and the γ-TuRC complex from the centrosome resulting in microtubule nucleation and anchoring defects (Delgehyr et al. 2005). In neurons ninein localises to the centrosome and non-centrosomal locales, non-centrosomal ninein is dispersed in the cytoplasm of neuronal and non-neuronal cells, but is particularly rich in the neuronal cytoplasm (Baird et al. 2004). Centrosomes are shown to have a key role in neurogenesis more specifically in axonal outgrowth which is important for the correct formation of neuronal circuits (de Anda et al. 2010). It has been shown that the polarised centrosome and Golgi predict the site of axon formation in cultured neurons (Andersen & Halloran 2012) . Neuronal polarisation occurs shortly after mitosis, this polarisation results in the establishment of dendrites and axons. In neurons, fewer microtubules are attached at the centrosome. Neurons express the microtubule severing protein katanin more than other cell types. It is thought higher levels of katanin in neurons is to obtain shorter microtubules that can be easily transported (Ahmad et al. 1999).

Mutations at the LRRK2 gene has been recently shown to affect centrosomal function (Madero-Pérez et al. 2018). This study showed in cells stably expressing the pathogenic LRRK2 mutation resulted in polarity defects with respect to the centrosome. Defects in centrosome positioning affected neurite extension, cell polarisation and cell migration (Madero-Pérez et al. 2018).

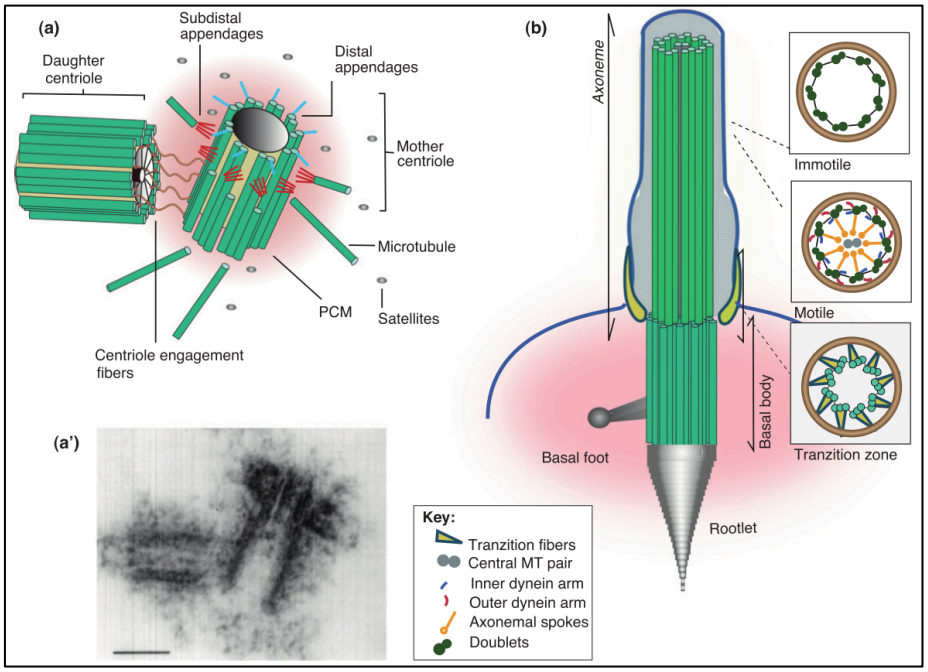

Figure 1.4 Centrosome and cilium structure.
A) The centrosome is composed of two cylindrical-based centrioles, each centriole is composed of 9 microtubule triplets. The centrioles are surrounded by a protein matrix called the pericentriolar material (PCM). The two centrioles are distinguished from on another by the presence of distal and subdistal appendages present on one of the two centrioles, known as the mother centriole. The second centriole is called the daughter centriole. The distal and subdistal appendages on the mother centriole facilitates centriole docking at the membrane, where the centriole forms the basal body, from which the microtubule-based axoneme extends. Satellite proteins are granular structures that surround the centrosome, they are involved in trafficking of proteins required for centrosome assembly and function. A') Electron micrograph of a centrosome, where the two centrioles are observed. B) During ciliogenesis the centrioles migrate to the apical surface of the membrane, where they dock via the subdistal /distal appendages to the membrane, forming the basal body. The centriole templates the microtubule axoneme. The cilia are assembled via Intraflagellar transport (IFT). Cilia structure determines whether it is primary or motile cilia. Primary cilia and motile cilia are made up of 9 microtubule doublets as the structural skeleton, motile cilia also have dynein arms and a central pair of microtubule doublets that enables cilia movement. Image taken from Bettencourt-Dias et al. (2011)

1.11 Cilia

Cilia are highly conserved organelles that project microtubule based protrusions from the surface of almost all cells. Cilia formation is a dynamic process coordinated with the cell cycle, whereby ciliogenesis is initiated when the cell exits the cell cycle (Plotnikova et al. 2009). Cilia have been classified into two main categories including motile and immotile cilia. Immotile cilia are also known as primary cilia (Mitchison & Valente 2017). Motile cilia are widely distributed throughout the body commonly found in large groups on the apical surface of epithelial cells such as those that line the trachea (Shah et al. 2009). Primary cilia are considered to be a sensory organelle that are able to detect fluid flow and pressure but also play a role in transducing intracellular signals. Primary cilia have distinct functions on different cells types and these functions are defined by the signalling

proteins that localise to the ciliary membrane commonly found on cells of the olfactory epithelium and on rods and cones in the retina (Goetz & Anderson 2010; Falk et al. 2015).

Cilia are made up of two key domains including the microtubule axoneme and the basal body derived from the two centrioles of the centrosome. Structurally composed of microtubule axoneme surrounded by the plasma membrane (Satir & Christensen 2008). The microtubule axoneme is made up of nine microtubule pairs, this typical arrangement of microtubules is associated with primary cilia whereas, motile cilia have an extra central pair of microtubules (Satir et al. 2010; Brooks & Wallingford 2014). The extra pair of microtubules facilitates cilia movement generally this movement results in fluid flow movement or cellular locomotion. As well as having a central pair of microtubules they have dynein arms that use energy from ATP hydrolysis to generate rhythmic movement of the axonemes (Goodenough & Heuser 1985). The microtubules serve as a scaffold to bind and organise the multitude of proteins needed to carry out the motility and sensory functions of cilia. Although their functions differ due to their structural arrangement, there are exceptions. For example, primary nodal cilia is able to exhibit rotational movement (Mitchison & Valente 2017).

Cilia assembly and disassembly is highly coordinated event, its assembly is dependent on centrioles which form the basal body of the cilium which convey on them their characteristic nine-fold symmetry. Ciliogenesis initiates with the translocation of the centrosome to apical surface of the membrane where they are anchored via appendages also known as transition fibres (Tanos et al. 2013). Assembly of the outer microtubule doublets of the axoneme that forms the core of the cilium occurs by the direct extension of the centriolar microtubules, whereas the central pair of microtubules form independently to the basal body. Ciliogenesis occurs when cells exit mitosis and proceed into a quiescent/stationary state (G0) or when cells ultimately differentiate within specialized tissues. Ciliogenesis is a dynamic and highly regulated process that can follow two major pathways the intracellular and extracellular pathways which dependent on the cell type. In fibroblast cells primary ciliogenesis is initiated intracellularly while in renal polarised epithelial cells it's at the cell surface (extracellularly) (Sorokin 1968; Molla-

Herman et al. 2010). Cilia do not contain machinery for protein synthesis, so ciliary proteins are synthesised elsewhere and imported selectively into the cilium. Cilia form at the distal end of the mother centriole through the recruitment of preciliary membranes, intraflagellar transport (IFT) machinery and transition zone (TZ) components to enable microtubule based axonemal assembly (Breslow et al. 2013; Lechtreck 2015). The highly ordered process of ciliogenesis can be divided into key stages including all the events that occur before and after from when the basal body docks at the membrane.

The highly ordered process of ciliogenesis can be divided into key stages including all the events that occur before and after the basal body docks at the membrane, including; removal of negative regulators and recruitment of positive regulators, vesicle recruitment, basal body migration, basal body docking and axoneme elongation. A key early event in ciliogenesis is the removal of centrosomal protein CPP10 which is a negative regulator of ciliogenesis where it localises to the mother and daughter centriole. During ciliogenesis CP110 that localises at the distal end of the mother centriole is displaced by the positive regulator Tau tubulin Kinase-2 (TTBK2) which is recruited upon serum starvation (Spektor et al. 2007; Goetz et al. 2012). Similarly the microtubule affinity regulating kinase 4 (Mark4) is required for CP110 removal where it accumulates at the basal body as CP110 is removed (Kuhns et al. 2013).

In parallel recruitment of ciliary proteins begin to build the cilium via, vesicular transport from the Golgi to the centrosome. Vesicles containing ciliary proteins bud from the trans-Golgi network (TGN) that are directed to specific docking sites at the preciliary base where they tether to the ciliary membrane (Kim et al. 2014). Along this pathway small cytoplasmic vesicles known as distal appendage vesicles (DAVs) or preciliary vesicles (PCVs) start to accumulate at the distal appendages of the mother centriole (Wu et al. 2018). The accumulated vesicles fuse with incoming vesicles building the ciliary vesicle (CV), this event is regulated by membrane shaping proteins Esp15 homology domain (EHD) more specifically EHD1 and EHD3 (Lu et al. 2015). The membrane modulating proteins convert the PCVs into a single CV. Formation of the CV is associated with the removal of CP110, allowing extension of the microtubule axoneme (Spektor et al. 2007). The association of PCVs with the mother centriole is required for basal body formation

and ciliogenesis progression. The basal body is now able to extend its microtubules to invaginate the CV forming a sheath around the extending axoneme that later fuses with the plasma membrane externalising the cilium (Tanos et al. 2013).

The membrane trafficking regulator Rab small GTPases particularly the Rab11-Rabin8-Rab8 signalling cascade are required for ciliary membrane formation during ciliogenesis (Knödler et al. 2010; Westlake et al. 2011). In brief the regulatory principle of Rab proteins, is through their ability to function as molecular switch that alternate between GTP and GDP bound conformations where GTP bound form is considered the active form additionally they are known to be involved in controlling polarised membrane trafficking and regulate transport between organelles. In this cascade Rabin8 the guanine nucleotide exchange factor for Rab8, binds to Rab11 that is delivered to the centrosome on vesicles to activate Rab8 to promote ciliary membrane assembly (Yoshimura et al. 2007). The assembly of CV is a prerequisite step for TZ proteins and IFT20 recruitment (Lu et al. 2015). The CV faces and subsequently fuses with the plasma membrane where the distal appendages mature into transition fibers docking the basal body on the plasma membrane (Reiter et al. 2012).

Subsequently after the formation of the basal body, the transition zone (TZ) is formed an intermediate region between the basal body and ciliary axoneme. This zone is where the nine microtubules triplets of the basal body differentiate into microtubule doublets. The microtubule doublets are connected by Y –link fibres to the overlying ciliary membrane a structural feature of the TZ. Mutations affecting the TZ have shown to result in ciliopathies such as Joubert syndrome (Sang et al. 2011). The TZ is said to act like molecular sieve as it said to serve as a gate for all proteins entering and leaving the ciliary domain, this comparable to the nuclear pore (Lechtreck 2015). The distal appendages mature into the transition fibers where they dock onto the membrane , the distal appendages are assembly points for the recruitment of IFT proteins (Deane et al. 2001).

Following the transition zone, the axoneme is constructed. The ciliary axoneme is elongated via IFT, ciliary extension occurs exclusively at the distal end of the outer doublets (Rosenbaum & Child 1967). Intraflagellar transport (IFT) was first discovered by

Kozminski et al. (1993) in the flagella of green alga *Chlamydomonas* (Kozminski et al. 1993). Characterised by the bidirectional movement of ciliary proteins along the length of the cilia. This bi-directional motility is important in cilia maintenance and function. IFT is a transport system mediated by molecular motors and IFT particles, composed of two complexes IFT-A and IFT-B which direct retrograde and anterograde movement of ciliary proteins respectively. IFT-B transports the building blocks for axonemal growth which is kinesin-II associated (Cole et al. 1998) whereas, components that need to be internalised are returned by the IFT-A complex dependent on dynein-2 (Pazour et al. 1998). Additionally, the maintenance of ciliary morphology and function requires continuous IFT achieved through the bidirectional cargo movement. Ciliary extension is limited at the tip of the growing axoneme where tubulin is transported to the tip of cilia by IFT (Hao et al. 2011). As well as regulating ciliary maintenance by regulating continuous tubulin turnover at the distal end of the axoneme, a subset of neuronal cilia contains G protein-coupled receptors (GPCRs) that are also trafficked via IFT (Schou et al. 2015).

Defects in cilia formation or structure, result in a group of diseases termed 'ciliopathies', including Bardet Biedl syndrome (BBS), polycystic kidney disease (PKD), Joubert Syndrome (JBTS) and Meckel-Gruber Syndrome (MKS) (Boltshauser & Isler 1977; Saeki et al. 1984; Ansley et al. 2003; Dawe et al. 2007). These diseases affect multiple tissues and manifest as a constellation of features that include retinal degeneration, renal disease and cerebral anomalies, reflecting the diverse role of cilia in different tissues(Waters & Beales 2011). Many ciliopathies have prominent neurological phenotypes reflecting the importance of neuronal cilia in the brain function (Boltshauser & Isler 1977). Though the functional role of primary cilia play in overall neuronal function is unclear (Green & Mykytyn 2014). It is thought they have the ability to act as non-synaptic sensory and signalling organelles. Interestingly a study by Basto et al, showed acentriolar flies can develop normally but die at early adulthood due to lack of sensory cilia (Basto et al. 2006). In mice, it was shown the dopamine receptor 1 (D1) localises to the cilia therefore implicating neuronal cilia in dopamine signalling (Domire et al. 2011). Another study by Miyoshi et al, showed lack of dopaminergic inputs elongated the primary cilia (Miyoshi et al. 2014). Cilia dysfunction is a common feature of neurodegenerative diseases including Alzheimer's and Huntington's disease (Keryer et al. 2011; Chakravarthy et al.

2012; Kaliszewski et al. 2015). Loss of smell is a common symptom for neurodegenerative diseases including Parkinson's (R. L. Doty et al. 1988). Olfaction is an involuntary sense. The olfactory epithelium is a multi-ciliated tissue. Cells normally use one centriole to build a single cilium. The centrioles are thought to be multiplied at the cell body of the olfactory sensory neuron. By long distant dendritic transport the centrioles are transported to olfactory epithelium , where they can form cilia. . The olfactory receptors that are housed on olfactory cilia are GPCRs. Interestingly the repertoire of genes contributing to the diversity of the GPCRs is equivalent to 1% (388) of the genome (Niimura & Nei 2003). The olfactory sensory neurons are the only neurons exposed to the external environment. A unique feature of these neurons, is their ability to regenerate through adult life (Graziadei & Graziadei 1979). The regenerative capacity of the olfactory neurons decreases with age (Keller & Malaspina 2013). Disruption of the olfactory cilia is known to cause anosmia or dysosmia, reflecting the importance of olfactory cilia in odour detection (Jenkins et al. 2009).

1.12 Aims and objectives

Parkinson's is a multisystem disorder, disruption in key pathways contribute to the pathogenesis of this disease including, autophagy, ubiquitin proteasome, cytoskeletal proteins and mitochondria. In this project, I looked at the possible connection between aggresomes and the centrosome in relation to Parkinson's. As Lewy bodies are thought to be derived from aggresomes, I looked to test whether aggresomes effect centrosomal function. To do this, I first need to generate aggresomes and then assess the multiple functions of the centrosome in the presence of these aggresomes. A number of centrosomal assays have been established including the microtubule regrowth assay, which would establish whether the centrosome is able to nucleate microtubules. I will test whether cell polarity is affected by scratch- wound assay as the centrosomes orientation, directs the route of migration and finally I'll test if ciliogenesis is affected. These experiments will be initially carried out in *in vitro* and then using zebrafish embryos as an *in vivo* model.

2. Materials and Methods

2.1 Cell culture

2.1.1 Media:

2.1.1.1 Media for HeLa and SH-SY5Y cell lines:

Culturing Media (50 ml)

- 44.5 ml Dulbecco's Modified Eagles Medium (Sigma #D5796)
- 5 ml foetal bovine serum (10 %; Gibco #10500-064)
- 500 μl L-Glutamine (2 mM final concentration; Gibco #A2916801)
- 500 μl Antibiotic-Antimycotic (100X) (5000 units/ml penicillin final concentration; 5000 μg/ml streptomycin final concentration; 12.5 μg/ml Gibco Amphotericin B final concentration; Gibco #15240062)

2.1.1.2 Media for RPE1-hTERT cell line:

Culturing Media (50 ml)

- 44.5 ml Dulbecco's Modified Eagles Medium with nutrient mixture G-12 Ham (Sigma #D6421)
- 5 ml foetal bovine serum (10 %; Gibco #10500-064)
- 500 μl L-Glutamine (2 mM final concentration; Gibco #A2916801)
- 500 μl Antibiotic-Antimycotic (100X) (5000 units/ml penicillin final concentration; 5000 μg/ml streptomycin final concentration; 12.5 μg/ml Gibco Amphotericin B final concentration; Gibco #15240062)

2.1.1.3 Media for Differentiating SH-SY5Y cell line:

Plating media (50ml):

- 44.5 ml Dulbecco's Modified Eagles Medium with nutrient mixture G-12 Ham (Sigma #D6421)
- 5 ml foetal bovine serum (10 %; Gibco #10500-064)
- 500 μl L-Glutamine (2 mM final concentration; Gibco #A2916801)
- 500 μl Antibiotic-Antimycotic (100X) (5000 units/ml penicillin final concentration; 5000 μg/ml streptomycin final concentration; 12.5 μg/ml Gibco Amphotericin B final concentration; Gibco #15240062)

Differentiation Media (50ml):

- 44.5 ml Dulbecco's Modified Eagles Medium with nutrient mixture G-12 Ham (Sigma #D6421)
- 500 μl foetal bovine serum (1 %; Gibco #10500-064)
- 500 μl L-Glutamine (2 mM final concentration; Gibco #A2916801)
- 500 μl Antibiotic-Antimycotic (100X) (5000 units/ml penicillin final concentration; 5000 μg/ml streptomycin final concentration; 12.5 μg/ml Gibco Amphotericin B final concentration; Gibco #15240062)
- 500 μl MEM NON-essential Amino Acid Solution (100X) (1 X final concentration Sigma #M7145)
- 50 μl Trans-Retinoic acid (10 μM final concentration #R2625)

2.1.1.4 Media for Mouse embryonic fibroblasts (MEFs) primary cultures:

Culturing Media (50 ml)

- 44.5 ml Dulbecco's Modified Eagles Medium (Sigma #D5796)
- 5 ml foetal bovine serum (10 %; Gibco #10500-064)
- 500 μl L-Glutamine (2 mM final concentration; Gibco #A2916801)
- 500 μl Antibiotic-Antimycotic (100X) (5000 units/ml penicillin final concentration; 5000 μg/ml streptomycin final concentration; 12.5 μg/ml Gibco Amphotericin B final concentration; Gibco #15240062)
- 500 μl MEM NON-essential Amino Acid Solution (100X) (1 X final concentration Sigma #M7145)

2.1.1.5 Media for Primary Basal Ganglion neurons:

Dissociation media (5ml final volume)

- 4.5 ml Dulbecco's Modified Eagles Medium (Sigma #D5796)
- 50 μl DNase (100 μg/ml final concentration)
- 0.5 ml Trypsin (Thermo Fisher #12604021)

Plating Media (50 ml final volume)

- 50 ml Dulbecco's Modified Eagles Medium (Sigma #D5796)
- 2.5 ml foetal bovine serum (10% Gibco #10500-064)
- 500 μl penicillin-streptomycin (100 units/ml penicillin final concentration; 100 μg/ml streptomycin final concentration Gibco #15140122)
- 500 μl L-Glutamine (2 mM final concentration; Gibco #A2916801)

Neurobasal Media (50 ml final volume)

- 48 ml Neurobasal media (Thermo fisher #21103049)
- 1 ml B27 supplement (Thermo fisher #17504044)
- 500 μl penicillin-streptomycin (100 units/ml penicillin final concentration; 100 μg/ml streptomycin final concentration Gibco #15140122)

- 500 μl Glutamax (2 mM final concentration; Thermo Fisher #35050061)

2.1.1.6 Media for Wound assay (50 ml final volume)

- 44.5 ml CO_2 Independent Media (Thermo Fisher #18045054)
- 5 ml foetal bovine serum (10 %; Gibco #10500-064)
- 500 μl L-Glutamine (2 mM final concentration; Gibco #A2916801)
- 500 μl Antibiotic-Antimycotic (100X) (5000 units/ml penicillin final concentration; 5000 μg/ml streptomycin final concentration; 12.5 μg/ml Gibco Amphotericin B final concentration; Gibco #15240062)

2.2 Cell lines and Storage

Cell lines used include: HeLa, provided by Prof George Dickson at Royal Holloway; neuroblastoma cell line SH-SY5Y, provided by Prof Robin Williams at Royal Holloway; immortalised human retinal pigment epithelial cells (RPE1-hTERT), kindly provided by Prof. Erich Nigg, Basel, Switzerland; mouse embryonic fibroblast cells (MEFs), provided by Dr Jenny Murdoch at Royal Holloway. Primary basal ganglion neurons were prepared by Dr Simona Ursu at Royal Holloway.

A number of cell lines were used including: Mouse embryonic fibroblasts (MEFs), HeLa, RPE1-hTERT and undifferentiated/ differentiated SH-SY5Y cells. All cell lines were cultured in the same way. The work was performed using sterile plastic ware inside a class 11 laminar flow hood. Culturing flasks, stripettes, 15 /50 ml falcon tubes, petri dishes, 6-well plates and 12-well plates came in sterile packaging, they were briefly sprayed with distel and placed in the hood. Pipette tips and 1.5/2 ml eppendorfs were autoclaved and similarly sprayed with distel before placed in the hood. The growth media used was dependent on the cell line (described 2.1.1 Media), working stocks were aliquoted into 50 ml falcons to limit contamination and stored at 4°C. Prior to use growth media and 1x PBS would be pre-warmed by incubating at 37°C for 20 minutes

2.2.1 Waking and plating cells

Frozen cell aliquots were either stored in liquid nitrogen or -80°C, were rapidly thawed in a water bath set at 37°C. Thawed cells were transferred to a 15 ml falcon tube, the cells were supplemented with 5 ml growth media and centrifuged at 2000 rpm for 3

minutes to pellet the cells. The supernatant was removed, and the cell pellet was gently resuspended in 10 ml of fresh growth media and transferred to a T75 cell culture flask. Cells were incubated at 37°C with 5% CO_2 in a humidified incubator. Cell confluency was checked using a light microscope, once the cells were at 90 % confluency, they were ready for passaging.

2.2.2 Splitting and sub-culturing cells

Spent media was aspirated, and cells were washed twice with 1 x phosphate buffer saline (PBS; Thermo Fisher #20012019). An aliquot of TrypLE (Thermo Fisher #12604021) was pre-warmed at 37°C for 3 minutes, 1 ml of TrypLE was added to the T75 culture flask, the flask was placed in the incubator at 37 °C for 3 minutes. By gentling tapping the edge of the flask the cells were assisted in detaching. Trypsin was inactivated by adding 5 ml of growth media. Cells were then washed from the surface of the flask and transferred to a 15ml falcon and pelleted by centrifuging at 2000 rpm for 3 minutes. The supernatant was removed, and the cell pellet was resuspended in 10 ml of growth media. 1 ml of the suspended cells were placed in a fresh T75 flask, with an additional 9 ml of growth media, this was considered as 1:10 split. Cells were allowed to grow in the incubator at 37 °C and 5% CO_2.

2.2.3 Freezing down cells

For long term storage cells were grown to 90% confluency, spent media was removed, and cells were washed twice with 1 x PBS. An aliquot of TrypLE was pre-warmed at 37°C for 3 minutes, 1 ml of TrypLE was added to the T75 culture flask, the flask was placed in the incubator at 37 °C for 3 minutes. By gentling tapping the edge of the flask the cells were assisted in detaching. Trypsin was inactivated by adding 5ml of growth media. Cells were then washed from the surface of the flask and transferred to a 15 ml falcon and pelleted by centrifuging at 2000 rpm for 3 minutes. The supernatant was removed, and the cell pellet was re-suspended at 1 x 10^5 cell per ml in freezing media (Thermo Fisher #12648010). Suspended cells were quickly aliquoted into cryovials (Thermo Fisher #377267), 1 ml was placed per vial. Vials were placed in a freezing container (Thermo

Fisher #5100-0001) and cooled slowly to -80°C. Cells were stored in liquid nitrogen for long-term storage.

2.2.4 SH-SY5Y Differentiation

SH-SY5Y's is a neuroblastoma cell line that is widely used in the study of Parkinson's. This cell line can be differentiated to represent a more realistic phenotype of neurons.

2.2.4.1 SHYSY-5Y Differentiation

Preparing SH-SY5Y cells for differentiation involved, removing spent media from a confluent culture of cells grown in a T75 flask, cells were washed twice with 1 x PBS. Cells were harvested by treating cells with 1 ml TrypLE, the trypsin was inactivated by adding 5 ml of growth media. Cells were pelleted at 2000 rpm for 3 minutes, the supernatant was removed and re-suspended in 10 ml of growth media. SH-SY5Y cells need to be seeded out on collagen-coated coverslips (as described above). Cells were seeded at 60,000 cells per well in growth media. Allowing 24 hours for cells to attach to the collagen matrix, the media was changed to differentiation media at a final volume of 2 ml per well. Thereafter 500 μl of media was removed and replaced with fresh 500 μl of differentiation media. Differentiation was achieved in seven days.

2.2.5 Preparing and culturing enriched cultures of dopaminergic neurons

2.2.5.1 Preparing PDL plates

Sterilised glass cover slips were placed into 6-well plates, then were coated with poly-D-lysine (PDL; 100 μg/ml in 1x PBS) and incubated at 37°C for 5 hours or at 4°C overnight. The PDL was aspirated, and wells were washed three times with sterile water. Plates were left to air dry and UV for 20 minutes.

2.2.5.2 Dissection

Enriched cultures of dopaminergic neurons were prepared by Dr Ursu in accordance with Home Office regulations and the Animals Scientific Act 1986. A pregnant Sprague-Dawley rat at E18 was euthanised, the embryos were removed and placed on ice. The head was severed, and the top of the skull was carefully peeled off. The brain was removed and

placed in ice cold 1 x PBS. Using a dissection light microscope, the meninges were removed. The basal ganglion was removed, carefully removing any non-basal ganglion tissue. The dissected basal ganglion tissue was cut into smaller pieces. The tissue was then transferred to a 15 ml tube, 5 ml of dissociation media was added. The tissue was dissected by pipetting and then incubated at 37°C for 10 minutes. The trypsin was inactivated by adding 1.5 ml of FBS, it was then incubated at 37°C for 5 minutes. The cells were pelleted by centrifuging at 1,500 rpm for 3 minutes. The supernatant was aspirated, and the cell pellet was resuspended in 1 ml of plating media. The cells were seeded at 400,000 cells per well of a 6-well plate. The cells were incubated in plating media for 24 hours at 37 °C and 5% CO_2. Following 24 hours, the plating media was aspirated and replaced with 2.5 ml of primary neuronal growth media per well. Plates were then incubated at 37 °C and 5% CO_2 for 18 days. During the 18 days in culture 0.5 ml of primary neuronal growth media was added to each well every seven days.

2.3 Transfections

2.3.1 Plating cells for transfection

Preparing cells for transfection included, removing spent media from a confluent culture of cells grown in a T75 flask, cells were washed twice with 1 x PBS. Cells were harvested by treating cells with 1ml TrypLE, the trypsin was inactivated by adding 5 ml of growth media. Cells were pelleted at 2000 rpm for 3 minutes, the supernatant was removed and re-suspended in 10 ml of growth media. Square glass coverslips (22 x22 mm) were sterilised by soaking them in 80% ethanol overnight. Cover slips were allowed to air-dry in the laminar flow hood, and UV exposure for 20 minutes. Glass cover slips were placed into each well of a 6-well plate. Cells were seeded at a high density aiming for 80% confluency the following day. For HeLa and SH-SY5Y cells 350,00 cells were seeded per well, for RPE1-hTERT cells 600,000 cells were seeded per well. The final volume per well was made up to 2 ml. Cells were placed in the incubator at 37 °C and 5% CO_2 for 24 hours. When at 80% confluency cells were ready for transfection.

2.3.2 Transfecting cells with DNA using Lipofectamine™ 2000

Lipofectamine 2000® (Thermo Fisher #11668019) was used to transiently transfect plasmid DNA into cells. Following manufacturer's instructions, 7 μl of Lipofectamine™ was added to 243 μl Opti-MEM in a 1.5 ml eppendorf (Thermo Fisher #11058021), 2.5 μg of plasmid DNA was diluted in Opti-MEM to a final volume of 250 μl, the diluted DNA and Lipofectamine was incubated at room temperature for 5 minutes. Both the diluted DNA and Lipofectamine were combined into a 1.5 ml eppendorf at a final volume of 500 μl. Lipid-DNA complexes were incubated at room temperature for 15 minutes. Once the complexes had formed, they were slowly added to the well, the final volume per well was 2 ml. Cells were then placed in the incubator (37 °C and 5% CO_2) for 5 hours. After 5 hours, the media was replaced with complete growth media an incubated for 24-72 hours depending on the assay.

2.3.3 RNA Interference

Small interfering RNAs (siRNAs) were designed with custom RNA synthesis tools (siDESIGN Center) provided by GE Dharmacon. siRNAs targeting BCAPα/ δ were designed targeting transcripts: NM_020729.2 (BCAPα) and NM_001184766.1 (BCAPδ).

Table 1 siRNA name and sequence

siRNA	Sequence	# Catalogue number
Hs*BCAP* siRNA 1	5′-GCAAGAAGCAGCUGAAAUAUU-3′ (sense)	TMOSLR-005597
	5′-GCAAGAAGCAGCUGAAAUAUU-3′ (antisense)	
Hs*BCAP* siRNA 2	5′-GGAGAAGGCUGUAAAUGAUUU-3′ (sense)	TMSOLR-005599
	5′-AUCAUUUACAGCCUUCUCCUU-3′ (antisense)	
Hs*BCAP* α	5′- UGAAGGAGUUAGAGCGUGUUU-3′ (sense)	CTM-294455
	5′-ACACGCUCUAACUCCUUCAUU-3′ (antisense)	
Hs*BCAP* δ	5′-AGUCUUGAGAAGUCGGAAAUU-3′ (sense)	CTM-294459
	5′-UUUCCGACUUCUCAAGACUUU-3′ (antisense)	
SMARTPool ON-TARGETplus –PCM-1	Sequence not provided	L-005165-00-0005
ON-TARGETplus NON-targeting Control Pool	Sequence not provided	D-001810-10-05

2.3.3.1 Preparing siRNAs

A SMARTPool ON-TARGETplus siRNA targeting PCM-1 (Dharmacon #L-005165-00-0005) was purchased from Dharmacon. The tube was briefly spun to collect contents to the

bottom. The oligonucleotides (PCM-1 5 nmol) were resuspended in 250 μl of RNase-free water to make a stock solution of 20 μM. The tube was placed on an orbital shaker for 30 minutes at room temperature. Working concentrations of 10 μM aliquots were made by diluting the 20 μM stock in RNase free water, both stocks were stored at -80°C. ON-TARGETplus Non-Targeting Control Pool (Dharmacon #D-001810-10-05) were previously prepared at 10 μM working stock. siRNAs targeting BCAPα and BCAPδ were prepared in the same way as siRNA for PCM-1. The oligonucleotides BCAPα and BCAPδ were at 20 nmol, they were resuspended in 200 μl of RNase-free water to make a stock solution of 100 μM, the tubes were placed on an orbital shaker for 30 minutes at room temperature working concentrations of 10 μM aliquots were made by diluting the 100 μM stock in RNase free water, both stocks were stored at -80°C.

2.3.3.2 Transfecting cell with siRNAs using Lipofectamine™ RNAiMAX

The reverse transfection protocol was used to transfect siRNAs into cells. This involves transfecting siRNA complexes to cell suspensions at the time of seeding the cells. Lipofectamine™ RNAiMAX was used to deliver the siRNAs (Thermo Fisher #13778037). Following manufacturer's instructions, 4 μl of Lipofectamine™ RNAiMAX was added to 46 μl of Opti-MEM in a 1.5 ml eppendorf, 1.5 μl of siRNA (15 nM final concentration) was added to 48.5 μl of Opti-MEM in a separate 1.5 ml eppendorf. The diluted siRNA and Lipofectamine™ RNAiMAX was incubated at room temperature for 5 minutes. The diluted siRNA and transfection reagent were then combined at a total volume of 100 μl. Lipid-siRNA complexes were incubated at room temperature for 15 minutes. The complexes were then transferred into wells of a 12-well plate, RPE1-hTERT cells were plated at 500,000 cells per well, growth media without any antibiotics was added to a final volume of 1 ml per well. Cells were then placed in the incubator (37 °C and 5% CO_2) for 24-72 hours.

2.3.3.3 Co-transfecting plasmid DNA and siRNAs

One of the experiments involved co-transfecting plasmid DNA and siRNA, designed as a rescue experiment, to show the knock-down of the siRNA is specific. More specifically, I transfected GFP-tagged mBCAP and siRNAs targeting all BCAP isoforms. When BCAP is

depleted the cells form cilia, when BCAP is overexpressed, BCAP inhibits ciliogenesis. I overexpressed mouse BCAP as the coding sequence is not completely identical with human BCAP at the target site of the siRNA. RPE1-hTERT cells were plated on ethanol-washed glass coverslips at 300,000 cells per well in a 12-well plate in antibiotic free growth media. At 80% confluency, the cells were ready for transfection. Lipofectamine 2000™ was used to deliver both plasmid DNA and siRNA. The complexes were assembled by adding: 46.5 μl Opti-MEM to a 1.5 ml eppendorf + 1.5 μl plasmid DNA (1μg/ μl) and 2 μl of siRNA (10 μM stock) the diluted plasmid DNA and siRNA were mixed gently by pipetting and incubated at room temperature for 5 minutes. In a separate 1.5 ml eppendorf, 3 μl of Lipofectamine 2000™ was added to 47 μl of Opti-MEM, this was mixed by pipetting gently and incubated at room temperature for 5 minutes. After the 5 minute incubation, the diluted plasmid DNA and siRNA were combined with the diluted Lipofectamine 2000™ at a total volume of 100 μl, the sample was mixed gently by pipetting and incubated at room temperature for 15 minutes allowing the complexes to form. The complexes were added to the wells with the total volume of 1 ml (100 μl of complexes + 900 μl antibiotic free growth media) the sample was mixed by gently rocking the plate back and forth. The cells were incubated at 37 °C and 5% CO_2 for 6 hours, the media containing transfection complexes was removed, and washed with 1 x PBS. 1 ml of serum free media was added per well and incubated at 37°C and 5% CO_2 for 24 hours. The cells were then fixed with 1 % formaldehyde (FA) in 0.2 % Triton + 1 x PBS for 10 minutes. The cells were washed twice with 1 x PBS and stored at 4°C, ready for immunostaining.

2.4 Aggresome Formation

Aggresomes were formed by either treating cells with MG-132 (Sigma #M7449) or overexpressing GFP-tagged αsyn wild-type or the two-familial mutations A30P and A53T. The optimal MG-132 concentration was determined for each cell line ranging from 1 μM to 10 μM (HeLa, 10 μM; SH-SY5Y, 1 μM; differentiated SH-SY5Y, 1μM; MEFs, 5 μM; RPE1-hTERT, 1 μM and rat neurons, 3 μM). MG-132 was thawed at room temperature and was added to growth media as the above final concentration. Cells were incubated with MG-

132 for 18 hours at 37°C in a humidified atmosphere with 5% CO_2. Once the aggresomes were formed the cells were processed for different centrosomal assays described below.

Constructs including; peGFP-C2, peGFP-αSYN, peGFP-αSYNA30P and peGFP-αSYNA53T were transiently transfected into cells as described above. After 72 hours post transfection, aggresomes were formed. The cells were processed for the centrosomal assays as described below.

2.5 Centrosomal Assays

Several centrosomal assays have been established that were used to assess centrosomal function. Assays were conducted with or without the presence of aggresomes.

2.5.1 Microtubule regrowth assay

Cells were plated onto ethanol-washed glass coverslips in serum-supplemented media. At 80% confluency, the cells were processed for aggresome formation by either MG-132 treatment or transfecting cells with GFP-tagged αsyn expression constructs. Cells were ready to be processed for the microtubule regrowth assay in 18 hours of MG-132 treatment. Cells transfected with GFP-tagged αsyn expression constructs were ready in 72 hours after transfection. A coverslip was removed and fixed in ice cold methanol (-20°C), the 6-well with 5 remaining coverslips was placed on ice for 30 minutes. The cold treatment depolymerises the network, another coverslip was removed and fixed with ice cold methanol (-20°C). The cells were then incubated with pre-warm (37°C) growth media. Samples were fixed at different time-points ranging from 0.5 minutes to 25 minutes, depending on the cell line. Cells were fixed for 10 minutes with ice cold methanol (-20°C), the fixative was removed and washed with 1 x PBS for 5 minutes on a shaking platform. Cells were stored in fresh 1 x PBS at 4°C ready for immunostaining.

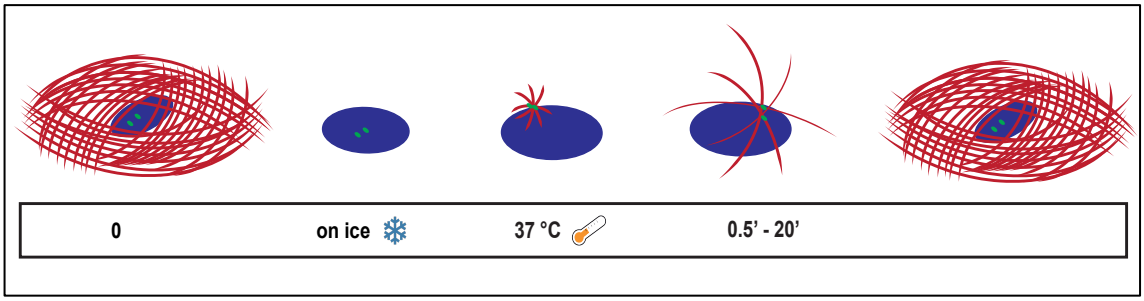

Figure 2.5 Schematic of microtubule regrowth assay.
Cells were plated onto ethanol-washed glass coverslips in a 6-well plate, at 80 % confluency, control cells were treated with DMSO or MG-132 (concentration dependent on the cell line used, ranging from 1 μM to 10 μM) to induce aggresome formation. Aggresomes were also formed by overexpressing GFP-tagged expression constructs encoding α-synuclein wild-type or two familial mutations (A30P or A53T). Control cells or cells where aggresomes were induced were processed for the microtubule regrowth assay. A coverslip was removed and fixed with ice cold -20°C methanol for 10 minutes. The 6-well plate was then transferred onto ice for 30 minutes, the cooling of cells, depolymerises the microtubule network. After 30 minutes, another coverslip was removed and fixed with ice cold -20°C methanol for 10 minutes. The remaining cells are then incubated with pre-warmed media at 37°Cat set time-points. Cells were fixed at different time-points ranging from 0.5 minutes to 30 minutes. Once the cells have been fixed with ice cold -20°C methanol for 10 minutes, the fixative is removed, and cells were washed with 1 x PBS. The cells were ready for immunostaining. Cells were stained with anti-α-tubulin and anti-γ-tubulin antibodies. Before cooling cells have an extensive microtubule network, the cooling of cells depolymerises the microtubule network. Incubating cells with pre-warmed media initiates microtubule nucleation. A characteristic aster is visible at the early stages of microtubule nucleation. The microtubules are seen nucleating from the centrosome. As warming continues, the microtubules continue to polymerise and extend further into the cell's cytoplasm, eventually re-establishing the microtubule network. The staining of the microtubule network prior cooling would be comparable to when the network has re-established itself.

2.5.2 Cell migration assay (Scratch-Wound assay)

MEFs, RPE1-hTERT and HeLa cells were used in the wound assay. The wound assay was carried out by either time-lapse microscopy, recording cell migration or fixing cells at set time-points, both ways were assessed in MEFs and RPE1-hTERT. HeLa cells were assessed by fixing at set time-points only.

2.5.2.1 Time-lapse

MEFs were plated into collagen-coated 35 mm Petri dishes (700,000 cells). Cells were treated with either 5 μM MG-132 for 18 hours to form aggresomes or DMSO as a control. At 100% confluency, a p200 pipetman tip was used make a wound, a vertical line was made going from one end of the Petri dish to the other. The media was aspirated, removing detached cells. The cells were washed twice with 1 x PBS to remove any remaining detached cells. Cells were supplemented with CO_2 independent media. Images

were taken using Nikon TE300 microscope with a 37°C chamber. The time-lapse was set for 24 hours with images taken every 2 minutes. Similarly, RPE-hTERT cells were processed for the wound assay, 750,000 cells were plated into 35 mm Petri dishes, Cells were treated with either 1 μM MG-132 for 18 hours to form aggresomes or DMSO as a control. The rest of the assay was carried out as the same with MEFs.

2.5.2.2 Immunostaining

MEFs, RPE1-hTERT and HeLa were all used for the wound assay, cell migration was assessed by immunostaining. MEFs were plated at 700,000 cells per well on collagen-coated glass coverslips. RPE1-hTERT and HeLa cells were plated onto ethanol-washed glass coverslips at 750,000 and 400,000 cells respectively in a 6-well plate. Cells were treated with MG-132 for 18 hours for aggresome formation or DMSO as a control. At 100% confluency, a p200 pipetman tip was used make a wound, a vertical line was made going from one end of the glass coverslip to the other end. The media was aspirated, removing detached cells. The cells were washed twice with 1 x PBS to remove any remaining detached cells. Cells were then incubated in growth media specific to that cell line. A coverslip was removed and fixed immediately with ice cold methanol (-20°C) as the first time-points. Cells were placed back in the incubator at 37°C and 5% CO_2. Cells were fixed at set time-points over 24 hours with ice cold methanol (-20°C). Cells were fixed for 10 minutes with ice cold methanol (-20°C), the fixative was removed and washed with 1 x PBS for 5 minutes on a shaking platform. Cells were stored in fresh 1 x PBS at 4°C ready for immunostaining.

2.5.2.3 Golgi orientation

A Golgi positioned within -45° and +45° of the wound was considered to be orientated towards the wound. The average angle of orientation was calculated using the formula $(\Sigma\sqrt{\alpha^2})/ n$ where α is the angle between the Golgi and a line perpendicular to the wound edge.

2.5.3 Ciliogenesis

Cells were plated onto glass coverslips sterilised by ethanol-wash in a 6 or 12-well plate in serum supplemented media. At 60% confluency cells, the cells were processed for aggresome formation by treating cells with either MG-132 or transfecting cells with GFP-tagged αsyn expression constructs. Cells were ready to be processed for the ciliogenesis assay in 18 hours of MG-132 treatment. Cells transfected with GFP-tagged αsyn expression constructs were ready 72 hours after transfection. Cells were washed with pre-warmed (37°C) 1 x PBS, cells were then incubated in serum free media for 24 hours to induce ciliogenesis. Before the cells were fixed they were briefly washed in room temperature 1 x PBS, cells were then fixed using 4% (v/v) formaldehyde (FA) for 10 minutes at room temperature. The fixative was removed and briefly washed in 1 x PBS. Cells were stored in fresh 1 x PBS at 4°C ready for immunostaining.

2.5.4 Cell-cycle synchronisation

RPE1-hTERT cells were plated out in 12-well plate on ethanol-washed glass coverslips. 450,000 cells were added per well supplemented with growth media. At 70-80% confluency cells were treated with 1.5 μM nocodazole arresting cells at G2/M transition phase. To release the cells from G2/M arrest, cells were twice washed with pre-warmed 1 x PBS and incubated in serum free growth media. Cells were incubated at 37°C and 5% CO_2. Cells were fixed at set time-points in 1 % Formaldehyde + 0.2% triton and 1 x PBS for 10 minutes. The fixative was removed and washed twice with 1 x PBS. Coverslips were stored in 1 x PBS at 4°C ready for immunostaining.

2.6 Molecular Biology

2.6.1 Cloning

Several constructs were cloned including; pcS2P-eGFPN αSYN, pcS2P-eGFPN αSYNA30P, pcS2P- eGFPN αSYNA53T, pcS2P-eGFPN BCAPα and pcS2P-eGFPN BCAPδ.

2.6.1.1 Cloning α-synuclein constructs

Dr Angeleen Fleming provided the plasmids peGFP- C2 αSYN, peGFP- C2 αSYNA30P and peGFP- C2 αSYNA53T. These constructs were used for generating aggresomes in cell lines. For mRNA synthesis αSYN and the two familial mutants were cloned in to pcS2P-eGFPN, where the Sp6 promoter was used to transcribe the mRNA. All three constructs were cloned in the same way.

2.6.1.1.1 Restriction digest of α-synuclein constructs

The peGFP- C2 αSYN (A30P and A53T) plasmids and pcS2P-eGFPN were digested with *Age*I (Thermo Fisher #ER1461) and *Sal*I (Thermo Fisher #ER0641). Digesting peGFP- C2 αSYN with AgeI and SalI removes the GFP tagged αSYN fragment (Figure 2.2), digesting the pcS2P-eGFPN with AgeI and SalI removes the GFP fragment which is then replaced when GFP tagged αSYN is ligated in. The reaction mixture contained; 2.5 μg of plasmid DNA + 5 μl of Buffer O (Thermo Fisher #BO5) + 0.2 μl AgeI (10U/μl) + 0.2 μl SalI (10U/μl) and molecular grade water was added to a final volume of 50 μl. The reaction mixture was incubated at 37°C in a heat block for 3 hours. A small volume of the digestion mixture was run on a 1% agarose gel to make sure digestion was complete. The reaction was then terminated by heat inactivation, the samples was incubated at 65°C for 15 minutes. The digest was run on a preparative gel, the 4kb fragment of the pcS2+eGFPN digest was excised and the 1.1kb fragment of the peGFP- C2 αSYN digest was excised. The gel fragments were gel purified.

2.6.1.1.2 Restriction digest of BCAPα/δ constructs

BCAPα and BCAPδ were inserted into the pcS2+eGFPN vector. BCAPα/δ cDNA was amplified from RPE1-hTERT cDNA using a high-fidelity polymerase (*Pfu* DNA polymerase), where 5' *Bam*H I and 3' *Sal*1 restriction sites were added to the cDNA during PCR amplification (primer sequence in table 2. The PCR products were purified using the Isolate II PCR and Gel Kit, following the protocol for PCR-clean up. The purified PCR products were then digested with *Bam*H I (Thermo Fisher #ER0051) and 3' *Sal*1, the reaction mixture contained; 0.5 μg of PCR product + 5 μl of *Bam*H I Buffer (10 x unique buffer for *Bam*H I; Thermo Fisher #ER0051) + 0.2 μl *Bam*H I (10U/μl) + 0.4 μl SalI (10U/μl) and molecular grade water added to a final volume of 50 μl. The reaction mixture was incubated at 37°C in a heat block for 3 hours. The digested PCR products were again purified using the Isolate II PCR and Gel Kit. The pcS2+eGFPN was digested with *Sal*1- *Bgl* II, the reaction mixture contained; 2.5 μg of plasmid DNA + 5 μl of Buffer O + 0.2 μl *Bgl* II (10U/μl) + 0.2 μl SalI (10U/μl) and molecular grade water to a final volume of 50 μl. The reaction mixture was incubated at 37°C in a heat block for 3 hours. The digest was run on a preparative gel, the 4.8 kb fragment was excised, and gel purified.

2.6.2 PCR Clean-up

The PCR reaction mixture of BCAPα and BCAPδ was purified using the Isolate II PCR and Gel Kit (Bioline #BIO-52058) following manufacturer's instructions. Each PCR reaction/ digest reaction was made up to 50 μl by adding molecular grade water. 100 μl of Binding Buffer CB was added to the sample and mixed by pipetting. The mixture was added to an Isolate II PCR and Gel column, it was centrifuged at 11,000 rpm for 30 seconds. The flow through was discarded and the membrane was washed by adding 700 μl Wash Buffer CW and centrifuged at 11,000 rpm for 30 seconds. The flow through was discarded and the sample centrifuged for another minute at 11,000 rpm to remove any residual ethanol. The DNA was eluted by adding 15 μl of Elution Buffer C to the membrane and incubating for 1 min at room temperature. The sample was centrifuged at 11,000 rpm for 1 minute. The purified PCR product was stored at -20°C for long term storage.

2.6.3 Gel Purification

The digested fragments were run on a 1% agarose gel at 70V for 45 minutes. The gel was visualised on a Blue Light Transilluminator to limit DNA damage. The appropriate fragments were excised using a metal scalpel. The DNA was then purified from the gel using the Isolate II PCR and Gel Kit (Bioline #BIO-52058). The gel fragment was placed in a 2 ml eppendorf and Binding Buffer CB was added to the gel fragment, the sample was then incubated at 50°C for 5-10 minutes (200 μl Binding Buffer CB per 100 mg of agarose gel). The sample was vortexed briefly to assist in dissolving the gel. The dissolved sample was then added to an Isolate II PCR and Gel column, it was centrifuged at 11,000 rpm for 30 seconds. The flow through was discarded and the membrane was washed three times by adding 700 μl Wash Buffer CW, the buffer was incubated on the silica membrane for 2 minutes for each wash, centrifuged at 11,000 rpm for 30 seconds. The sample was centrifuged at 11,000 rpm for 1 minute to remove any residual ethanol. The DNA was eluted by adding 15 μl of Elution Buffer C to the membrane and incubating for 1 min and centrifuged at 11,000 rpm for 1 minute. The DNA fragment was stored at -20°C for long term storage.

2.6.4 T4 DNA Ligase

To ligate the purified fragments into the pcS2+eGFPN vector the T4 DNA ligase kit was used (Promega #M1801) a 20 μl ligation reaction was assembled.

2.6.4.1 α-synuclein constructs

A 20 μl ligation reaction mixture contained: 150 ng of pcS2+eGFPN (cut with *Age*I –*Sal*I) + 50 ng of GFP-tagged α-syn fragment (in separate tubes fragments of GFP-tagged α-synA30P and GFP-tagged α-synA53T were added) + 2 μl of Ligase 10X Buffer + 1u of T4 DNA ligase (1-3u/ μl) and molecular grade water added to a final volume of 20 μl.

2.6.4.2 BCAPα/δ constructs

A 20 μl ligation reaction mixture contained: 150 ng of pcS2+eGFPN (cut with *Sal*1- *Bgl* II) + 50 ng of BCAPα (in separate tube the insert was BCAPδ) + 2 μl of Ligase 10X Buffer + 1u of T4 DNA ligase (1-3u/ μl) and molecular grade water to a final volume of 20 μl.

The ligation mixtures were incubated at 16°C for 18 hours and stored at 4°C. The ligated plasmids were then transformed into chemically competent cells.

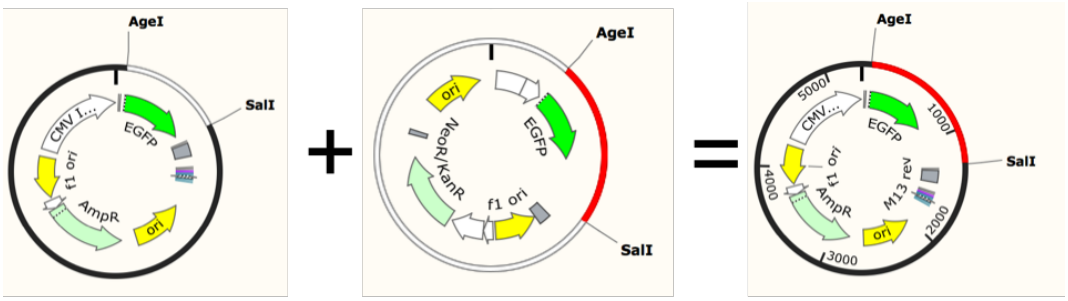

Figure 2.6 Illustration of cloning strategy of pcS2P+eGFPN αsyn.
The plasmid pcS2P+eGFPN was cut with AgeI-SalI, removing the GFP coding sequence. The plasmid peGFP-C2 αsyn was also cut with AgeI-SalI removing the GFP-αsyn sequence. Digested constructs were gel purified. The GFP- αsyn was then ligated into pcS2P+eGFPN by T4 DNA ligase forming a new construct pcS2P+eGFPN αsyn.

2.6.5 Bacterial Transformation

Chemical competent *Escherichia coli (E. coli)* cells (α-select™ silver efficiency Bioline #BIO-85026) were used for plasmid transformation, the cells were stored at -80°C. Competent cells were thawed on ice, 50 µl of cells were aliquoted to a pre-chilled 1.5ml eppendorf, 5µl of plasmid DNA or ligated DNA plasmids was added to the cells. The sample was mixed by lightly tapping the end of the tube. The cells were incubated on ice for 30 minutes. Cells were then heat-shocked for 42°C for 45 seconds in a water bath and immediately cooled on ice for 2 minutes. 950 µl of Lauria Bertani (LB) broth (Melford #L1704) was added to cells the cells were then incubated at 37°C for 1 hour.

Once the cells had recovered they were streaked onto LB- agar plates. To prepare the plates 15 g of agar (Formedium #AGR05) was added to freshly prepared LB broth (25 g/L). Once autoclaved the LB-agar was ready to use, the solution was allowed to cool, and the appropriate antibiotics were added (50 µg/ml ampicillin final concentration Formedium #AMP50; 50 µg/ml kanamycin final concentration Sigma #K4000-1G). The plates were prepared by adding 15 ml of LB-agar per sterile plastic plate, next to a Bunsen burner. The plates were set at room temperature and stored at 4°C until needed. Plates were warmed to 37°C and 20µl (re-transformation of a plasmid) or 200 µl (ligated plasmid) of cells were streaked out. Plates were incubated overnight at 37°C. Individual colonies

were then picked and inoculated in 5 ml LB broth with the appropriate antibiotics (ampicillin 50 µg/ml, kanamycin 50 µg/ml). The cultures were incubated at 37°C for 16 hours in a shaking incubator (250 rpm).

2.6.6 Mini-Prep of Plasmid DNA

To check if the new clone is of the right plasmid composition plasmid DNA was prepared in low quantities using the QIAprep spin Miniprep kit (Qiagen #27104). 5 ml starter cultures were prepared as described above, 2 ml of culture was transferred to a 2 ml eppendorf and centrifuged at 8,000 rpm for 3 minutes at room temperature. The supernatant was discarded, 250 µl of Buffer P1 was added to the pellet, the pellet was resuspended by pipetting. The resuspended sample was transferred to a 1.5 ml eppendorf. To lyse the bacteria, 250 µl of Buffer P2 was added, the sample was mixed by inverting the tube 4-5 times. The sample was incubated at room temperature for 3 minutes, to which 350 µl of Buffer N3 was added to. The sample was mixed by inverting the tube 4-5 times, forming a white precipitate. The sample was then centrifuged for 10 minutes at 13, 000 rpm. 800 µl of the supernatant was transferred to a QIAprep spin column. The sample was centrifuged at 13,000 rpm for 1 minute. The flow through was discarded and the column membrane was washed with 750 µl of Buffer PE, the sample was centrifuged at 13, 000 rpm for 1 minute. The flow through was discarded and the sample was centrifuged again to remove any residual wash buffer. The QIAprep spin column was transferred to a 1.5 ml eppendorf, the plasmid DNA was eluted by adding 50 µl of elution buffer (EB) to the membrane, the EB was incubated at room temperature for 1 minute and then centrifuged at 13,000 rpm for 1 minute.

To check if the new clone was correct, the plasmids were digested with key restriction enzymes that would give specific fragments size. Constructs that gave the correct restriction digest pattern were sent for sequencing. The sequence data verified plasmid composition.

2.6.7 Midi-Prep of Plasmid DNA

To increase plasmid DNA quantity the QIAGEN® plasmid Midi Kit (Qiagen #12143) was used. From the starter culture, 60 µl of culture was inoculated to 30 ml of LB, in a sterile conical flask, the appropriate antibiotics were added. Cultures were incubated at 37°C for 16 hours in a shaking incubator (250 rpm). The bacterial culture was transferred to a 50-ml falcon tube, the cells were harvested by centrifuging at 5000 *x g*, for 20 minutes at 4°C. The pelleted cells were resuspended in 4 ml Buffer P1. 4 ml of Buffer P2 was added, the sample was mixed by inverting the tube 4-5 times, causing the lysate to become viscous. The lysis reaction was incubated at room temperature for 4 minutes. 4 ml of chilled buffer P3 (4°C) was added, the sample was mixed by inverting the tube 4-5 times and then incubated on ice for 15 minutes. The sample was then filtered to remove the white precipitate. Filter paper was folded and placed in a funnel, the lysate was filtered through to a beaker. The QIAGEN-tip 100 was equilibrated by adding 4 ml of Buffer QBT, the buffer flows through the column by gravity flow. The supernatant containing plasmid DNA was added to the column, once the supernatant had passed through by gravity flow the membrane was washed twice with 10 ml of Buffer QC. Once the wash solution had moved through by gravity flow the DNA was eluted by adding 5 ml of Buffer QF. The 5 ml of DNA was precipitated by adding 3.5 ml of room temperature isopropanol to a 15 ml falcon and centrifuged at 5000 *x g*, for 60 minutes at 4°C. The clear DNA pellet was then washed with 70% ethanol and centrifuged at 5000 *x g*, for 60 minutes at 4°C. The ethanol was removed, another quick spin to collect and remove any residual ethanol. The pellet was left to air-dry for 5 minutes at room temperature. The pellet was resuspended in 120 µl of EB buffer. The plasmid DNA is stored at -20°C for long term storage.

2.6.8 RNA Extraction

Total RNA was extracted from cells using the TRIzol protocol. Spent media was aspirated, the cells were briefly washed with room temperature 1 x PBS, the PBS was replaced by adding 500 µl of Trizol (Thermo Fisher #15596026) directly to the cells, pipetting several times to achieve homogenisation. For phase separation, 100 µl (one fifth of Trizol volume used) of chloroform was added, the sample was mixed by inverting 3-5 times followed by

a 5 minute incubation at room temperature. The sample was centrifuged at 12,000 rpm for 15 minutes at 4°C. After centrifugation, the three phases were visible, total RNA was contained in the upper aqueous layer, this layer was carefully collected avoiding any contact with the middle phase (genomic DNA) and transferred to a clean 1.5 ml eppendorf. The RNA was precipitated by adding 250 µl (half the volume of Trizol) of room temperature isopropanol, mixed by inverting 4-5 times and incubated at room temperature for 10 minutes. The sample was then centrifuged at 12,000 rpm for 10 minutes at 4°C. After careful removal of the supernatant, the pellet was washed with 75% ethanol followed by another centrifugation at 7,500 rpm for 5 minutes at 4°C, again carefully discarding the supernatant. The sample was briefly spun again to collect any residual ethanol, this was removed by pipetting. The RNA pellet was air dried by leaving at room temperature for 5 minutes. The pellet was re-suspended in 40ul of RNase free water. To check RNA quality, the sample was run on a gel, two bands were visible (if smearing was observed some of the RNA has degraded).

2.6.9 cDNA synthesis

For cDNA synthesis two different reagents were used: AccuScript High Fidelity 1st Strand cDNA Synthesis kit (Agilent Technologies #200820) or GoScript^{TM} Reverse Transcriptase (Promega #A500).

2.6.9.1 AccuScript High Fidelity 1st Strand cDNA Synthesis

The high-fidelity enzyme was used for DNA products used for cloning or samples required for sequencing. Following manufacturer's instructions, first strand reaction mixture was assembled; 5 µg of RNA + 1 µl of Oligo (dT_{20}) primers (0.5 µg/µl; Invitrogen #18418020) + 2 µl of AccuScript RT Buffer (10 x) + 0.8 µl of dNTP mix (100 mM Promega #U1240) + DNase/RNase free water to a total volume of 16.5 µl. The reaction mixture was incubated at 65°C for 5 minutes in a heat block. The reaction mixture was then cooled to room temperature for 5 minutes allowing the primers to anneal to the RNA. To complete the reaction mixture to a final volume of 20 µl, 2 µl of Dithiothreitol (DTT; 100 mM) + 1 µl of AccuScript RT and 0.5 µl of RNase Block ribonuclease inhibitor (40U/ µl Promega #N2111) was added to the reaction mixture. The reaction mixture was incubated at 42°C for 1

hour in a heat block. The reaction was terminated by incubating the reaction mixture at 70°C for 15 minutes in a heat block. The cDNA was stored at -20°C for long term storage.

2.6.9.2 GoScript™ Reverse Transcriptase

cDNA synthesis using GoScript™ Reverse Transcriptase involved assembling a 20 µl reaction mixture containing; 5 µg of RNA + 1 µl of Oligo (dT_{15}) (0.5 µg/ µl) + RNase/DNase free water to make up to 5 µl. This was incubated at 70°C for 5 minutes in a heat block. The reaction mixture was immediately chilled on ice for a minimum of 5 minutes, the sample was briefly centrifuged and then placed back on ice. In a separate 1.5 ml eppendorf, the remaining components of the reaction mixture were assembled containing; 4 µl of GoScript 5 x Reaction Buffer + 2 µl of $MgCl_2$ (2.5 mM final concentration) 4 µl of dNTP mix (0.5 mM final concentration) + 0.5 µl of Recombinant RNasin® ribonuclease inhibitor + 1 µl of GoScript™ reverse transcriptase and RNase/DNase free water to a total volume of 15 µl. The 5 µl of RNA and primer mix was combined with the 15 µl reverse transcription reaction mixture with a final volume of 20 µl. The reaction mixture was mixed by pipetting, and then incubated at 25°C for 5 minutes in a heat block. It was then incubated at 42°C for 1 hour, the reaction was terminated by incubating at 70°C for 15 minutes. The cDNA was stored at -20°C for long term storage.

2.6.10 Polymerase chain reaction (PCR)

The DNA was amplified using either *Pfu* DNA polymerase (Promega #M7741) a high-fidelity DNA polymerase or GoTaq® DNA Polymerase kit (Promega #M3001).

2.6.10.1 *Pfu* DNA polymerase

The cDNA mix prepared using the high-fidelity AccuScript kit was used in this reaction mixture. A 25 µl reaction mixture was assembled containing; 2.5 µl of 10 x *Pfu* DNA Polymerase buffer with $MgSO_4$ + 2 µl of dNTP mix (200 µM of each dNTP final concentration) + 1 µl of forward primer (0.4 µM final concentration) + 1 µl of reverse primer (0.4 µM final concentration) + 0.5 µl of cDNA template (125 ng final concentration) + 0.25 µl of *Pfu* DNA Polymerase (0.625 units final concentration) and 17.75 µl of molecular grade water. The PCR reactions was performed in a Chromo 4™ Thermo cycler

(Bio-Rad #CFB-3240) with the following heat cycle: 95°C for 2 minutes, 30 cycles of 95°C for 1 minute, 57°C for 30 seconds and 72°C for 4 minutes followed by a final extension step of 72°C for 5 minutes. PCR samples were then stored at 4°C.

2.6.10.1 GoTaq® DNA Polymerase

The cDNA mixed prepared using GoScript™ Reverse Transcriptase was used in this reaction mixture. A 25 µl reaction mixture was assembled containing; 5 µl 5 X colourless GoTaq® Reaction Buffer + 2.5 µl of dNTP mix (0.2 mM each dNTP final concentration) + 1 µl of forward primer (0.4 µM final concentration) + 1 µl of reverse primer (0.4 µM final concentration) + 0.75 units of GoTaq® DNA Polymerase and molecular grade water to a final volume of 25 µl. The PCR reactions was performed in a Chromo 4™ Thermo cycler (Bio-Rad #CFB-3240) with the following heat cycle: 95°C for 2 minutes, 30 cycles of 95°C for 1 minute, 57°C for 30 seconds and 72°C for 1 minute/kb (depending on the size of amplicon) followed by a final extension step of 72°C for 5 minutes. PCR samples were then stored at 4°C.

Table 2 Primer names and sequence

Target gene	Primer Sequence		Amplicon size bp
Human β- actin	Forward Primer	5′-ATTCCTATGTGGGCGACGAG-3′	643
	Reverse Primer	5′-GGAGTTGAAGGTAGTTTCGTGG-3′	
h*BCAP*	Forward Primer	5′-ATGGAGAAGGCTGTAAATGA-3′	613
	Reverse Primer	5′-CTTTCAACTTATCGTTCTCG-3′	
h*BCAP*α cloning	Forward Primer	5′-tttgggatcctgATGGAGAAGGCTGTAAATGA-3′	2,061
	Reverse Primer	5′-tttgtcgacTCATGGAGTCTCTGGATCAC-3′	
h*BCAP*δ cloning	Forward Primer	5′-tttgggatcctgATGGAGAAGGCTGTAAATGA-3′	1,863
	Reverse Primer	5′-tttgtcgacTTATTCAAACATTGTTACATAA-3′	
h*BCAP*α siRNA	Forward Primer	5′-GGAAGATCTGAAGAAAATGG-3′	255
	Reverse Primer	5′-ATTTCAGCTGCTTCTTGC-3′	
h*BCAP*δ siRNA	Forward Primer	5′-GCAAGAAGCAGCTGAAATAG-3′	416 and 218
	Reverse Primer	5′-CAAGCTCTTTATTTTCTGCG-3′	

2.6.11 Agarose gel Electrophoresis

DNA was analysed by gel electrophoresis using agarose gels. A 50 x stock solution of Tris-acetate-EDTA was prepared (TAE; 40 mM Tris, 20 mM acetic acid and 1 mM EDTA). A 1.5 % gel was prepared by adding 0.375 g of agarose (Bioline #BIO-41025) to 25 ml of 1 x TAE buffer, the sample was heated in a microwave until fully dissolved, the sample was let to cool for 2 minutes at room temperature, 0.35 µl Web Green Advance DNA Stain (Web Scientific #WG-04) was added to the dissolved agarose solution, the stain was mixed by swirling the beaker until the orange dye was no longer visible. The solution was poured into a gel cast and allowed to set for 20 minutes. Gel electrophoresis tanks (Mini ReadySub-Cell GT Cell #1704887EDU) were used to run the samples. Samples were prepared with 5 x loading dye (1 x final concentration; Bioline #BIO-37045) water was added to make up to 5 µl or 10 µl, depending on the volume of product to be loaded. 5 µl of a 1 kb HyperLadder™ (Bioline #BIO-33053) or 50bp HyperLadder™ (Bioline #BIO-33054) were also loaded on the gel. Gels were run at 90 V for 45 min and the bands were

visualised using a UV transilluminator. For a preparative gel where DNA product will be gel purified a 1% agarose gel was used.

2.6.12 mRNA synthesis

2.6.12.1 Plasmid digest

The following plasmids were used to transcribe mRNA using the Sp6 promoter: pcS2P-eGFPN, pcS2P- eGFPN +αSYN, pcS2P-eGFPN+αSYNA30P and pcS2P- eGFPN +αSYNA53T. 5 μg of plasmid DNA was digested with NdeI (Buffer D 10 μl; 1 unit of enzyme; final reaction volume 100 μl; Promega #R6801) for 3 hours at 37°C. The linearised plasmid was purified using MicroCLEAN DNA Clean up (Web Scientific #2MCL-5). Equal volume of microCLEAN was added to the linearised plasmid, the samples were mixed by pipetting and incubated at room temperature for 5 minutes. Samples were centrifuges at 12,000 rpm for 7 minutes. The supernatant was carefully discarded, samples were spun briefly to collect and remove any residual reagent. The pellet was resuspended in 10 μl DNase/RNase free water.

2.6.12.2 mRNA Transcription

RiboMAX Large Scale RNA Production System (Promega #P1280) was used to transcribe mRNA from the linearised plasmids. The reaction was assembled at room temperature in the order shown in table 3. The reaction mixture was incubated in a heat block set at 37°C for 4 hours. The mRNA was purified using the RNA Clean and Concentrator kit. (Zymo Research #RCC5). Following the manufacturer's instructions, 100 μl of RNA Binding Buffer (2 x the volume of sample to be purified) was added to the mRNA reaction mixture, the sample was mixed by pipetting, 150 μl of 100% ethanol (volume of mRNA + RNA Binding Buffer) was added to the sample, mixed by pipetting, the sample was then added to the column and centrifuged at 10,000 rpm for 30 seconds, discarding the flow through. 400 μl of RNA Prep Buffer was added to the column, centrifuged at 10,000 rpm for 30 seconds. The column membrane was washed by adding 700 μl of RNA Wash Buffer, this was then centrifuged at 10,000 rpm for 30 seconds. The column was then transferred to a clean RNase/DNase free 1.5 ml eppendorf. To elute the mRNA, 15 μl of DNase/RNase free water was directly added to the column membrane, this was then centrifuged at

10,000 rpm for 30 seconds. The sample was then run on a gel to check if synthesis was successful and to assess the quality of mRNA. Typically, two bands should be observed, if smearing is observed some of the mRNA has degraded. The mRNA samples were stored at -80°C.

Table 3 Sp6 reaction mixture components

SP6 Reaction Components	**Volume**
SP6 Transcription 5 x Buffer	12 μl
rNTPs (25 mM ATP, CTP, GTP, UTP)	12 μl
Linear DNA template (5 μg)	9 μl
Enzyme Mix Sp6	5 μl
Final volume	50 μl

2.7 Zebrafish

2.7.1 Animal studies

In this study zebrafish fry less than 5 day post fertilisation (d.p.f.) were used. Rats were killed by Schedule 1 methods, according to Home Office regulations, in compliance with the Animals (Scientific Procedures) Act, 1986.

The AB and TL wild-type strains of zebrafish *Danio Rerio* were used. Zebrafish were maintained and bred at 26.5°C and embryos were raised at 28.5 °C. Both strains of zebrafish were used in these experiments.

2.7.2 Fish breeding and embryo collection

To harvest embryos for experiments female and male fish were put together with a barrier in between overnight (28±1°C) Female and male fish were kept together in a ratio of 1:1. the following morning the barriers were lifted, where spawning was induced by first light. The eggs were fertilised by the male fish once the female fish has released the eggs. The embryos were collected and placed into embryo media (EM3: NaCl, 13.7 mM; KCl, 0.54 mM; $MgSO_4$, 1.0 mM; $CaCl_2$, 1.3 mM; Na_2HPO_4, 0.025 mM; KH_2PO_4, 0.044 mM; $NaHCO_3$, 4.2 mM) and incubated at 28±1°C.

2.7.3 Microinjection

2.7.3.1 Preparing and loading needles for microinjection

Microinjection needles were prepared by placing glass capillaries (Borosil 1.0 mm O.D × 0.5 mm I.D, Frederick Haer & Co., Inc., USA) in a Flaming Brown micropipette puller (Sutter instruments). The needles were pulled and stored in a plastic petri dish ready for use. The pulled glass capillary was attached to a micromanipulator, to which a syringe was attached. The needle tip was placed in the mRNA solution to be loaded, by pulling the syringe the mRNA loaded into the needle. The micromanipulator- mounted micropipette was attached to a Picospritzer microinjector (World Precision Instruments). Allowing small volumes to be injected. Once the needle was loaded, the injection volume was adjusted to final a concentration of 150-200 pg.

2.7.3.2 Injecting into the zebrafish yolk

Zebrafish embryos at 1-4 cell stage were aligned onto a glass slide that had been mounted in a petri dish, excess embryo media was removed. Around 50 embryos can be aligned in one set of injections. The embryos were injected using a light dissecting microscope. The mRNA was injected into the yolk, as the needle penetrates through the chorion and then into the yolk sac. Injected embryos were placed in embryo media in a glass petri dish and were incubated at 29°C. After 24 hours, dead embryos were removed, and Phenylthiourea (PTU; 0.003% final concentration) was added to the embryo medium to inhibit melanin production. Embryos were fixed at 24 hours post fertilisation (h.p.f), 48 h.p.f and 72 h.p.f with Dent's fixative or 4 % FA. Embryos were ready for whole mount immunostaining.

2.7.4 Treating zebrafish embryos with MG-132

To treat zebrafish embryos with MG-132, 1 ml of embryo media containing PTU and 50 μM MG-132 were added to per well in a 12-well plate. 5 embryos were added to each well. Embryos were incubated at 29°C and fixed at 24 to 48 hours of MG-132 treatment.

2.8 Immunostaining

2.8.1. Antibodies

Table 4 Antibodies and dilutions

Primary Antibody	Species	IHC	Supplier
Anti-Vimentin	Mouse	1:1000	Sigma #V6389
Anti-γ-tubulin	Mouse	1:1000	Sigma #T6557
Anti-γ-tubulin	Rabbit	1:1000	Sigma #T5192
Anti-Acetylated-α-tubulin	Mouse	1:1000	Sigma #T7451
Anti-Golgi-97	Mouse	1:1000	Thermo Fisher #Q92805
Anti- BCAP	Rabbit	1:100	Proteintech #23887-1-AP
Anti-α-tubulin	Mouse	1:1000	Sigma #T6199
Anti-Tyrosine Hydroxylase	Rabbit	1:1000	Merck-Millipore #AB152
Anti-α-synuclein	Rabbit		Cell signalling #D37A6
Anti-PCM-1	Rabbit	1:200	Sigma #HPA23374
Anti-PCM-1	Mouse		Sigma #CL0206
Anti-ODF2	Rabbit	1:500	Abcam #ab4380
Secondary Antibody	**Species**	**IHC**	**Supplier**
Anti- mouse Alexa Fluor 594	Goat	1:1000	Invitrogen #A11032
Anti-rabbit Alexa Fluor 594	Goat	1:1000	Invitrogen #A11036
Anti-mouse Alexa Fluor 488	Goat	1:1000	Invitrogen #A11029
Anti- rabbit Alexa Fluor 488	Goat	1:1000	Invitrogen #A11008

2.8.2 Immunocytochemistry

Cells were grown on glass coverslips, sterilised with 80% ethanol in 6-well plates. Cells were fixed with either ice cold -20°C methanol or 4% FA. The fixative was removed and washed with room temperature 1 x PBS, 3 washes, each wash was for 5 minutes on a

shaking platform. The PBS was replaced with 2 ml of blocking solution, 3% bovine serum albumin (BSA) made in 1 x PBS for 30 minutes at room temperature. After blocking, coverslips were placed on parafilm on a flat surface, 150 μl of primary antibody solution made in 1% BSA in 1 x PBS was added to cells. Cells were incubated with the primary antibody either for 3 hours at room temperature on a shaking platform or overnight at 4°C on a shaking platform. After primary antibody incubation, the cells were placed back into a 6- well plate and washed with 1x PBS, 3 washes, each wash was 5 minutes on a shaking platform. For secondary antibody incubation, the coverslips were again transferred onto parafilm on a flat surface, 150 μl of secondary antibody made in 1% BSA in 1 X PBS was added to the cells for 1 hour at room temperature on a shaking platform, cells were covered with foil to prevent bleaching. After secondary incubation, the coverslips were transferred back to a 6-well plate and washed with 1x PBS, 3 washes, each wash was 5 minutes on a shaking platform. To mount the coverslips, 10 μl of FluorSave (Calbiochem # 345789) was placed vertically on the edge of Superfrost Plus glass slides (Thermo Scientific #J1800AMNT), excess PBS was removed by dabbing it on paper, the edge of the coverslip was placed on the mounting media, lowered slowly allowing the mounting media to move across and avoiding any air bubbles. Mounting media was allowed to set for 30 minutes at room temperature. The coverslips were sealed with clear nail polish around the edges of the coverslips. Slides were stored at 4°C. Images were taken using a Nikon Ni-E fluorescence microscope. Images were analysed using ImageJ.

2.8.3 Whole mount immunostaining

Zebrafish embryos were grown in the presence of 0.0012% PTU, to inhibit pigment formation. Embryos at 24 hours post fertilisation (h.p.f) to 72 h.p.f were fixed with Dent's fixative (80:20, methanol: DMSO) prepared fresh on the day or 4% (v/v) FA overnight at 4°C. The fixative was removed the following day; embryos fixed with Dent's fixative were stored in 100% methanol at -20°C; FA fixed embryos were stored in PBS+0.2% Triton +0.02% sodium azide. Embryos fixed with Dent's fixative were permeabilised by incubating 100% methanol for 30 minutes at -20°C. The embryos were rehydrated by washing in serial dilutions of methanol in PBS including: MeOH: PBS at 70:30, 50:50 and

30:70, each rehydration step was for 30 minutes at room temperature on a shaking platform, followed by a final wash in PBS. Embryos fixed with FA were permeabilised by incubating embryos in 0.25% trypsin-EDTA in PBS for 10 minutes on ice and then washed three times for 30 minutes in PBS +0.2% Triton. Embryos were blocked in 10 % heat-inactivated goat serum, 1% BSA and 0.2% Triton in PBS for 4 hours on a shaking platform. Embryos were incubated with primary antibody in 1% BSA and 0.2% Triton in PBS for 48 hours at 4°C on a shaking platform. After primary antibody incubation embryos were washed three times for 30 minutes in PBS +0.2% Triton. Embryos were incubated in secondary antibody in 1% BSA and 0.2% Triton in PBS for 36 hours. Embryos were washed again three times for 30 minutes in PBS +0.2% Triton. Once staining was complete embryos were stored in PBS +0.2% Triton +0.02% sodium azide. Confocal stacks were imaged with an Olympus FX81/FV1000 laser confocal system using Ar gas laser and He-Ne diode laser. Stacks were taken in 1µm thickness and are represented as maximum-intensity projections. Stacks were analysed using ImageJ.

2. 9 Statistics

Statistical analyses were carried out using Graph Pad PRISM using version 7.0a. Student's t-test was used when comparing two treatments to test for statistically significant difference in the means of the control and treated group. When comparing more than two treatments one-way Analysis of Variance (ANOVA) was used. to test for statistically significant differences in the means. n numbers represent the experimental unit, either number of embryos or separate cell culture experiments.

3. Aggresome formation

3.1 Introduction

Protein inclusions are a pathological hallmark for many neurodegenerative diseases including Parkinson's, Alzheimer's and Huntington's diseases (Ross & Poirier 2004). Lewy bodies are protein inclusions known to cause a group of eponymous diseases. The disease manifested is dependent on the distribution of these protein inclusions (Beyer et al. 2009). In Parkinson's these protein inclusions are found in dopaminergic neurons of the substantia nigra. Lewy bodies are made up of a number proteins, with up to 76 proteins being identified so far, including: α-synuclein, heat shock proteins, cytoskeleton components, and parts of the ubiquitin-proteasome machinery (Spillantini et al. 1997; Kuusisto et al. 2003; Wakabayashi et al. 2007; Beyer et al. 2009). The main constituents of these Lewy bodies is α-synuclein (Spillantini et al. 1997; Wakabayashi et al. 2007). The function of Lewy bodies is debated, with some evidence suggesting the presence of these protein inclusions may have a protective role in assisting cell survival (Tompkins & Hill 1997), while other reports suggest the presence of Lewy bodies directly correlates with neuronal loss in the substantia nigra (Greffard et al. 2010). The orderly organisation of Lewy bodies suggests that they do not form randomly or by nonspecific passive diffusion (Kuusisto et al. 2003) . These protein inclusions are generated by a regulated pathway to control excessive amounts of unfolded proteins by an aggresome-related process (McNaught, et al. 2002). Lewy bodies are thought to be derived from aggresomes since they share similar protein components, including heat shock proteins and components of the ubiquitin-proteasome system (Kopito 2000; McNaught et al. 2002).

Aggresomes are juxtanuclear inclusion bodies. They form as a response to misfolded proteins, when the proteasome is overwhelmed (Johnston et al. 1998). Similar to Lewy bodies, aggresomes are believed to form as a cytoprotective response to collect and degrade potentially toxic proteins. In sporadic cases of Parkinson's, functional and structural defects of the proteasome machinery have also been observed at the substantia nigra (McNaught & Jenner 2001). The ubiquitin proteasome system is a degradative pathway responsible for degrading over 80-90% of proteins (Rock et al. 1994). The aggregated protein is transported towards the centrosome, by dynein motors in a microtubule dependent manner, confining the protein to a single location (Johnston et al. 1998; Ahmad et al. 1998; Johnston et al. 2002).

A number of proteins get recruited to the aggresome including heat shock proteins, cytoskeletal proteins and components of the ubiquitin proteasome system (Johnston et al. 1998; García-Mata et al. 1999; Junn et al. 2002; Olzmann et al. 2008). One of the standard molecular markers for aggresomes is vimentin, an intermediate filament that has an extended cytoplasmic distribution (Franke et al. 1979; Franke et al. 1987; Johnston et al. 1998). Upon aggresome formation the vimentin filaments get rearranged caging the aggregated protein inclusion body (Johnston et al. 1998). Another marker for the aggresome is γ-tubulin (Johnston et al. 1998). In normal conditions γ-tubulin appears as two punctae staining the material around the two centrioles components of the centrosome (Oakley et al. 1990; Stearns et al. 1991; Joshi et al. 1992). In aggresomes, γ-tubulin is incorporated into the aggresome and its staining appears as a large zone next to the nucleus (Johnston et al. 1998; Diaz-Corrales et al. 2005). Indeed, the aggresome is formed right next to the centrosome (McNaught, Shashidharan, et al. 2002; Vora & Phillips 2016). The centrosome is the main microtubule organising centre found next to the nucleus in eukaryotic cells (Osborn & Weber 1976; Gould & Borisy 1977). Since aggresomes are in close proximity and share components of the centrosome the presence of aggresomes could affect the function of the centrosome. In its role as the microtubule organising centre the centrosome affects, cell polarity, cellular locomotion and the internal structure of the cell(Koonce et al. 1984; de Anda et al. 2005; Brangwynne et al. 2006). The centrosome is also involved in forming cilia. The microtubule network itself is used for intracellular transport. This includes transport of neurotransmitter vesicles and positioning of organelles such as mitochondria, which are essential for neuronal function(Hollenbeck 1996; Hendricks et al. 2010). If the aggresome inhibits the centrosome neuronal survival could be compromised through lack of intracellular transport and lack of orientated organelles in the cells.

To explore the link between aggresomes and centrosomes, I need to establish cellular conditions that induce the formation of aggresomes and to be able to assay various centrosome functions and then assess whether the function is disrupted in the presence of aggresomes. These assays would need to be compatible with the conditions needed to create aggresomes. Several assays for centrosomal function are well established e.g. microtubule regrowth assay and cell locomotion (see chapter 4 and 5)(Brabander et al.

1986; Nobes & Hall 1999). Aggresomes can be induced experimentally by inhibiting the proteasome or by overexpressing particular proteins that are prone to aggregation (Johnston et al. 1998; Boeddrich et al. 2003). In Parkinson's, the major aggregate found in cells is α-synuclein. Increase in α-synuclein expression is shown to be upregulated by oxidative stress, mitochondrial damage and high concentrations of metal ions (Shavali et al. 2006). Additionally, α-synuclein has increased predisposition to aggregate and form filamentous fibrils at higher concentrations (Dawson & Dawson 2003). A study by Mclean et al. (2001), showed that overexpression of α-synuclein in mouse hippocampal neurons, caused the formation of protein inclusions (McLean et al. 2001). In addition, though the majority of Parkinson's cases are sporadic, around 10% occur as familial forms, and two point mutations in α-synuclein have been identified amongst the 8 genes linked with familial Parkinson's. This includes an alanine to proline mutation at position 30 of the protein and alanine to threonine change at position 53 (Polymeropoulos et al. 1997; Krüger et al. 1998; Hill-Burns et al. 2016).

In this chapter, I describe how I established the conditions to make aggresomes in cell lines under conditions compatible with the centrosomal assays that I will use in chapters 4 and 5. I first try to generate aggresomes in HeLa and RPE1-hTERT cells, as the centrosomal assays have been established in these cell lines, before progressing onto more physiologically relevant (dopaminergic) cells. Two approaches were used to generate aggresomes, either by treating cells with the proteasome inhibitor MG-132 or overexpression of α-synuclein protein. MG-132 is a synthetic peptide aldehyde that inhibits the 20S subunit of the proteasome and has been widely used to induce aggresomes (Han et al. 2009; Orlowski & Wilk 2000). I also overexpressed GFP-tagged α-syn fusion proteins including both the wildtype form and the mutant forms known to predispose Parkinson's. Aggresome formation was confirmed by staining for known aggresomal markers, vimentin and γ-tubulin (Johnston et al. 1998).

3.2 Results

3.2.1 Aggresomes form at the centrosome in HeLa cells

Aggresomes form when the proteasome system is overwhelmed (Johnston et al. 1998). MG-132 is a commonly used proteasome inhibitor which prevents proteasome activity, the accumulated protein forms into an aggresome (Junn et al. 2002). I treated HeLa cells with 10 μM MG-132 or with DMSO (as a control) for 18 hours, the cells were then fixed and stained with anti-vimentin, anti- γ-tubulin and anti-αsynuclein. In control conditions the vimentin staining appears as a fibrous network of filaments around the nucleus (Figure 3.1 A-A'). Upon proteasome inhibition with MG-132 (10 μM MG-132 for 18 hours) the vimentin staining pattern changes to a condensed structure, next to the nucleus (Figure 3.1 B-B'). Similarly, when stained with γ-tubulin, in control DMSO-treated conditions γ-tubulin labels the centrosome which appears as two punctae (Figure 3.1 C-C'). When aggresome formation is induced by MG-132 treatment the two characteristic dots of the centrosome change to a distinct condensed structure similar to that seen with the vimentin staining (Figure 3.1 D-D'). Aggresomes juxtaposed to the nucleus were observed in this cell line following MG-132 treatment. As the centrosome and aggresome are in close proximity to one another it appears the aggresome smothers the centrosome. In some cases, the γ-tubulin staining is more prominent at the centrosome making it easier to distinguish the centrosome (Figure 3. 1 D-D'). The aggresomal staining by γ-tubulin appears weaker surrounding the centrosome (Figure 3.1 D-D'). Since in Parkinson's the main constituent of Lewy bodies is α-synuclein, we tested for whether these aggresomes also contain aggregated α-synuclein protein. In control conditions, endogenous α-synuclein has a diffuse expression throughout the cytoplasm (Figure 3.1 E-E'', G-G''). Following MG-132 treatment, the α-synuclein stain changed to accumulate

next to the nucleus, which is indicative of an aggresome. α-synuclein stain also co-localised with aggresomal markers vimentin and γ-tubulin (Figure 3.1 F-F'', H-H'').

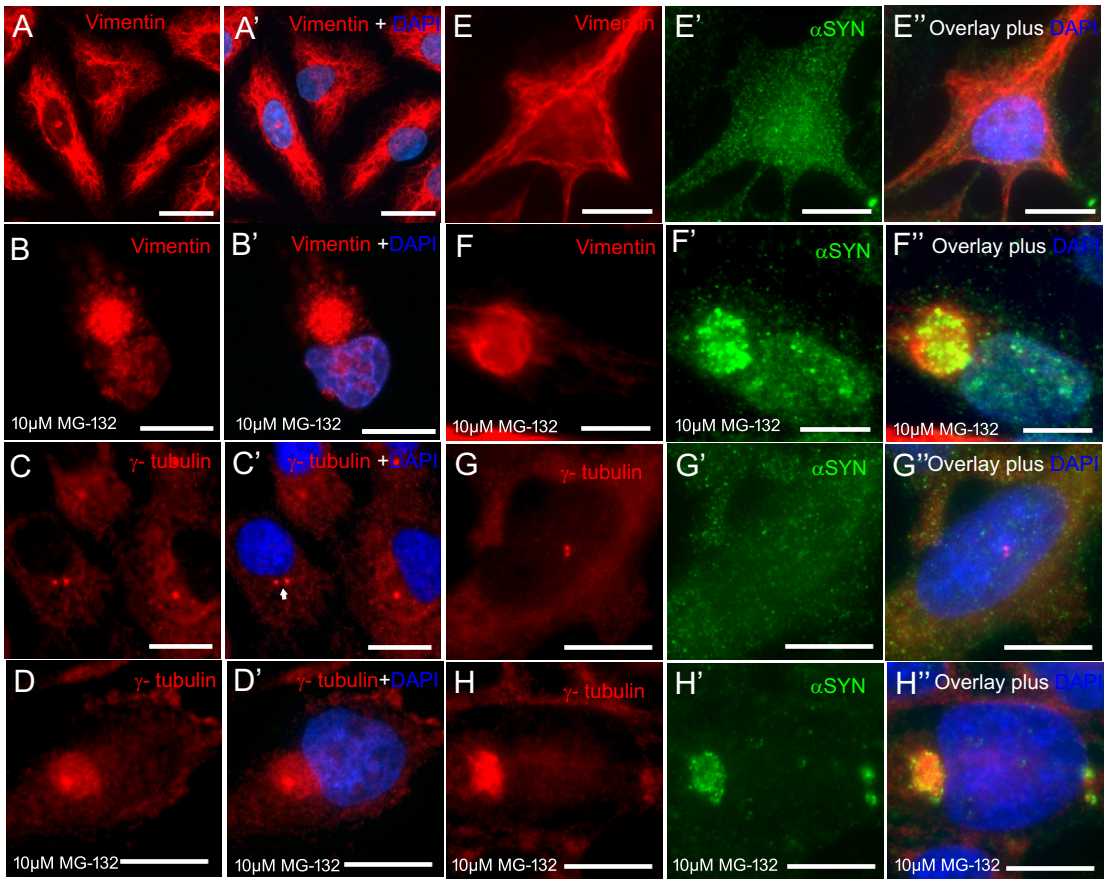

Figure 3.1 HeLa cells form aggresomes when treated with MG-132.
Vimentin (A-A') (red) in control HeLa cells forms a fibrous network, around the nuclei (DAPI- blue). (B-B') When treated with 10 μM MG-132 for 18 hours, vimentin positive aggresomes appear in cells, juxtaposed to the nucleus. The vimentin stain changes from a filamentous stain around the nuclei to caging the aggresome. Similarly, γ-tubulin (red) staining in control HeLa cells (C-C') labels the centrosomes as two punctae. Following MG-132 treatment, γ-tubulin forms a condensed structure around the aggresome (D-D'). The expression pattern of endogenous α-synuclein was also investigated to determine whether this protein co-localises within the aggresome. (E'-E'') In control cells, α-synuclein (green) staining was widespread and diffuse within the cytoplasm with vimentin (red) forming a filamentous network. (F'-F'') Following MG132 treatment, α-synuclein aggregates were observed and co-localised with vimentin staining within the aggresomes. (G'-G'') In control cells, γ-tubulin (red) was observed as two punctae with α-synuclein diffuse within the cytoplasm. (H-H'') γ-tubulin staining (red) also co-localises with endogenous α-synuclein in the aggresome when treated with MG-132. DNA /nuclei stained with DAPI. Scale bars 10 μm.

3.2.2 Aggresomes form at the centrosome in SH-SY5Y cells

SH-SY5Y is a neuroblastoma cell line known to express several neuronal markers e.g. nestin, tyrosine hydroxylase and βIII tubulin (Lopes et al. 2010; Dwane et al. 2013). I next tested whether exposure of SH-SY5Y cells to MG-132 also induces aggresome formation. I treated SH-SY5Y cells with 1 μM MG-132 for 18 hours or control treated with DMSO, the cells were then fixed and stained with either anti-vimentin or anti-γ-tubulin. In control conditions the vimentin staining again appears as a filamentous network surrounding the nucleus, as observed in HeLa cells even though the cell body is smaller in SH-SY5Y cells (Figure 3.2 A-A'), Similarly, the γ-tubulin stain appears as two punctae labelling the centrosome (Figure 3.2 C-C'). In cells treated with MG-132, the vimentin stain changes to a condensed structure, while γ-tubulin stain appears as a larger zone of staining next to the nucleus characteristic of aggresomes (Figure 3.2 B-B'). Having established that SH-SY5Y cells can form aggresomes, cells were also stained with α-synuclein, to check whether α-synuclein also localises to the aggresome. In control cells, endogenous α-synuclein had a diffuse staining pattern throughout the cytoplasm with a more pronounced stain at the periphery of the cells (Figure 3.2 : E-E'' and G-G''). After MG-132 treatment, α-synuclein localises to a large area next to the nucleus indicative of an aggresome. The staining co-localises with both vimentin and γ-tubulin confirming α-synuclein is at the aggresome. The vimentin stain is seen to cage around the aggresome while, γ-tubulin stains the aggresome (Figure 3.2 : F-F'' and H-H'').

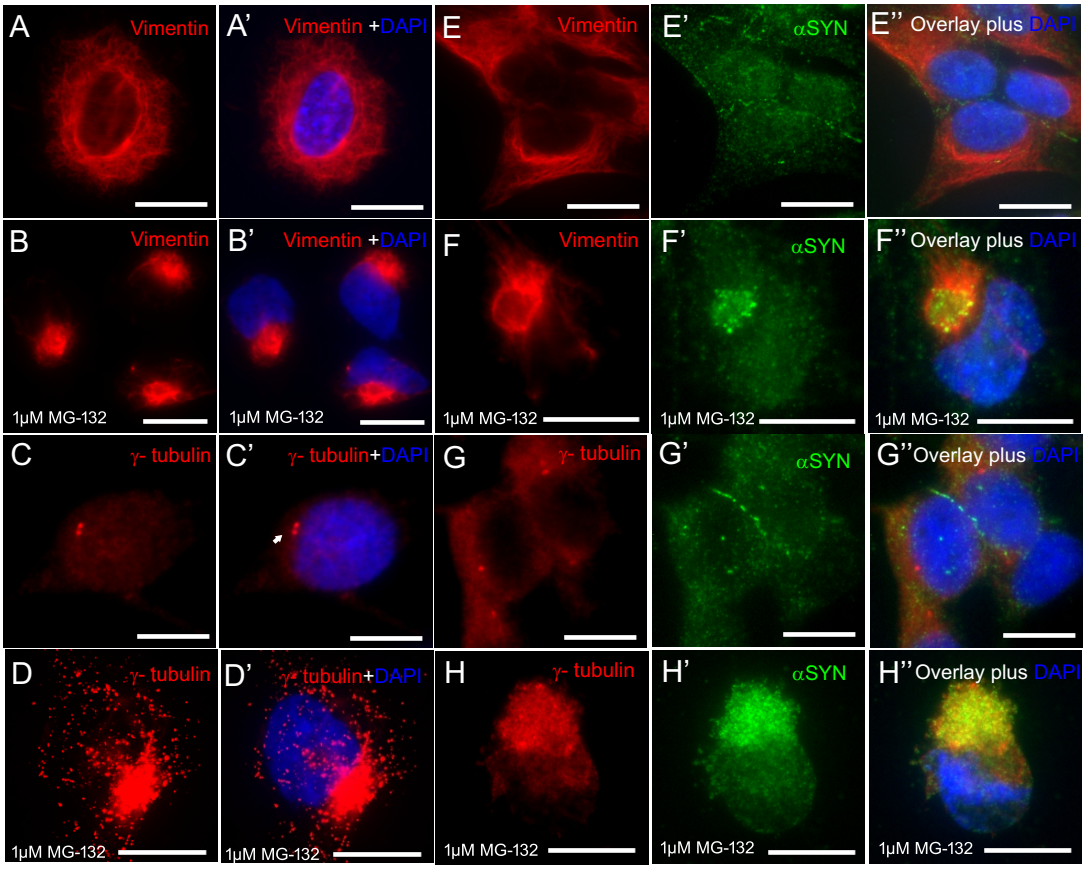

Figure 3.2 SH-SY5Y cells form aggresomes when treated with MG-132.

A-A') Control treated (DMSO) SH-SY5Y cells were stained with vimentin (red) where a filamentous network was observed. B-B') Following MG-132 exposure, the vimentin staining changes to a condensed staining around the aggresome (MG-132 at 1 μM for 18 hours). C-C'- D-D') The γ-tubulin staining (red) changes from two dots characteristic of the centrosome to label the condensed aggregated protein. E-E'', G-G'') Endogenous α-synuclein was detected as a diffuse cytosolic staining in control conditions. F-F'', H-H") Following MG-132 treatment, α-synuclein aggregates appeared caged by vimentin or γ-tubulin. DNA/nuclei stained with DAPI (blue), where indicated. Scale bars 10 μm.

3.2.3 SH-SY5Y cells can be differentiated by retinoic acid

SH-SY5Y cells have a useful feature that they can undergo differentiation. This causes them to further resemble dopaminergic neurons both in morphology and biochemically (Dwane et al. 2013). Increased expression of neuronal markers is observed including tyrosine hydroxylase (TH) (Khwanraj et al. 2015). Tyrosine hydroxylase is the rate limiting enzyme for dopamine synthesis and is used as a marker for dopaminergic neurons (Daubner et al. 2011). SH-SY5Y cells were differentiated by plating proliferating cells on collagen-coated coverslips, upon attachment cells were supplemented with 10 μM retinoic acid. Media was replenished every two days with differentiation achieved in seven days (Figure 3.3 A). Proliferating SH-SY5Y cells have a neuroblastoma-like morphology while differentiated cells adopted a neuronal morphology by forming and extending neurites (Figure 3.3 B). The cells were fixed and stained with anti-TH antibody. The presence of dopaminergic neurons was confirmed by positive TH staining (Figure 3 .3 C). Approximately over 90% of cells are considered to be differentiated, confirmed by tyrosine hydroxylase staining.

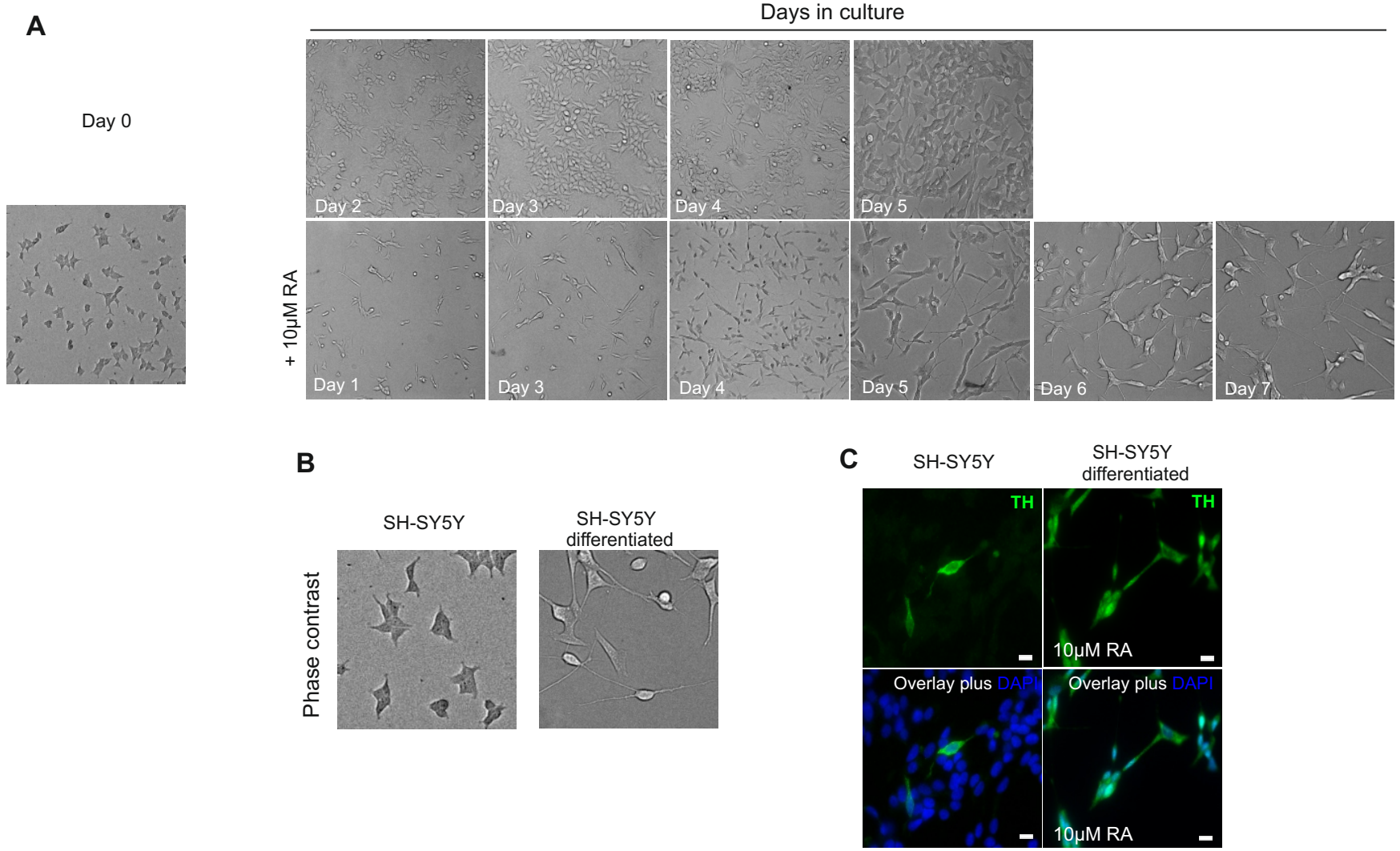

Figure 3.3 SH-SY5Y cells can be differentiated Retinoic acid.

A) Undifferentiated SH-SY5Y cells have a neuroblastoma morphology, SH-SY5Y cells treated with retinoic acid (RA) over seven days become differentiated where they adopt neuronal like morphology and biochemical properties of neurons while, cells that have not been exposed to RA continue to proliferate with no change in morphology. B) One key characteristic feature that validates differentiation is change in morphology with evidence of neurite outgrowth and smaller cell body. C) Tyrosine hydroxylase (TH) is a marker used for dopaminergic neurons, in differentiated cultures increased staining of tyrosine hydroxylase is seen. DNA/nuclei stained with DAPI (blue), where indicated. Scale bars 10 µm.

3.2.4 Differentiated SH-SY5Y cells form aggresomes when the proteasome is inhibited

After SH-SY5Y cells were differentiated with retinoic acid, confirmed by neuronal morphology and positive tyrosine hydroxylase staining, I treated differentiated SH-SY5Y cells with MG-132 to see if they too form aggresomes. Differentiated SH-SY5Y cells were treated with 1 μM MG-132 for 18 hours or control treated with DMSO. The cells were then fixed and stained with aggresomal markers, anti-vimentin and anti-γ-tubulin antibodies or with anti-TH antibody to confirm the presence of dopaminergic-like cells. In control differentiated SH-SY5Y cells, the vimentin staining is compact around the nucleus and the extended neurites (Figure 3.4 A-A''). The γ-tubulin staining labels the centrosome with two punctae visible near the nucleus, while tyrosine hydroxylase staining is diffused throughout the cytoplasm (Figure 3. 4 C-C''). Differentiated cells treated with 1 μM MG-132 for 18 hours showed the vimentin stain to accumulate next to the nucleus, indicative of an aggresome (Figure 3.4 B-B''). The tyrosine hydroxylase staining mainly remained diffuse throughout the cytoplasm. However, closer observations show increased staining next to the nucleus, suggesting tyrosine hydroxylase can also localise to the aggresome (Figure 3.4 B-B''). Similarly, in MG-132 treated cells the γ-tubulin staining is seen to label the centrosome and an increased zone of staining around the centrosome, representative of an aggresome (Figure 3.4 D-D'').

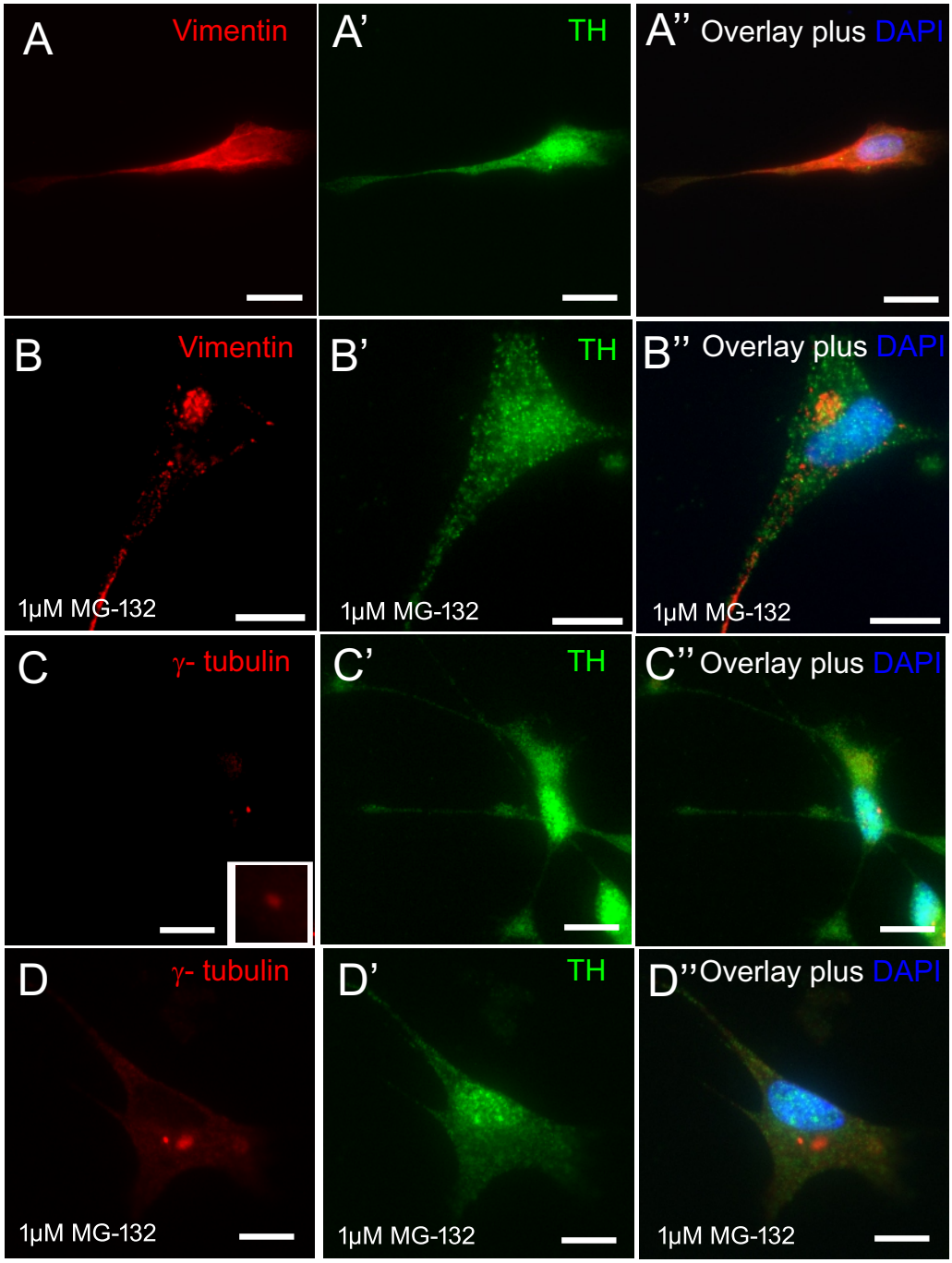

Figure 3.4 Differentiated SH-SY5Y cells form aggresomes induced by MG-132 treatment.

A-A") Differentiated SH-SY5Y cells were treated with DMSO as a control, the vimentin (red) staining was observed surrounding the nuclei as well as along the axon. B-B") Cells treated with MG-132 (1 μM for 18 hours) the vimentin staining changed to a compact structure near the nuclei, indicative of an aggresomes. C-C") In control cells treated with DMSO the γ-tubulin stain is observed as two punctae next to the nucleus. D-D") Following MG-132 treatment, aggresomes were detected by γ-tubulin staining, as a larger zone of staining is visible. Differentiated SH-SY5Y cells are tyrosine hydroxylase positive (green). DNA/nuclei stained with DAPI. Scale bars 10 μm.

3.2.5. Primary neuronal cultures can be made to form aggresomes

The closest one can get to physiological conditions without performing *in vivo* work is to use cultured primary neurons. The basal ganglion comprises an extensive dopaminergic network with the substantia nigra being a structural component (Labandeira-Garcia et al. 2017). Enriched cultures of dopaminergic neurons were prepared from rat embryos and used at 18 days *in vitro* (DIV). The presence of dopaminergic neurons in these cultures was confirmed by anti-TH antibody staining with 25% of cells showing positive tyrosine hydroxylase staining (Figure 3.5 A-A''). Neuronal cultures were treated with 3 μM MG-132 for 18 hours or control treated with DMSO. In control neurons, the vimentin staining pattern is similar to that of differentiated SH-SY5Y cells, with the vimentin compactly labelling the axons and cell body (Figure 3.5 A-A''). Tyrosine hydroxylase staining was very prominent throughout the cell body while at the axon this staining was weaker (Figure 3.5 A-A''- C-C''). In control cells, the γ-tubulin staining appears as a single punctum, labelling the centrosome (Figure 3.5 C-C''). Treating neuronal cultures with MG-132 showed, the vimentin stain to accumulate next to the nucleus symbolic of positive aggresome staining (Figure 3.5 B-B''). The γ-tubulin, staining pattern changed to a larger zone of staining (Figure 3.5 D-D''). The aggresomal markers showed consistent staining when aggresomes were induced by MG-132 treatment. The condensed aggresome structures can be seen to take up substantial space within the cell body of the neurons (Figure 3. 5B-B'' and 3. 5D-D'').

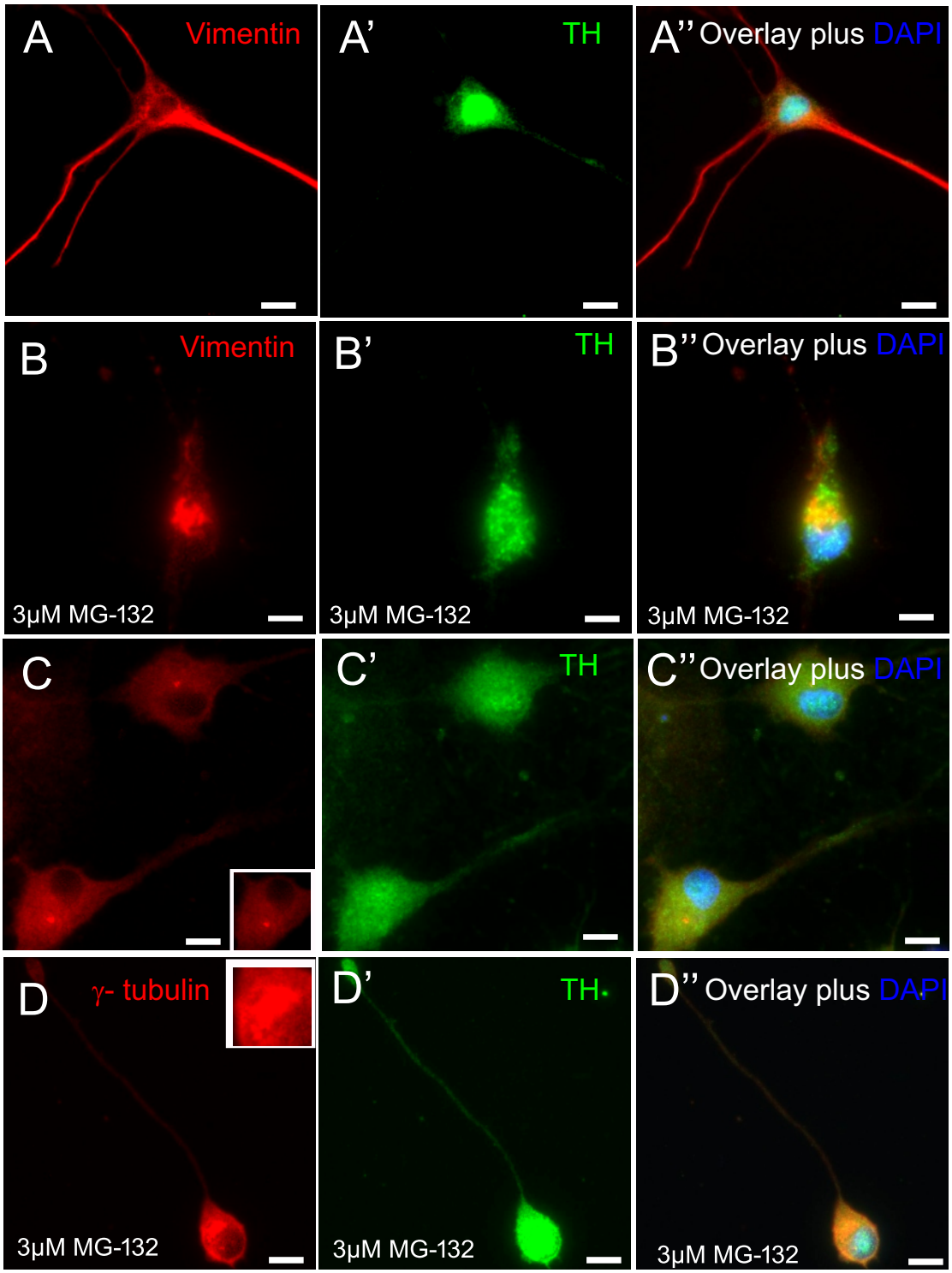

Figure 3.5 Enriched culture of dopaminergic neurons form aggresomes when treated with MG-132.
A- A'') Primary neuronal cultures from the rat basal ganglion contain dopaminergic neurons confirmed by positive tyrosine hydroxylase staining (green), while the vimentin staining (red) is abundant around the nuclei and along the axon. B-B'') When treated with MG-132 (3 μM for 18 hours), vimentin gets rearranged and localises to the aggresome. C-C'') In control, rat basal ganglion neurons treated with DMSO, the γ-tubulin is observed as a single punctum as the two centrioles are close together located close to the nucleus. D-D'') Following MG-132 treatment, the γ-tubulin staining now appears as a large zone of staining next to the nucleus representative of an aggresome. DNA/nuclei stained by DAPI. Scale bars 10 μm.

3.2.6 Overexpression of α-syn causes the formation of aggresomes in HeLa cells

Since MG-132 inhibits the proteasome in all conditions, it could have other effects on cell biochemistry beyond causing the formation of aggresomes. I thought to test if aggresomes could be generated in another way. To do this I overexpressed human α-synuclein wild type and familial mutant forms in cells with the aim of generating aggresomes. As overexpression of α-synuclein has been previously reported to form aggresomes (McLean et al. 2001). The GFP expression constructs encoding human α-synuclein wild type and familial mutant forms were provided by Dr Angeleen Fleming (see chapter 2 materials and methods). Again, I first tested this in a less specialised cell line using HeLa cells. HeLa cells were transfected with either GFP- tagged α-syn wild-type, familial mutant constructs or GFP alone. After 72 hours of overexpression cells were fixed and stained with anti- vimentin antibody. In control cells, in which GFP alone was overexpressed the vimentin stain appeared as a filamentous network around the nucleus with the GFP distributed through the cytoplasm (Figure 3.6 A-A''). In cells overexpressing GFP- tagged α-syn the vimentin staining appears as a condensed structure next to the nucleus (Figure 3.6 B-B''). The vimentin filaments can be seen to cage the aggregated GFP-α-syn protein. Additionally, GFP-α-syn is also seen throughout the cytoplasm (Figure 3.6 B-B''). Similarly, overexpression of GFP-α-synA30P, one of the familial mutant forms, also shows the vimentin staining to accumulate next to the nucleus. The vimentin stain appears as a condensed structure, though it is less apparent than the αsyn wild-type. Overexpression of GFP-α-synA30P is seen through the cytoplasm, with subtle aggregation that co-localises with the vimentin stain. (Figure 3.6 C-C''). Overexpression of GFP-α-synA53T also showed the vimentin stain to form a condensed structure next to the nucleus, characteristic of aggresomes (Figure 3.6 D-D''). These aggresomes are comparable to the aggresomes present in cells where either GFP-α-syn or GFP-α-synA30P were overexpressed. Similarly, the GFP signal is seen through the cytoplasm with a more noticeable expression at the nucleus. The aggregated protein co-localises with the vimentin stain appearing as a condensed structure (Figure 3.6 D-D''). Distortion of the nuclear envelope to accommodate the aggresome is recognised as a feature of aggresomes (Johnston et al. 1998; Taylor et al. 2003). Aggresomes generated by the

overexpression of all three forms of α-synuclein show evidence of nuclear distortion, which further validates the positive aggresome staining.

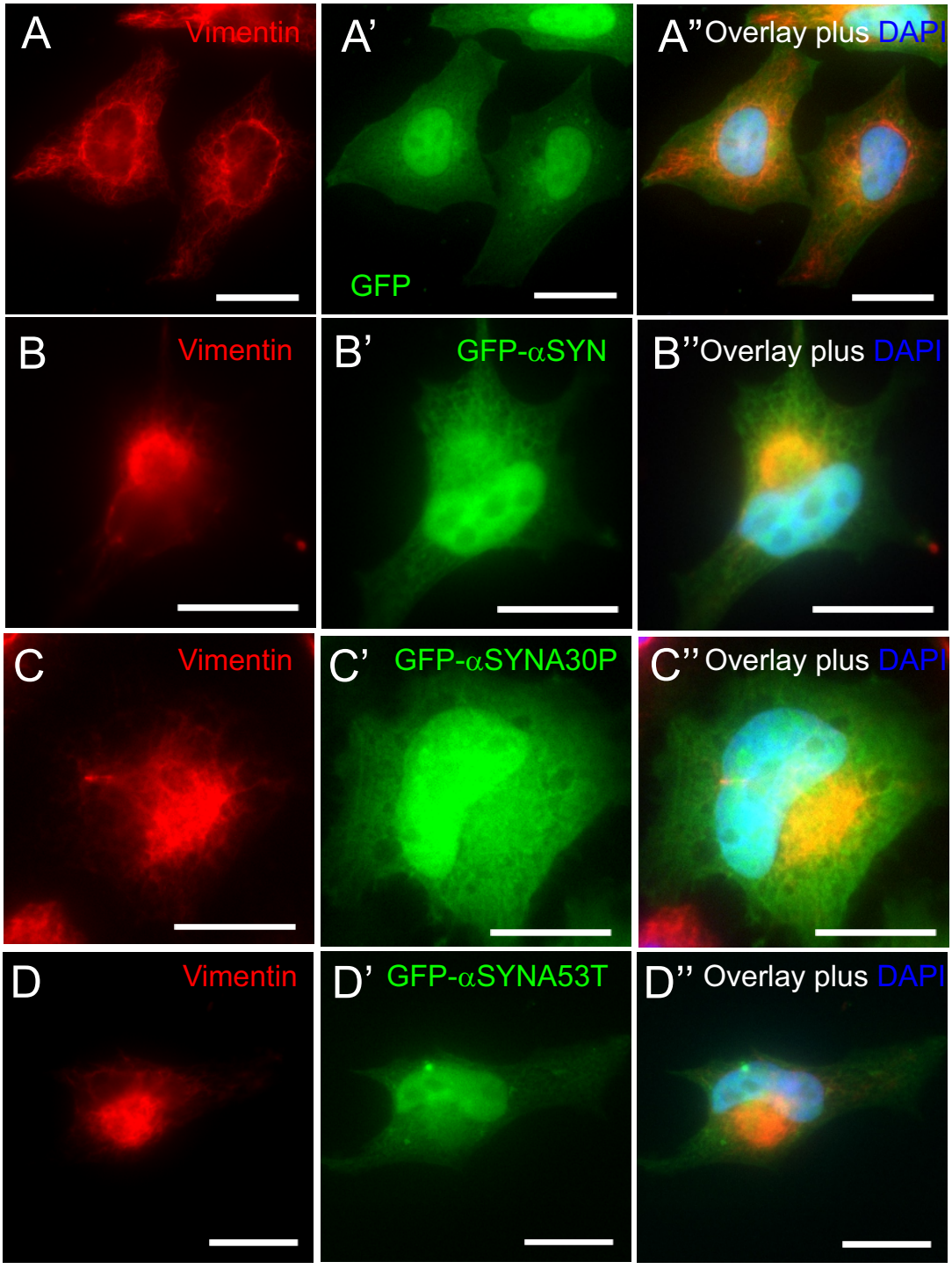

Figure 3.6 The overexpression of GFP-tagged α-syn and the familial mutants forms, induce the formation of aggresomes in HeLa cells.

A) In control cells, where GFP alone is overexpressed the vimentin filaments extend through the cell cytoplasm and cage around the nucleus. The GFP signal is widespread through the cytoplasm. B, C and D'') In cells overexpressing GFP-tagged α-syn, wild-type or the two familial mutant forms (A3OP and A53T), (green) the vimentin stain changes to a condensed structure next to the nucleus (red), the vimentin filaments cage the aggregated protein of α-synuclein, which is not observed upon GFP expression alone, in HeLa cells. DNA/nuclei stained by DAPI. Scale bars 10 μm.

3.2.7 Overexpression on α-syn forms aggresomes in SH-SY5Y cells.

I next repeated these experiments using more specialised cells, the SH-SY5Y cells. SH-SY5Y cells were transfected with GFP alone or GFP-tagged α-syn wild-type and familial mutants to see whether the accumulation of this protein would form aggresomes. SH-SY5Y cells were transfected with GFP alone or GFP-tagged α-syn wild-type and familial mutants (A30P and A53T). After 72 hours, the cells were fixed and stained with anti-vimentin antibody. In control, GFP-transfected cells, the GFP is seen throughout the cytoplasm while the vimentin staining appears as a filamentous network around the nucleus and the vimentin filaments seen extending towards the periphery of the cell (Figure 3.7 A-A''). Cells transfected with GFP-tagged α-syn show diffuse cytoplasmic expression with noticeable aggregation of the protein next to the nucleus (Figure 3.7 B-B''). The vimentin stain is seen to cage the aggregated α-syn protein. Similarly, overexpression of GFP-α-synA30P shows the vimentin staining caging the aggregated (Figure 3.7 C-C''). The same is the case for cells transfected with GFP-tagged α-synA53T, the vimentin staining accumulates around the aggregated protein next to the nucleus characteristic of aggresomes (Figure 3.7 D-D''). The vimentin stain has changed from a fibrous network of filaments as seen in control GFP transfected cells to a condensed structure caging the aggregated protein (Figure 3.7 D-D''). Although the overexpression of all three forms α-synuclein show aggresomes caged by vimentin, some cells showed larger aggresomes as there is increased vimentin staining. As a result, the larger aggresome caused distortion of the nucleus, a feature indicative of an aggresome (Figure 3.7 D-D''). Aggregation of protein is only observed when GFP-tagged α-syn wild-type or the familial mutants, are overexpressed, not when GFP alone is overexpressed.

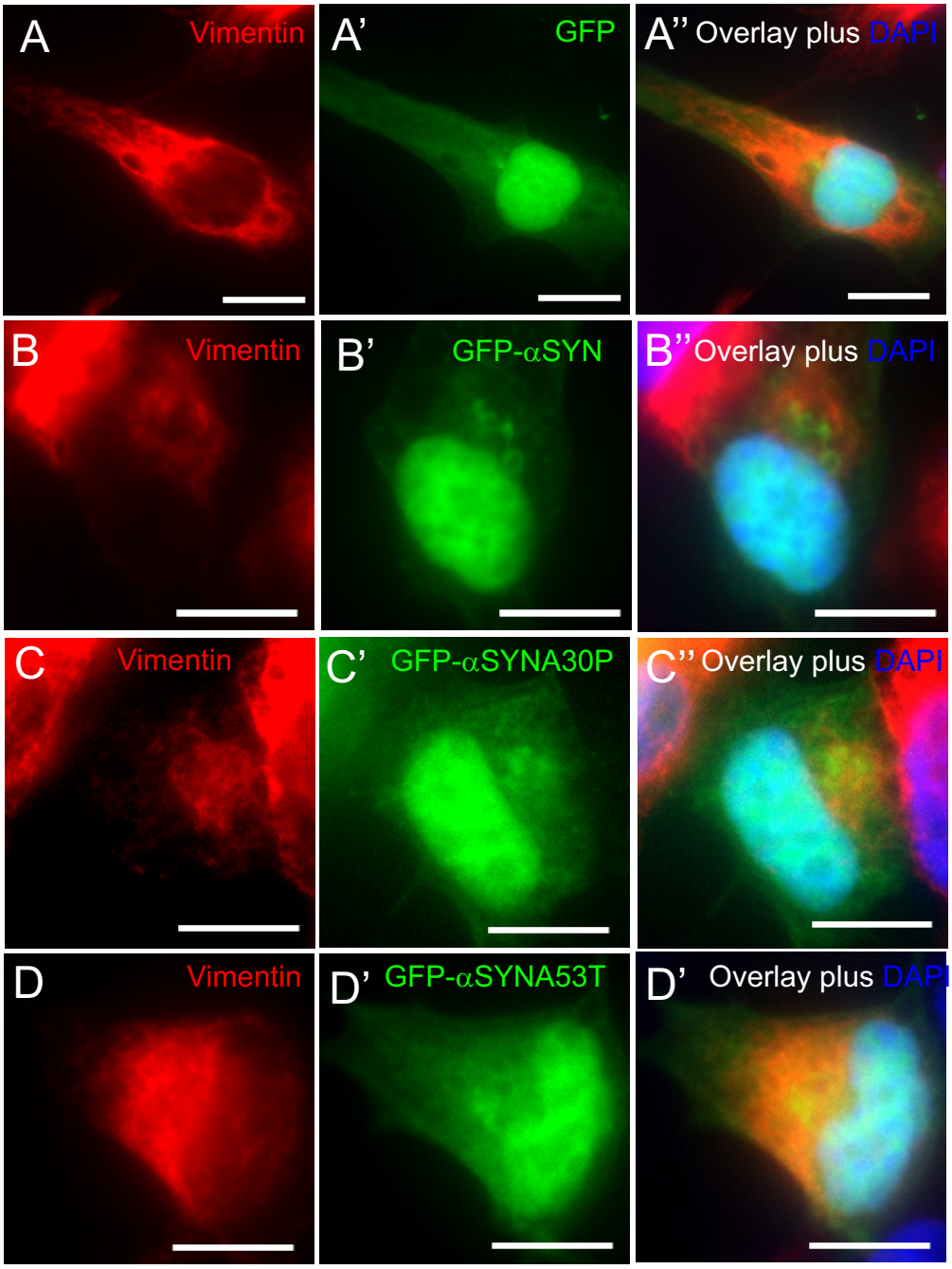

Figure 3.7 The overexpression of GFP- tagged α-syn and the familial mutants induce aggresome formation in SH-SH5Y cells.

A-A'') In control cells, where GFP alone is expressed the vimentin filaments form a fibrous network, stretching across the cytoplasm and cage around the nuclei (red), overexpression of GFP appears diffuse within the cytoplasm (green). B-B'') The overexpression of GFP-tagged α-syn (green) causes formation of aggresomes as the vimentin staining (red) changes to caging the aggregated protein, protein aggregates can be seen next to the nucleus. C-C'') The overexpression of GFP-tagged α-synA30P (green) a familial mutant form also forms aggresome as the vimentin staining (red) changes to a condensed staining around the aggregated protein. D-D'') Similarly, overexpression of GFP-tagged α-synA53T (green) forms an aggresome, with aggregated protein localising juxtaposed to the nucleus and the vimentin staining (red) surrounding the aggregated protein. DNA/ nuclei stained with DAPI. Scale bar 10 μm.

3.3 Discussion

Aggresomes form as a response to the presence of misfolded proteins, at a perinuclear location(Johnston et al. 1998). Comparable to Lewy bodies, aggresomes contain components of the cytoskeleton, centrosome and ubiquitin proteasome machinery (Johnston et al. 1998; Junn et al. 2002). In this chapter, I demonstrate aggresomes can be formed when cells are treated with MG-132 or when GFP-tagged α-syn (wild-type or familial mutants) were overexpressed. I show aggresomes can be induced in several cell lines ranging from less specialised cell lines such as HeLa to a more comparable physiological model including differentiated SH-SY5Y cells and primary neuronal cultures.

Cells were treated with varying concentrations of MG-132 or control treated with DMSO for 18 hours, and then fixed and stained with anti-vimentin or anti-γ-tubulin antibodies to determine the presence of aggresomes. Aggresome formation was also tested in differentiated SH-SY5Y cells. SH-SY5Y cells were treated with retinoic acid over seven days, inducing morphological changes where neurite formation was observed. The presence of dopaminergic cells was confirmed by tyrosine hydroxylase staining with over 90% showing positive staining. In all cell models tested, under control conditions vimentin staining showed an extended cytoplasmic distribution of intermediate filaments. The γ-tubulin stain labelled the centrioles appearing as two punctae next to the nucleus. When aggresome formation was induced both markers appeared as a condensed structure next to the nucleus. The vimentin stain would cage the aggregated protein, while γ-tubulin would appear as a larger zone of staining. HeLa and SH-SY5Y cells were also co-stained with anti-α-syn, which showed α-synuclein becomes aggregated and localises at the aggresome. As aggresome formation was tested in several cell lines, it was noticeable the more specialised cell lines required a lower concentration of MG-132, ranging from 1 μM to 10 μM for differentiated SH-SY5Y and HeLa cells respectively. This agrees with the current published data that the ubiquitin proteasome system is more sensitive in post-mitotic cells (Urushitani et al. 2002; Ciechanover & Brundin 2003). Additionally, it was also apparent the aggresome appeared smaller as I progressed through to more neuronal like cells. This change in size could be explained by the smaller cell body of these specialised cells.

While proteasome inhibition by MG-132 is a commonly used technique for aggresome formation, it is possible to have unknown affects other than inducing aggresome formation. For this reason, I tested whether the overexpression of GFP-tagged α-syn could also form aggresomes by overwhelming the proteasome machinery. Similar to MG-132 treated cells, HeLa and SH-SY5Y cells were transfected with GFP-tagged αsyn including the wild-type or the familial mutants, and cells were fixed and stained with anti-vimentin. In the GFP alone transfected cells, an extended cytoplasmic distribution of intermediate filaments was observed, while overexpression of GFP-tagged α-syn wild-type or GFP-tagged mutant α-syn showed increased aggregation next to the nucleus with the vimentin caging the aggregated protein. The MG-132 treatment and the overexpression of GFP-tagged α-syn formed aggresomes of similar size. These methods of aggresome formation are based on either inhibiting or overloading the ubiquitin proteasome machinery, respectively. Nonetheless, the ubiquitin proteasome machinery is compromised as the end result. Interestingly, mutations found at the ubiquitin proteasome system have an associated risk factor for familial Parkinson's (McNaught & Olanow 2003).

I show aggresomes can be induced by the overexpression of GFP-tagged α-syn in both HeLa and SH-SY5Y cells. Protein aggregation of GFP-tagged α-syn appears more prominent in SH-SY5Y cells than in HeLa cells. Post-mitotic cells are said to be more sensitive to perturbations of the ubiquitin proteasome system (UPS) (Urushitani et al. 2002; Ciechanover & Brundin 2003), such that overexpression of α-synuclein could be more demanding for the UPS system in SH-SY5Y cells to manage. Additionally, overexpression of α-synuclein has shown to have selective toxicity in catecholaminergic neurons of primary midbrain cultures (Tanaka et al. 2004). Although, SH-SY5Y cells are not considered to be post-mitotic, they are known to possess many characteristics of dopaminergic neurons. This includes expression of neuronal markers; tyrosine hydroxylase, dopamine transporter and dopamine-beta hydroxylase(Lopes et al. 2010; Korecka et al. 2013; Khwanraj et al. 2015). Increased sensitivity to UPS perturbations or selectivity toxicity may explain the increase in aggregation observed in SH-SY5Y cells compared to HeLa. Although, some studies have reported an increase in aggregation of mutant α-synuclein such as the A30P and A53T compared to wild-type α-synuclein, no

difference was seen in either HeLa or SH-SY5Y cells. Also, though vimentin staining is shown to localise to the aggresome, slight variations in staining pattern is sometimes observed as sometimes the vimentin filaments are seen to cage the aggresome and at other times the vimentin filaments appear collapsed at the aggresome, the two staining patterns were observed concurrently (Figures 3.6 and 3.7). The vimentin stain either cages or localises to the aggresome, both staining patterns have been observed in the same culture and treatment, so it is not specific to a cell line or a method of aggresome formation.

Cellular features of aggresomes include: juxtanuclear location, nuclear distortion and caging by cytoskeletal proteins (Johnston et al. 1998). Aggresomes generated either by proteasome inhibition or overexpression of GFP-tagged α-syn presented these characteristic features, verifying these protein inclusions. Aggresome formation is a microtubule dependent process (Ahmad et al. 1998). Similar to aggresomes the microtubule organising centre of the cell also has a juxtanuclear location (Osborn & Weber 1976; Gould & Borisy 1977). Misfolded or toxic proteins are collected and recruited towards the centrosomes via microtubules (Johnston et al. 1998). As a result, the aggresome is in close proximity of the centrosome and in many cases, the aggresome ends up smothering the centrosome. Increasing evidence suggests that Lewy bodies in Parkinson's are a form of expanded aggresomes. One of the key differences between these two protein inclusions is their cellular localisation, with the presence of Lewy bodies in the cytoplasm while aggresomes have a juxtanuclear location. It is possible aggresomes retain this central location next to the centrosome since, the centrosome nucleates the microtubules that provide the direction for collection and deposition of unwanted proteins. Another explanation why Lewy bodies do not have this juxtanuclear location could be the difference in microtubule organisation in different cell types including neuronal and non-neuronal cells. Neurons are polarised cells determined by their microtubule arrangement. In non-neuronal cells microtubules nucleate from the centrosome, while this is also the case in neurons, the microtubules are quickly released from the centrosome by microtubule severing protein katanin (Ahmad et al. 1999). Interestingly, neurons are shown to express higher levels of katanin than other cell types, with fewer microtubules attached to the centrosome (Yu et al. 1993). Additionally, the centrosomal protein ninein, responsible for re-capturing minus-end microtubules when

released from the centrosome, has also been observed at non-centrosomal locales in cultured neurons. Although non-centrosomal ninein is also found in non-neuronal cells, there is notable abundance in the cytoplasm of neurons. It is possible cytoplasmic ninein could compete with centrosomal ninein, impeding the recapture of microtubules by the centrosome after their release (Baird et al. 2004). As the neuronal centrosome has poorly anchored and fewer microtubules attached it is possible the presence of aggresome could further weaken this attachment by affecting the centrosome's ability to nucleate microtubules. If this is the case, the aggresome would not able to retain this central location for too long resulting in large inclusions dispersed in the cytoplasm that could go onto form Lewy bodies. Another interesting morphological similarity between aggresomes and Lewy bodies, is that they both contain a central core of ubiquitinated protein suggesting it is possible that aggresomes could go on to form larger protein inclusions. This could also explain how Lewy bodies attained this core of ubiquitinated protein.

I show we can generate aggresomes in several cell lines either by the overexpression of GFP-tagged α-syn (wild-type or familial mutations) or proteasome inhibition by treating cells with MG-132. As aggresomes envelope the centrosome, this close association could hinder centrosomal function.

4. Aggresomes affect microtubule activity and cell polarity

4.1 Introduction

The cytoskeleton is an organised network of fibrillary structures that extends through the cells cytoplasm. Architecturally the cytoskeleton is composed of three key constituents including; actin, microtubules and intermediate filaments (Gall 1966). Key functions of the cytoskeleton include; spatial organisation of cellular content, cellular trafficking, maintaining structural integrity and connecting the cell both physically and biochemically to the external environment (Kapitein & Hoogenraad 2015). The neuronal cytoskeleton is a dynamic network that changes depending on the physiological and pathological condition of the cell (Lavedan et al. 2002). The microtubule network is an integral component of the cytoskeleton providing cells with structural integrity but also serving as a means of transportation within the cell (Utton et al. 2005) . In eukaryotic cells, the centrosome is the main microtubule organising centre (MTOC) (Joshi et al. 1992). In neurons, the microtubule network differs from other cell types, they consist of different compartments that have distinct microtubule organisation which establishes neuronal polarity (Baas et al. 1988). Neuronal function is largely dependent on this polarity. As a result, the development and maintenance of the neuronal cytoskeleton is crucial in maintaining this asymmetric shape and polarity. The microtubule network is also important in regulating neuronal morphology as this is important in regulating formation of specific connections to both pre-and post- synaptic neighbouring cells (Dubey et al. 2015).

The microtubule network is a dynamic intracellular matrix where microtubules form as parallel bundles of asymmetric protofilaments. Microtubules are inherently polarised structures, composed of α and β tubulin heterodimers (Bergen & Borisy 1980). They can switch between growth and shrinkage depending on the need of the cell known as dynamic instability (Mitchison & Kirschner 1984a). In neurons, the axon and the dendritic compartment have microtubules orientated in different orientations . Axons contain microtubules with a uniform orientation whereas, in dendrites microtubule orientation is mixed. The specific organisation of microtubules drives selective transport routes for

the sorting of cargo either to axons or dendrites (Baas et al. 1988; Kapitein & Hoogenraad 2011). This intrinsic polarity of microtubules is crucial for precise trafficking of cargo within a neuron. Disorganisation of microtubule polarity results in the incorrect localisation of cargo. In *Drosophila*, loss of dynein motors or microtubule associated LIS1 resulted in axons having both plus and minus- end distal microtubules which resulted in mis-trafficking of dendritic proteins into axons (Liu et al. 2000; Zheng et al. 2008).

Axonal microtubules have been demonstrated to be more stable than dendritic microtubules. Increase in microtubule stability by Taxol treatment has shown to form multiple neuronal processes that exhibit characteristics of typical axons. A study by Bauer and Richter-Landseberg also showed stabilisation of microtubules by Taxol treatment disrupted the formation of aggresomes. Although aggresome formation is a microtubule dependent event, requiring an intact microtubule network, its dynamic instability of shrinking and polymerising is also needed (Bauer & Richter-Landsberg 2006). Difference in microtubule stability between axons and dendrites is also regulated by microtubule associated proteins (MAPs)including; MAP2, tau and post-translational modifications including acetylation and tyrosination. These regulatory mechanisms result in microtubules with spatially and temporally dependent characteristics. Mutations found at the tau gene has been associated with many neurodegenerative diseases including Alzheimer's and Parkinson's (Bancher et al. 1993; Tobin et al. 2008). Hyper-phosphorylation of tau is believed to destabilise microtubules affecting protein trafficking (Harada et al. 1994). Defects in axonal transport may contribute to the initiation or progression of neuronal dysfunction.

Microtubules serve as tracts for long distance transport. In Parkinson's the affected dopaminergic neurons, extend their process from the substantia nigra through to the basal ganglion. Long distant, axonal transport is necessary for normal functioning of dopaminergic neurons. Additionally, proteins associated with Parkinson's including α-synuclein, Parkin and LRRK2 have been shown to modify microtubule stability. Microtubule stability has also been implicated in other neurodegenerative diseases such as Huntington's and Alzheimer's disease. In Huntington's disease loss of microtubule mass is observed in the affected neurons. Cellular transport is pivotal for cell survival whereby in neurons this includes vesicle transport. The centrosome organises

microtubules by regulating nucleation and microtubule anchoring (Mitchison & Kirschner 1984b). The presence of γ-tubulin is common in microtubule nucleating sites, whereby nucleation is initiated at the γ- tubulin ring complex. Microtubule polymerisation begins when α- and β- tubulin dimers associate with the γ- tubulin ring complex, forming and elongating microtubules (Keating & Borisy 2000).

Aggresome formation is also a microtubule dependent event, as aggregated protein is transported by microtubule associated motor proteins along microtubules to the centre of the cell (Johnston et al. 1998; Ahmad et al. 1998). I have shown in the previous chapter aggresomes form at close vicinity to the centrosome. It is possible this large protein inclusion could hinder the centrosome from nucleating and maintaining the microtubule network. One of the ways in which the microtubule activity of the centrosome can be assessed is by the microtubule regrowth assay. This assay involves depolymerising the microtubule network by cold treating cells, and then letting it reform by warming. Cells are fixed at different time-points to asses both network integrity and whether the network can be re-established. Key observations which would reflect on whether the centrosome is able to nucleate and maintain the microtubule network includes the complexity of the microtubule network prior depolymerisation. Formation of a microtubule aster, usually appearing within 1' of warming. Microtubule polymerisation is a very quick and dynamic process, with the network resembling a mature network of untreated cells by 10'. The rate at which this network is re-established is dependent on the cell line, with some cell lines establishing this network quicker than others.

The polarised neuronal structure is governed by microtubule organisation which, gets reorganised in response to polarity cues. Similarly, centrosomal location in maturing neurons determines the site of axon elongation (de Anda et al. 2005). Cellular polarisation requires changes in microtubule biochemistry to achieve asymmetric polarisation of cells, which requires the microtubules to be organised asymmetrically. In migrating cells, the Golgi and centrosome are re-orientated to face the direction of cell locomotion. The centrosome nucleates microtubules, that are either attached to the centrosome or released, together they aid cell migration (Abal et al. 2002). This centrosome function can be tested by the wound assay. In brief, a strip of cells is removed

from a confluent cell culture, where cells at the edge of the wound would migrate to close the gap.

The microtubule regrowth assay and wound assay will be carried out in the presence of aggresomes either generated by MG-132 or overexpression of GFP-tagged α-syn constructs. As in chapter 3, I first carried out these assays in HeLa and then moved onto more specialised cell lines.

4.2 Results

4.2.1 Microtubule regrowth assay to assess the centrosomes microtubule activity

The centrosome is the main microtubule organising centre (MTOC) of the cell. Microtubules provide structural integrity and serve as tracks for intracellular transport including cellular transport of vesicles, important for neuronal function. Microtubule stability has been implicated in many neurodegenerative diseases including Alzheimer's and Parkinson's, more precisely in axon degeneration and axonal transport (Saha et al. 2004; Rodríguez-Martín et al. 2013). As aggresomes are formed at close vicinity of the centrosome it is possible this large structure could hinder the ability of the centrosome to nucleate microtubules and maintain the microtubule network. Also, aggresome formation is a microtubule dependent event as, aggregated protein is transported along microtubules towards the centrosome. To test if aggresomes affect the centrosome from discharging its function of nucleating microtubules, cells were assessed by the microtubule regrowth assay. In brief, this involves depolymerising the microtubule network and then letting it reform by warming. I first tested this in HeLa cells as this cell line has been routinely used for this assay. To establish how the microtubule network appears in control HeLa cells, cultured cells on coverslips were fixed and stained with anti-α-tubulin to visualise the microtubules and anti-γ-tubulin to detect the centrosome. The staining shows microtubule filaments extending and stretching through the cells cytoplasm up to the periphery of the cell (Figure 4.1 A-A''). Cooling the cells for 30 min, depolymerises the microtubules as α-tubulin staining appears diffused through the cytoplasm (Figure 4.1 B-B''). Upon warming to 37°C, the centrosome is seen to nucleate microtubules and re-establish this network. Microtubule nucleation is a dynamic process with microtubules observed within 0.5 min of warming. The characteristic aster is observed reflecting proficient centrosomal nucleating activity (Figure 4.1 C-C''). As warming proceeds, long and short microtubules are seen with abundant microtubule staining orchestrating from the centrosome (Figure 4.1 D-D'', E-E'' and F-F'').

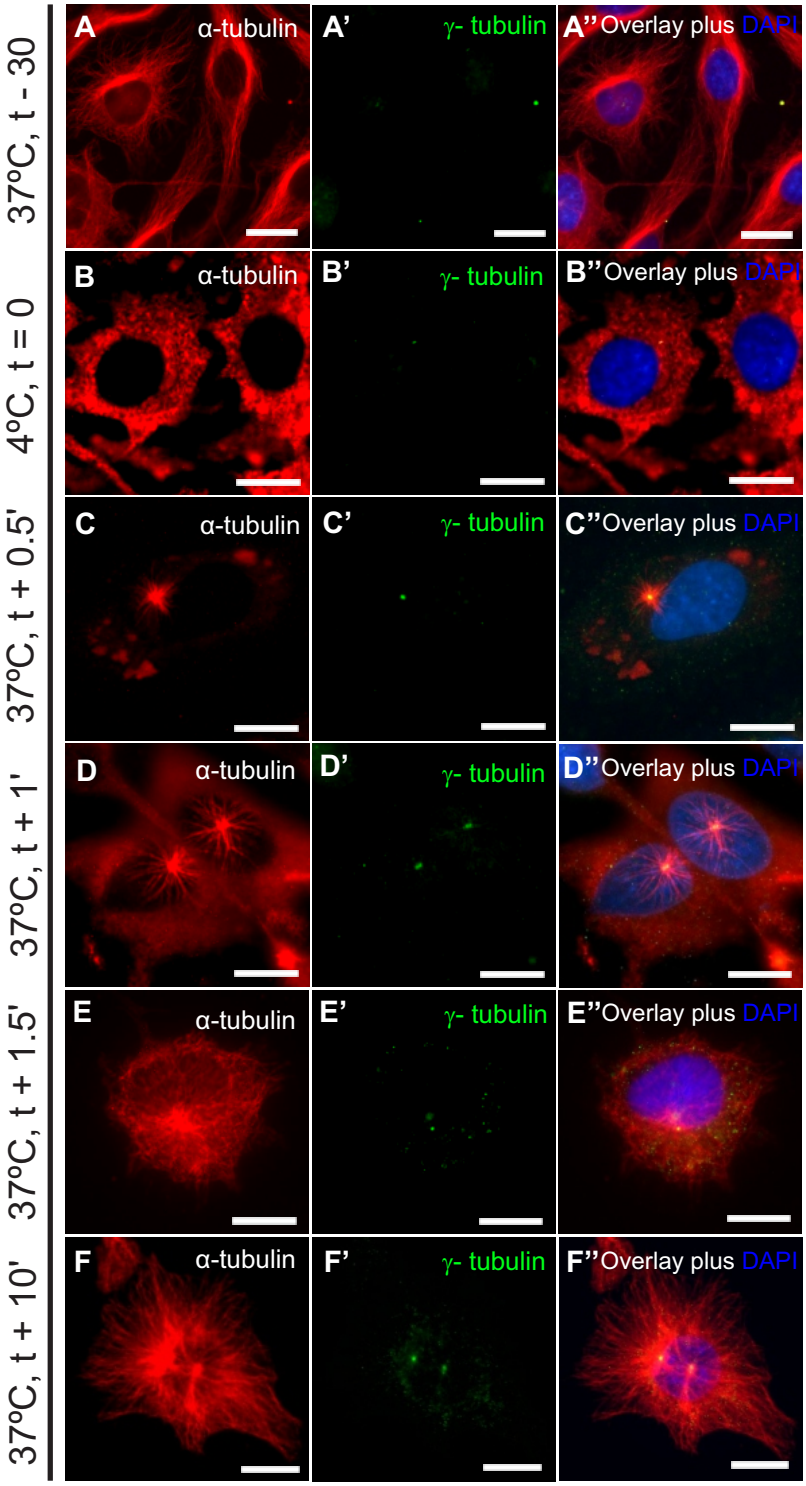
37°C, t - 30
4°C, t = 0
37°C, t + 0.5'
37°C, t + 1'
37°C, t + 1.5'
37°C, t + 10'
A α-tubulin
A' γ- tubulin
A" Overlay plus DAPI
B α-tubulin
B' γ- tubulin
B" Overlay plus DAPI
C α-tubulin
C' γ- tubulin
C" Overlay plus DAPI
D α-tubulin
D' γ- tubulin
D" Overlay plus DAPI
E α-tubulin
E' γ- tubulin
E" Overlay plus DAPI
F α-tubulin
F' γ- tubulin
F" Overlay plus DAPI

Figure 4.1 HeLa cells can re-establish the microtubule network within 10 minutes.
A-A'') HeLa cells at the interphase of the cell cycle have an extensive microtubule network, microtubules visualised by α-tubulin , γ-tubulin staining the centrosome. **B-B'')** Cold treating the cells depolymerises the microtubules, as microtubule staining is no longer visible but alpha tubulin is, diffuse in cytoplasm. **C-C'')** Upon warming, microtubules begin to nucleate from the centrosome forming a characteristic aster by 0.5'. **D-D'')** At 1' the aster continues to grow, E-E'') The microtubule network is still re-establishing itself at 1.5' with increased microtubule staining visible. **F-F'')** By 10' the network has re-established itself with the microtubules originating from the centrosome , the microtubule organising center of the cell. DNA/nuclei stained with DAPI. Scale bars 10 μm.

4.2.2 Aggresomes disrupt the centrosome's ability to nucleate microtubules in HeLa cells.

I have shown in control untreated HeLa cells, there is an extensive microtubule network. The centrosome is able to nucleate microtubules and re-establish a new microtubule network. As aggresomes form next to the centrosome it could structurally obstruct the centrosome from nucleating microtubules and maintaining this network. The microtubule regrowth assay was carried out on HeLa cells in the presence of aggresomes. HeLa cells were treated with 10 μM MG-132 for 18 hours followed by the microtubule regrowth assay. Cells were fixed at different time points including; before cooling, depolymerisation of microtubules by cooling, and then warming, ranging from 0.5 mins to 10 mins. The microtubules were visualised by staining with anti-α-tubulin and anti-γ-tubulin for the centrosome. In the presence of aggresomes, the microtubule network is severely reduced as minimal microtubule staining is observed with majority of the staining localising to the aggresome, that is seen next to the nucleus. The γ-tubulin labels the centrosome with the characteristic dot observed as well as increased aggregation around the centrosome also co-localising to the aggresome (Figure 4.2 A-A''). Cold treating the cells for 30 mins depolymerised the microtubules as α-tubulin predominantly localised to the aggresome and diffused through the cytoplasm (Figure 4.2 B-B''). Upon warming to 37°C, there is no immediate change in α-tubulin staining, as microtubule nucleation is not observed (Figure 4.2 C-C'' and D-D''). Only after 1.5' of warming there is some microtubule staining visible around the centrosome though, the microtubules appear disordered. (Figure 4.2 E-E''). By 10 mins there is no apparent increase in microtubule staining however, a few longer microtubules can be seen extending across the cytoplasm (Figure 4.2 F-F''). The γ-tubulin stain localises to both the centrosome and aggresome with the centrosome confined to the aggresome. Although

these cells were left for over 10 mins of warming there was no change in microtubule staining.

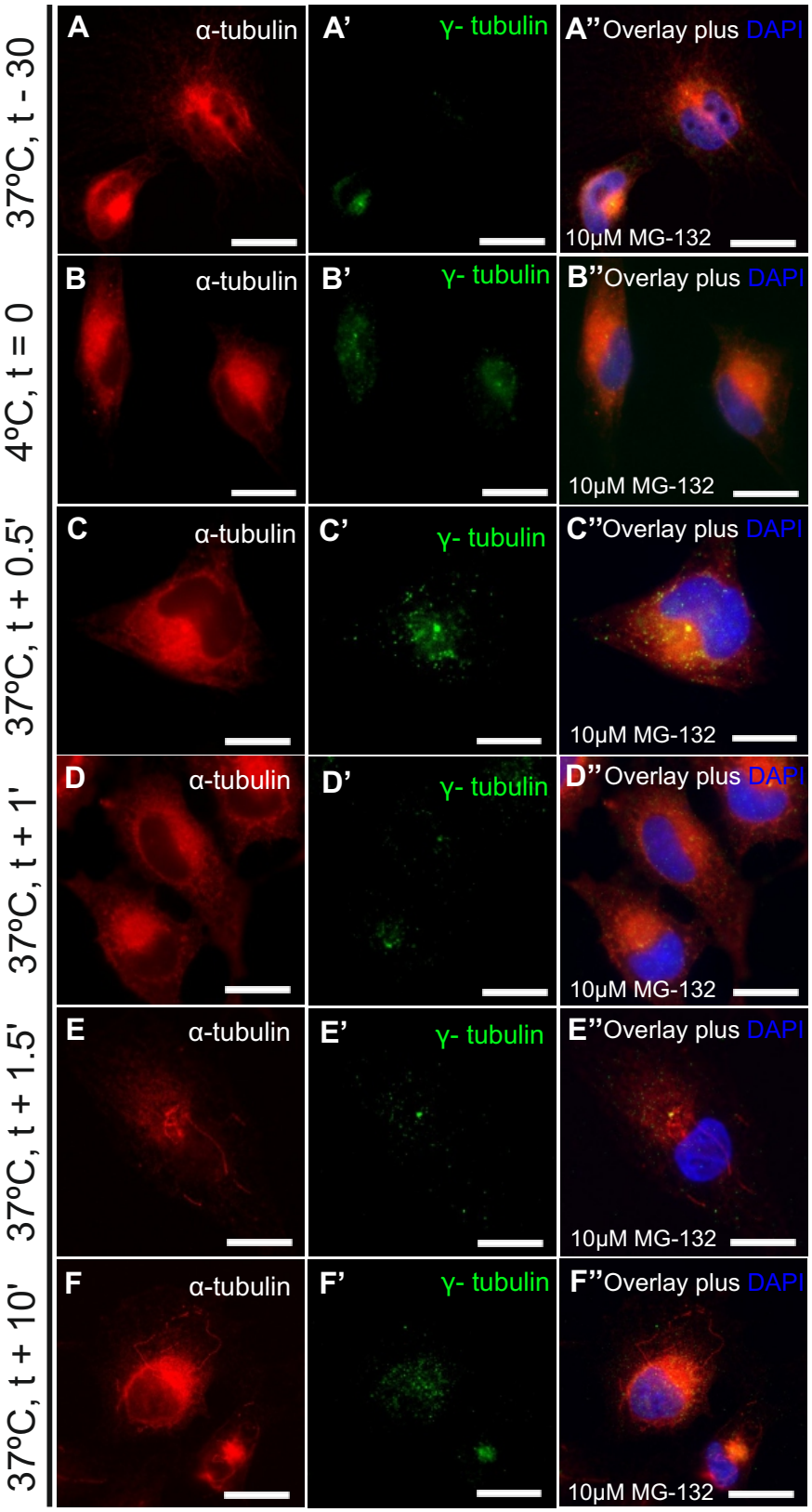

Figure 4.2 Presence of aggresomes disrupts re-establishing the microtubule network in HeLa cells.
HeLa cells were treated with 10 μM MG-132 to form aggresomes. Microtubules are visualised by α-tubulin and the centrosome is labelled by γ-tubulin. **A-A'')** The microtubule filaments appear very short, mainly localising to the aggresome. A few long microtubules can be seen extending into the cells cytoplasm. Similarly, the γ-tubulin stain does not detect the centrosome, as a larger zone of staining is observed next to the nucleus, indicative of an aggresome. **B-B'')** Cold treating the cells, depolymerises the microtubules, with the α-tubulin stain localising to the aggresome and diffused through the cytoplasm. γ-tubulin detects both the aggresome and the centrosome with, the centrosome in close proximity to the aggresome. **C-C'' and D-D'')** Upon warming, the α-tubulin continues to stain and localise to the aggresome as well as diffused cytoplasmic staining, with no microtubule staining visible. **E-E'' and F-F'')** By 1.5 'of warming microtubule staining is visible, appearing short with a random organisation, a few long microtubules are visible stretching across the cells cytoplasm, as warming continues there is no obvious change in microtubule staining, short microtubule can be seen near the aggresome and a few long microtubules stretching across the cells cytoplasm. The γ-tubulin stain does not change upon warming, it localises to the centrosome appearing as a single punctum or a large zone of staining next to the nucleus . DNA/nuclei stained with DAPI. Scale bars 10 μm.

4.2.3 Overexpression of GFP does not affect microtubule activity in HeLa cells

Seeing that aggresomes generated through proteasome inhibition had a detrimental effect on the centrosome's ability to nucleate and maintain the microtubule network, I next tested whether aggresomes generated by the overexpression of α-syn would have a similar effect. As a control, I overexpressed GFP alone in HeLa cells for 72 hours followed by the microtubule regrowth assay. As before cells were fixed at different time-points and stained with anti-α-tubulin and anti-γ-tubulin to visualise the microtubules and the centrosome respectively. Before depolymerising the microtubule network, the α-tubulin labels a well-established network of microtubules. The abundance of microtubules is similar in both the transfected and untransfected cell while, the GFP signal is seen diffused throughout the cytoplasm (Figure 4.3 A-A''). Following on, microtubules were depolymerised as α-tubulin staining is seen diffused throughout the cytoplasm (Figure 4.3:B-B''). Upon warming to 37°C, microtubule nucleation at the centrosome is observed with the characteristic aster appearing by 0.5 mins (Figure 4.3 C-C''). As warming continues microtubule nucleation and polymerisation continues as longer microtubule filaments are observed stretching further to the cell periphery. Increase in microtubule staining is seen, including microtubules orchestrating from the centrosome (Figure 4.3 D-D'' and E-E''). Within 10 min of warming, the centrosome has established a new microtubule network with comparable microtubule staining and organisation in the transfected and untransfected cell (Figure 4.3 F-F'').

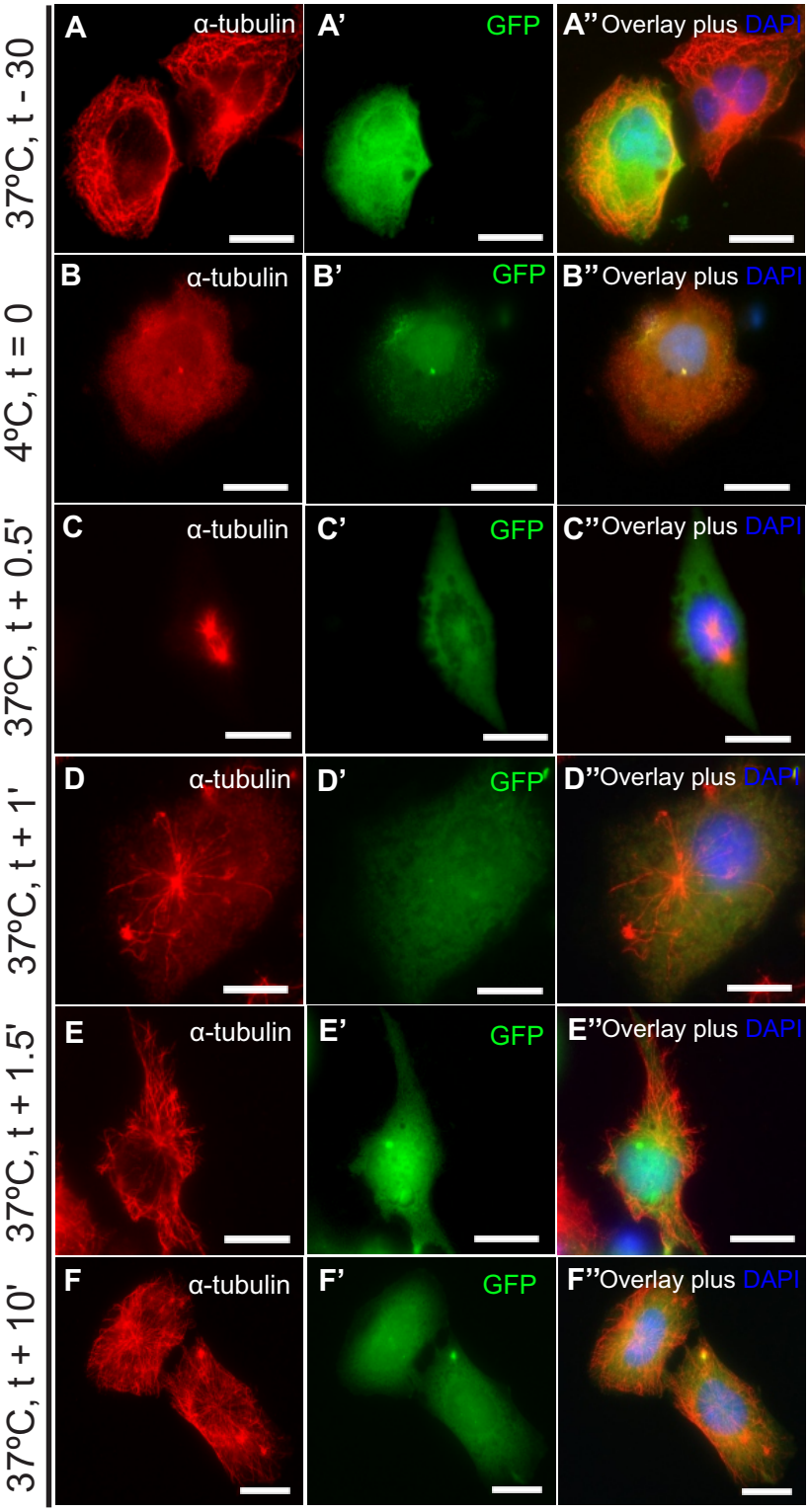
37°C, t - 30
4°C, t = 0
37°C, t + 0.5'
37°C, t + 1'
37°C, t + 1.5'
37°C, t + 10'
A α-tubulin
A' GFP
A'' Overlay plus DAPI
B α-tubulin
B' GFP
B'' Overlay plus DAPI
C α-tubulin
C' GFP
C'' Overlay plus DAPI
D α-tubulin
D' GFP
D'' Overlay plus DAPI
E α-tubulin
E' GFP
E'' Overlay plus DAPI
F α-tubulin
F' GFP
F'' Overlay plus DAPI

Figure 4.3 HeLa cells can re-establish the microtubule network when GFP is over-expressed.
A-A'') HeLa cells transfected with GFP alone expression construct have an extensive microtuble newtork similar to untransfected cells. Microtubules stained by α-tubulin with GFP being expressed throughout the cytoplasm. **B-B'')** Cold treating the cells depolymerise the microtubules where α-tubulin staining is no longer visible while, the GFP expression remains unchanged. **C-C'')** Upon warming ,microtubules begin to nucleate from the centrosome by 0.5' , a characteristic aster is observed. **D-D'')** At 1' the microtubules continue to polymerise establishing this network. **E-E'')** By 1.5' the mcirotubules have further established this network with the aster becoming less visible. **F-F'')** Within 10' the microtubule network has re-established itself comparable to cells prior to cold treating. DNA/nuclei stained with DAPI. Scale bars 10 μm.

4.2.4 HeLa cells fail to re-establish the microtubule network when GFP-α-syn is overexpressed.

I have previously shown (Chapter 3) that overexpression of GFP- tagged α-syn forms aggresomes. I next tested whether these aggresomes affect the microtubule nucleating function of the centrosome. As, aggresomes generated through proteasome inhibition did. HeLa cells were transfected with GFP-tagged α-syn for 72 hours, followed by the microtubule regrowth assay. Cells were fixed at different time-points of the assay and stained with anti-α-tubulin antibody to visualise the microtubules. Overexpression of GFP- tagged α-syn formed aggresomes next to the nucleus. The α-tubulin staining is predominantly localising to the aggresome and the cytoplasm with reduced microtubule filaments observed (Figure 4.4 A-A''). By depolymerising the microtubule network α-tubulin staining is seen throughout the cytoplasm and at the aggresome (Figure 4.4 B-B''). Upon warming, microtubule nucleation is not observed at earlier time-points as majority of α-tubulin staining seen at the cytoplasm and aggresome while microtubule nucleation is observed at the untransfected cell and that too in the form of an aster. The overexpression of GFP- tagged α-syn is seen to cause nuclear distortion, considered to be indicative of an aggresome (Figure 4.4 C-C'', D-D'' and E-E''). It is only at 10 mins of warming, when microtubules are observed however, they are disorganised with only a few nucleating from the centrosome with many distributed around the cell (Figure 4.4 F-F''). Overexpression of GFP-tagged α-syn forms aggresomes which disrupts the microtubule network. As the centrosome is not able to efficiently nucleate microtubules to build a new network.

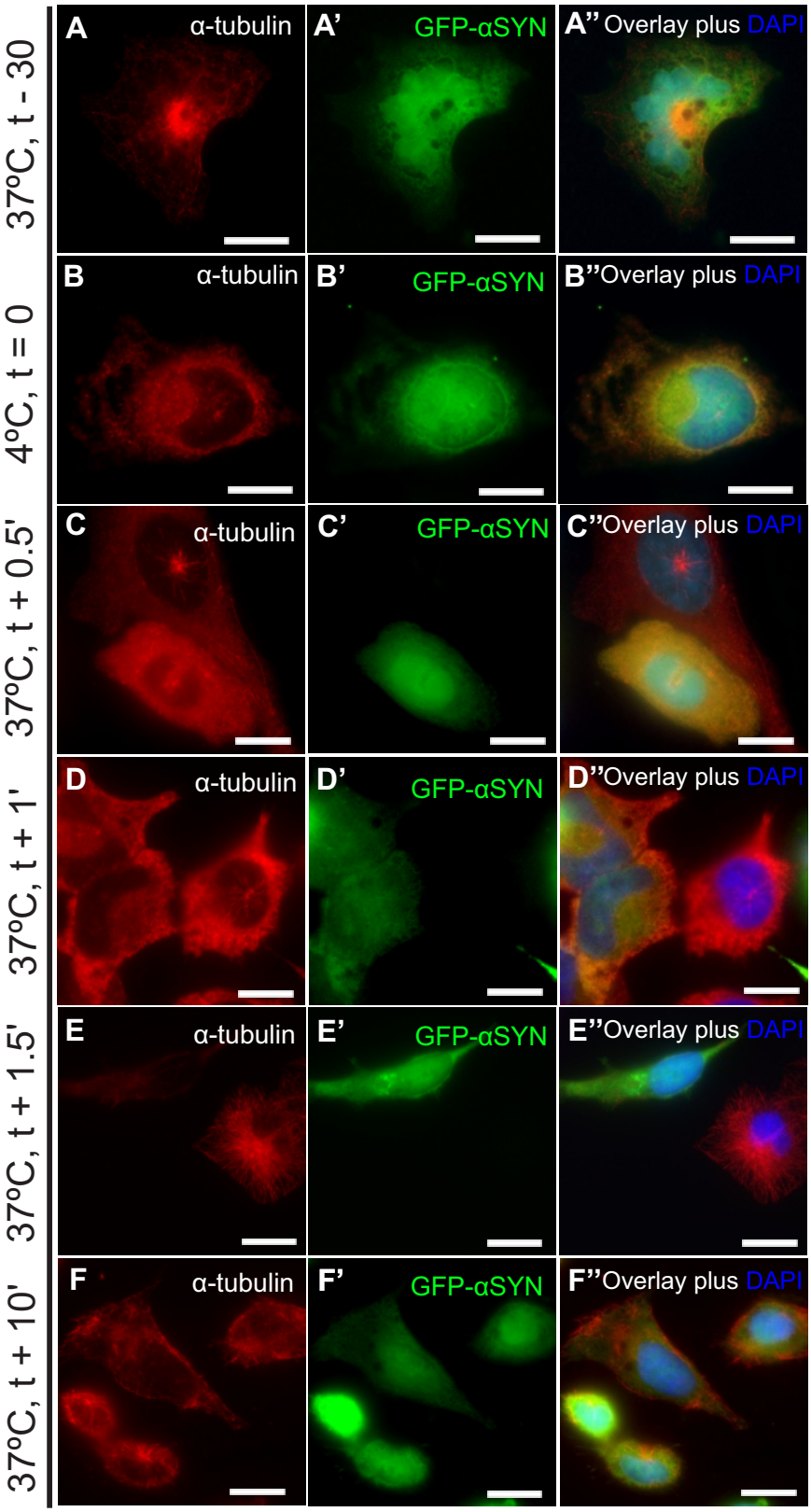
A α-tubulin
A' GFP-αSYN
A" Overlay plus DAPI
B α-tubulin
B' GFP-αSYN
B"Overlay plus DAPI
C α-tubulin
C' GFP-αSYN
C"Overlay plus DAPI
D α-tubulin
D' GFP-αSYN
D"Overlay plus DAPI
E α-tubulin
E' GFP-αSYN
E"Overlay plus DAPI
F α-tubulin
F' GFP-αSYN
F"Overlay plus DAPI
37°C, t - 30
4°C, t = 0
37°C, t + 0.5'
37°C, t + 1'
37°C, t + 1.5'
37°C, t + 10'

Figure 4.4 Microtubule nucleation is disrupted in HeLa cells in the presence of aggresomes created by overexpressing GFP-α-syn.
A-A'') Overexpression of GFP-αsyn compromises microtubule integrity with reduced microtubule filament staining, visualised by α-tubulin. The α-tubulin detects the aggresome at the nucleus, while GFP-αsyn is expressed throughout the cytoplasm concentrating at the aggresome. **B-B'')** Cold treating the cells depolymerises the microtubules as the microtubule staining disappears without affecting GFP-αsyn expression. **C-C'')** At 0.5' of warming the transfected cell is not able to nucleate any microtubules, while the untransfected cell has microtubules nucleating from the centrosome forming a aster. **D-D'')** By 1' the tranfected cell still does not have any microtubule staining , with the GFP-αsyn aggregating next to the nucleus. **E-E'')** At 1.5' of warming the untranfected cell has extensive microtubule staining close to re-establishing the network while the GFP-αsyn expressing cell has no α-tubulin staining with increased GFP-αsyn aggregation seen at the nucleus. **F-F'')** By the final time-point of 10' of warming limited microtubule filaments can be seen from cells overexpressing GFP-αsyn. While some of them are showing microtubules nucleating from the centrosome and forming the aster other cells have small sporadic microtubule staining around the cyotplasm of the cell. DNA/nuclei stained with DAPI. Scale bars 10 μm.

4.2.5 Aggresomes generated by overexpressing GFP-α-synA30P, disrupt centrosomes ability to re-establish the microtubule network.

Patients with mutations found at the α-synuclein gene have increased predisposition for Parkinson's . This includes the point mutation α-syn-A30P which is an alanine for proline substitution at position 30 of the protein. Similarly, I show in chapter 3, overexpression of GFP-tagged α-synA30P forms aggresomes. Since aggresomes generated by proteasome inhibition and overexpression of GFP-tagged α-syn disrupted the microtubule network as the centrosome struggled to nucleate microtubules, it is also possible this point-mutation could have similar effects. I next tested whether aggresomes generated through the overexpression of GFP-tagged α-synA30P hinders the centrosome, from maintaining and nucleating microtubules in HeLa cells. HeLa cells were transfected with GFP-tagged α-synA30P for 72 hours and then processed for the microtubule regrowth assay. Cells were fixed at different time-points of the assay and stained with anti-α-tubulin to visualise the microtubules. Overexpression of GFP-tagged α-synA30P is seen throughout the cytoplasm with increased aggregation next to the nucleus where it is seen to cause nuclear distortion. Microtubule staining is compact with a few microtubule filaments observed originating from a local point (Figure 4.5 A-A''). Once microtubules were depolymerised, α-tubulin localised to the cytoplasm (Figure 4.5 B-B''). Upon warming to 37°C, microtubule nucleation is delayed with α-tubulin continued to be distributed through the cytoplasm (Figure 4.5 C-C''). Microtubules are mainly observed randomly at the periphery of the cell however; some cells were able to

nucleate microtubules in the form of a characteristic aster (Figure 4.5 D-D'' and E-E''). After 10 mins of warming, microtubule staining remained limited, with short microtubules at the boundary of the cells with no apparent arrangement (Figure 4.5 F-F''). Although, there is evidence of microtubule nucleation, the limited microtubules are insufficient to establish a new network.

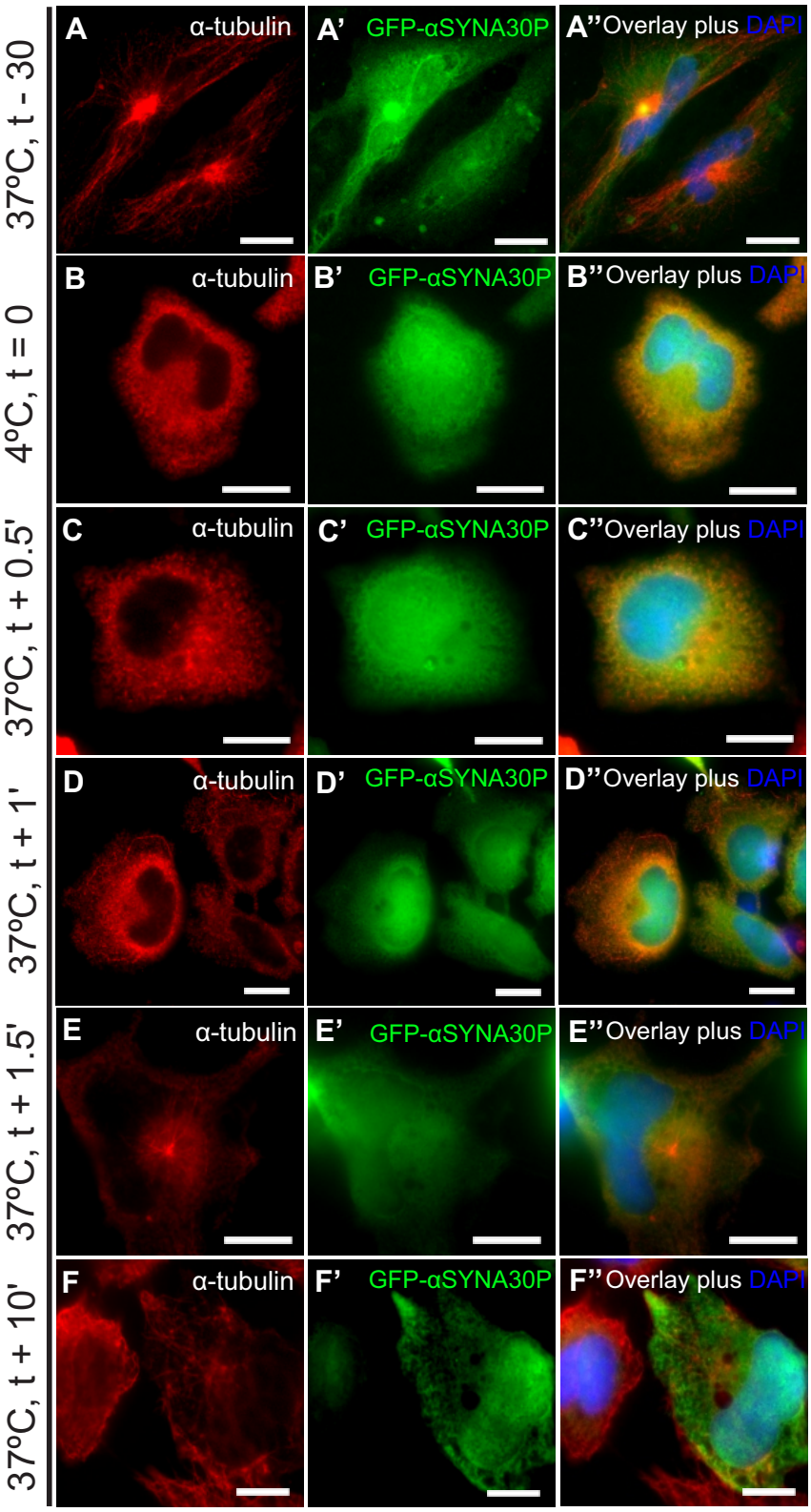

Figure 4.5 Microtubule nucleation is disrupted in HeLa cells in the presence of aggresomes created by overexpressing GFP-α-synA30P.
A-A'') Overexpression of GFP-α-synA30P compromises microtubule integrity with reduced microtubule filament staining, visualised by α-tubulin. The α-tubulin detects the aggresome at the nucleus, while GFP-α-synA30P is expressed throughout the cytoplasm concentrating at the aggresome. **B-B'')** Cold treating the cells depolymerises the microtubules as the microtubule staining disappears without affecting GFP-α-syn expression. **C-C'')** At 0.5' of warming the transfected cell is not able to nucleate any microtubules. **D-D'')** By 1' of warming short and long microtubules can be seen at the periphery of the cell with the GFP-α-synA30P aggregating next to the nucleus. **E-E'')** At 1.5' of warming, a characteristic aster can be seen nucleating from the centrosome which is surrounded by the aggressome generated by overexpressing GFP-α-synA30P. **F-F'')** By the final time-point of 10' of warming limited microtubule filaments can be seen from cells overexpressing GFP-α-synA30P. Short microtubule staining can be seen at the cell particulalry at the periohery of the cell while the untransfected cell has able to re-eatblish this network. DNA/nuclei stained with DAPI. Scale bars 10 μm.
5

4.2.6 Aggresomes generated by overexpressing GFP-α-synA53T, disrupt centrosome's ability to re-establish the microtubule network in HeLa cells

I have shown (chapter 3) aggresomes are formed when GFP-tagged α-synA53T is overexpressed. Similarly, HeLa cells were transfected with GFP-tagged α-synA53T for 72 hours and then assessed whether these aggresomes disrupt microtubule nucleation as it has done for GFP-tagged αsyn and GFP-tagged α-synA30P. Microtubule nucleation was assessed by the microtubule regrowth assay. Cells were fixed at different time-points of the assay and stained with anti-α-tubulin to visualise the microtubules. Overexpression of GFP-tagged α-synA53T is seen throughout the cytoplasm, with increased aggregation at the centre of the cell causing nuclear distortion. The complexity of the microtubule network is reduced with α-tubulin labelling fewer microtubules. Most of the microtubules are situated at the periphery of the cell with some caging the aggregated protein (Figure 4.6 A-A''). Following depolymerisation of microtubules, α-tubulin is observed at the cytoplasm and aggresome, co-localising with the aggregated protein formed by the overexpression of GFP-tagged α-synA53T (Figure 4.6 B-B''). Warming the cells to 37°C did not change α-tubulin staining, as it continued to be localised at the cytoplasm although the untransfected cell is seen to have microtubule staining (Figure 4.6 C-C'', D-D'' and E-E''). It is only at the final time-point, microtubule nucleation is observed, where the microtubules have arranged as the characteristic aster however, the number and arrangement of microtubules is few, inefficient for a new network to be established (Figure 4.6 F-F'').

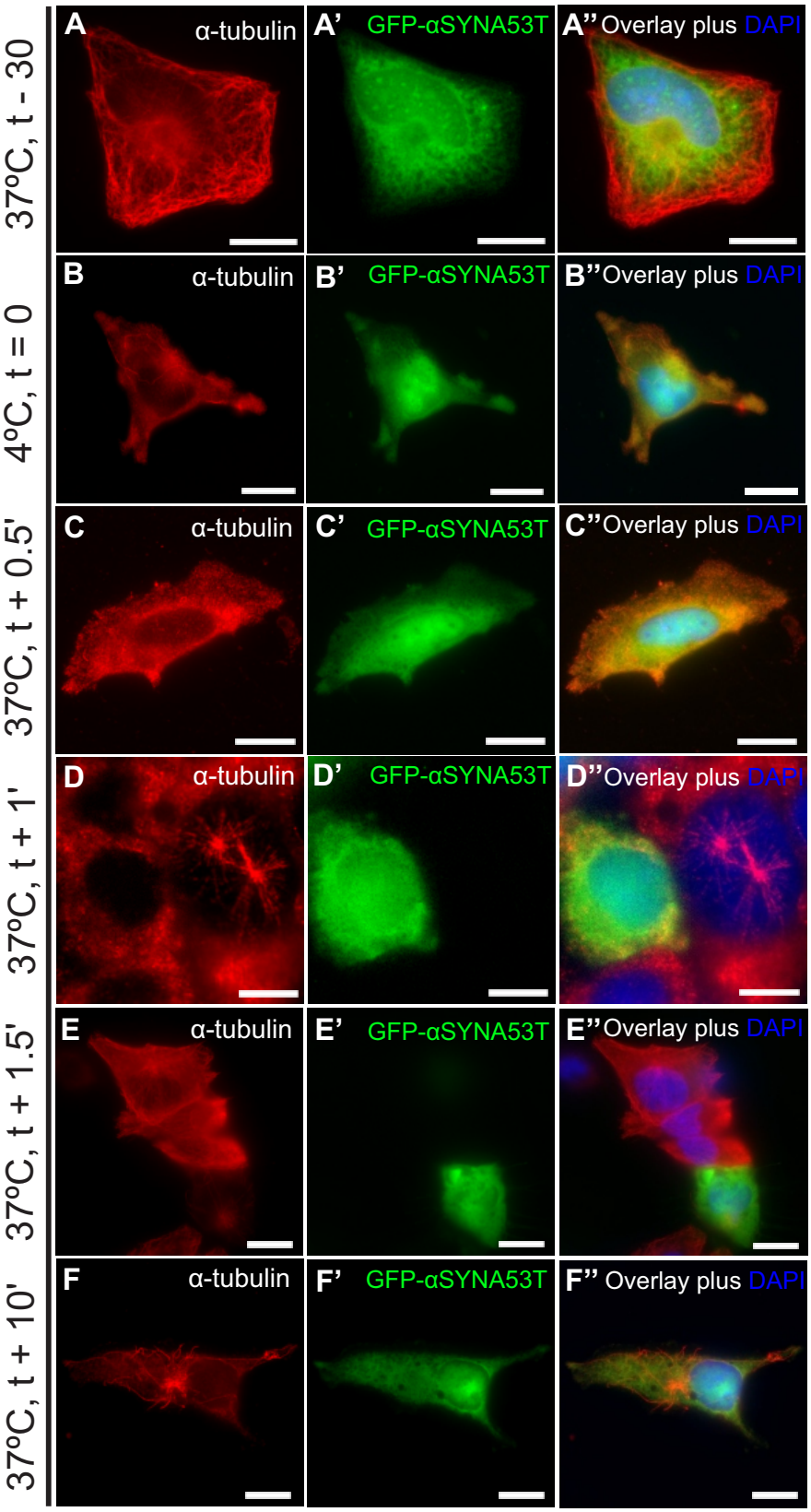
37°C, t - 30
4°C, t = 0
37°C, t + 0.5'
37°C, t + 1'
37°C, t + 1.5'
37°C, t + 10'
A
α-tubulin
A'
GFP-αSYNA53T
A''
Overlay plus DAPI
B
α-tubulin
B'
GFP-αSYNA53T
B''
Overlay plus DAPI
C
α-tubulin
C'
GFP-αSYNA53T
C''
Overlay plus DAPI
D
α-tubulin
D'
GFP-αSYNA53T
D''
Overlay plus DAPI
E
α-tubulin
E'
GFP-αSYNA53T
E''
Overlay plus DAPI
F
α-tubulin
F'
GFP-αSYNA53T
F''
Overlay plus DAPI

Figure 4.6 Microtubule nucleation is disrupted in HeLa cells in the presence of aggresomes created by overexpressing GFP-α-synA53T.
A-A'') Overexpression of GFP-αsynA53T form aggresomes in HeLa cells, aggresome positive cells have a reduced microtubule network, visualised by α-tubulin. **B-B'')** Cold treating the cells depolymerised the microtubules as the staining disappears, while the aggresome created by the overexpression of GFP-αsynA53T can bee seen juxtaposed at the nucleus. **C-C'')** At 0.5' of warming, microtubule nucleation is not seen with GFP-αsynA53T expressed throughout the cytoplasm. **D-D'')** At 1' of warming microtubule nucleation as a characteristic aster can be seen at the untransfected cell, though the cell overexpressing GFP-αsynA53T has no microtubule staining. **E-E'')** By 1.5' of warming, the untransfected cells have re-established the microtubule network with extensive α-tubulin staining yet, there are no microtubules seen at the cell overexpressing GFP-αsynA53T, with increased aggreagtion observed. **F-F'')** At 10' of warming microtubule staining is visible appearing as a characteristic aster near the nucleus, with GFP-αsynA53T expressed throughout the cytoplasm. DNA/nuclei stained with DAPI. Scale bars 10 μm.

4.2.7 SH-SY5Y cells can dynamically re-establish the microtubule network after cooling.

As aggresomes generated through proteasome inhibition or overexpression of GFP-tagged αsyn or the familial mutants drastically reduced microtubule nucleation, resulting in a compromised microtubule network. It would be interesting to see whether this is the same for SH-SY5Y cells since, this cell line is commonly used in Parkinson's research as they are considered to hold biochemical properties similar to neurons. As in HeLa, SH-SY5Y cells were assessed for microtubule nucleation by the microtubule regrowth assay. SH-SY5Y cells were fixed at different time-points during the assay including before and after depolymerisation of microtubules and after warming allowing the network to reform. Cells were then stained with anti-α-tubulin to visualise the microtubules and γ-tubulin for the centrosome.SH-SY5Y cells, have an extensive structured microtubule network, visualised by α-tubulin. The microtubules can be seen nucleating from the centrosome as they extend and stretch across the cytoplasm (Figure 4.7 A-A''). Following depolymerisation α-tubulin localises to the cytoplasm (Figure 4.7 B-B''). Upon warming to 37°, microtubule nucleation is observed as microtubules emerge from the centrosome (Figure 4.7 C-C''). As warming continues increase in microtubule staining can be seen, with both long and short microtubules extending into the cytoplasm. Some microtubules have detached from the centrosome while, others continue to nucleate from the centrosome as they elongate (Figure 4.7 D-D'' and E-E''). By 10 mins a new network has formed, microtubules have been arranged in organised network with a few microtubules maintaining contact with the centrosome (Figure 4.7 F-F'').

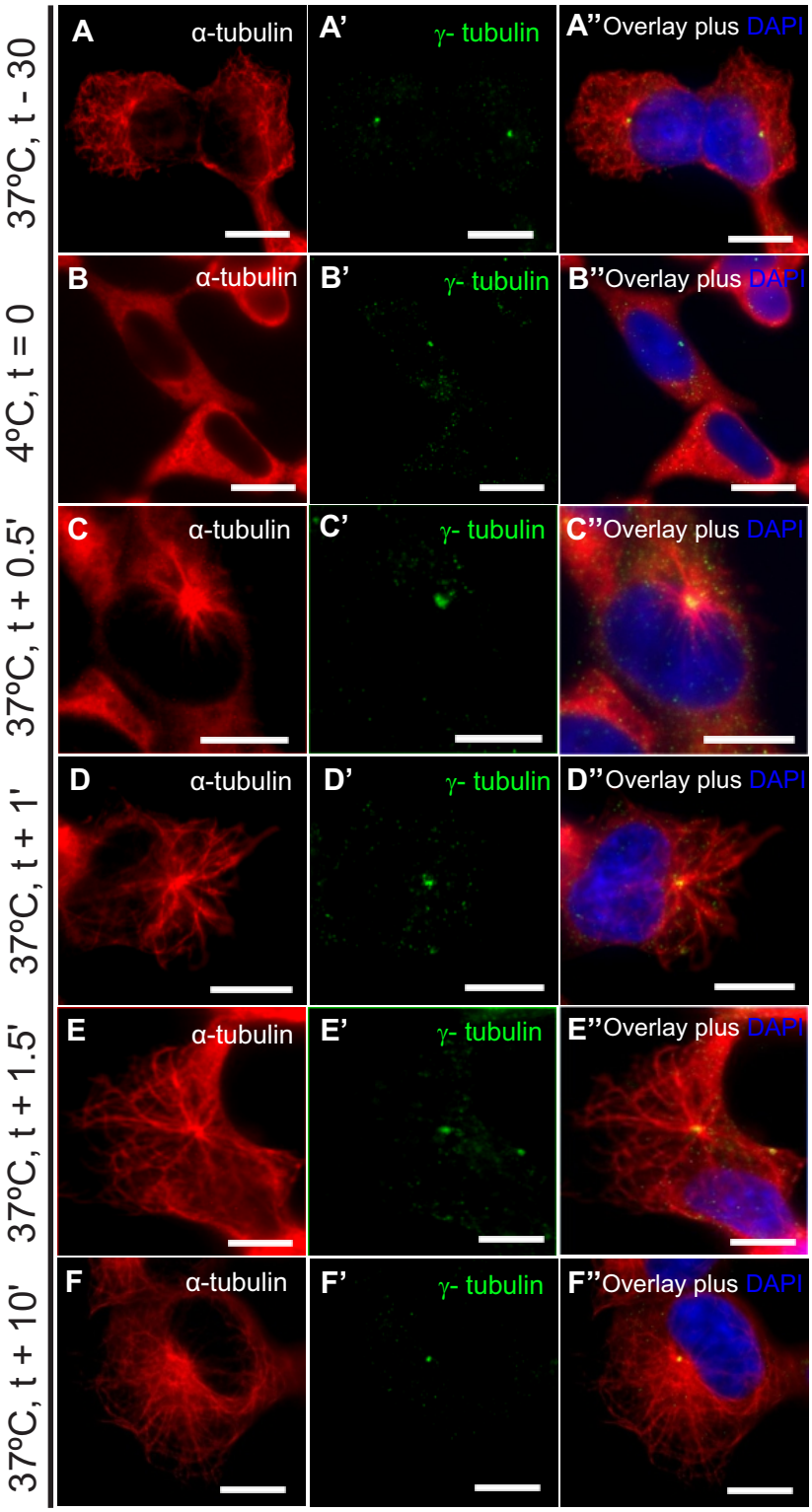
37°C, t - 30
4°C, t = 0
37°C, t + 0.5'
37°C, t + 1'
37°C, t + 1.5'
37°C, t + 10'
A α-tubulin
A' γ- tubulin
A" Overlay plus DAPI
B α-tubulin
B' γ- tubulin
B" Overlay plus DAPI
C α-tubulin
C' γ- tubulin
C" Overlay plus DAPI
D α-tubulin
D' γ- tubulin
D" Overlay plus DAPI
E α-tubulin
E' γ- tubulin
E" Overlay plus DAPI
F α-tubulin
F' γ- tubulin
F" Overlay plus DAPI

Figure 4.7 SH-SY5Y cells can re-establish the microtubule network within 10 minutes.
A-A'') SH-SY5Y cells have an extensively structured microtubule network, microtubules visualised by α-tubulin. The network is maintained by the centrosome stained by γ-tubulin, where it nucleates microtubules that extend across the cell. **B-B'')** Cold treating the cells for 30' depolymerises the microtubule filaments as microtubule staining disappears and α-tubulin appears diffuse through the cytoplasm. **C-C'')** Upon warming for 0.5', microtubules nucleate from the centrosome forming a characteristic aster near the nucleus. **D-D'')** At 1' of warming increased microtubule staining is apparent as the microtubule aster has increased size, extending microtubules further through the cytoplasm. **E-E'' and F-F'')** By 10' the microtubule filaments have further stretched through the cytoplasm reaching the periphery of the cell, with the aster appearing fuller of microtubules. DNA/nuclei stained with DAPI. Scale bars 10 μm.

4.2.8 In the presence of aggresomes SH-SY5Y cells fail to re-establish the microtubule network

I have shown that SH-SY5Y have a well-established microtubule network, I next tested whether aggresomes would obstruct microtubule nucleation affecting microtubule network integrity as seen in HeLa cells. SH-SY5Y cells were treated with 1 μM MG-132 for 18 hours, cells were assessed for microtubule nucleation activity by the microtubule regrowth assay. Cells were fixed at different time-points during the assay including before and after microtubule depolymerisation and warming when the network reforms. They were stained with anti-α-tubulin and anti-γ-tubulin to visualise the microtubules and centrosome respectively. In the presence of aggresomes, microtubule staining is severely reduced, as most of α-tubulin staining localises to the aggresome. Microtubules are drastically reduced in length with a few at the periphery of the cell, with no obvious microtubule arrangement. The characteristic punctae representing the centrosome is also not visible as, γ-tubulin staining localises to the aggresome and the cytoplasm (Figure 4.8 A-A''). Depolymerisation of microtubules resulted in α-tubulin localising to the cytoplasm and aggresome, closer observations show increased α-tubulin staining around the aggresome. Since, the size of the aggresome varies, it is sometimes difficult to distinguish the centrosome as larger aggresomes envelope the centrosome. In this image, the γ-tubulin staining shows localisation to the aggresome as well as the centrosome while, γ-tubulin expression at the centrosome appears more profuse (Figure 4.8 B-B''). Upon warming to 37°C, there is no sign of microtubule nucleation as α-tubulin continues to localise to the cytoplasm and the aggresome (Figure 4.8 C-C'', D-D'' and E-E''). Microtubule nucleation is severely delayed as, microtubules are only seen at 10 min of warming. Though microtubules can be seen emanating from the centrosome, microtubule length is reduced with only a few extending across the cytoplasm and that

too with a disoriented arrangement. Fewer microtubules result in an incomplete network (Figure 4.8 F-F'').

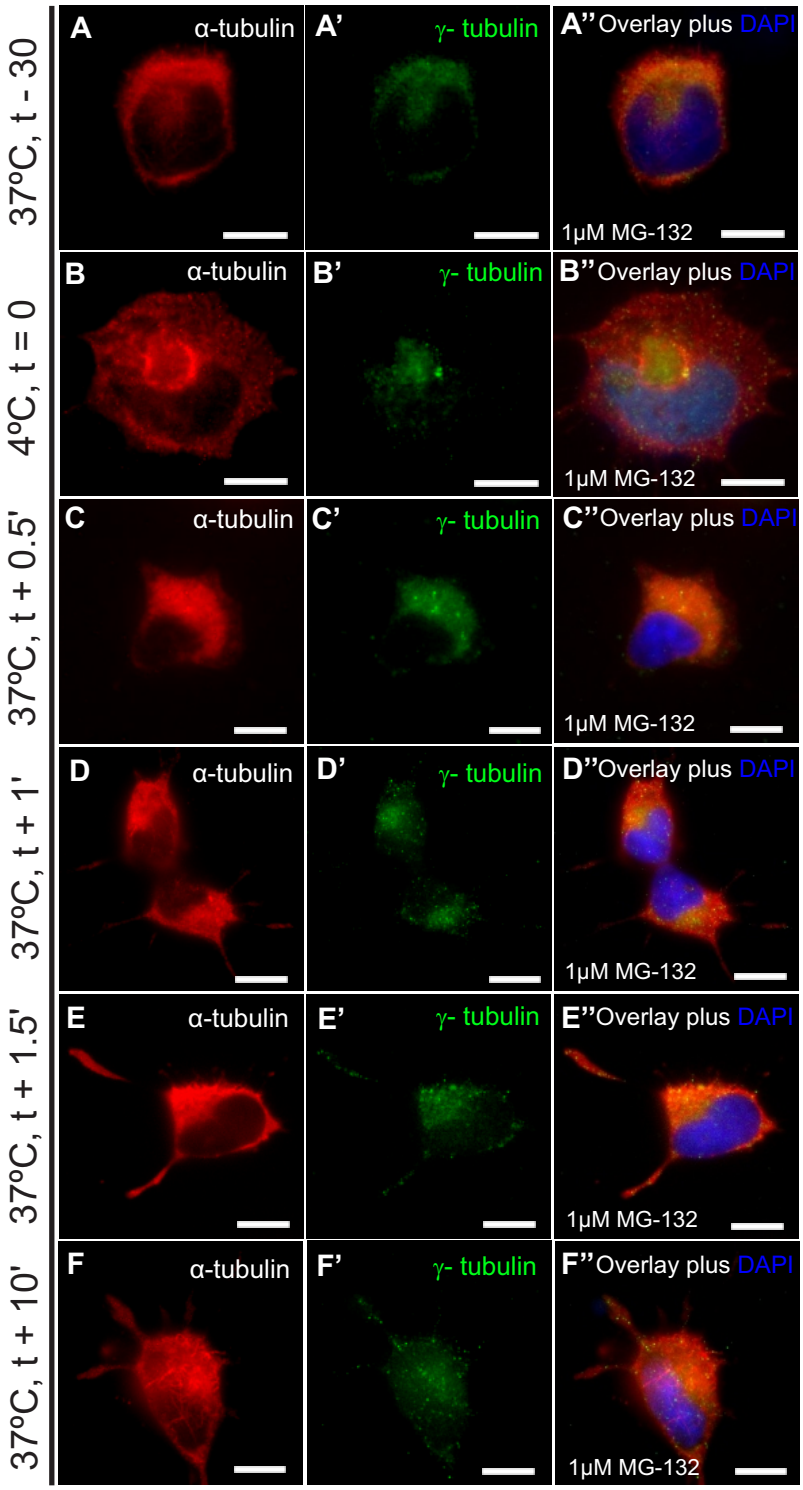

Figure 4.8 In the presence of aggresomes SH-SY5Y cells fail to re-establish the microtubule network.
SH-SY-5Y cells were treated with MG-132 to form aggresomes. Microtubules are visualised by α-tubulin and the centrosome is labelled by γ-tubulin. **A-A'')** The microtubule filaments appear very short, mainly localising to the aggresome and the periphery of the cell. Similarly, the γ-tubulin stain does not detect the centrosome, as it also marks the aggresome. **B-B'')** Cold treating the cells, depolymerises the microtubules, with the α-tubulin stain localising to the aggresome and diffused through the cytoplasm. γ-tubulin detects both the aggresome and the centrosome with, the centrosome in close proximity to the aggresome. **C-C'', D-D'' and E-E'')** Upon warming, the α-tubulin continues to mark the aggresome as well as diffused cytoplasmic staining, with no microtubule staining visible. **F-F'')** By 10' of warming microtubule staining is visible, appearing short with a random organisation. DNA/nuclei stained with DAPI. Scale bars 10 μm.

4.2.9 Overexpression of GFP alone does not affect microtubule nucleating activity of the centrosome in SH-SY5Y cells

Aggresome formation by MG-132, showed severely reduced microtubule nucleation activity in SH-SY5Y cells, where cells failed to build a new microtubule network. As aggresomes generated through proteasome inhibition had such drastic affects it is also possible aggresomes generated by the overexpression of GFP-tagged αsyn or the familial mutants could have similar effects as, it did in HeLa cells. I next tested if this is the case. As a control, SH-SY5Y cells were transfected with GFP alone for 72 hours followed by the microtubule regrowth assay. Cells were fixed at set stages of the assay including before and after microtubule depolymerisation and warming when a new network is formed. Cells were stained with α-tubulin to visualise the microtubules. Overexpression of GFP is seen throughout the cytoplasm. An intact and well-established microtubule network is visible as microtubules extend across the cytoplasm to the periphery of the cell. Microtubule staining is comparable in cells were GFP is overexpressed and in cells without (Figure 4.9 A-A''). Depolymerisation of microtubules resulted in diffused α-tubulin staining at the cytoplasm (Figure 4.9 B-B''). Upon warming to 37°C, microtubule staining is visible as microtubules nucleate from the centrosome forming the characteristic aster (Figure 4.9 C-C''). As warming continues, microtubules lengthen and extend towards the boundary of the cell. Microtubules have an ordered arrangement as they radiate from the centrosome, as some microtubules continuously maintain contact with the centrosome (Figure 4.9 D-D'' and E-E''). Cells overexpressing GFP show similar microtubule staining and arrangement throughout the assay as cells without GFP. SH-SY5Y cells overexpressing GFP are able to construct a new microtubule network (Figure 4.9 F-F'').

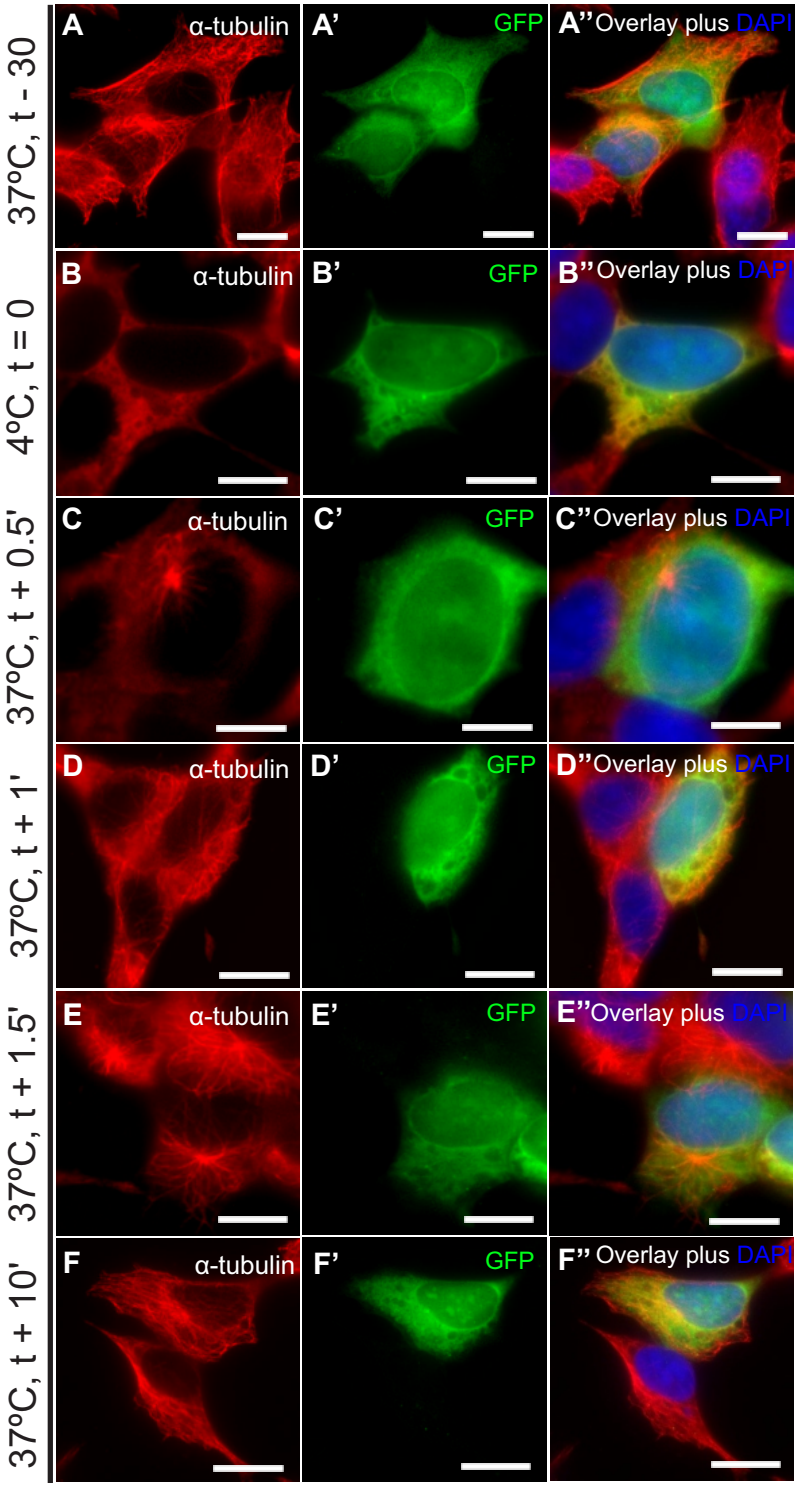
37°C, t - 30
4°C, t = 0
37°C, t + 0.5'
37°C, t + 1'
37°C, t + 1.5'
37°C, t + 10'
A
α-tubulin
A'
GFP
A"Overlay plus DAPI
B
α-tubulin
B'
GFP
B"Overlay plus DAPI
C
α-tubulin
C'
GFP
C"Overlay plus DAPI
D
α-tubulin
D'
GFP
D"Overlay plus DAPI
E
α-tubulin
E'
GFP
E"Overlay plus DAPI
F
α-tubulin
F'
GFP
F" Overlay plus DAPI

Figure 4.9 Overexpression of GFP does not affect microtubule nucleating activity of the centrosome in SH-SY5Y cells.
SH-SY5Y cells were transfected with control GFP expression construct, after 72 hours cells were processed for the microtubule regrowth assay, they were fixed before cooling, immediately after cooling and when warmed up to 37°C. Cells were stained with anti-α-tubulin. **A-A'')** SH-SY5Y cells have an extensive microtubule network, with microtubules seen extending through the cells cytoplasm **B-B'')** Cooling depolymerises the microtubules as -α-tubulin is now seen at the cytoplasm. **C-C'', D-D'', E-E'' and F-F'')** Upon warming to 37°C, microtubule nucleation is observed with the characteristic aster observed within in 0.5', as warming continues microtubules extend and stretch to the periphery of the cell while microtubules emanating from the centrosome continue to be observed. By 10' of warming the microtubule network has been re-established, as comparable microtubule staining is observed to prior cooling. DNA/nuclei stained with DAPI. Scale bar 10 μm.

4.2.10 SH-SY5Y cells fail to build a new microtubule network when GFP-tagged α-syn is overexpressed

Overexpression of GFP-tagged α-syn form aggresomes in SH-SY5Y cells. I next tested if these aggresomes supress microtubule nucleation in SH-SY5Y cells. SH-SY5Y cell were transfected with GFP-tagged α-syn for 72 hours, followed by the microtubule regrowth assay. SH-SY5Y cells were fixed at set time-points of the assay and stained with anti-α-tubulin to visualise the microtubules. Overexpression of GFP-tagged α-syn is seen throughout the cytoplasm with increased aggregation next to the nucleus. Microtubule density is severely reduced as, microtubule staining is seen mainly to localise at the aggresome with a few microtubules at the cytoplasm with no obvious arrangement (Figure 4.10 A-A''). When microtubules were depolymerised the α-tubulin appeared diffused within the cytoplasm. It is also seen localising at the aggresome where increased aggregation of GFP-tagged α-syn is observed (Figure 4.10 B-B''). By warming cells to 37°C, microtubule nucleation is not observed at the earlier time-points as α-tubulin continues to appear diffused throughout the cytoplasm and staining the aggresome (Figure 4.10 C-C'', D-D'' and E-E''). Only at later time-points there is evidence of microtubule nucleation, though there are very few microtubules that have no clear arrangement (Figure 4.10 F-F''). While, cells overexpressing GFP-tagged α-syn showed partial microtubule nucleation suppression as there is some evidence of microtubule nucleation but not enough to establish a new network. Nearby cells that did not get transfected were able to efficiently build a new structured network.

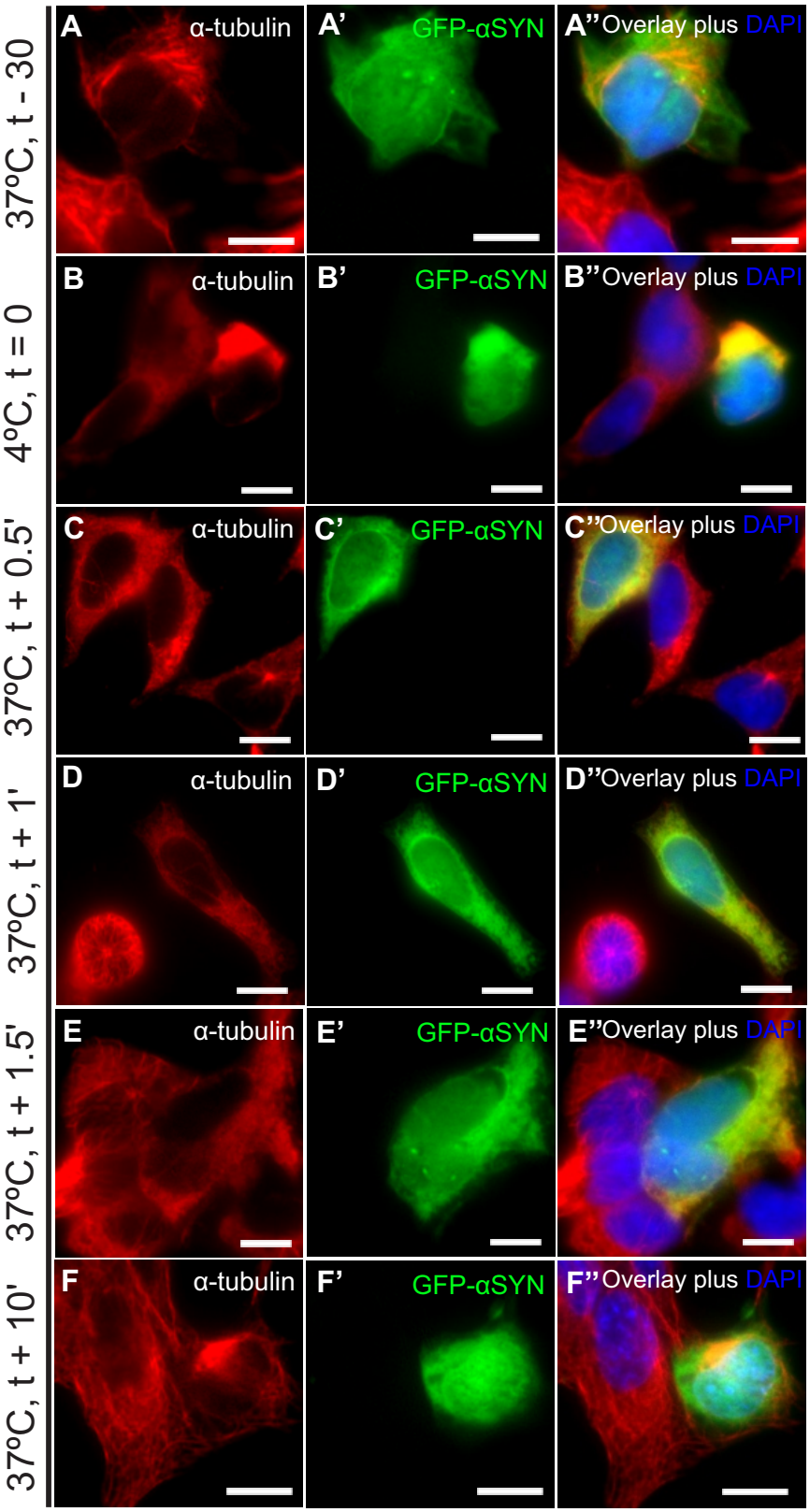
37°C, t - 30
4°C, t = 0
37°C, t + 0.5'
37°C, t + 1'
37°C, t + 1.5'
37°C, t + 10'
A α-tubulin
A' GFP-αSYN
A" Overlay plus DAPI
B α-tubulin
B' GFP-αSYN
B" Overlay plus DAPI
C α-tubulin
C' GFP-αSYN
C" Overlay plus DAPI
D α-tubulin
D' GFP-αSYN
D" Overlay plus DAPI
E α-tubulin
E' GFP-αSYN
E" Overlay plus DAPI
F α-tubulin
F' GFP-αSYN
F" Overlay plus DAPI

Figure 4.10 Overexpression of GFP-tagged α-syn disrupts microtubule nucleation in SH-SH5Y cells.
SH-SY5Y cell were transfected with GFP-tagged α-syn, after 72 hours cells were processed for the microtubule regrowth assay. Cells were fixed before cooling, immediately after cooling and upon warming to 37°C. Cells were stained with anti-α-tubulin. **A-A'')** Cells overexpressing GFP-tagged α-syn have a reduced microtubule network as reduced α-tubulin staining is observed. α-tubulin staining predominantly localises to the aggresome seen next to the nucleus. Overexpression GFP-tagged α-syn, is widespread throughout the cytoplasm though increased aggregation is also seen next to the nucleus, co-localising with α-tubulin staining. **B-B'')** Cooling depolymerises the microtubules as α-tubulin is now seen at the cytoplasm, increase α-tubulin staining is seen localising at the aggresome which also co-localises to the increased aggregation signal of GFP-tagged α-syn. **C-C'', D-D'', E-E'' and F-F'')** Upon warming to 37°C, α-tubulin staining continues to localise at the cytoplasm, reduced microtubule staining is observed even at longer incubations time-points. The limited microtubule staining observed appears random with no obvious nucleation pattern, with either very short sporadically positioned microtubules or a few very long microtubules, while cells that have not been transfected in same field of view are able to nucleate microtubules and re-establish the network. DNA/nuclei stained with DAPI. Scale bars 10 μm.

4.2.11 SH-SY5Y cells fail to establish a new microtubule network when GFP-tagged α-synA30P is overexpressed

I have shown aggresomes formed by the overexpression of GFP-tagged α-syn supresses microtubule nucleation in SH-SY5Y cells, preventing cells from re-building a new network. I next tested whether aggresomes formed by the overexpression of GFP-tagged α-synA30P has a similar affect. SH-SY5Y cells were transfected with GFP-tagged α-synA30P for 72 hours followed by the microtubule regrowth assay to assess microtubule nucleation. Cells were fixed at set time-points of the assay and stained with anti-α-tubulin to visualise the microtubules. Overexpression of GFP-tagged α-synA30P is seen throughout the cytoplasm as well as the overexpression forming aggregates. Microtubule staining is limited with very diffused α-tubulin staining at the cytoplasm, while neighbouring cells have an organised microtubule network (Figure 4.11 A-A''). After, microtubule depolymerisation α-tubulin continues to localise to the cytoplasm (Figure 4.11 B-B''). When cells were warmed up to 37°, microtubule nucleation is not observed as, α-tubulin continues to localise to the cytoplasm (Figure 4.11 C-C''). As warming continues even till the last time-point there is no evidence of any microtubule nucleation activity, as α-tubulin staining does not change (Figure 4.11 D-D'' E-E'' and F-F''). Only cells that do not overexpress GFP-tagged α-synA30P show microtubule staining, where nucleating microtubules form an aster which eventually extend across to establish a new microtubule network.

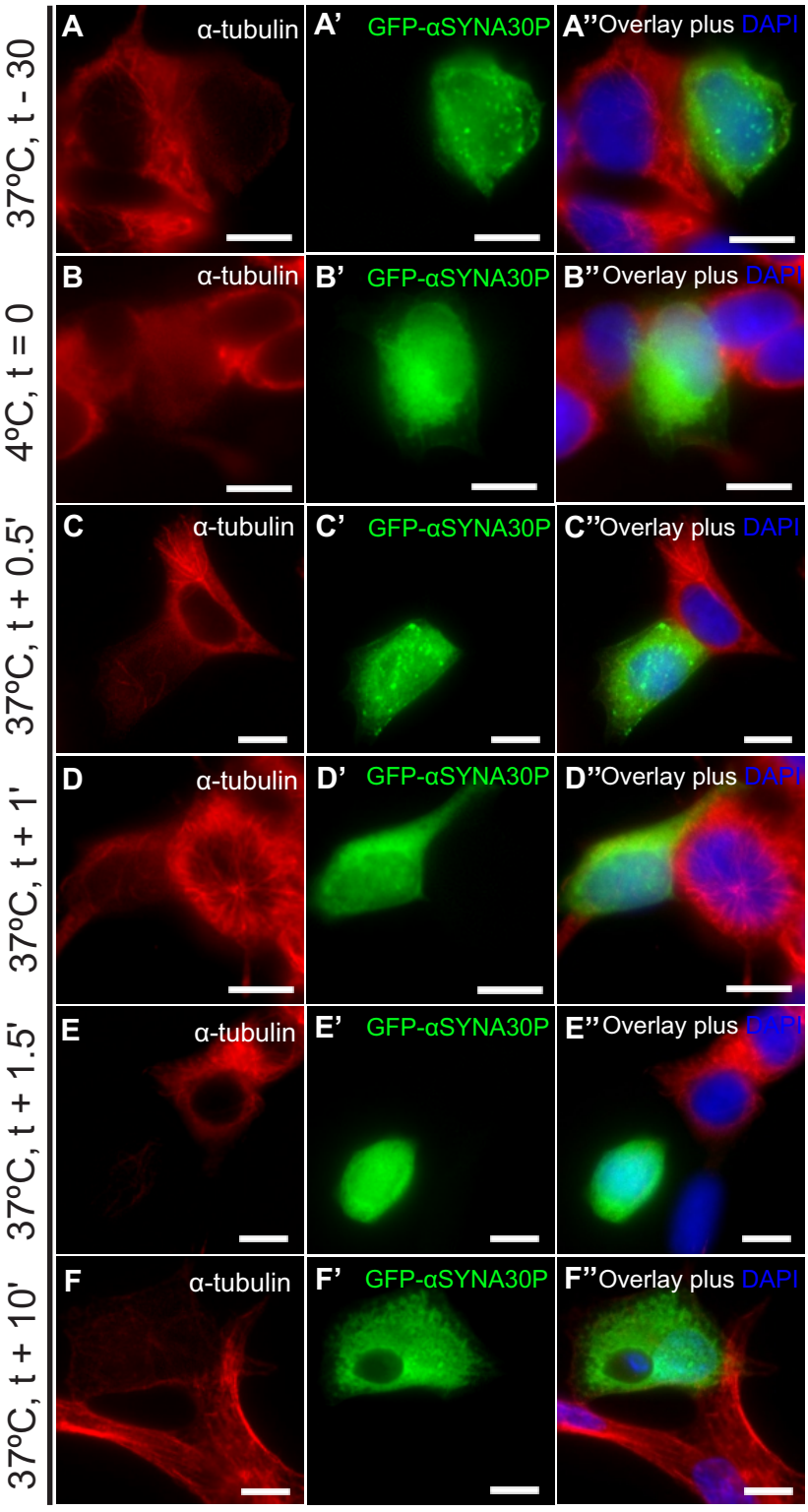
A
α-tubulin
A'
GFP-αSYNA30P
A"Overlay plus DAPI
B
α-tubulin
B'
GFP-αSYNA30P
B"Overlay plus DAPI
C
α-tubulin
C'
GFP-αSYNA30P
C"Overlay plus DAPI
D
α-tubulin
D'
GFP-αSYNA30P
D"Overlay plus DAPI
E
α-tubulin
E'
GFP-αSYNA30P
E"Overlay plus DAPI
F
α-tubulin
F'
GFP-αSYNA30P
F"Overlay plus DAPI
37°C, t - 30
4°C, t = 0
37°C, t + 0.5'
37°C, t + 1'
37°C, t + 1.5'
37°C, t + 10'

Figure 4.11 Overexpression of GFP-tagged α-synA30P, prevents the re-establishment of the microtubule network in SH-SH5Y cells.
SH-SY5Y cells were transfected with GFP-tagged α-synA30P, after 72 hours cells were processed for the microtubule regrowth assay. Cells were fixed at different time-points including, before cooling, immediately after cooling and when warmed up to 37°C, at set incubation time-points. Cells were stained with anti-α-tubulin to visualise the microtubules. **A-A'')** The microtubule network is reduced in cells overexpressing GFP-tagged α-synA30P, with α-tubulin localising to the cytoplasm. **B-B'')** Cooling the cells depolymerises the microtubules, the GFP signal is seen throughout the cytoplasm, while increased aggregation of GFP-tagged α-synA30P is seen next to the nucleus. **C-C'', D-D'', E-E'' and F-F'')** Upon warming to 37°C, minimal microtubule nucleation is seen, as reduced microtubule filaments are observed. Either short or long microtubules are observed sporadically distributed within the cytoplasm. Cells that are not overexpressing GFP-tagged α-synA30P are able to re-build the microtubule network as comparable α-tubulin staining is observed before cooling and at the last time-point of warming. DNA/nuclei stained with DAPI. Scale bars 10 μm.

4.2.12 SH-SY5Y cells fail to establish a new microtubule network when GFP-tagged α-synA53T is overexpressed

Overexpression of GFP-tagged α-synA30P in SH-SY5Y cells completely inhibited microtubule nucleation. It is possible GFP-tagged α-synA53T could also disrupt microtubule nucleation. I next tested if aggresomes generated through overexpression of GFP-tagged α-synA53T as shown in chapter 3 could also hinder microtubule nucleation. SH-SY5Y cell were transfected with GFP-tagged α-synA53T for 72 hours, followed by microtubule regrowth to assess microtubule nucleation. Transfected cells were fixed at set time-points of the assay including, before and after microtubule polymerisation and warming as the network is reforming. Cells were stained with anti-α-tubulin to label the microtubules. Cells overexpressing GFP-tagged α-synA53T have a reduced microtubule network with majority of α-tubulin staining localising to the aggresome, cytoplasm and the few microtubules at the periphery of the cell. Overexpression is seen throughout the cytoplasm with regions of increased aggregation next to the nucleus (Figure 4.12 A-A''). Once microtubules were depolymerised α-tubulin had a diffused stain at the cytoplasm (Figure 4.12 B-B''). Upon warming to 37°C, microtubule nucleation is severely delayed as there is no microtubule staining visible at earlier time-points (Figure 4.12 C-C'' and D-D''). It is only in the last two time-points microtubule nucleation is observed. Although, microtubules appear to be emitting from the centrosome, there is no obvious arrangement such as the characteristic aster seen in control cells (Figure 4.12 E-E''). Microtubules appear both short and long with majority of them localising at the periphery of the cell, with no focal point (Figure 4.12 F-F'').

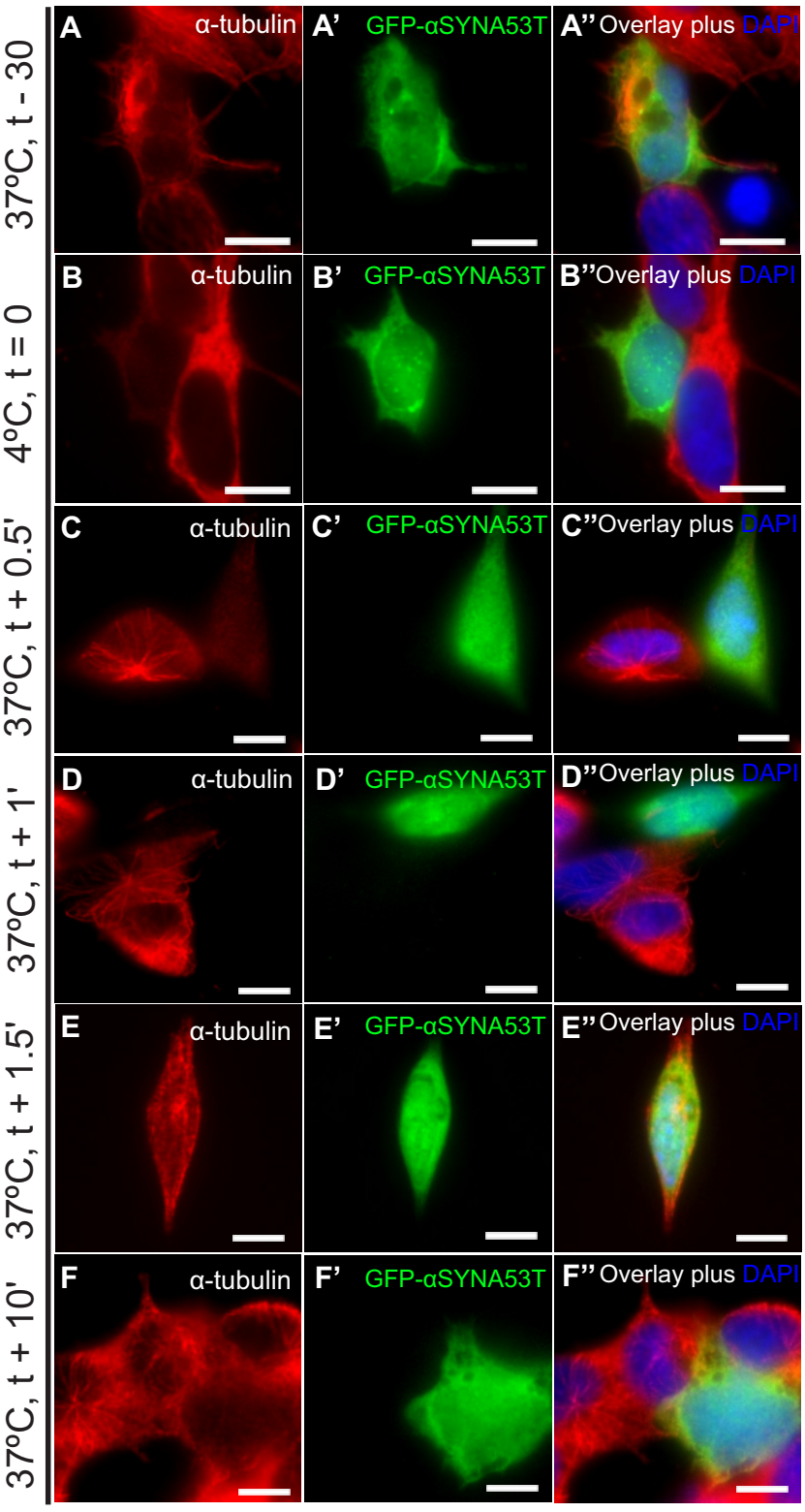
A
α-tubulin
A'
GFP-αSYNA53T
A"
Overlay plus DAPI
B
α-tubulin
B'
GFP-αSYNA53T
B"
Overlay plus DAPI
C
α-tubulin
C'
GFP-αSYNA53T
C"
Overlay plus DAPI
D
α-tubulin
D'
GFP-αSYNA53T
D"
Overlay plus DAPI
E
α-tubulin
E'
GFP-αSYNA53T
E"
Overlay plus DAPI
F
α-tubulin
F'
GFP-αSYNA53T
F"
Overlay plus DAPI
37°C, t - 30
4°C, t = 0
37°C, t + 0.5'
37°C, t + 1'
37°C, t + 1.5'
37°C, t + 10'

Figure 4.12 Overexpression of GFP-tagged α-synA53T prevents SH-SY5Y cells from re-building the microtubule network.
SH-SY5Y cells were transfected with GFP-tagged α-synA53T, after 72 hours cells were processed for the microtubule regrowth assay. Cells were fixed before cooling, immediately after cooling and upon warming to 37°C. Microtubules were visualised by staining cells with anti-α-tubulin. **A-A'')** Microtubule staining is reduced in cells overexpressing GFP-tagged α-synA53T, α-tubulin localises to the cytoplasm and the aggresome where increased staining is observed. The GFP signal is seen throughout the cytoplasm as well as, increased aggregation next to the nucleus. **B-B'')** Cooling the cells, depolymerised the microtubules as α-tubulin stains the cytoplasm. **C-C'', D-D'', E-E'' and F-F'')** Upon warming to 37°C, microtubule nucleation is not seen at earlier incubation time-points as α-tubulin continues to localise to the cytoplasm. It is only at the last two time-points microtubule staining is observed, microtubules appear short with majority of them localising at the periphery of the cells. Cells that have not been transfected with GFP-tagged α-synA53T were able to re-establish the microtubule network as increased structured microtubule staining observed. DNA/nuclei stained with DAPI. Scale bars 10 μm.

4.2.13 Differentiated SH-SY5Y cells re-establish the microtubule network after microtubule network has depolymerised.

I have shown aggresomes disrupt microtubule nucleation in HeLa and SH-SY5Y cells, whether aggresomes were generated through proteasome inhibition or overexpression of GFP-tagged α-syn (or the familial mutants). It would be interesting to see if a similar effect is observed in a more neuronal like model such as differentiated SH-SY5Y cells. I have shown (chapter 3) SH-SY5Y cells can be differentiated, resembling neurons both morphologically and biochemically. I have also shown differentiated SH-SY5Y cells can form aggresomes when treated with MG-132 (chapter 3). I next tested if aggresomes had an effect on microtubule nucleation and microtubule network integrity. As a control differentiated SH-SY5Y cells were assessed for microtubule nucleation activity by the microtubule regrowth assay. Cells are fixed at different time-points of the assay including, before and after microtubule depolymerisation and when network is reformed during warming. They were then stained with anti-α-tubulin to visualise microtubules and anti-TH to confirm dopaminergic cells. Differentiated SH-SY5Y cells, have extensive microtubule staining. Microtubules appear compact at the developing neurites whereas at the cell body microtubules have a fibrous appearance similar to network in HeLa and SH-SY5Y cells. Tyrosine hydroxylase is expressed throughout the cytoplasm though, some regions have a more profuse staining (Figure 4.13 A-A''). Depolymerising the microtubule shows α-tubulin appearing diffused throughout the cytoplasm (Figure 4.13 B-B''). Upon warming to 37°C, microtubule nucleation is observed where microtubules nucleate forming the characteristic aster (Figure 4.13 C-C'' and D-D''). As warming continues

microtubules extend and stretch across the cytoplasm as microtubules polymerise. The microtubules arrange themselves in an organised arrangement where again they appear tightly compact around the extending neurite and as a filamentous network around the cell body (Figure 4.13 E-E'' and F-F''). By 15 mins of warming differentiated SH-SY5Y cells have established a new microtubule network after the network was depolymerised.

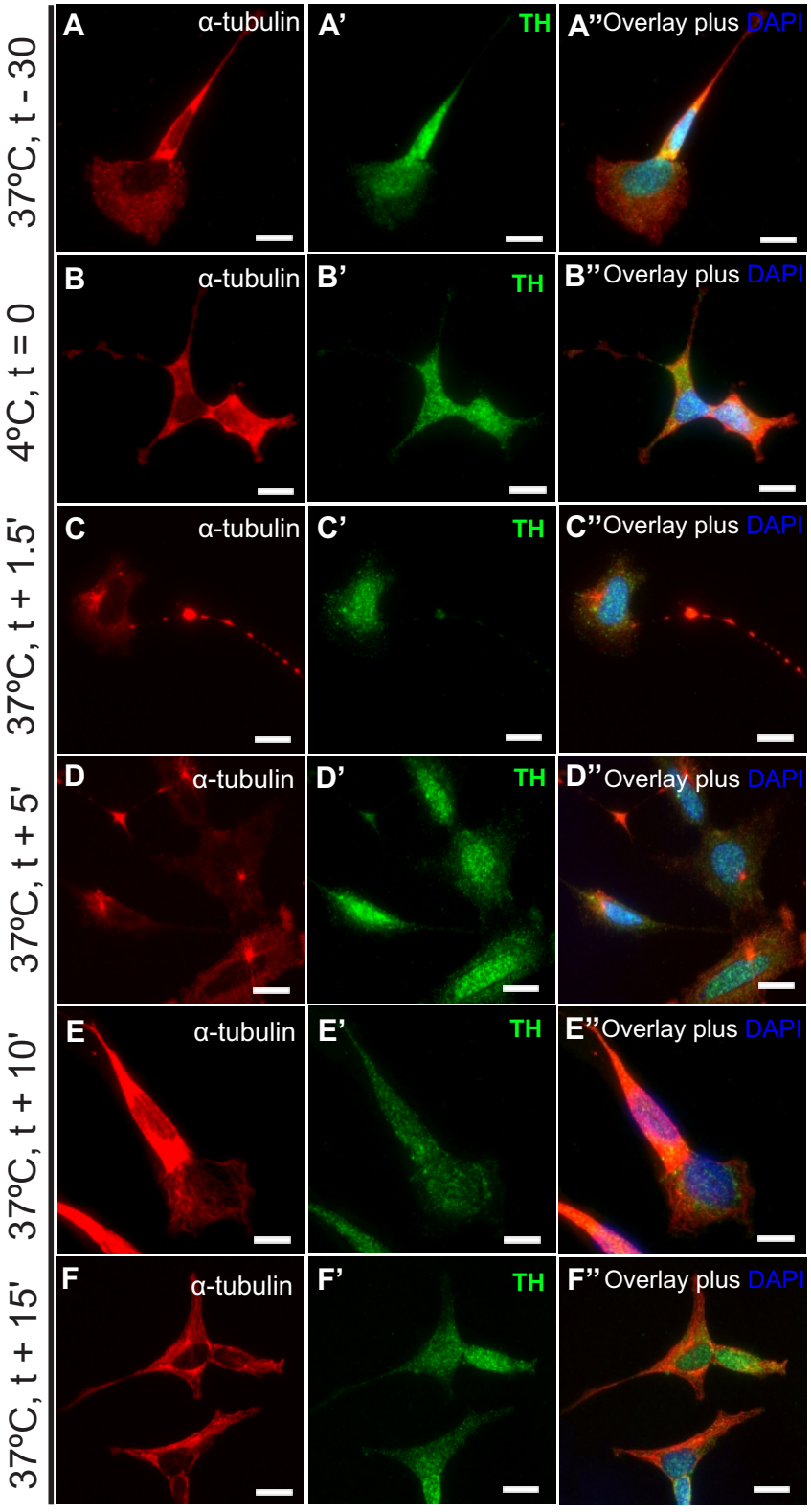

Figure 4.13 Differentiated SH-SY5Y cells can re-build the microtubule network after the microtubule network has been depolymerised.
SH-SY5Y cells were differentiated by treating cells with 10 μM retinoic acid over a period of seven days. Differentiation was assessed by tyrosine hydroxylase (TH) staining and morphological changes including the extension of neurites and a smaller cell body. Differentiated SH-SY5Y cells were processed for the microtubule regrowth assay. Cells were fixed before cooling, immediately after cooling and upon warming to 37°C at set incubation time-points. Cells were stained with anti-α-tubulin to stain microtubules and anti-TH to confirm dopaminergic like cells. **A-A'')** The microtubule network of differentiated SH-SY5Y cells is very compact around the extending neurite, while at the cell body a filamentous network is observed. Positive tyrosine hydroxylase staining confirms cells are of dopaminergic nature. **B-B'')** Cooling the cells, depolymerised the microtubule network, as α-tubulin stain localises to the cytoplasm. **C-C'', D-D'', E-E'' and F-F'')** Upon warming to 37°C, microtubule nucleation is observed, the characteristic microtubule aster is seen at the cell body. As warming continues, the microtubules increase in length, stretching further across the cell body. By 10' comparable microtubule staining is seen to prior cooling with a similar arrangement of microtubules. The microtubule staining around the neurite is very compact while at the cell body the microtubules have a filamentous appearance. At longer incubation time-points the microtubule network has fully re-established with microtubules arranged in an organised manner, stretching and extending across cytoplasm and extending neurite. DNA/nuclei stained with DAPI. Scale bars 10 μm.

4.2.14 Differentiated SH-SY5Y cells fail to re-establish the microtubule network in the presence of aggresomes

I have shown differentiated SH-SY5Y cells have an established microtubule network and form aggresomes when treated with MG-132. I next tested if the presence of aggresomes obstruct the centrosome from nucleating microtubules and maintaining an organised microtubule network. Differentiated SH-SY5Y cells were treated with 1 μM MG-132 for 18 hours followed by the microtubule regrowth assay. Cells were fixed at different time-points during the assay including, before and after microtubules depolymerisation and during warming when the network is reformed. They were stained with anti-α-tubulin and anti –TH to visualise microtubules and confirm the presence of dopaminergic cells respectively. Tyrosine hydroxylase staining is observed throughout the cytoplasm confirming cells are of dopaminergic nature. In the presence of aggresomes, microtubule staining is severely reduced particularly, at the cell body. Closer observations show α-tubulin staining the aggresome seen next to the nucleus. The overall density of microtubules is reduced as individual tubulin filaments can be seen (Figure 4.14 A-A''). By depolymerising microtubules α-tubulin staining is seen diffused throughout the cytoplasm and at the aggresome (Figure 4.14 B-B''). Upon warming to 37°C, microtubule nucleation is delayed as microtubule staining is only observed at 15 mins of warming. At early time-points α-tubulin does not change from when the network was depolymerised

as α-tubulin continues to appear diffused throughout the cytoplasm (Figure 4.14 C-C'', D-D'' and E-E''). The microtubules nucleating at the last time-point, show unorganised arrangement of microtubule nucleation which have not extended across the cell body. As insufficient number of microtubules have nucleated from the centrosome, cells failed to build a new network (Figure 4.14 F-F'').

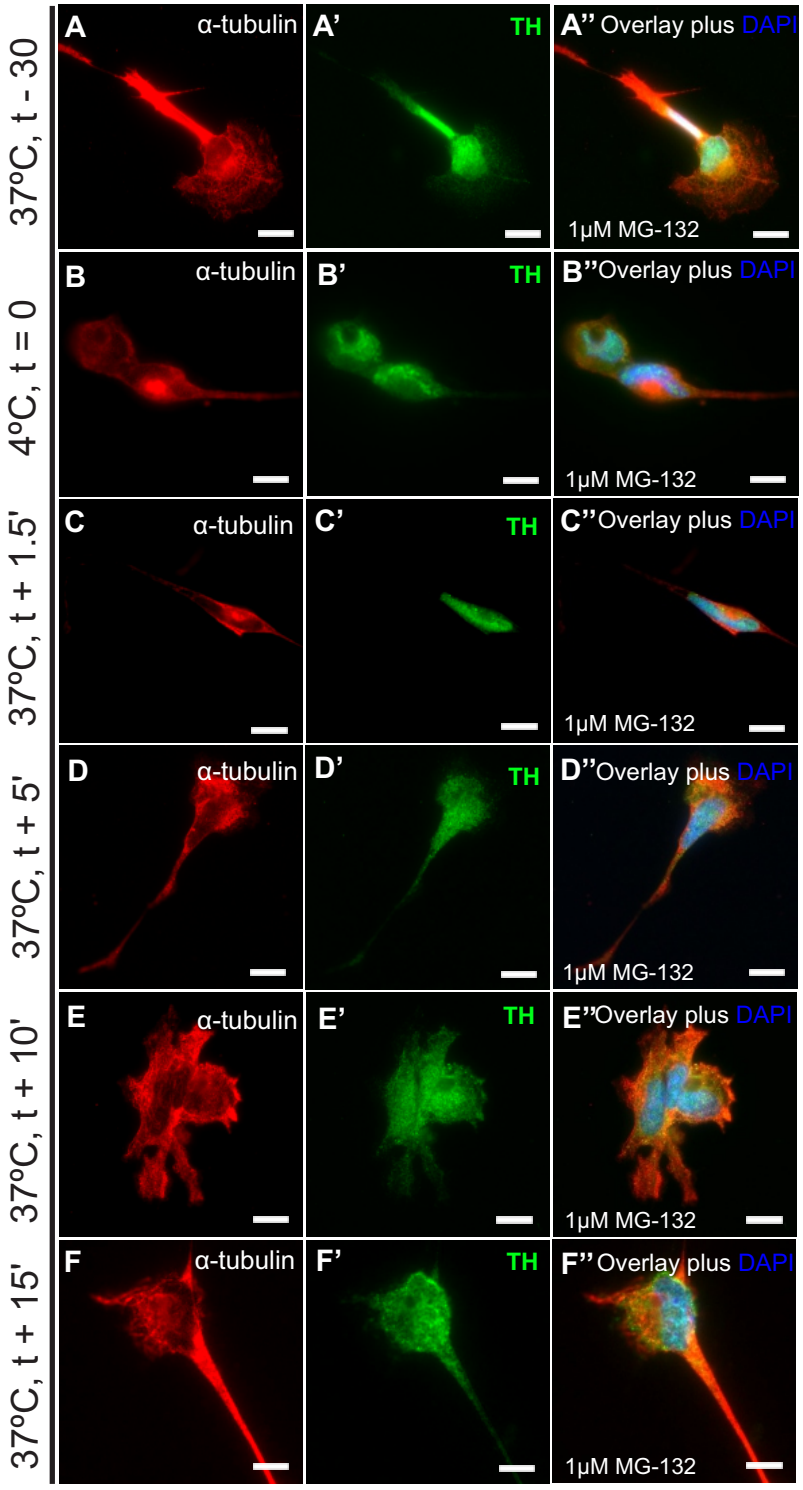

Figure 4.14 In the presence of aggresomes, differentiated SH-SY5Y cells fail to re-build the microtubule network.
Differentiated SH-SY5Y cells were treated with 1μM MG-132 for 18 hours to generate aggresomes. Cells were then processed for the microtubule regrowth assay, in brief, they were fixed before cooling, immediately after cooling and upon warming to 37°C at set incubation time-points. Cells were stained with anti-α-tubulin and anti-TH antibodies. A-**A'')** In the presence of aggresomes, reduced microtubule staining is observed, particular at the cell body of the cell, α-tubulin labels the microtubules as well as the aggresome, seen next to nucleus. Tyrosine hydroxylase is seen throughout the cytoplasm, indicative of dopaminergic like cell. **B-B'')** Cooling the cells, depolymerises the microtubule network, as α-tubulin now stains within the cytoplasm. **C-C'', D-D'', E-E'' and F-F'')** Upon warming to 37°C, α-tubulin staining continues to localise to the cytoplasm and the aggresome, only at the last incubation time of 15' microtubule staining was visible. Short microtubules can be seen next to nucleus, though they do not appear to a have structured organisation however the staining around the neurite reappears. DNA/nuclei stained with DAPI. Scale bars 10 μm.

4.2.15 Aggresomes prevent the re-establishment of the microtubule network

In summary, I have shown that aggresomes generated by MG-132 treatment or the overexpression of GFP-tagged α-syn wild-type or familial mutants disrupts the centrosome from nucleating and maintaining the microtubule network. Aggresomes generated via proteasome inhibition, by treating cells with MG-132 showed more severe affects than aggresomes generated through overexpression of GFP expression constructs encoding α-synuclein (Figure 4.15 A and C). Over 70% of control treated cells were able to re-establish the microtubule network in either condition, while this was less than 25% in the presence of aggresomes (Figure 4.15 A-D).

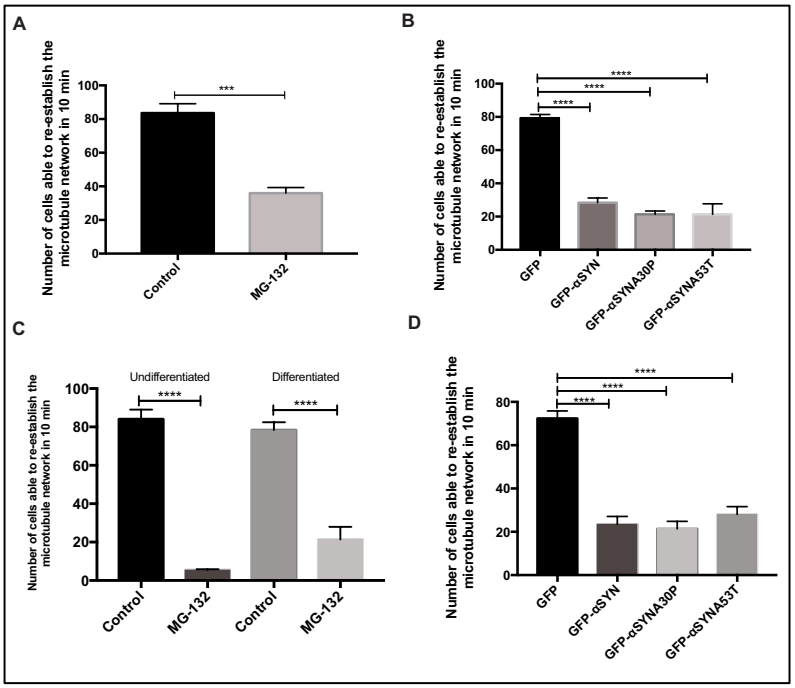

Figure 4.15 Aggresomes prevent the centrosome from re-establishing the microtubule network. Aggresomes generated by MG-132 treatment or the overexpression of GFP-tagged α-syn wild-type or familial mutants prevent the centrosome from nucleating and maintaining the microtubule network. Microtubule nucleation and re-establishment of this network was quantified by scoring cells (yes or no) whether the network was re-established in 10 mins. **A)** Quantification of microtubule regrowth in HeLa cell when treated with MG-132 (P<0.001, by Student's t-test, 100 cells, n=3. **B)** Quantification of microtubule regrowth in HeLa cells when α-synuclein was over expressed (P<0.0001, one way- ANOVA, 100 cells, n=3).**C)** Quantification of microtubule regrowth in undifferentiated and differentiated SH-SY5Y cells when treated with MG-132 (P<0.0001, by Student's t-test, 100 cells, n=3). **D)** Quantification of microtubule regrowth in SH-SY5Y when α-synuclein was over expressed (P<0.0001, one way- ANOVA, 100 cells, n=3).

4.2.16 HeLa cells fail to close the wound in the presence of aggresomes

Neurons are highly polarised cells; neuronal polarity is determined by microtubule arrangement, resulting in different functional compartments comprising of axons and dendrites. The microtubule network is also rearranged in response to polarity cues. In maturing neurons, the centrosome's location determines site of axon formation. Similarly, in cell migration the Golgi and centrosome orientate themselves towards the direction of cell locomotion. It is possible aggresomes could also disrupt this centrosomal function. One of the ways this can be assessed is by the wound assay. In brief, this involves removing a strip of cells from a confluent monolayer of cultured cells. Cells at the edge of the wound would migrate to close the gap. I first tested this in HeLa cells as I have shown they can form aggresomes when treated with MG-132 and are known to migrate. A confluent monolayer of cultured HeLa cells was treated with 10 μM MG-132 for 18 hours. A strip of cells is then removed using a p200 tip, changing media immediately after to remove detached cells. Cells were fixed at different time-points of the assay including 0 hours of migration, 5, 12 and 24 hours of migration. They were stained with anti-Golgi97 to visualise Golgi orientation and DAPI for whole cell migration. In control HeLa cells, DAPI staining shows cells have moved in to close the wound as the gap between the wound gets smaller. By 24 hours the cells have fully migrated in to close the wound (Figure 4.16 A-A'''). In the presence of aggresomes, cell migration is observed as the distance between the wound is narrower however, the rate of migration is reduced whereby in 24 hours the wound is still visible (Figure 4.16 B-B''' and D).

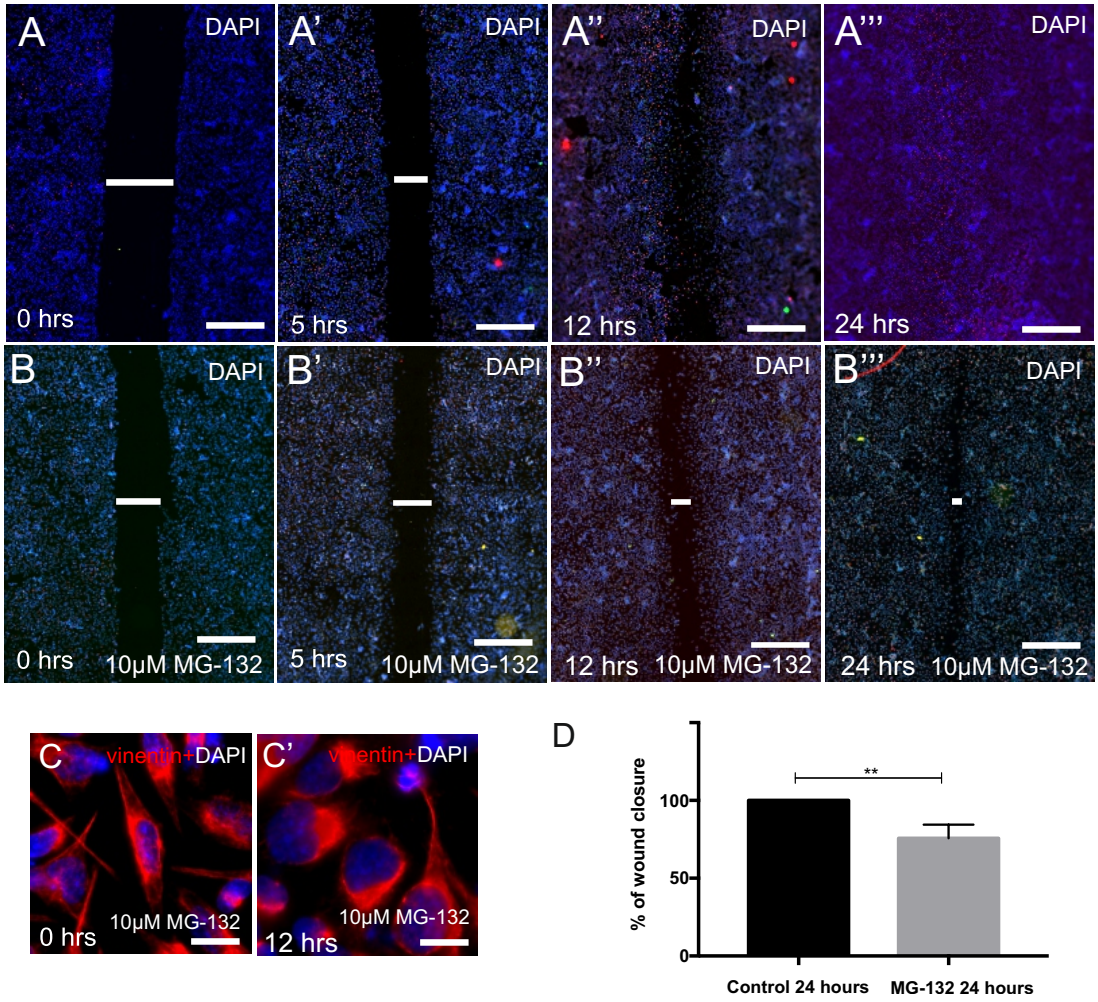

Figure 4.16 HeLa cells fail to close the wound in the presence of aggresomes.
A confluent monolayer of HeLa cells was either treated with 10 μM MG-132 or DMSO for 18 hours. Using a p200 tip a strip of cells is removed creating a wound, media is replenished removing detached cells. Cells were fixed at set time-points and stained with DAPI to visualise the nuclei. **A-A''')** In control treated cells, cell migration is observed as the distance between the wound gets smaller as the cells migrate to close the wound. Cell migration is observed within 5 hours of when the wound was created, cells continue to migrate, by 24 hours cells have migrated in and wound closure is observed. **B-B''')** In the presence of aggresomes, cells are able to migrate but at a much slower rate as the distance between the wound gets smaller however, by 24 hours the wound is still visible as cells were not able to migrate fast enough to close the wound. **C-C')** HeLa cells were treated with 10 μM MG-132 or DMSO for 18 hours, as a preliminary check to ensure aggresomes where formed, cells were stained with anti-vimentin antibody. In control treated cells the vimentin staining appears as a filamentous network caging the nuclei and extending across the cytoplasm. When treated with MG-132, vimentin staining changes to cage around the aggresome seen next to the nucleus. **D)** Quantification of wound closure $P<0.01$ by Student's *t*-test. A-A'''-B-B''')Scale bars 200 μm. C-C' Scale bars 10 μm.

4.2.17 The Golgi is not able to re-orientate itself towards the wound in the presence of aggresomes in HeLa cells

I have shown in control HeLa cells, wound closure is observed by 25 hours however, in the presence of aggresomes cell migration is slower where cells are not able to close the wound in 24 hours. Cells were stained with anti-Golgi97 and DAPI. A Golgi orientated within -45° and +45° of the wound was considered orientated towards the wound. In control HeLa cells, Golgi staining shows Golgi orientation is random from when the wound was formed. By 12 hours of migration cells at the leading edge of the wound show the Golgi has re-orientated itself towards the wound (Figure 4.17 A-A'). HeLa cells treated with 10 μM MG-132 also show random Golgi orientation at the beginning of the migration assay. However, at 12 hours of migration the number of cells with their Golgi orientated towards the wound is less than half (Figure 4.17 B-B'). In control cells over 60% of the cells had re-orientated their Golgi while this was only 40% in MG-132 treated cells.

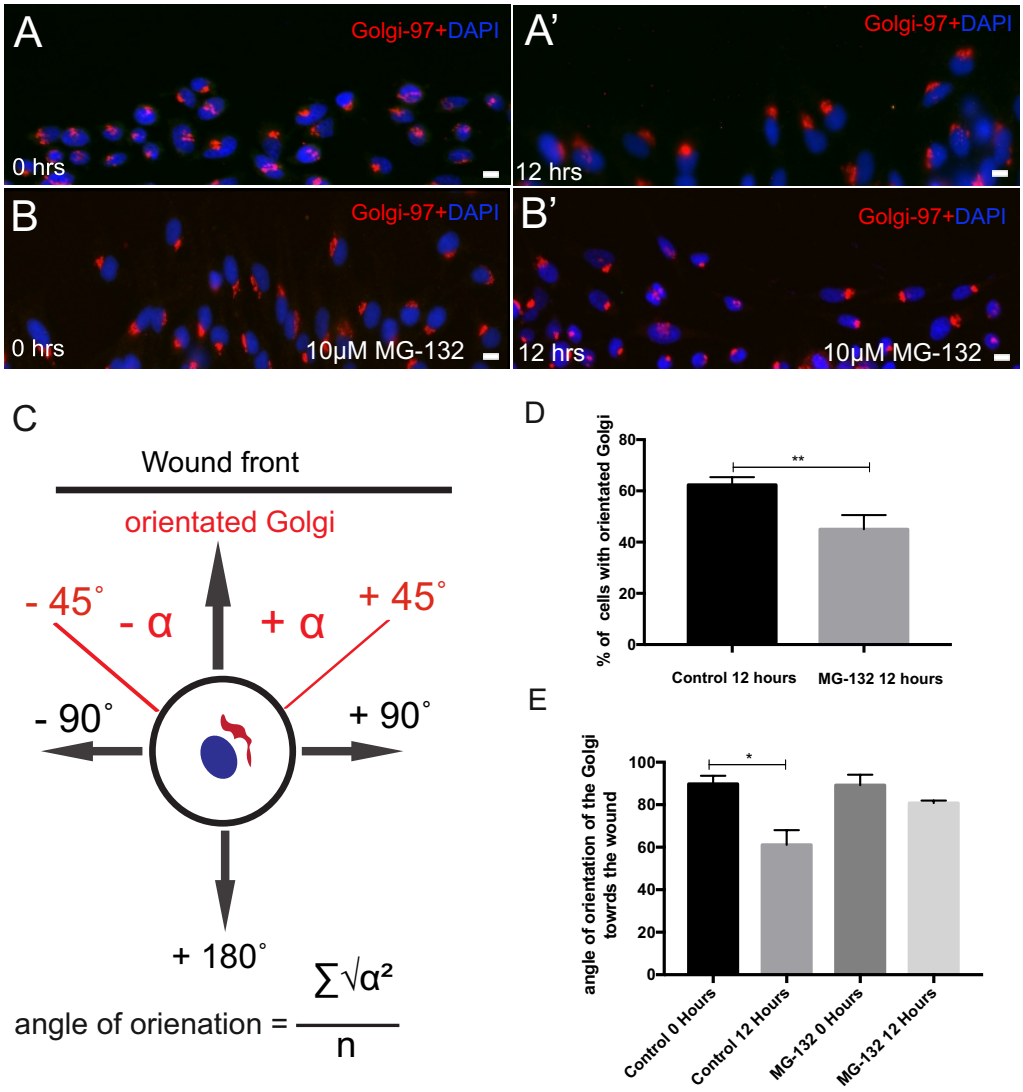

Figure 4.17 The Golgi is not able to re-orientate itself towards the wound in the presence of aggresomes.
A confluent monolayer of HeLa cells was either treated with 10 μM MG-132 or DMSO for 18 hours. Using a p200 tip a strip of cells is removed creating a wound, media is replenished removing detached cells. Cells were fixed at set time-points and stained with anti-Golgi-97 antibody staining the Golgi and DAPI to visualise the nuclei. **A-A')** In control treated cells when the wound is initially created the Golgi has a random orientation, by 12 hours of when the wound was created, the Golgi of cells at the leading edge of the wound has re-orientated it-self towards the wound. **B-B')** In the presence of aggresomes, the Golgi also has a random orientation from when the wound was formed, by 12 hours of when the wound was created, less than half of the cells have the Golgi orientated towards the wound. **C)** A schematic illustration of how the Golgi orientation was measures, a Golgi orientated within -45° and +45° of the wound was considered orientated towards the wound. **D)** Quantification of number of cells with a Golgi orientated towards the wound ($P< 0.01$, by Student's *t*-test, 100 cells, n=3). **E)** Quantification of change in angle of orientation during cell migration $P< 0.05$, by Student's *t*-test, 100 cells, n=3). Scale bars 10 μm.

4.2.18 In the presence of aggresomes MEFs cells fail to close the wound

I have shown in the presence of aggresomes, the slow rate of cell migration in HeLa cells prevents wound closure. As HeLa cells migrate very slowly, and to avoid the possibility of cells dividing and filling up the wound rather than cell migration I decided to use mouse embryonic fibroblast cells (MEFs) as fibroblast cells are frequently used to study cell migration due to their migration capability. At first, I needed to test whether these cells can form aggresomes. MEFs were treated with 5 μM MG-132 for 18 hours and stained with anti-vimentin and anti-γ-tubulin. In control MEFs, the vimentin staining appeared very diffused throughout the cytoplasm, with a few short and sporadically distributed intermediate filaments. Vimentin is also seen at the nucleus while, γ-tubulin staining shows the two characteristic punctae representative of the centrosome (Figure 4.18 A-A' and C-C'). When treated with MG-132 the vimentin stain is seen to aggregate next to the nucleus, similarly the γ-tubulin localises to the large aggresome (Figure 4.18 B-B' and D-D'). I next followed on to the wound assay. A confluent monolayer of cultured MEFs was treated with 5 μM MG-132 for 18 hours. A wound was created, and cells were subsequently fixed at set time-points. Cells were stained with DAPI to visualise cell migration. In control MEFs, cell migration is observed within 3 hours as the distance of the wound gets smaller. By 5 hours the wound is not clearly visibly, within 8 hours, cells have fully closed the wound (Figure 4.18 E-E'''' and G) . In the presence of aggresomes, cell migration is only visible at 5 hours, however, the distance covered is marginal with relatively no change by 8 hours (Figure 4.18 F-F'''' and G).

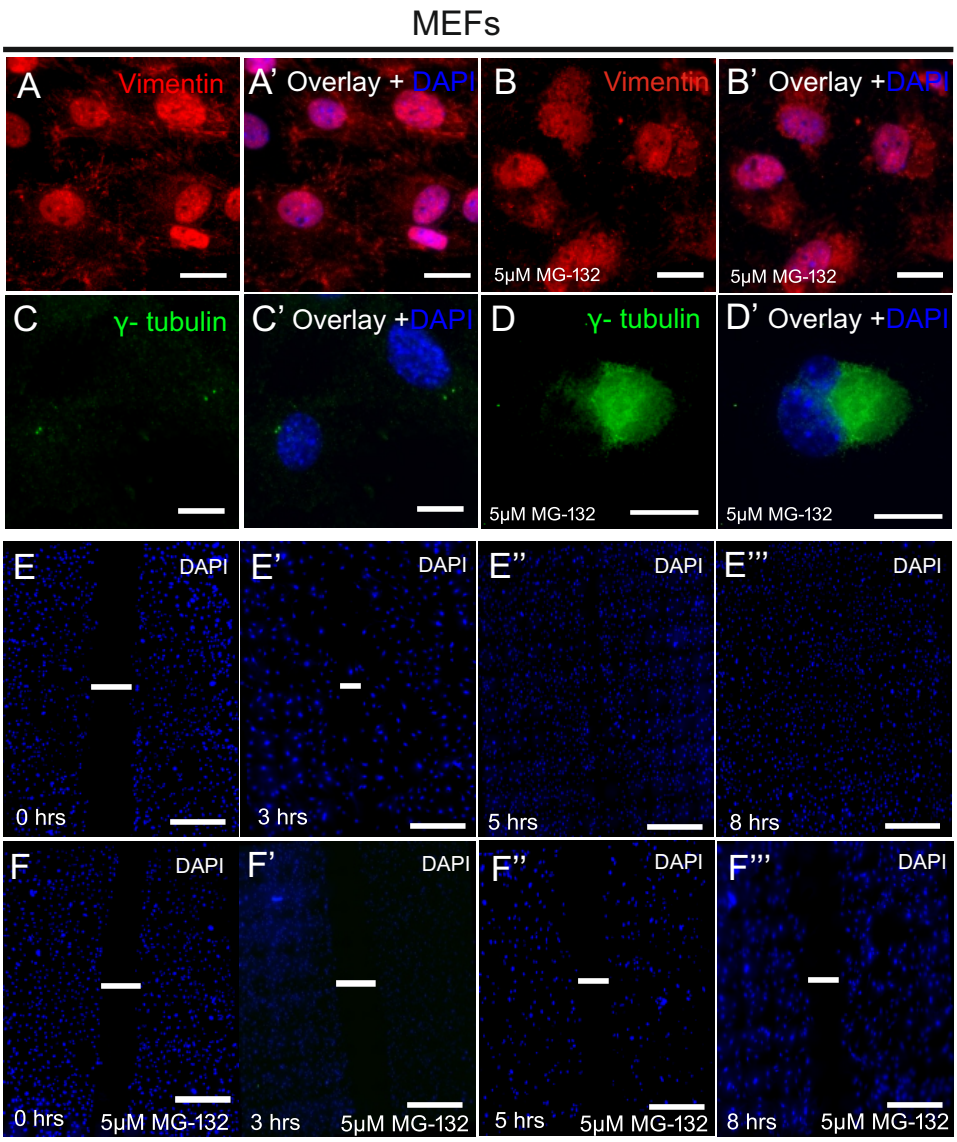
MEFs
A
Vimentin
A' Overlay + DAPI
B
Vimentin
B' Overlay +DAPI
5μM MG-132
5μM MG-132
C
γ- tubulin
C' Overlay +DAPI
D
γ- tubulin
D' Overlay +DAPI
5μM MG-132
5μM MG-132
E
DAPI
E'
DAPI
E''
DAPI
E'''
DAPI
0 hrs
3 hrs
5 hrs
8 hrs
F
DAPI
F'
DAPI
F''
DAPI
F'''
DAPI
0 hrs
5μM MG-132
3 hrs
5μM MG-132
5 hrs
5μM MG-132
8 hrs
5μM MG-132

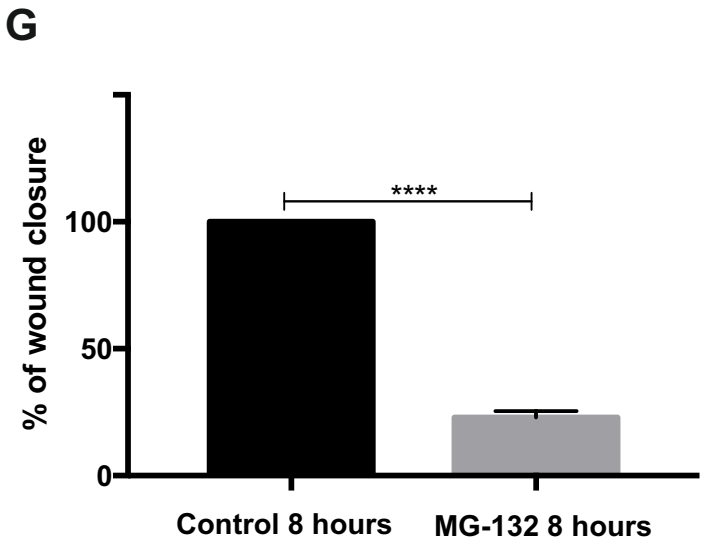
G
% of wound closure
100
50
0
****
Control 8 hours
MG-132 8 hours

Figure 4.18 In the presence of aggresomes MEFs fail to close the wound.
MEFs cells were treated with 5 μM MG-132 or with DMSO for 18 hours. Cells were fixed and stained with anti-vimentin or anti-γ-tubulin antibodies. **A-A' and C-C')** In control treated cells, the vimentin staining appears diffused throughout the cytoplasm with short sporadically distributed vimentin filaments, the γ-tubulin labels the centrioles of the centrosome appearing as two punctae. **B-B') and D-D')** When treated with proteasome inhibitor, the vimentin staining appears more compact next to the nucleus, while the γ-tubulin staining has an increased zone of staining indicative of an aggresome. A confluent monolayer of MEFs cells were treated with 5 μM MG-132 or with DMSO for 18 hours, a strip of cells is removed using a p200 tip, the media is replenished removing detached cells and cells were fixed at set time-points. Cells were stained with DAPI to visualise the nuclei. **E-E''')** In control cells, cell migration is observed within 3 hours of when the wound was created, as the distance between the wound has decreased, by 5 hours the cells have fully migrated in and closed the wound. **F-F''')** In the presence of aggresomes, cell migration is only observed at 5 hours of when the wound was created, as the distance between the wound has decreased slightly. The rate of cell migration is reduced as the cells fail to close the wound at 8 hours of migration. The distance between the wound from 5 hours to 8 hours has marginally decreased as a result of slow cell migration. **G)** Quantification of wound closure P<0.0001, by Student's *t*-test, n=3. A-D') Scale bars 10 μm. E-F''') Scale bars 200 μm.

4.2.19 In the presence of aggresomes MEFs cells fail to close the wound

I have shown MEFs form aggresomes when treated with MG-132, snapshots of the assay show presence of aggresomes, slow down cell migration where wound closure is inhibited. Ideally live imaging would allow us to visualise individual cell movement. I next tested if time-lapse of live imaging agrees with the snapshot images which would strengthen previous data. A confluent monolayer culture of MEFs were treated with 5μM MG-132 for 18 hours. A strip of cells was removed, and media was replenished removing detached cells. In control MEFs, cell migration is seen within 3 hours. Individual cells can be seen extending their processes as they move into close the wound. By 12 hours, cells have moved in and complete closure of the wound is observed (Figure 4.19 A-A'''). In the presence of aggresomes, cell migration is not observed until 5 hours, cells can also be seen to be extending their processes facilitating cell migration. Although individual cells are seen migrating towards the wound, cells have sparsely migrated as a result wound closure is not observed (Figure 4.19 B-B'''). Control MEFs show 100% wound closure while, in the presence of aggresomes this is reduced to 45% (Figure 4.19 C).

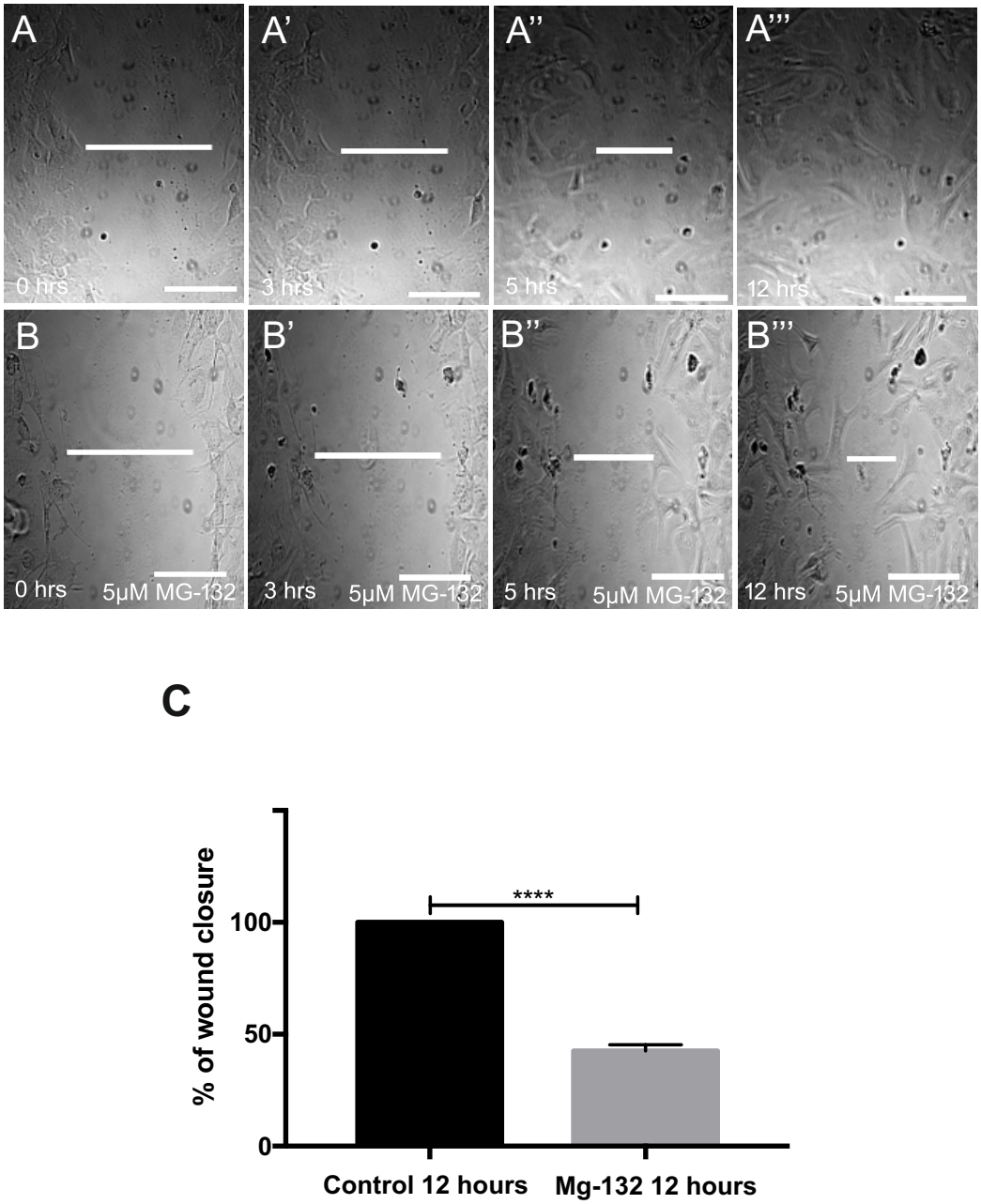

Figure 4.19 Stills from time-lapse showing MEFs fail to close the wound in the presence of aggresomes.
MEFs cells were treated with 5 μM MG-132 or with DMSO for 18 hours. A strip of cells is removed using a p200 tip, detached cells are removed by replacing the media. Cells were incubated in CO_2 independent media, by time-lapse microscopy cell migration was recorded. **A-A'''**) In control cells, stills from time-lapse show cells migrating within in 3 hours of when the wound was created, cells extending their process to migrate can be seen. The distance of the wound decreases as cells migrate, by 12 hours cells have migrated in and closed the wound. **B-B'''**) In the presence of aggresomes, stills of time-lapse show a delay in cell migration, cell migration is observed by 5 hours of when the wound is created. By 12 hours of cell migration, cells extending their processes are seen, the distance of the wound has decreased but has not fully closed as cells are seen to have sparsely filled the wound. **C)** Quantification of wound closure ($P< 0.0001$, by Student's *t*-test, n=3). Scale bars 200 μm.

4.2.20 In the presence of aggresomes RPE1-hTERT cells fail to close the wound

In the presence of aggresomes, rate of cell migration is severely reduced where incomplete wound closure is observed. Though MEFs were ideal for this cell migration assay I also wanted to test whether aggresomes generated by overexpressing GFP-tagged αsyn would also reduce rate of cell migration. However, this proved challenging as MEFs were proving difficult to transfect as a high transfection efficiency is required for this assay. As a result, I moved onto using RPE1-hTERT cells as they too have migrating means and are easier to transfect. To begin with I had to check if RPE1-hTERT cells can form aggresomes. RPE1-hTERT cells were treated with 1 μM MG-132 for 18 hours, cells were fixed and stained with anti-γ-tubulin antibody. In control cells, γ-tubulin staining appears as two punctae, representative of the centrosome, upon aggresome formation a larger zone of staining is observed, indicative of an aggresome (Figure 4.20 A-A' and B-B'). I next moved on to testing if these aggresomes affect cell migration in RPE1-hTERT cells. A confluent monolayer of cultured RPE1-hTERT cells was treated with 1 μM MG-132 for 18 hours or control treated with DMSO . A wound was created, and media was replenished removing detached cells. Cells were fixed at set time-points capturing snap shots of cell migration. Cell migration was observed by immunofluorescence analysis, were cells were stained with anti-Golgi97 antibody and DAPI. In control cells, cell migration is observed as the distance between the wound decreases. Cell migration is seen within 3 hours of when the wound was created as DAPI staining shows more cells at the wound. By 8 hours, the wound is near enough to complete closure (Figure 4.20 C-C'''). In the presence of aggresomes, cell migration is delayed as migration is observed at 5 hours by, 8 hours there is marginal change in cell migration resulting in incomplete wound closure (Figure 4.20 D-D'''). In control RPE1-hTERT cells, wound closure was at 85% while, cell treated with MG-132 showed 45% wound closure (Figure 4.20 E).

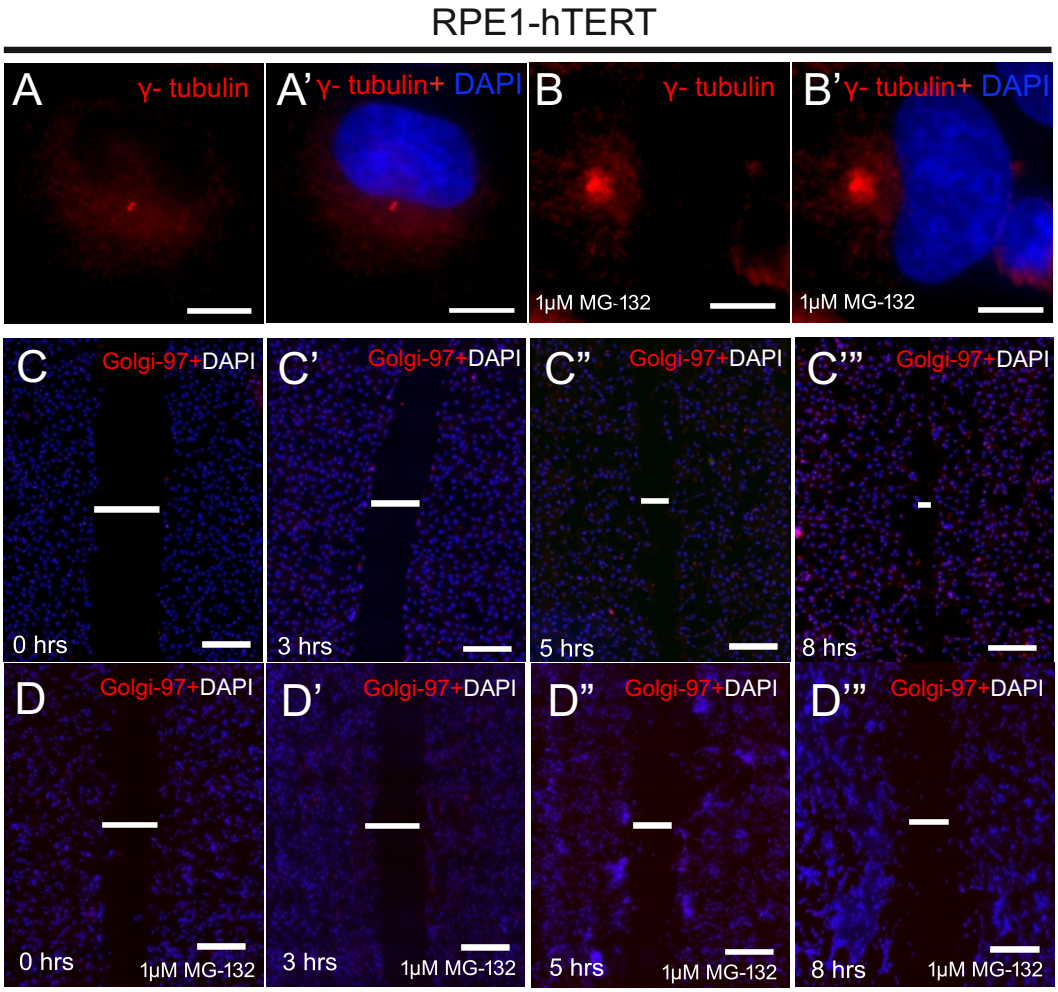
RPE1-hTERT
A
γ- tubulin
A'
γ- tubulin+ DAPI
B
γ- tubulin
1μM MG-132
B'
γ- tubulin+ DAPI
1μM MG-132
C
Golgi-97+DAPI
0 hrs
C'
Golgi-97+DAPI
3 hrs
C"
Golgi-97+DAPI
5 hrs
C'"
Golgi-97+DAPI
8 hrs
D
Golgi-97+DAPI
0 hrs
1μM MG-132
D'
Golgi-97+DAPI
3 hrs
1μM MG-132
D"
Golgi-97+DAPI
5 hrs
1μM MG-132
D'"
Golgi-97+DAPI
8 hrs
1μM MG-132

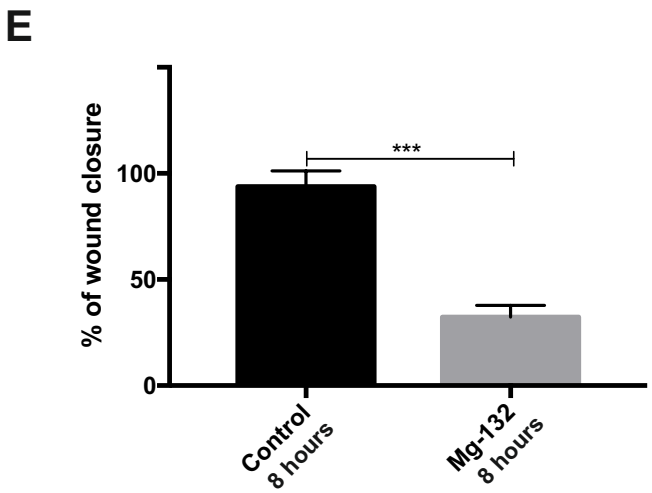
E
% of wound closure
100
50
0
***
Control
8 hours
Mg-132
8 hours

Figure 4.20 In the presence of aggresomes, RPE1-hTERT cells fail to close the wound.
RPE1-hTERT cells were treated with 1 μM-MG-132 or DMSO for 18 hours, cells were fixed and stained with anti-γ-tubulin antibody. **A-A' and B-B')** In control cells, the γ-tubulin labels the centrioles, seen as two punctae, in the presence of aggresomes the γ-tubulin is observed as a larger zone of staining next to the nucleus, indicative of an aggresome. A confluent monolayer culture of RPE1-hTERT cells was treated with 1 μM MG-132 or DMSO for 18 hours, a wound was created by removing a strip of cells using a p200 tip. The media was replenished removing detached cells. Cells were fixed at set time-points and stained with anti-Golgi 97 antibody and DAPI. **C-C''')** In control cells, cell migration is observed within in 3 hours as cell nuclei are seen to narrow the wound, as migration continues the distance of the wound closes. By 8 hours, majority of the cells have moved in to close the wound, with only a marginal distance remaining. **D-D''')** In the presence of aggresomes, the rate of cell migration is reduced as cell migration is observed at 5 hours of when the wound was formed. By 8 hours there is no obvious changes in cell migration as the distance between the wound is similar, the reduced rate of cell migration inhibits the cells from closing the wound. **E-E)** Quantification of wound closure ($P<0.001$, by Student's *t*-test, n=3). **A-B')**Scale bars 10 μm. C-D''') Scale bars 200 μm

4.2.21 In the presence of aggresomes the Golgi is not able to re-orientate towards the wound in RPE1-hTERT cells

I have shown rate of cell migration is reduced in RPE1-hTERT cells, when in the presence of aggresomes. As both the centrosome and Golgi are involved in directing cell migration towards the wound, cells were stained with anti-Golgi97 antibody to visualise change in Golgi orientation. A Golgi orientated within -45° and +45° of the wound was considered orientated towards the wound. In control cells, the Golgi is seen to have a random orientation at the time the wound was initially formed (Figure 4.21 A). At 5 hours, the Golgi staining shows cells at the edge of the wound have orientated the Golgi towards the wound (Figure 4.21 A'). Similarly, cells treated with MG-132 also show random Golgi orientation at the time of when the wound was created (Figure 4.21 B). At 5 hours of migration, there are some cells that have re-orientated the Golgi towards the wound while, majority of the cells continue to have randomly orientated Golgi (Figure 4.21 B'). In comparison 60 % of cells in the control showed Golgi orientated towards the wound while, 30% in the presence of aggresomes (Figure 4.21 D).

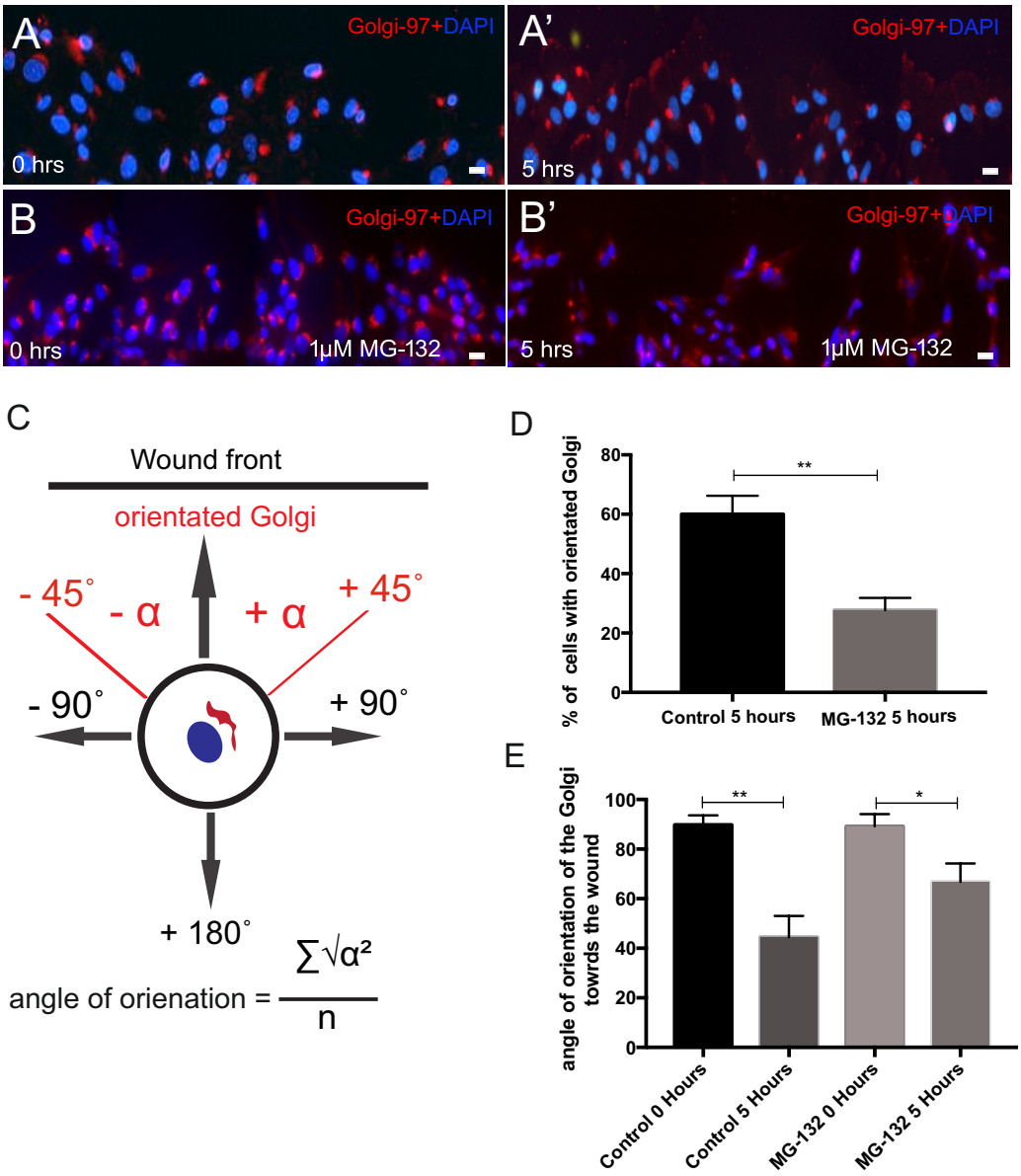

Figure 4.21 In RPE1-hTERT cells the Golgi is not able to re-orientate itself towards the wound in the presence of aggresomes.

A confluent monolayer of RPE1-hTERT cells was treated with 1 μM MG-132 or DMSO for 18 hours. Using a p200 tip a strip of cells is removed creating a wound, media is replenished removing detached cells. Cells were fixed at set time-points and stained with anti-Golgi-97 antibody staining the Golgi and DAPI to visualise the nuclei. **A-A')** In control treated cells when the wound is initially created the Golgi has a random orientation, by 5 hours from when the wound was created, the Golgi of cells at the leading edge of the wound has re-orientated it-self towards the wound. **B-B')** In the presence of aggresomes, the Golgi also has a random orientation from when the wound was formed, by 5 hours of when the wound was created, less than half of the cells have the Golgi orientated towards the wound. **C)** A schematic illustration of how the Golgi orientation was measures, a Golgi orientated within -45° and +45° of the wound was considered orientated towards the wound. **D)** Quantification of number of cells with a Golgi orientated towards the wound ($P < 0.01$, by Student's *t*-test, 100 cells, n=3). **E)** Quantification of change in angle of orientation during cell migration $P < 0.01$, $P<0.05$ by Student's *t*-test, 100 cells, n=3). Scale bars 10 μm.

4.2.22 In the presence of aggresomes RPE1-hTERT cells fail to close the wound

Immunofluorescence analysis shows aggresomes slow down cell migration in RPE1-hTERT cells and fewer cells were able to orientate its Golgi towards the wound. I followed on by assessing cell migration by live imaging. A strip of cells was removed from a confluent monolayer culture of RPE1-hTERT cells. Media was replenished removing detached cells. In control cells stills from time-lapse shows gradual closure of the wound cell migration is seen at 3 hours with cells extending their processes facilitating cell migration (Figure 4.22 A-A'''). In the presence of aggresomes, marginal cell migration is observed, cells are seen trying to extend their processes with a few cells seen moving, however cell migration is largely inhibited (Figure 4.22 B-B'''). In control cells, there was over 80-% wound closure while, cells treated with MG-132 showed very little wound closure at 12% (Figure 4.22 C).

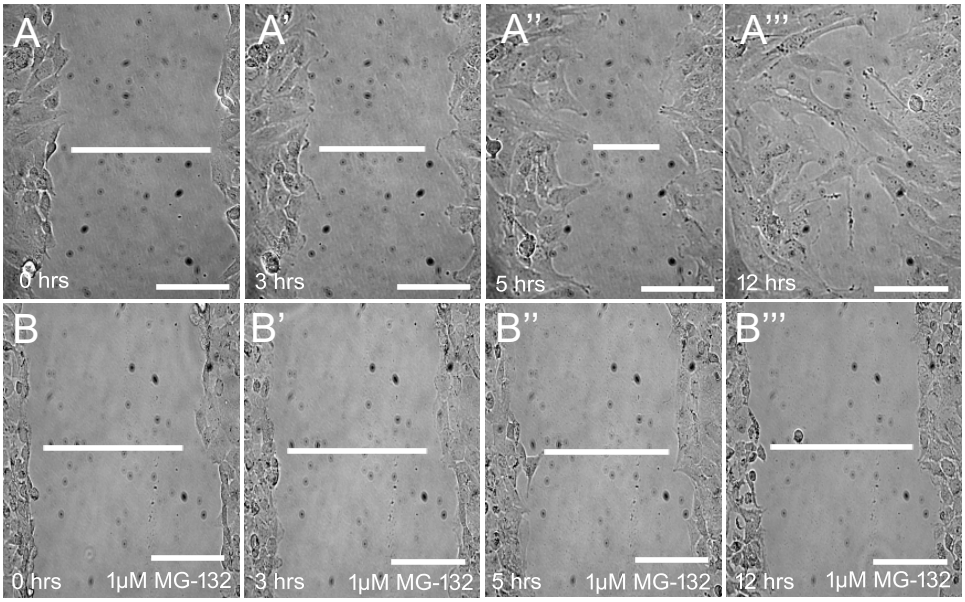

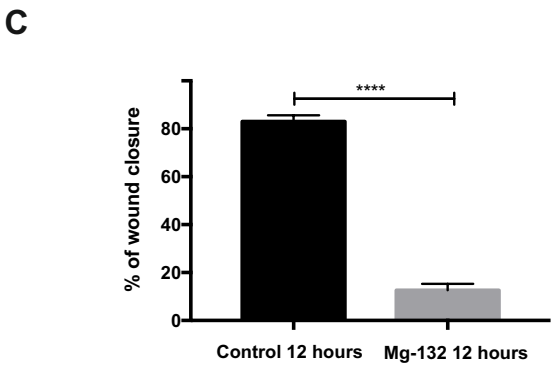

Figure 4.22 Stills of time-lapse showing RPE1-hTERT cells fail to close the wound in the presence of aggresomes. RPE1-hTERT cells were treated with 1 μM MG-132 or with DMSO for 18 hours. A strip of cells is removed using a p200 tip, detached cells are removed by replacing the media. Cells were incubated in CO_2 independent media, by time-lapse microscopy cell migration was recorded. **A-A''')** In control cells, stills from time-lapse show cells migrating within in 3 hours of when the wound was created as the distance of the wound is smaller, cells are seen extending their process to migrate. The distance of the wound decreases as cells migrate, by 12 hours cells have migrated in and closed the wound. **B-B''')** In the presence of aggresomes, stills of time-lapse show a few individual cells extending their processes, only a few of the cells are able to migrate, the cells fail to migrate and close the wound. **C)** Quantification of wound closure ($P < 0.0001$, by Student's *t*-test, n=3). Scale bars 200 μm

4.3 Discussion

The integrity of the microtubule network is essential in neuronal function. Microtubule organisation specifies axons and dendritic compartments establishing neuronal polarity and functional components of neurons. Microtubules are tracks where cargo is transported along. Microtubule degeneration is associated with many neurodegenerative diseases including Alzheimer's and Parkinson's. In this chapter I tested whether aggresomes inhibit centrosomal microtubule nucleation activity since aggresomes are formed in close vicinity of the centrosome. I have shown in several cell lines, starting from HeLa to differentiated SH-SY5Y cells, aggresomes severely reduce microtubule nucleation activity of the centrosome where the microtubule network is not able to establish be when the network was depolymerised.

HeLa and SH-SY5Y cells both have a similar arrangement of microtubules, appearing as a filamentous network. Microtubules are seen extending across the cytoplasm to the periphery of the cells. At the interphase stage of the cell cycle and during microtubule nucleation there is constant radial array of microtubules associating with the centrosome. In differentiated SH-SY5Y cells the microtubule staining differs, with compact microtubule staining at the extending neurite and more of a fibrous network around the cell body. In control conditions, all cell types tested were able to dynamically build a new microtubule network. The characteristic aster was also seen in all cell types. However, microtubule nucleation and building a new network took slightly longer in differentiated SH-SY5Y cells. When aggresomes were formed by treating cells with MG-132, microtubule integrity was affected. The extensive microtubule network was compromised as fewer microtubules are seen and the loss of radial array of microtubules at the centrosome. The few microtubules nucleated at the last time-point were not able to conform to any structural organisation seen in control cells. Insufficient microtubule nucleation meant cells were not able to establish a new network. MG-132 generated aggresomes showed drastic effects on centrosome's ability to nucleate microtubules with the same effect observed across all three cell lines.

Similarly, aggresomes formed by overexpressing GFP-tagged αsyn or familial mutants showed a comparable effect. In both HeLa and SH-SY5Y cells, loss of microtubule integrity is observed however not to the same extent as seen when aggresomes were formed by MG-132 treatment. While there is reduce microtubule staining in HeLa cells the characteristic array of microtubules is still visible. It appears network integrity in SH-SY5Y cells is more severely affected as the array of microtubules is not seen. Microtubule nucleation is delayed in both cell types, with microtubule staining only visible at the later stages of the assay. Again, it appears microtubule nucleation is more severely affected in SH-SY5Y cells as, aster formation is seen in HeLa cells with overall increase in microtubule staining but not in SH-SY5Y cells. Microtubules also appear to be longer with more apparent microtubule arrangement at times.

Aggresomes generated by proteasome inhibition showed more severe effects on microtubule nucleation than aggresomes formed by overexpressing GFP-tagged αsyn. In the presence of aggresomes formed by MG-132 the radial microtubule array is not seen. Since proteasome inhibition impairs degradation of all proteins, it is possible the composition and density aggresomes generated by MG-132 treatment differs to aggresomes generated via overexpressing GFP-tagged αsyn or the familial mutants. One would assume aggresomes generated through proteasome inhibition would be denser as it is a composition of many proteins plus overexpression of GFP-tagged αsyn forms aggresomes by burdening the proteasome machinery, which means protein degradation can still occur but at a slower rate. If this is the case, it can be assumed the difference in protein composition and density of the aggresomes could explain why aggresomes generated by proteasome inhibition showed more drastic effects on the centrosome from nucleating microtubules and forming a new network. Certain features including formation of an aster, and continually radial microtubule association reflects efficient microtubule nucleation activity of the centrosome. While, aggresomes generated by either MG-132 or overexpression of GFP-tagged αsyn, would both envelope the centrosome, microtubule nucleation forming the characteristic aster was only observed in cells where aggresomes were generated by the overexpression of GFP-tagged αsyn. In instances where the aggresome had engulfed the centrosome, radial array of

microtubules can be seen emerging from the aggresome. Assuming it is the case of differences in protein densities that allow microtubules to nucleate and emerge from a less compact structure. Again, this could be explained by the possibility of aggresomes formed by the different means having different structural densities. As it was aggresomes generated through overexpression of GFP-tagged αsyn or the familial mutants, the characteristic aster is seen. Although, this was not often, it was not observed at all when cells were treated with MG-132.

I also tested if aggresomes affect cell migration and polarity changes since the centrosome is involved in directing cells towards the wound. In control cells, including HeLa, MEFs and RPE1-hTERT cells, cells gradual migrate to close the wound. Time-lapse of MEFs and RPE1-hTERT show cells extending their processes as they migrate towards the wound. In the presence of aggresomes, rate of cell migration was reduced in all three cell lines with RPE1-hTERT affected the most. The immunofluorescence data agrees with the time-lapse showing limited cell migration in RPE1-hTERT whereas MEFs show a reduced rate of cell migration. The effects of MG-132 are reversible, when MG-132 is removed from the media, the proteasome is able to resume its function. This might explain why at the early stages of cell migration there was a delay in comparison to control cells and as the aggresome gets smaller the cells are able to migrate. While it would have been interesting to see if aggresomes formed by the overexpression of GFP-tagged α-syn or the familial mutants had any effect on cell migration this proved difficult to test. MEFs proved difficult to transfect and since a high transfection efficiency is required we decided to use RPE1-hTERT as they are also known to migrate and are easier to transfect. However, cells failed to move even in the control GFP assay including both the transfected and untransfected cells of the same culture. The wound assay is a sensitive assay were a sparse or an over confluent culture is not optimal for cell migration to be observed. Since aggresomes are only observed when cells overexpress for 72 hours together with the transection reagent used, I assume the cells are stressed and conditions are not optimal for cell migration.

I have shown that microtubule nucleation is severely compromised in the presence of aggresomes. An efficient microtubule network is required for trafficking cargo but also organelle positioning. Microtubule stability has been widely researched as axonal

degeneration is a feature observed in Parkinson's and other neurodegenerative diseases. While there will be different possibilities of how microtubule stability and function is affected, it is possible protein inclusions sterically hinder the centrosome from nucleating microtubules and maintaining the network. As, microtubule nucleation was observed, both the delay and unorganised structure could accumulate eventually leading to neuronal death.

5. Aggresomes inhibits ciliogenesis

5.1 Introduction

Centrosomes and cilia have a coordinated relationship, where the mother centriole forms the basal body from which the microtubule axoneme extends (Sorokin 1968). Primary cilia have distinct functions in different cells types, they are considered to be a sensory organelle that are able to detect fluid flow and pressure but also play a role in transducing intracellular signals (Mahjoub 2013). Defects in cilia formation or structure, result in a group of diseases termed 'ciliopathies'. Many ciliopathies have prominent neurological phenotypes reflecting the importance of neuronal cilia in the brain function (Boltshauser & Isler 1977). Neurons throughout the mammalian brain possess primary cilia yet, their precise functions remain unclear (Guemez-Gamboa et al. 2014). In the previous chapter I show that aggresomes disrupt the centrosome from nucleating and maintaining the microtubule network. The aggresomes also slow down or inhibit cell migration. Seeing that aggresomes affect two functions associated with the centrosome it is then possible the aggresome could affect ciliogenesis.

Cilia dysfunction is a common feature of neurodegenerative diseases (Armato et al. 2011; Kaliszewski et al. 2015). A study by Chakravarthy and colleagues (2012) overexpressed the toxic mutant form of tau and Amyloid β ($A\beta_{1-42}$) protein, in a mouse model of Alzheimer's. They found the cilia of the hippocampal dentate gyral cells had shorter cilia as the cilia length was reduced by half. They also found as the age of the mice increased the cilia length decreased, suggesting as the proteins accumulate the cilia becomes shorter (Chakravarthy et al. 2012). Similarly, another study showed by depleting IFT20, a protein important in the assembly of cilia, resulted in lack of primary cilia in mature dentate granule cells which impaired memory and long-term plasticity (Rhee et al. 2016). Defects in cilia have also been observed in Huntington's disease and Amyotrophic lateral sclerosis. Huntington's disease (HD) is caused by a single gene mutation at the huntingtin (HTT) gene, clinically characterised by progressive motor dysfunction, cognitive decline and psychiatric disturbances. Htt is shown to localise to the centrosome in a microtubule

dependent manner. A study by Keryer et al, showed depletion of Htt disrupts PCM-1 localisation and impaired primary cilia formation. In the mouse model of HD increased cilia length resulted in abnormal cerebral spinal fluid (CSF) flow that in turn affected neuroblast migration from the subventricular zone to the olfactory bulb (Keryer et al. 2011). In mice, it was shown the dopamine receptor 1 (D_1) localises to the cilia (Domire et al. 2011). Another study by Miyoshi et al, showed that lack of dopaminergic inputs elongated the primary cilia, implicating neuronal cilia in dopamine signalling (Miyoshi et al. 2014).

More recently autophagy has shown to have a functional interaction with ciliogenesis, autophagy is involved in removing negative regulators of ciliogenesis such as OFD1, which is essential for cilia formation to occur (Tang et al. 2013). Autophagy has shown to inhibit ciliogenesis by limiting trafficking of components needed for ciliary growth (Pampliega et al. 2013). Ciliogenesis and autophagy are both up-regulated in serum free conditions. Basal autophagy prevents the formation of a primary cilium, one of the ways by which this is achieved is by the degradation of IFT20 protein (Pampliega & Cuervo 2016). Since, intraflagellar transport (IFT) proteins are required for cilia assembly, serum deprivation then switches from basal to induced autophagy. IFT20 protein is no longer degraded and recruited to the basal body to assist in primary cilia formation (Pampliega et al. 2013). This process reflects the tight coordination between autophagy and cilia formation. Aberrant primary cilia and autophagic dysfunction is also seen in Huntington's disease (Liu & Zeitlin 2011). Autophagy is also involved in the clearing of aggresomes (Iwata et al. 2005). A study by Bang et al. (2016) showed that over expression of mutant LRRK2 protein, that is an associated risk factor for Parkinson's , generated protein inclusions which failed to get cleared by the autophagy pathway suggesting underlying autophagy dysfunction (Bang et al. 2016). The dynein /dynactin complex is essential for aggresome formation as well as the delivery of autophagosomes to lysosomes for lysosomal degradation (Johnston et al. 2002; Kimura et al. 2008).

During ciliogenesis, centriole translocation is dependent on cytoplasmic dynein-1 motors, via microtubules where mutations of cytoplasmic dynein 1 block translocation and ciliogenesis (Li et al. 2017). Since there is a functional interaction between autophagy, aggresomes and ciliogenesis it is then possible there is a connection between

aggresomes and cilia and the possible hindrance of aggresomes on cilia structure and function. A study by Sharma et al. (2011) showed that limiting the supply of free tubulin by treating cells with Taxol resulted in cilia loss or shortening (Sharma et al. 2011). As the primary cilium is composed of a microtubule based antennae, and in chapter 4 I have shown that aggresomes result in the rearrangement of the cytoskeleton particularly the microtubule network and the intermediate filaments, suggest it is possible aggresomes could also affect the cilia.

Intriguingly, loss of smell is a pre-clinical symptom associated with Parkinson's (Haehner et al. 2014). The receptors that detect smell, are housed on olfactory cilia (Jenkins et al. 2009). The loss of smell could be due to the presence of the pathological protein inclusions found in Parkinson's patients, which could hinder cilia maintenance and function. However, it is not known what exactly is causing this loss of odour detection. Clinically, some olfactory tests are being developed as a tool to determine anosmia (Daum et al. 2000). In the hope to detect Parkinson's early and by doing so able to reduce disease progression. While it appears to be a connection between cilia and the pathogenesis of Parkinson's, only a few studies have looked at the molecular pathology of the olfactory bulb in relation to Parkinson's but not looked at cilia at the olfactory bulb (Huisman et al. 2004; Fleming et al. 2008).

I next tested if the presence of aggresomes prevents cells from making cilia. I first tested this in RPE1-hTERT cells that are known to ciliate when in serum free media. Aggresomes were generated by treating cells with MG-132 or overexpressing GFP-tagged α-syn constructs. Similarly, as with the other assays I progressed to more neuronal like cells, first testing if they can form cilia and then testing in the presence of aggresomes. I also checked the olfactory cilia in zebrafish larvae.

5.2 Results

5.2.1 RPE1-hTERT cells fail to ciliate in the presence of aggresomes

RPE1-hTERT cells are routinely used to study primary cilia, as cilia formation can be induced by placing cells in serum-free media for 24 hours. In chapter 3 I showed that RPE1 –hTERT cells can form aggresomes when treated with MG-132. RPE1-hTERT cells were treated with 1 μM MG-132 for 18 hours or with DMSO in serum free media. Cells were fixed and stained with anti-acetylated tubulin and anti-γ-tubulin antibodies and DAPI. In control treated cells, cilia are seen extending from the centrioles, visualised by γ-tubulin (Figure 5.1 A-A''). In MG-132 treated cells, acetylated tubulin is confined to the aggresome next to the nucleus; cilia are not observed. The γ-tubulin staining changes to a large zone of staining co-localising with acetylated tubulin staining (Figure 5.1 B-B''). In serum free media, over 80% of cells ciliate compared to 20% of cells in the presence of aggresomes (Figure 5.1 C).

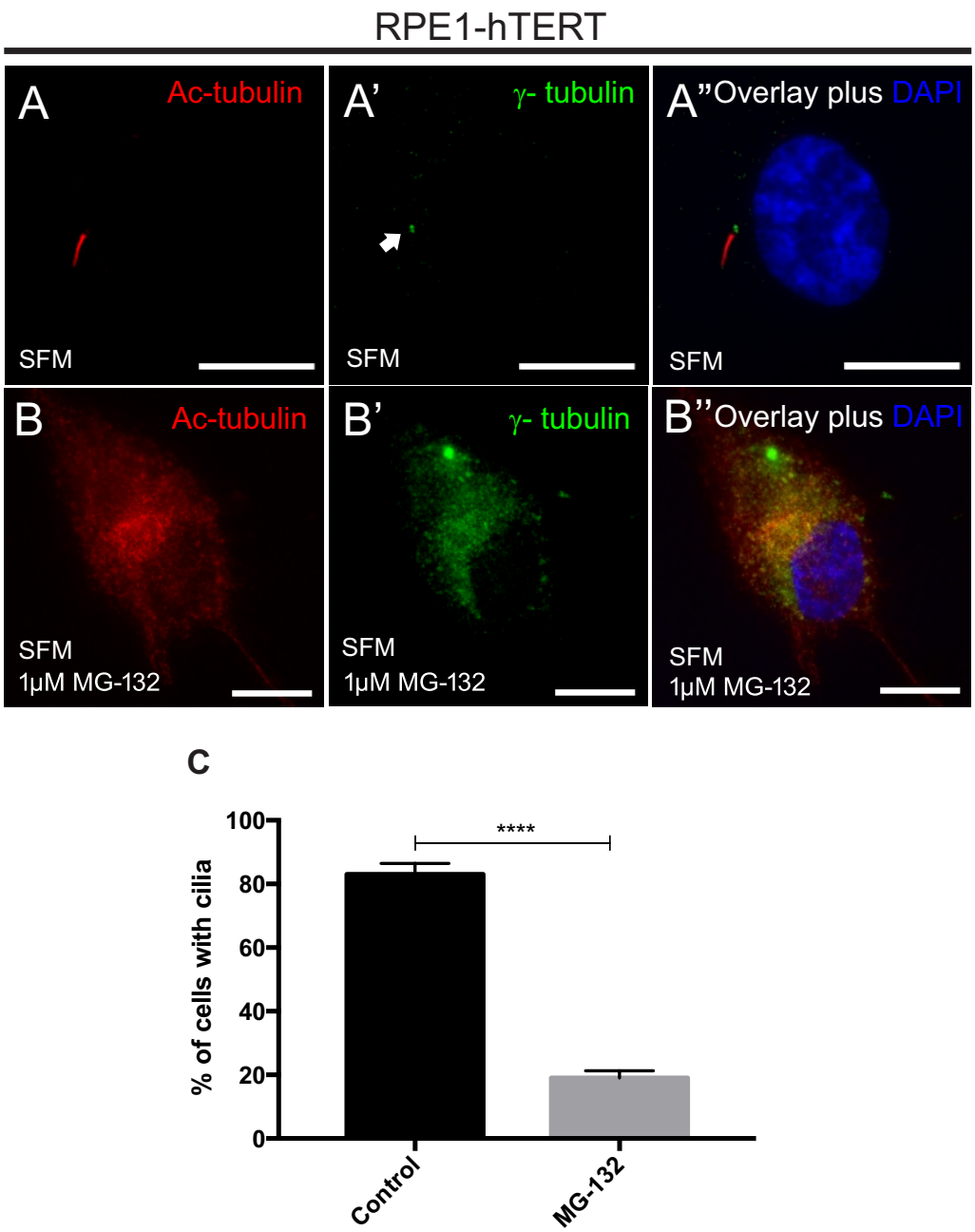

Figure 5.1 Aggresomes inhibit cilia formation in RPE1-hTERT cells.
RPE1-hTERTcells can form cilia readily upon serum starvation. **A-A'')** RPE1-hTERT cells form cilia in serum free conditions (24hours) as visualised by acetylated (ac-) tubulin staining (red) with γ-tubulin (green) marking the basal body of the cilium. **B-B'')** RPE1-hTERT cells treated with 1 μM MG-132 for 18 hours form aggresomes B') γ-tubulin showing aggresomal staining. In the presence of aggresomes, cilia are unable to form. **C)** Over 80% of control cells form cilia in serum free conditions compared to only 20% in aggresome positive cells. Quantification of ciliation in RPE1-hTERT cells untreated vs. MG-132, P< 0.0001; by Student's t-test, 100 cells, n=3. Scale bars 10 μm. DNA/nuclei stained with DAPI.

5.2.2 Overexpression of α-syn inhibit cilia formation in RPE1-hTERT cells

I next tested if aggresomes generated by overexpressing GFP-tagged α-syn wild-type or the two familial mutants would inhibit ciliogenesis similar to when aggresomes were induced by treatment with MG-132. RPE1-hTERT cells were transfected with either control GFP or GFP-tagged α-syn or the two familial mutants for 72 hours. Cells were fixed and stained with anti-acetylated tubulin antibody. In control transfected GFP cells, the GFP signal is expressed throughout the cytoplasm and cells are readily able to form cilia, visualised by acetylated tubulin (Figure 5.2 A-A''). In cells overexpressing any form of GFP-tagged α-syn, increased aggregation is observed next to the nucleus (Figure 5.2 B-B'', C-C'' and D-D''). The increase in aggregation, observed next to the nucleus is similar between all three forms of α-synuclein; cilia are only seen in untransfected cells. In control transfected GFP cells, 70% of cells ciliate while less than 20% of cell ciliate when GFP-tagged α-syn or familial mutants were overexpressed (Figure 5.2 E). In cells overexpressing GFP-tagged α-synA30P, it appears ciliogenesis is suppressed the most with only 15 % of cells able to form cilia (Figure 5.2 E). Since, control GFP cells and untransfected cells in GFP-tagged α-syn conditions are able to ciliate it suggests inhibition of cilia formation is a result of aggregates seen when α-synuclein is overexpressed.

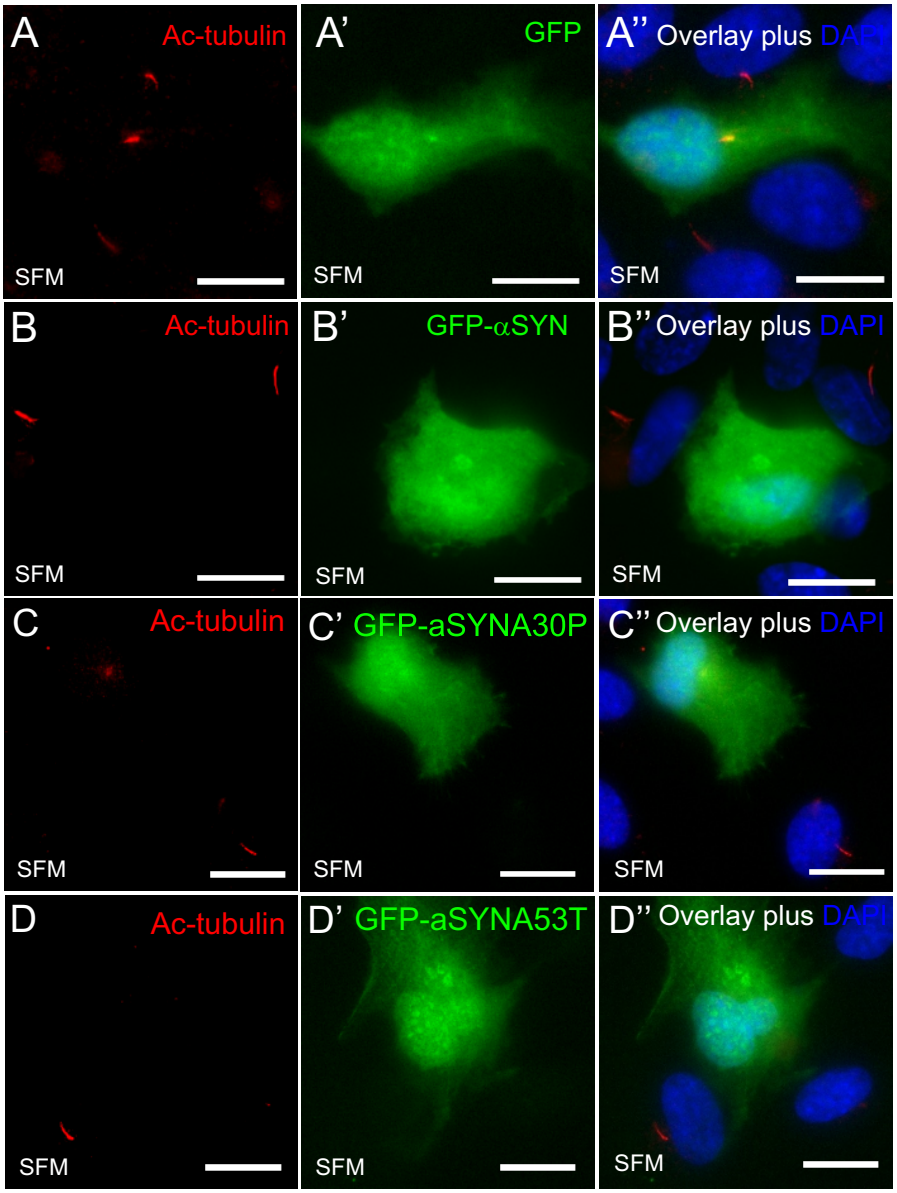
A
Ac-tubulin
SFM
A'
GFP
SFM
A''
Overlay plus DAPI
SFM
B
Ac-tubulin
SFM
B'
GFP-αSYN
SFM
B''
Overlay plus DAPI
SFM
C
Ac-tubulin
SFM
C'
GFP-aSYNA30P
SFM
C''
Overlay plus DAPI
SFM
D
Ac-tubulin
SFM
D'
GFP-aSYNA53T
SFM
D''
Overlay plus DAPI
SFM

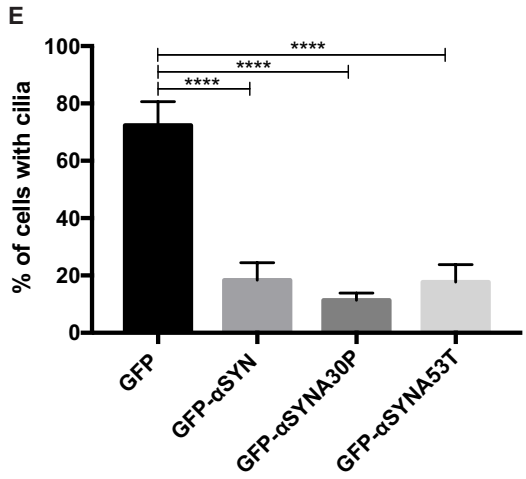
E
% of cells with cilia
100
80
60
40
20
0
****
****
****
GFP
GFP-αSYN
GFP-αSYNA30P
GFP-αSYNA53T

Figure 5.2 Overexpression of α-syn inhibits ciliogenesis in RPE1-hTERT cells.
RPE1-hTERT cells were transfected with control GFP plasmid and GFP-tagged αsyn wild-type or the two familial mutations for 72 hours. **A-A'')** In control GFP-transfected cells and (green) untransfected cells, cilia are formed as normal stained by acetylated α-tubulin (red). **B-B'', C-C'' and D-D'')** Overexpression of α-syn (green) inhibits cilium formation when either form of α-synuclein is overexpresses. In the neighbouring cells of the α-syn transfected cell cilia forms as normal. **E)** In control GFP overexpression 70% of the cells formed cilia compared to 20% of cells for the overexpression of α-syn. Quantification of ciliation in RPE1-hTERT cells GFP expressing vs. α-syn P<0.0001, by one-way ANOVA, 100 cells, n=3). Scale bar 10 μm. DNA/nuclei stained with DAPI.

5.2.3 Aggresomes inhibit ciliogenesis in MEFs

I next thought to test whether the presence of aggresomes inhibits ciliogenesis in a primary cell culture model. In chapter 4 I show that MG-132 treatment induces aggresome formation in MEFs. MEFs cells were treated with 5 μM MG-132 or control treated with DMSO for 18 hours in serum supplemented media. Cells were fixed and stained with anti-acetylated tubulin and anti-γ-tubulin antibodies. In control cells, treated with DMSO acetylated tubulin labels the cilia seen elongating from the basal body visualised by γ-tubulin (Figure 5.3 A-A''). When aggresomes are induced, acetylated tubulin localises to the centrioles and aggresome, while cilia are not seen. Similarly, the γ-tubulin continues to localise to the centrioles. However, a larger zone of staining is also observed indicative of the aggresome. The aggresome can be seen next to the centrosome (Figure 5.3 B-B''). 70% of control cells ciliated while only 20% of cells with aggresomes ciliated in the presence of aggresomes (Figure 5.3-C). Although it would have been interesting to see whether aggresomes generated by the overexpression of α-syn would also inhibit cilia formation, transfection efficiencies were considerably low with less than 1% of cells transfected with the relevant plasmids.

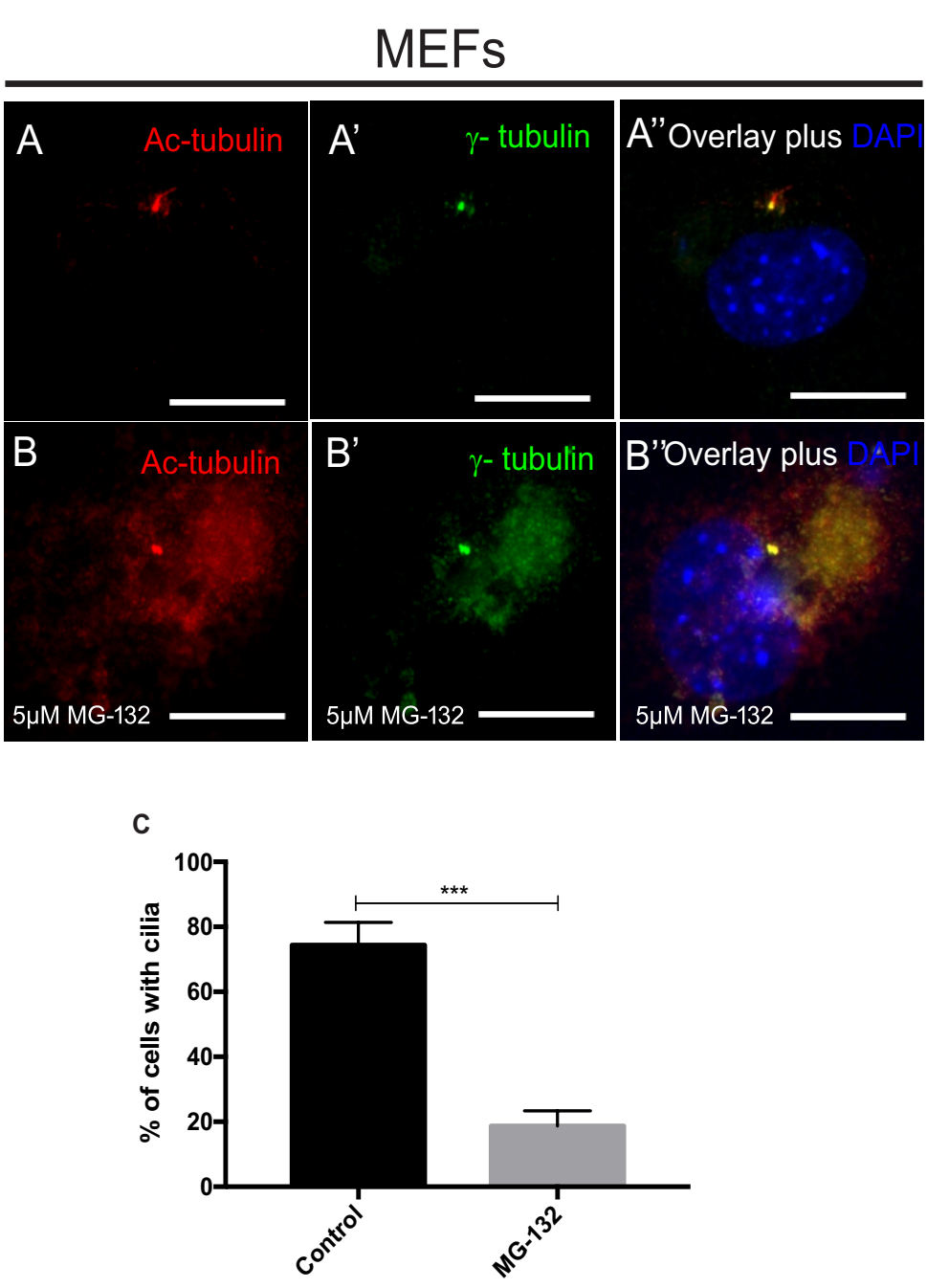

Figure 5.3 MEFs fail to form cilia in the presence of aggresomes.
A-A'') MEFs form cilia in the presence of serum, cilia is visualised by acetylated α-tubulin (red) and basal body by γ-tubulin (green). **B-B'')** when treated with 5 μM MG-132 for 18 hours cilia is no longer detected, both the acetylated α-tubulin and γ-tubulin stain concentrates at the centrosome and the aggresome. **C)** In control cells 70% of cell ciliate whereas, only 20% ciliate in treated cells with aggresomes. Quantification of number of cilia in untreated vs. MG-132 treated MEFs ($P<0.001$; by Student's t-test, n=3). Scale bar 10 μm. DNA/nuclei stained with DAPI.

5.2.4 Aggresomes inhibit cilia formation in the neuroblastoma SH-SY5Y cell line

In Parkinson's, the dopaminergic neurons of the substantia nigra deteriorate. I wanted to test whether cilia are affected in a more neuronal- like cell line. I used the human neuroblastoma SH-SY5Y cell line. SH-SY5Y cells are not widely used for studying cilia. The only published data is in a review by Whitefield et (2015), that demonstrated by immunostaining, that SH-SY5Y cells can form cilia (Whitfield et al. 2015). It would be interesting to see whether aggresomes affect cilia in a neuronal-like cell type as it may be relevant to the dopaminergic neurons affected in early Parkinson's. SH-SY5Y cells form cilia when in serum free media for 24 hours. SH-SY5Y cells were treated with 1 μM MG-132 or DMSO for 18 hours and subsequently changed to serum free media for 24 hours. Cells were fixed and stained with anti-acetylated tubulin and anti-γ-tubulin antibodies. In control treated SH-SY5Y cells, cilia are visualised by acetylated tubulin staining. The cilia are seen elongating from the basal body which is stained by γ-tubulin (Figure 5.4 A-A''). In the presence of aggresomes, acetylated tubulin staining is confined to the aggresome. Cilia are not observed. The centrosome is not completely consumed by the aggresome as γ-tubulin is still able to label the centrosome, which is seen as a single punctum as the two centrioles are close together. In addition, there is a large zone of staining surrounding the centrosome, characteristic of an aggresome (Figure 5.4 B-B''). In control cells 35% of cells form cilia. In the presence of aggresomes this drops to only 2% forming cilia (figure 5.4 C).

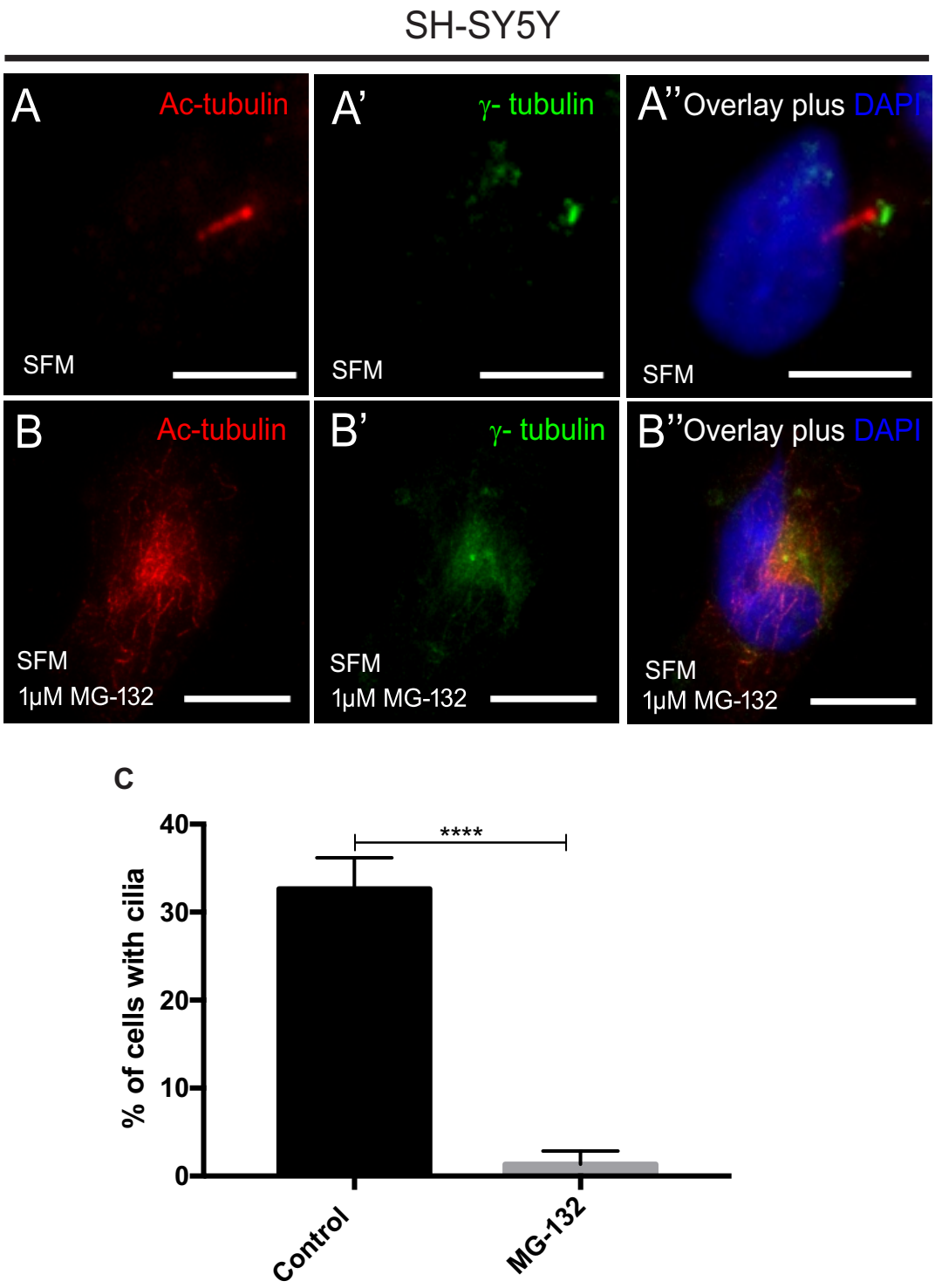

Figure 5.4 Aggresomes inhibit cilia formation in undifferentiated SH-SY5Y cells.
A-A'') Undifferentiated SH-SY5Y form cilia under serum free conditions. Cilia is visualised by acetylated α-tubulin (red) and γ-tubulin (green) staining the cilium basal body. **B-B'')** Cells treated with 1 μM MG-132 for 18 hours form aggresomes, when serum starved for 24 hours cells fail to ciliate. Both acetylated α-tubulin and γ-tubulin staining concentrate at the aggresome. **C)** In serum, free media 35% of undifferentiated SH-SY5Y cells form cilia compared to 2% of cells forming cilia in the presence of aggresomes. Quantification of ciliation in undifferentiated SH-SY5Y cells untreated vs. MG-132, $P<0.0001$, by Student's t-test, 100 cells, n=3. DNA/nuclei stained with DAPI. Scale bar 10 μm.

5.2.5 Overexpression of α-syn inhibits ciliogenesis in undifferentiated SH-SY5Y cells

As aggresomes generated by proteasome inhibition inhibited ciliogenesis in SH-SY5Y cells, the next step was to see if a similar result would be observed when aggresomes were generated through overexpression of GFP-tagged α-syn or the familial mutants. SH-SY5Y cells were transfected with control GFP construct, or GFP-tagged α-syn or the familial mutants for 72 hours. Cells were fixed and stained with anti-acetylated tubulin antibody. In control cells, where GFP alone is overexpressed, the GFP signal is distributed throughout the cytoplasm. Cilia are formed as normal, as visualised by acetylated tubulin staining (Figure 5.5 A-A''). In cells overexpressing either form of GFP-tagged α-syn, GFP signal is distributes throughout the cytoplasm with increased aggregation observed next to the nucleus. Cilia are not observed when cells overexpress either form of GFP-tagged α-syn (Figure 5.5 B-B'', C-C'' and D-D''). In control, transfected cells 30% of cells transfected have a cilium whereas, less than 5% form cilia when either form of GFP-tagged α-syn is overexpressed. As untransfected cells ciliate. This strengthens the case that it is the aggresome that is inhibiting ciliogenesis.

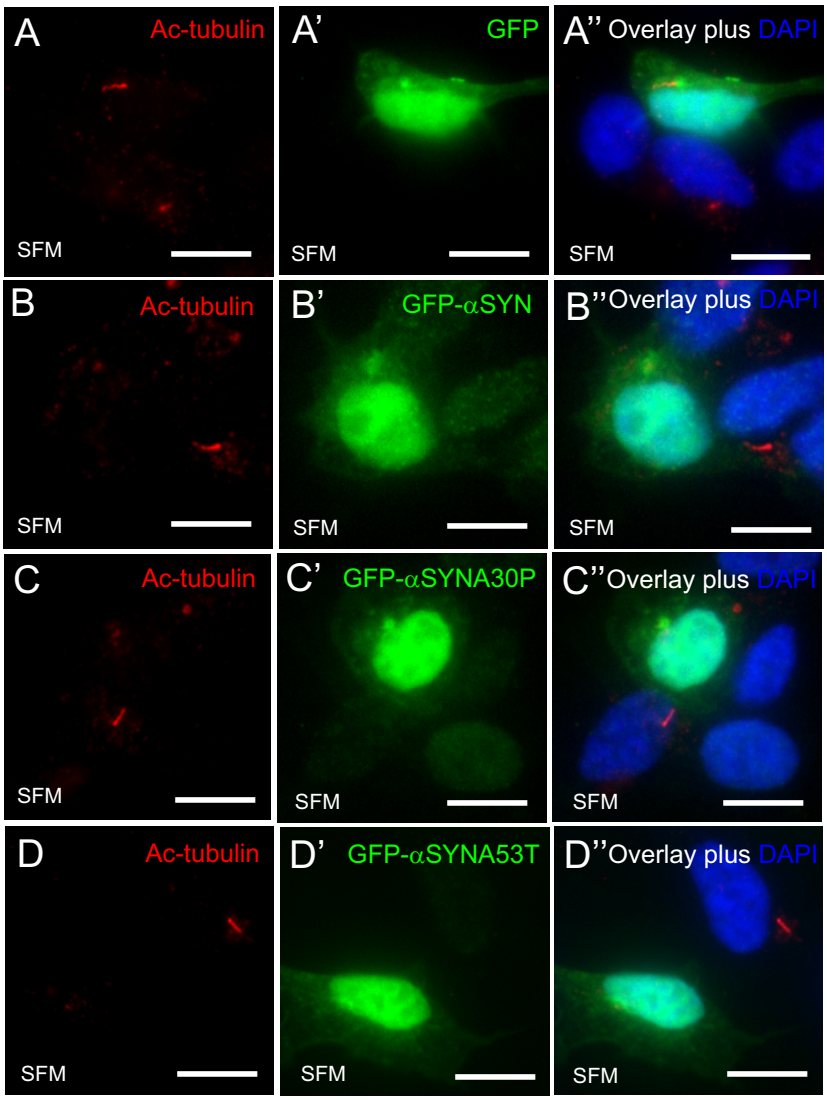
A
Ac-tubulin
SFM
A'
GFP
SFM
A" Overlay plus DAPI
SFM
B
Ac-tubulin
SFM
B'
GFP-αSYN
SFM
B"Overlay plus DAPI
SFM
C
Ac-tubulin
SFM
C'
GFP-αSYNA30P
SFM
C"Overlay plus DAPI
SFM
D
Ac-tubulin
SFM
D'
GFP-αSYNA53T
SFM
D"Overlay plus DAPI
SFM

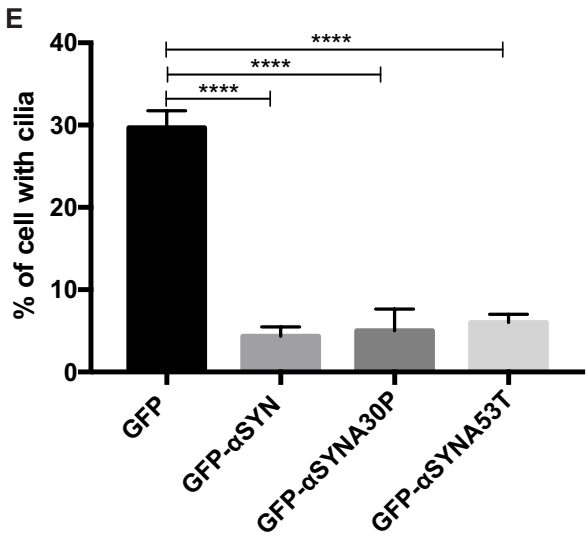
E
% of cell with cilia
40
30
20
10
0
****
****
****
GFP
GFP-αSYN
GFP-αSYNA30P
GFP-αSYNA53T

Figure 5.5 Overexpression of α-syn inhibits ciliogenesis in undifferentiated SH-SY5Y cells. Undifferentiated SH-SY5Y cells were transfected with control GFP plasmid and α-syn for 72 hours. **A-A'')** In control GFP-transfected cells and untransfected cells, cilia are formed as normal. Cilia is visualised by acetylated α- tubulin. **B-B'', C-C'' and D-D'')** Overexpression of α-syn inhibits cilium formation with all three forms of α-syn. In the neighbouring cells of the α-syn transfected cell cilia forms as normal. **E)** In control GFP overexpression 30% of the cells formed cilia compared to 5% of cells for the overexpression of α-syn. Quantification of ciliation in undifferentiated SH-SY5Y cells, GFP expressing vs. α-syn expression, p=0.0003, by one-way ANOVA, 100 cells, n=3). Scale bar 10 μm. DNA/nuclei stained with DAPI.

5.2.6 Differentiated SH-SY5Y cells fail to ciliate in the presence of aggresomes

I have shown in previous chapters that SY-SY5Y cells can be differentiated to adopt more neuronal-like characteristics. I next tested if aggresomes affect cilia formation in differentiated SH-SY5Y cells. When cells differentiated induced by, retinoic acid, cilia are formed. However, this percentage is increased from 55% to 75% in the absence of serum. Increase in cilia number in differentiated cells has also been observed in rat tracheal epithelial cells and muscle cells (Clark et al. 1995; Fu et al. 2014). SH-SY5Y cells were differentiated by treating cells with 10 μM retinoic acid. Differentiated cells were then treated with 1 μM MG-132 or DMSO for 18 hours and cells were grown in serum free media for 24 hours. Cells were fixed and stained with anti-acetylated tubulin and anti-γ-tubulin antibodies. In control, differentiated cells, cilia are observed by acetylated tubulin staining. The cilium is seen extending from the basal body, as visualised by γ-tubulin staining (Figure 5.6 A-A''). In cells where aggresomes are present, the γ-tubulin staining does not distinctly stain the centrioles as a larger area of staining is observed, that is consuming the centrosome (Figure 5.6 B-B''). Acetylated tubulin stains the aggresome (Figure 5.6 B-B''). Similarly, in control differentiated SH-SY5Y cells, 75% of cells ciliate, only 20% of cells form cilia in the presence of aggresomes (Figure 5.6 C). Aggresomes generated by the overexpression of GFP-tagged α-syn were also checked to see whether they inhibit ciliogenesis in differentiated SH-SY5Y. However, in contrast to previous experiments, when GFP alone was overexpressed cells were able to ciliate; inhibition of cilia formation was only observed in cells when α-synuclein was overexpressed. In differentiated SH-SY5Y cells overexpression of GFP alone also inhibited ciliogenesis.

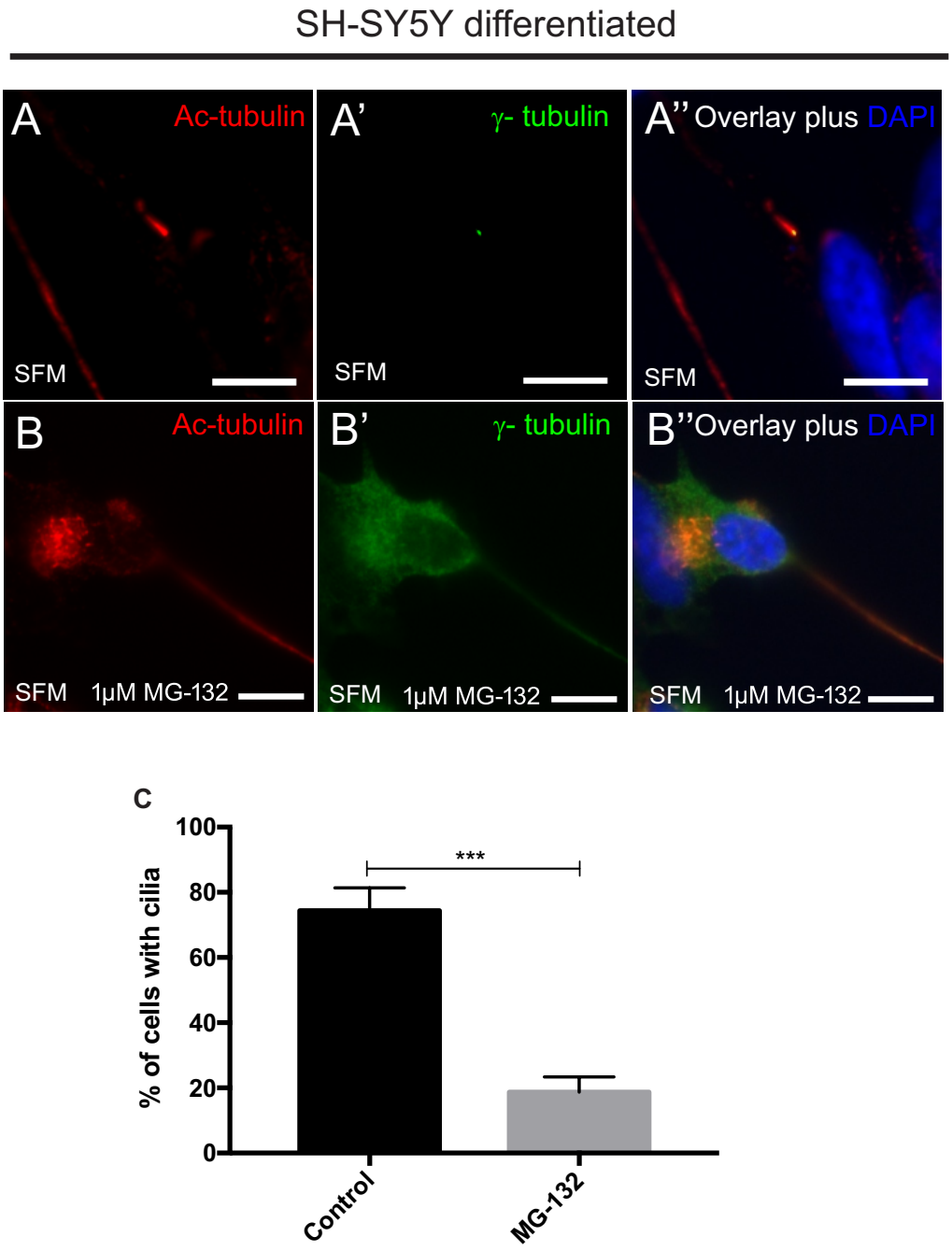

Figure 5.6 Differentiated SH-SY5Y fail to form cilia in the presence of aggresomes.
Undifferentiated SH-SY5Y were differentiated over a period of seven days by plating cells on collagen coated coverslips and treating cells with 10 μM retinoic acid, were the media was replaced every two days. Differentiated SH-SY5Y cells can form cilia in serum free condition over 24 hours. **A-A'')** Cilia is visualised by acetylated α-tubulin (red) and γ-tubulin (green) staining the cilium basal body**. B-B'')** Cells treated with 1 μM MG-132 for 18 hours form aggresomes, when serum starved for 24 hours cells fail to ciliate. Both acetylated α-tubulin and γ-tubulin staining concentrate at the aggresome. **C)** In serum, free media 75% of differentiated SH-SY5Y cells form cilia compared to 20% of cells forming cilia in the presence of aggresomes. Quantification of cilia in differentiated SH-SY5Y cells when treated with MG-132 ($P<0.0001$; by Student's t-test, 100 cells counted, n=3. Scale bar 10 μm. DNA/nuclei stained with DAPI.

5.2.7 Enriched culture of dopaminergic neurons cannot retain cilia in the presence of aggresomes

I have shown that the presence of aggresomes inhibits ciliogenesis in several cell line models including MEFs, representing a primary cell model, and differentiated SH-SY5Y, which are more representative of dopaminergic neurons. Primary neuronal cultures are even closer to neurons *in vivo*. A better representation of the dopaminergic neurons affected in Parkinson's. Basal ganglion neurons from rats were cultured as the basal ganglion is known to have an extensive dopaminergic network (Bäckman et al. 1996). I first checked whether these neurons possessed cilia, cilia were visualised by acetylated tubulin in serum conditions. The cilia of these neurons are a lot smaller than the other cell models as reported in literature (Marley & von Zastrow 2010). I also tested if neuronal cultures were supplemented in serum free condition, would this increase cilia number or cilia length. However, no difference was observed in cilia number or length, though neurons appeared morphologically stressed with increase in cell death observed. I showed that in chapter 3 neuronal cultures from rat basal ganglion can form aggresomes when treated with MG-132. I next tested if these aggresomes affect cilia of primary neurons. Neuronal cultures at 18 DIV were treated with 3 μM MG-132 for 18 hours or control treated with DMSO in serum supplemented media. Cells were fixed and stained with anti-acetylated tubulin and anti-TH antibodies. Positive tyrosine hydroxylase staining is observed, tyrosine hydroxylase is expressed throughout the neuronal cytoplasm, staining confirms the neuron is of dopaminergic nature (Figure 5.7 A-A''). In control neurons, cilia are visualised by acetylated tubulin. In the presence of aggresomes, increased acetylated tubulin staining is observed localising to the aggresome. However, the cilia are no longer seen. Tyrosine hydroxylase staining did not change, though increase in tyrosine hydroxylase intensity is observed at the nucleus (Figure 5.7 B-B''). Around 25% of dopaminergic neurons in control dishes possessed cilia while only 5% of neurons had cilia when aggresomes were induced (Figure 5.7 C).

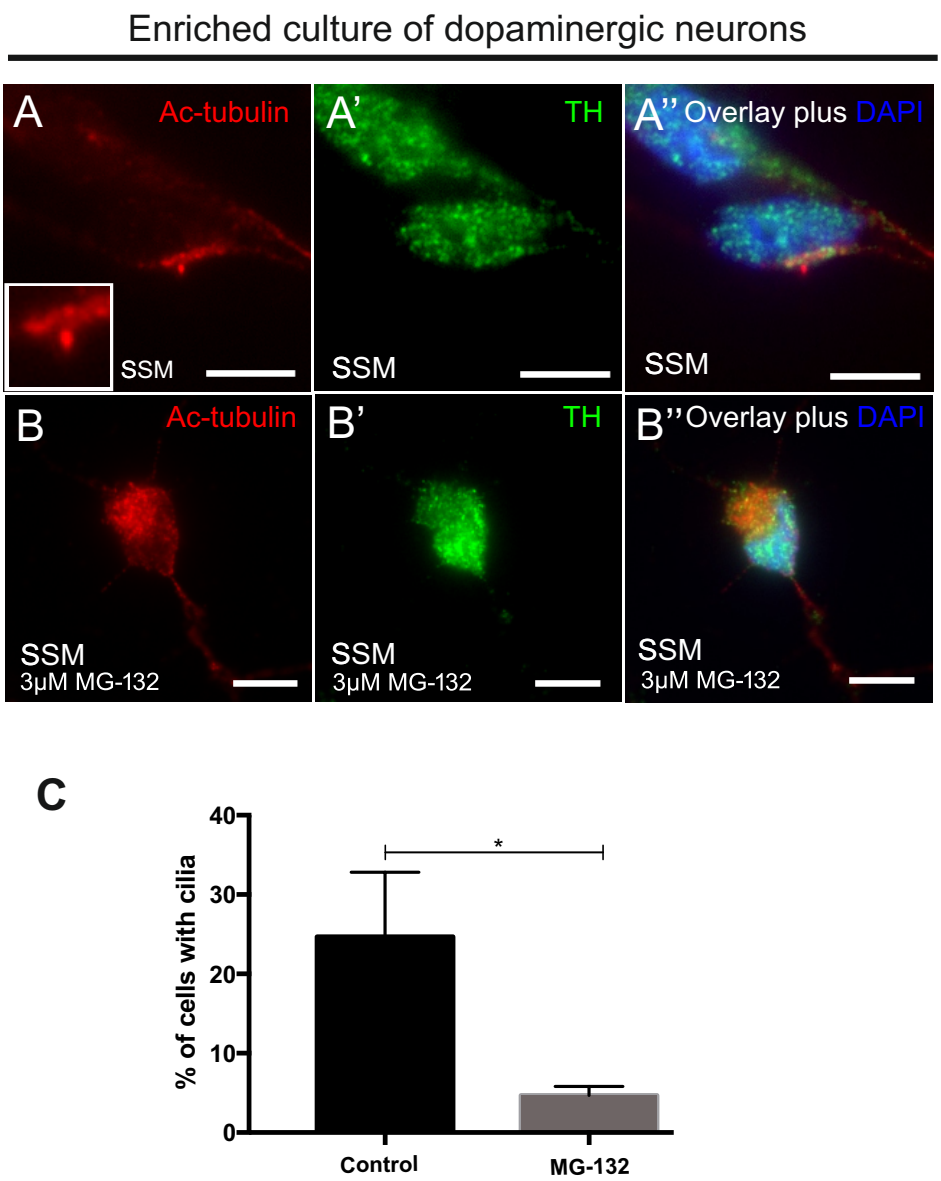

Figure 5.7 Aggresomes inhibit cilia in enriched culture of dopaminergic neurons .
A-A'') Enriched culture of dopaminergic neurons were cultured in-vitro for 21 days. Cells were stained with tyrosine hydroxylase (green) for dopaminergic positive neurons. In serum supplemented media they form cilia visualised by acetylated α- tubulin (red). B-B'') Neurons treated with 3 μM MG-132 for 18 hours failed to ciliate. The acetylated α- tubulin stain confines to the aggresome. C) In serum supplemented media 25% of dopaminergic neurons have cilia whereas, in the presence of the aggresome only 5% retain the cilia. Quantification of cilia for Enriched culture of dopaminergic neurons when treated with MG-132 ($P<0.0126$ by Student's t-test, 100 cells counted, n=3). DNA/nuclei stained with DAPI. Scale bars 10 μm.

5.2.8 Zebrafish larvae have a dopaminergic network and olfactory cilia

I have shown that the aggresomes supress cilia formation in different cell line model as well as cilia maintenance in primary neurons that already possess cilia. I next wanted to test whether aggresome formation affected ciliogenesis in an *in vivo* model. To do this I used zebrafish as the model organism as they are widely used to study cilia and are experimentally accessible. Since one of the early symptoms of Parkinson's is loss of smell, and olfactory receptors are housed in cilia on the olfactory neurons, I decided to test the state of such cilia in embryonic zebrafish in which aggresomes were induced. The olfactory pit in larval zebrafish is highly ciliated and accessible to observation by confocal microscopy. To check when cilia are observed at the olfactory pit, zebrafish embryos from 24 h.p.f to 72 h.p.f were fixed and stained with anti- acetylated tubulin. At 2 d.p.f the olfactory pit is highly ciliated in zebrafish embryos (Figure 5.8 B). I next established that dopaminergic neurons with cilia could be observed in the olfactory pit. To check this, zebrafish larvae at 3 d.p.f were fixed and stained with anti-acetylated tubulin and anti-TH antibodies. The dopaminergic network in zebrafish is detectable from 24 h.p.f and continues to develop as the embryo grows. At 3 d.p.f the establishment of the developing dopaminergic network can be observed by staining cells with tyrosine hydroxylase (Figure 5.8 A) with acetylated α-tubulin staining the axon tracts and cilia (Figure 5.8 A and B). The tyrosine hydroxylase and acetylated tubulin staining has some overlap, suggesting the olfactory bulb contains dopaminergic neurons. After microinjection of control GFP mRNA, cilia at the olfactory pit still form (Figure 5.8 C).

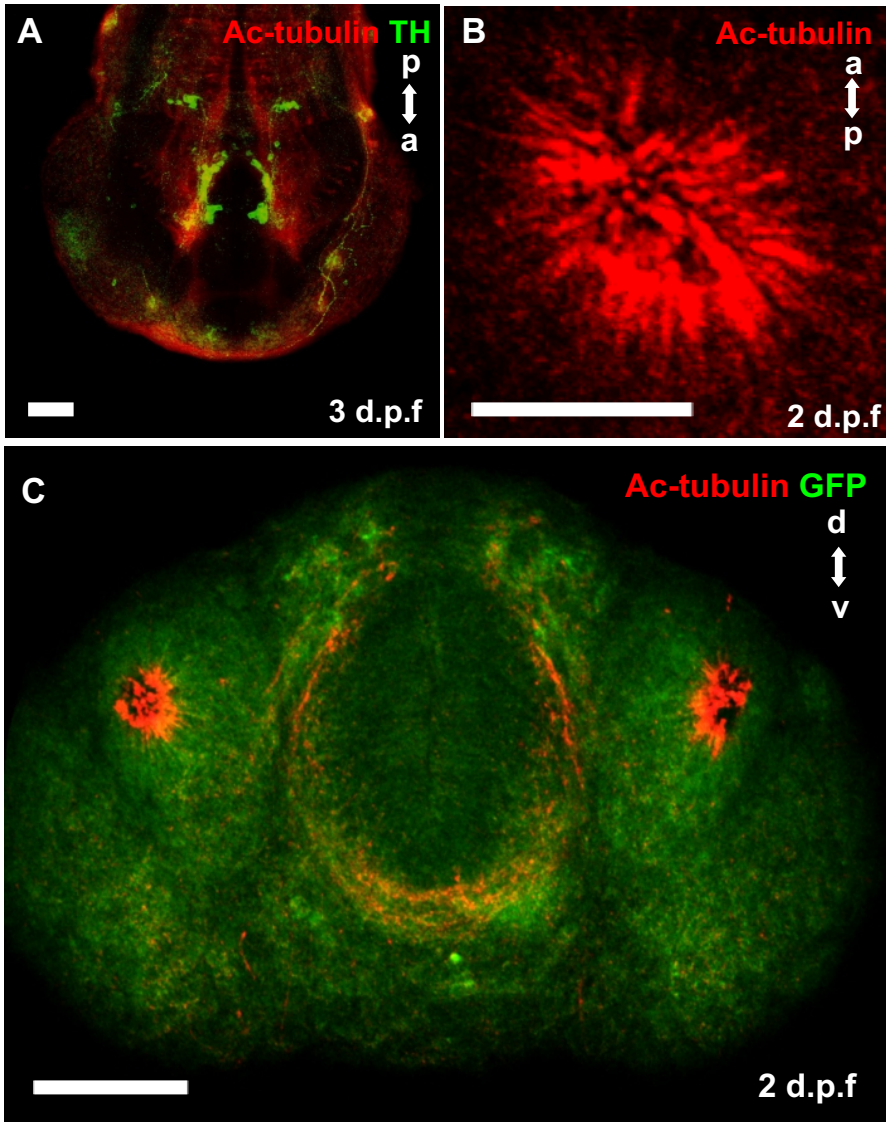

Figure 5.8 Dopaminergic network and olfactory cilia in zebrafish larvae.
A) The neuronal dopaminergic network in zebrafish is detectable from 24 h.p.f. and continues to develop during larval stages. By 3 d.p.f. a developing network is present in the forebrain of the larva when viewed from the dorsal aspect. This is clearly evident by TH-positive staining (green). TH staining is also seen around the olfactory pit. Acetylated tubulin (red) stains axon tracts and cilia. **B)** At 2 d.p.f the olfactory pit is highly ciliated as visualised by acetylated tubulin staining (red). **C)** After microinjection of control GFP mRNA, cilia at both the olfactory pits can be seen when viewed from the anterior axis. (acetylated tubulin, red). Scale bars 100 μm.

5.2.9 Olfactory cilia in zebrafish larvae are severely reduced when aggresomes are generated by treatment with MG-132

I have shown zebrafish larvae have a developing dopaminergic network at 3 d.p.f, with a highly ciliated olfactory pit. I next tested if aggresomes generated by MG-132 treatment would affect cilia at the olfactory pit. Zebrafish embryos at 24 h.p.f were treated with 50 μM MG-132 or DMSO for 48 hours. Zebrafish larvae were fixed and stained with anti-acetylated tubulin. In control embryos at 3.d.p.f the olfactory pit is highly ciliated with an average of 60 cilia. Cilia at the olfactory pit form in a ring like structure (Figure 5.9 A-B). However, when treated with MG-132 for 48 hours, there is a severe reduction in length and number of cilia with less than 20 cilia observed (Figure 5.9 C-E). Moreover, the ring like structure observed in control embryo changes to a circular mass of cilia.

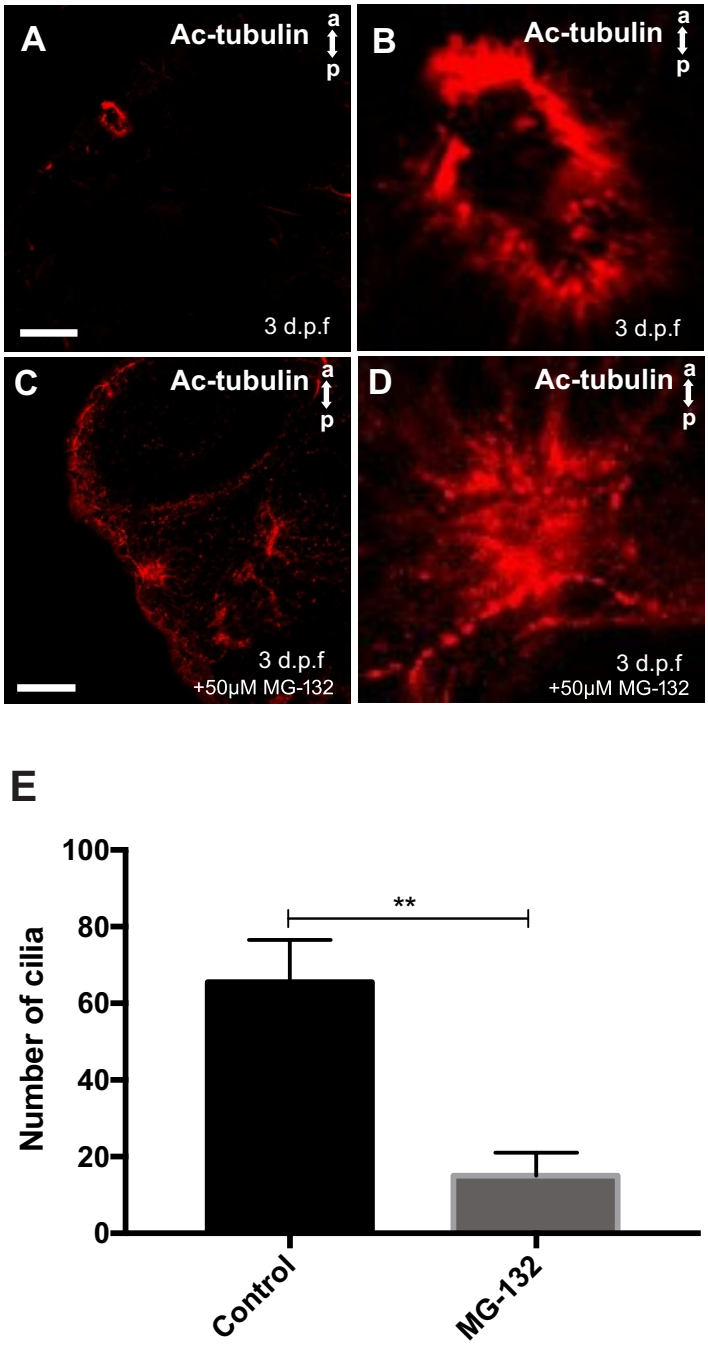

Figure 5.9 MG-132 treatment reduces the number of olfactory cilia in zebrafish larvae.
A) By 3 d.p.f extensive numbers of cilia are visible at the olfactory pit acetylated α-tubulin (red). B) zoomed in of A). C-D) Embryos treated with MG-132 50 μM for 48 hours, showed an extensive reduction in number of cilia (D zoomed in of C). E) Quantification of cilia numbers when embryos are treated with MG-132 ($P<0.0024$, by Student's t-test, n=4) A reduction of 70% is seen. Scale bars 100 μm.

5.2.10 Overexpression of α-syn in zebrafish larvae severely reduces number of cilia in the olfactory pit

Aggresomes generated through MG-132 treatment in zebrafish embryos severely reduced cilia length and cilia number at the olfactory pit. I next checked if overexpressing GFP-α-syn mRNA or any of the familial mutants also affected cilia at the olfactory pit. Zebrafish embryos at 1-4 cell stage were injected with mRNA encoding, control GFP or GFP -α-syn wild-type or familial. At 2 d.p.f the embryos were fixed and stained with anti-acetylated tubulin antibody. In control GFP injected embryos the olfactory pit is multi-ciliated with an average of 40 cilia (Figure 5.10 A). In embryos injected with GFP α-syn mRNA or any variant there was a severe reduction in the number and length of cilia as reduced acetylated tubulin staining is observed (Figure 5.10 B-F). In control embryos in which GFP alone is over-expressed, individual cilia can be easily distinguished in the olfactory pit, (Figure 5.10 A). However, the confocal images for the overexpression of α-synuclein and familial mutants show acetylated tubulin staining restricted to the periphery of the olfactory pit, where individual cilia are difficult to distinguish. Although from the merged confocal stacks individual cilia are difficult to delineate, it was easier to distinguish cilia in the individual stacks, which showed the cilia were significantly shorter (Figure 5.10 F). The presence of aggresomes in cell-based models, showed acetylated tubulin staining to localise to the aggresome. The acetylated tubulin staining observed at the periphery of the olfactory pit could be comparable to the staining observed in cells. As some of the acetylated tubulin staining at the olfactory pit was not staining the cilia, it could be that acetylated tubulin staining observed is staining of the aggresomes (Figure 5.10 B-D).

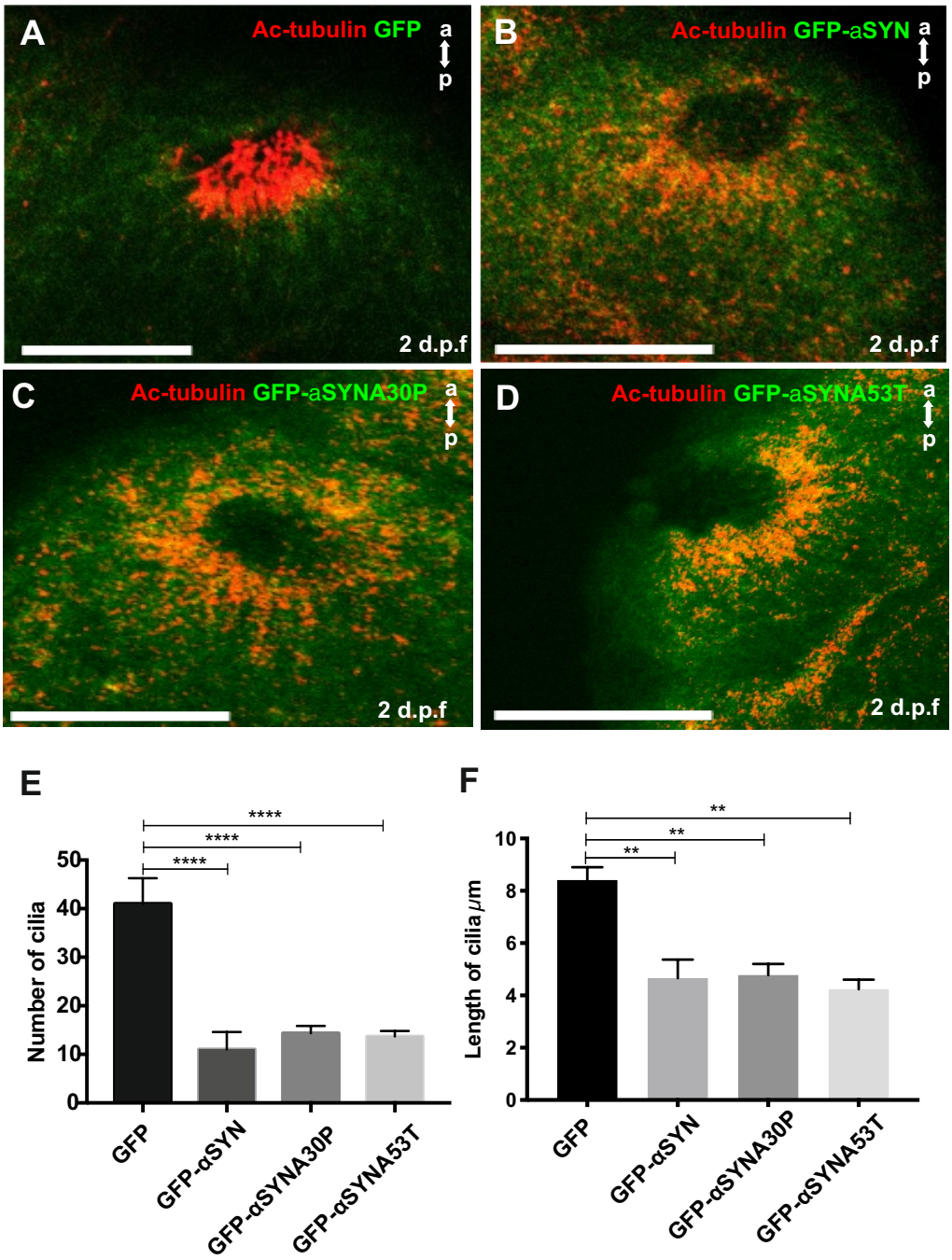

Figure 5.10 Overexpression of α-syn reduces the length and number of olfactory cilia in zebrafish larvae. **A)** In control GFP-injected embryos, cilia are seen in the olfactory pit in large numbers. Cilia is visualised by acetylated α-tubulin (red). **B-D)** Overexpression of any of the three forms of α-syn severely reduces numbers of cilia. Cilia length is also reduced. **E)** Quantification of cilia numbers in zebrafish embryos when α-syn is over expressed ($P<0.001$; by one-way ANOVA, n=3,). **F)** Quantification of length of cilia when α-syn is overexpressed in zebrafish embryos ($P<0.0088$; by one-way ANOVA, n=3). Scale bar 100 µm.

5.2.11 Overexpression of α-syn does not cause developmental abnormalities in zebrafish larvae

As I observe a reduction in the number and length of cilia when GFP-α-syn or the familial mutants are overexpressed in zebrafish larvae the absence of cilia or shorter cilia is known to cause other defects during embryogenesis, for example hydrocephaly, left-right asymmetry defects and pronephric cysts yet, none of these defects were observed (Figure 5.11 A-D). Control GFP mRNA or α-syn wildtype or familial mutant mRNA, was injected into the yolk of zebrafish embryos at 1-4 cell stage. The mRNA was overexpressed for 48 hours, widespread GFP expression can be seen throughout the embryos. The levels of expression in the embryos appear to be similar as expected as each construct was injected at 400 ng/µl. Nonetheless, it is also evident some embryos show increased expression in particular regions. This is seen when any of the three GFP-α-syn were overexpressed more specifically increased expression is observed around the eyes, brain and notochord (Figure 5.11 B-D). It is possible this localised increased expression is a result of GFP-α-syn aggregating and forming aggresomes and so the GFP signal is intensified. Overall the gross anatomy of these embryos appeared normal, no curvature or cysts in the kidney where observed.

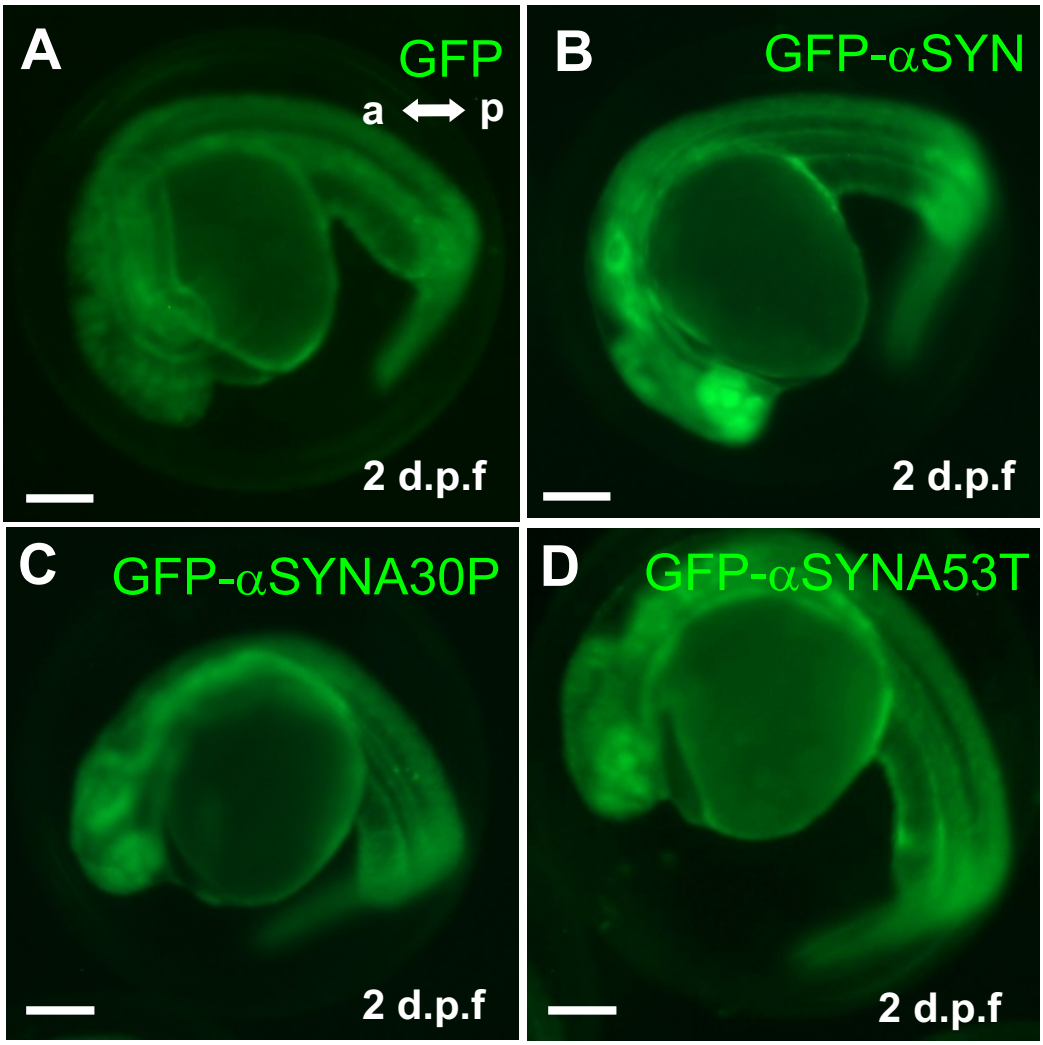

Figure 5.11 Overexpression of α-syn does not cause any developmental abnormalities in zebrafish larvae. **A-D)** 400pg of control GFP mRNA or α-syn was microinjected into zebrafish embryos at the 1-cell stage. Over expression of either control GFP mRNA or α-syn mRNA does not cause any anatomical defects in zebrafish larvae with similar levels of expression detected by overall fluorescence intensity. Overexpression is seen throughout the developing embryo, structural features such as eye and brain ventricles are clear visible. Scale bar 100 μm.

5.3 Discussion

Ciliogenesis is a dynamic process which requires translocation of the centrioles from the centre of the cell to the membrane (Pitaval et al. 2017). I show that aggresomes generated by either MG-132 or overexpression of GFP-tagged α-syn inhibit ciliogenesis in several lines, with aggresomes induced by MG-132 showing more severe affects. In RPE1 –hTERT, MEFs, undifferentiated and differentiated SH-SY5Y cell lines, aggresomes generated through MG-132 treatment prevented cilia form being formed. The number of cells ciliating drop more than 60%, compared to control cells. The cilia marker and centriole marker both strongly stained the aggresome. The γ-tubulin staining localising to the two centrioles changed to a larger zone of staining where the characteristic two dots of the centrosome were no longer visible indicating the aggresome has encaged the centrosome. I went onto show primary neuronal cilia from the basal ganglion already possess cilia. In the presence of aggresomes the cilia are not observed. Since these cells possess cilia in serum supplemented media, it shows that the aggresome is affecting ciliary maintenance. When zebrafish embryos were treated with MG-132 or injected with GFP- αsyn wild-type and familial mutants, the olfactory cilia in zebrafish are severely affected with reduced number of cilia and reduced ciliary length observed. Although ciliary defects in zebrafish larvae are associate with particular characteristic phenotypes, including hydrocephalus, increased number of otoliths and body curvature, none of these were observed. The embryos developed as normal. It has also been proposed olfactory cilia show increased sensitivity due to their localisation at the nasal cavity (Pinto 2011).

The inhibition of cilia formation could be due to number of reasons. The simplest is that the aggresome cages the centrioles and sterically hinders any further biochemical reactions of the centriole. This steric hindrance would structurally sequester the centrosome at its location near the nucleus which would physically block the centrosome from moving and forming a cilium. Since the aggresome is located in close proximity of the nucleus, even in serum free conditions, it suggests the centrosome is trapped. Similarly, when aggresomes were generated by overexpressing α-syn, the aggregated protein was also juxtaposed to the nucleus whilst in serum free conditions. In normal conditions the translocation of the centrosome is driven by dynein 1 motors along the microtubules (Johnston et al. 2002; Li et al. 2017) where the microtubules serve as a track

for the dynein motors. As I have shown in the previous chapter aggresomes inhibit microtubule nucleation. This could mean, the restricted microtubule activity or that a reduced number of microtubules are available for dynein-1 motors to transport the centrosome via the microtubule track.

Seeing that it is possible that the lack of microtubule nucleation prevents the dynein motors from collecting and transporting the centrosome it is also possible other components that are required to be delivered or removed from the centrosome for ciliogenesis to precede are prevented from doing so. For example, rabin8 which is a Rab8-guanine nucleotide exchange factor, is recruited to the centrosomes before ciliogenesis begins and that localises to the centrosome, rabin8 vesicle transport is microtubule dependent (Westlake et al. 2011). Nocodazole treatment blocked rabin8 localisation to the centrosome while depletion of rabin8 inhibited ciliogenesis (Chiba et al. 2013). In another study Zaarur et al. (2014) showed proteasome inhibition supressed the overall microtubule transport around the centrosome as proteasome inhibition was shown to create an entrapment zone (EZ) (Zaarur et al. 2014).

As an intact microtubule network is required for increased efficiency and selectivity of autophagic degradation (Kimura et al. 2008). A study by Tang et al. (2013) showed OFD1 is removed from centriolar satellites via autophagy mediated protein degradation to promote ciliogenesis, and when autophagy was compromised shorter and fewer cilia were observed (Tang et al. 2013). If aggresomes reduce microtubule activity, it is likely components such as OFD1 that need to be removed for ciliogenesis to proceed fail to do so resulting in absence of cilia. Similarly, the ubiquitin proteasome system is involved in removing centrosomal proteins for ciliogenesis to initiate. One study showed that the ubiquitin proteasome initiates ciliogenesis by removing centriolar trichoplein which is known to be a negative regulator of ciliogenesis (Kasahara et al. 2014). When trichoplein is stabilised by inhibiting the proteasome ciliogenesis is blocked. Seeing that MG-132 inhibits the proteasome and similarly overexpression of α-syn also compromises proteasome function to form these aggresomes it is likely, other proteins similar to centriolar trichoplein that need to be removed for ciliogenesis to follow are not able to do so as the proteasome function is impaired.

More recently it was shown the migration of centrosome is dependent on microtubules, where cells that were treated with nocodazole blocked centrosome migration and ciliogenesis (Pitaval et al. 2017). Additionally, they showed centrosome migration occurred 2-4 hours upon serum starvation and in parallel there was an increase of microtubules surrounding the centrosome which emphasises the need of microtubules for centrosome migration to the membrane. Pitaval et al. (2017) showed centrosomal migration towards the membrane to initiate ciliogenesis is driven by the remodelling of the cytoskeleton including the microtubule and actin networks. More specifically they showed the microtubule network compacted and bundled around the centrosome, where the orientation of the bundle between the centrosome and basal pole suggested it was exerting mechanical force towards the membrane. Both actin and microtubules were shown to rearrange and form asymmetrical networks at the basal end of cilia exerting a mechanical force to drive centrosome migration. It is possible in the presence of aggresomes, the force generated is not sufficient to drive centrosome migration. Interestingly they showed when cep164 was depleted from cells this remodelling did not occur and centrosomes failed to migrate and in turn cilia was not formed. Similarly, if centrosomal proteins cannot be delivered or removed from the centrosome, downstream events such as the remodelling of the cytoskeleton cannot occur.

The cytoskeleton is shown to modulate ciliogenesis and cilia function, where branched actin networks are shown to supress cilia formation. One of the mechanisms thought to result in cilia inhibition is through regulatory role in the transport of cilia directed vesicles by creating a mechanical barrier for vesicle movement or membrane remodelling required for ciliogenesis. The role in regulating vesicle transport is supported by observations that actin disassembly results in a transient accumulation of cilia-targeted positive vesicles at the basal body (Kim et al. 2015). The branched actin network could therefore block rapid vesicle transport that is necessary for cilia elongation. As the neuronal model already possessed cilia, which were no longer present when aggresomes were induced suggests ciliary maintenance is affected. The axoneme serves as a track for IFT driven by kinesin (anterograde) and dynein (retrograde) motors where, mis-localisation of ciliary components including structural as well as signalling components result in ciliary defects. As previously mentioned the branched actin network is thought

to act as a mechanical barrier, this could be a comparable affect, of the large insoluble aggregates which could similarly act as a mechanical barrier. Inhibiting trafficking of ciliary proteins which would affect cilia maintenance resulting in short or fewer cilia.

One of the early but unexplained symptom of Parkinson's is the loss of smell, it is possible it is due to the loss of olfactory cilia and associated odorant receptors. Approximately 90% of patients with early stage Parkinson's exhibit olfactory dysfunction (Doty et al. 1988). Presence of LBs have also been confirmed in the anterior olfactory nucleus (AON) which has been associated with significant neuronal loss (Pearce et al. 1995). The Braak staging also report the neuropathology , particularly Lewy bodies and Lewy neurites begin within the olfactory bulb, AON and dorsal motor nucleus of the vagus nerve (dmX) which continues to advance through other regions (Braak et al. 2003). Additionally, direct connections are present between the olfactory system and the substantia nigra. Anosmia is also seen in a number of ciliopathies including Bardet –Biedl syndrome (BBS), Primary ciliary dyskinesia (PCD) and Polycystic kidney disease (PKD) whereby the causative proteins localize to the basal body or the cilium. This suggests cilia dysfunction might contribute to the loss of smell observed in Parkinson's patients. Similarly, in AD loss of dopamine receptors in the olfactory bulb has been observed (Loopuijt & Sebens 1990). Reduction in number of cilia has also been shown in a mouse model of ALS where olfactory impairment was also observed (Ma et al. 2011; Takeda et al. 2014). Loss of smell has been reported in AD and ALS patients.

I have shown that cilia formation and cilia maintenance is inhibited in the presence of aggresomes both in an *in vivo* and *in vitro* model. Our model proposes this is likely due to the aggresome acting as a mechanical barrier for centrosome re-location and the recruitment of ciliary components necessary for its assembly. As well as preventing trafficking of ciliary proteins in the cilia. It is possible, that the loss of smell seen in Parkinson's patients and other in other neurodegenerative diseases could be explained by the loss of cilia that house the olfactory receptors at the olfactory bulb. Future clinical-experiments would include examining the olfactory cilia in patients with Parkinson's by taking nasal tissue of affected patients. To check if cilia number or length is affected. Additionally, to look at whether the aggresome inhibits other pathways that regulate

ciliogenesis, such as autophagy. As autophagy is involved in cilia formation and the clearance of aggresomes.

6. BCAP a centriolar satellite protein and an inhibitor of ciliogenesis

6.1 Introduction

The centrosome is the main microtubule organising centre (MTOC) of animal cells, that regulates cell division, motility and polarity (Gotlieb et al. 1981; Piel et al. 2000). Centrosomes are cytoplasmic structures composed of a pair of cylindrically shaped centrioles, surrounded by an electron-dense protein matrix, the pericentriolar material (PCM) (Bornens 2002). Each centriole is structurally composed of nine triplet microtubules, that acts as a template for the axoneme, the skeleton of the cilium (Sorokin 1968; Anderson & Brenner 1971). Primary cilia are microtubule-based organelles that protrude from the surface of many mammalian cells. They house receptors and signalling proteins that are involved in many signalling pathways(Goetz & Anderson 2010). Mutations in ciliary components give rise to a group of diseases termed ciliopathies, including Bardet Biedl syndrome (BBS), polycystic kidney disease (PKD), Joubert Syndrome (JBTS) and Meckel-Gruber Syndrome (MKS) (Boltshauser & Isler 1977; Saeki et al. 1984; Ansley et al. 2003; Dawe et al. 2007). These diseases affect multiple tissues and manifest as a constellation of features that include retinal degeneration, renal disease and cerebral anomalies, reflecting the diverse role of cilia in different tissues(Waters & Beales 2011).

The transition between centriole and basal body is tightly regulated. Through genomic and proteomic screens, positive and negative regulators of ciliogenesis have been identified (Wheway et al. 2015). A genomic screen carried out by Kim et al. (2010), found 36 positive and 13 negative regulators of ciliogenesis, while some are solely involved in ciliogenesis and others involved in other regulatory networks (Kim et al. 2010). While key mechanisms exist between these regulators it is largely not fully understood. Though there are many protein components identified as positive regulators for ciliogenesis, there are far fewer known proteins that inhibit ciliogenesis. Of the few known negative regulators, some are satellite proteins. This includes the oral-facial-digital syndrome 1 (OFD1) protein. OFD1 localises to the centrioles and to centriolar satellites; the centriolar satellite pool of OFD1 is degraded via autophagy, promoting ciliogenesis (Tang et al.

2013). In another study by Spektor and colleagues (2007), it was demonstrated that two centrosomal proteins, Cep97 and CP110, act as negative regulators of ciliogenesis, as depletion of these proteins resulted in cilia formation (Spektor et al. 2007). Satellite proteins cluster around the centrosome, however, they are not static but move around the centrosome and assist in centrosome assembly and ciliogenesis.

In my MRes studies, I investigated the role of two proteins in zebrafish development. I looked at Outer Dense Fiber 2 (ODF2) and Outer Dense fiber 2-Like (OFD2l). ODF2 and ODF2L were depleted in zebrafish embryos using morpholinos. Due to their name, one might expect the role in centrosome biology and zebrafish development to be similar, however, it should be noted there is only 28% identity and 51% similarity between them. ODF2 is a centriolar appendage protein, localising to one of the two centrioles; removal of ODF2 inhibits cilia formation by preventing basal body docking at the membrane (Ishikawa et al. 2005). In zebrafish, ODF2 depletion was shown to affect brain development (Novorol et al. 2013). When ODF2-like was depleted the phenotype observed was similar to that of centriolar satellite proteins (Stowe et al. 2012). Although it has got the name ODF2l it has been previously published as Basal Body Centriole-Associated Protein (BCAP) (Ponsard et al. 2007). Paul de Saram (PdS) then followed on this project and showed it to be a satellite protein (de Saram et al., 2017). He showed that ODF2l/BCAP behaves as a negative regulator of ciliogenesis as depletion of ODF2l/BCAP resulted in cilia formation. Initial we assumed BCAP/ODF2L would have similar localisation pattern to ODF2. However, unexpectedly BCAP/ODF2L staining appears speckled around the centrosome, co-localising with other centriolar satellite proteins. As ODF2L was first named BCAP and was described to localise to the basal bodies. We will also continue to refer to it as BCAP as initial data shows differences in function and localisation to ODF2, suggesting it is not 'like' ODF2.

BCAP was first identified by Ponsard et al.(2007) and colleagues, who demonstrated BCAP localisation within basal bodies of motile ciliating tissues and at centrioles of proliferating cells (Ponsard et al. 2007). They went onto observe increased expression of BCAP in trachea and testes, but also detected expression of different isoforms between the tissues. Contrary to their observations, we observed BCAP as a cloud of small punctae around the centrosome, a staining pattern characteristic of centriolar satellites.

Additionally, we observed co-localisation between BCAP and other centriolar satellite proteins, suggesting BCAP is a centriolar satellite protein. Further characterisation of BCAP revealed that BCAP levels decrease markedly when ciliogenesis is induced by serum starvation. BCAP is seen around the centrosome in proliferating cells; this staining disappears in ciliating cells also confirmed by western blotting. Similarly, when BCAP was depleted by RNAi in serum conditions, cilia were observed. However, when these experiments were repeated with another BCAP antibody slight differences were observed, with BCAP disappearing then reappearing after ciliogenesis with a slight reduction in expression levels. This led us to think BCAP could have multiple isoforms with different roles as both the NCBI database predicts 4 transcript variants and Ponsard et al. identified five isoforms by Northern blotting, where they suggested different isoforms having slightly different function (Ponsard et al. 2007).

Since I was interested in the inhibition of ciliogenesis, I became interested in its regulation in case aggregates and aggresomes were affecting the normal regulation of ciliogenesis, possibly through autophagy, which is a pathway common to both processes. In this chapter I look at further elucidating the role of BCAP by exploring the potentially different or redundant roles of the splice variants predicted in the NCBI database to resolve difference seen between two antibodies. In this chapter I will explore the role of BCAP in ciliogenesis. The work was initiated by PdS which I continued and published.

6.2 Results

6.2.1 Localisation of BCAP

The function of BCAP was largely unknown, with a previous study observing basal body localisation in ciliating tissues (Ponsard et al. 2007). This figure summarises the work carried out by PdS, Figure 6.1a and b is an amalgam of figures 1,3,4 and 5 from the paper de Saram et al. (2017). In brief, BCAP staining using the anti-BCAP antibody (Biorybt) showed satellite-like staining, appearing as speckled granular punctae around the centrioles (Figure 6.1a A-C and I). BCAP staining localised with the prototypical centriolar satellite protein, PCM-1 (Figure 6.1a H). BCAP was then overexpressed, which also showed similar centriolar satellite staining that also co-localised with the BCAP antibody and PCM-1 (Figure 6.1a D-G and J-L). Since BCAP showed centriolar satellite staining, and centriolar satellites are known to be involved in ciliogenesis, expression and localisation of BCAP in ciliating cells was tested. In ciliating cells, BCAP staining disappeared, confirmed and by Western blotting BCAP was removed. (Figure 6.1a M-N and Q-R). Consistent with a possible inhibitory role, overexpression of BCAP inhibited ciliogenesis in serum free media (Figure 6.1a O-P). BCAP was then depleted by RNAi in serum supplemented media. BCAP staining was no longer seen around the centrioles (Figure 6.1b C) and BCAP depletion was confirmed by RT-PCR (Figure 6.1b F-G). Consistent with the overexpression experiments, these cells now ciliated in conditions where cells do not normally form cilia (Figure 6.1b D). Additionally, an increase in cilium length was observed (Figure 6.1b E). When these experiments were repeated using another commercially available antibody anti-BCAP (Proteintech), slightly different results were obtained. As before, proliferating cells show BCAP as having a satellite-like staining, around the centrioles (Figure 6.1b A). However, in serum free conditions, BCAP is seen to localise at the base of the cilia or clustered away from it (Figure 6.1b B). Western blot data showed only a 30% reduction in BCAP levels when cells ciliate in serum free media (Figure 6.1b H-I). I first aimed to resolve this discrepancy then further understand the role of BCAP in control of ciliogenesis.

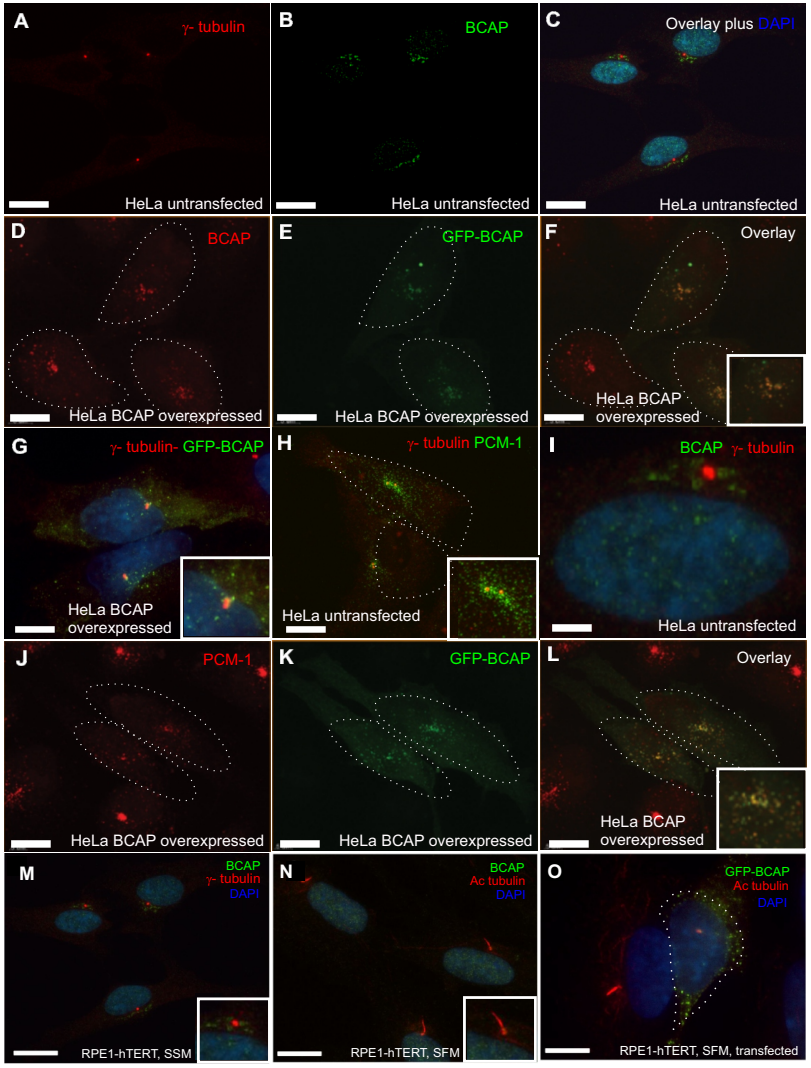

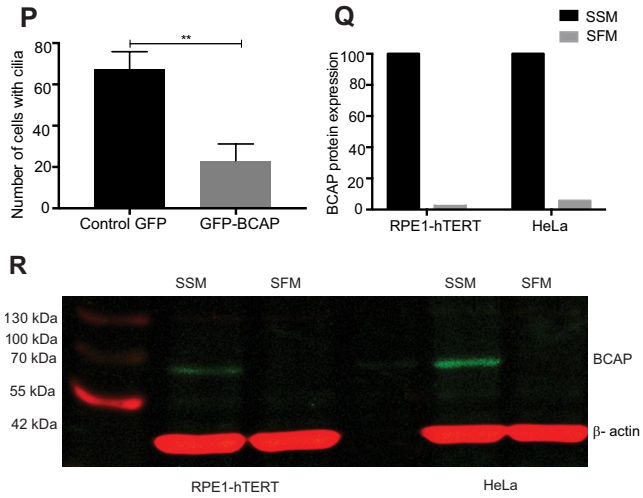

Figure 6. 1 A Localisation of BCAP and ciliogenesis.
A-C) HeLa cells stained with anti-γ-tubulin antibody (red), anti-BCAP (Biorbyt) antibody (green) and DAPI (blue) overlay image, **C)** cloud of small granular spots clustered around the centrosome, 1-2 punctae of γ-tubulin. **D-F)** anti-BCAP staining (red) co-localises with GFP-mBCAP fluorescence (green), **E)** overlay signals are shown in F. **G-*H*)** GFP-mBCAP appears as punctate staining around the centrosome, visualised by γ-tubulin (red). HeLa cells stained with ant-PCM1 antibody (green) show similar punctate staining around the centrosome (red), characteristic of centriolar satellite staining. **I)** This is a magnified image shown in C, BCAP (green), staining is around the centrosome but not at the centrioles (red), BCAP staining does not overlap with γ-tubulin. **J-L)** PCM1 staining (red) coincides with GFP-mBCAP staining (green) overlay image shown in L. **M)** In cycling RPE1-hTERT cells in serum supplemented media (SSM), endogenous BCAP visualised by anti-BCAP (Biorbyt) antibody (green) localises in satellites around the centrosome (γ-tubulin, red) next to the nucleus (DAPI, blue). **N)** in serum-free media (SFM), cilia visualised by acetylated tubulin (red) are formed where BCAP staining (green) disappears (DAPI in blue). **O)** When cells are transfected with a GFP-mBCAP expression plasmid, untransfected cells form a cilium, whereas the transfected cells do not (GFP-mBCAP in green, acetylated tubulin (red) and DAPI in blue. **P)** There is a 40% reduction in the number of cells with cilia when GFP-mBCAP is overexpressed ($P<0.001$ by Student's t-test, 100 cells counted, 3 independent experiments. **Q-R)** Western blotting confirms BCAP (green; running at ~70 kDa) does not disperse, instead the protein disappears on both HeLa and RPE1-hTERT cells. BCAP levels drop over 90% when cells ciliate. Scale bars: 10 μm. Data from de Saram et al. (2017)

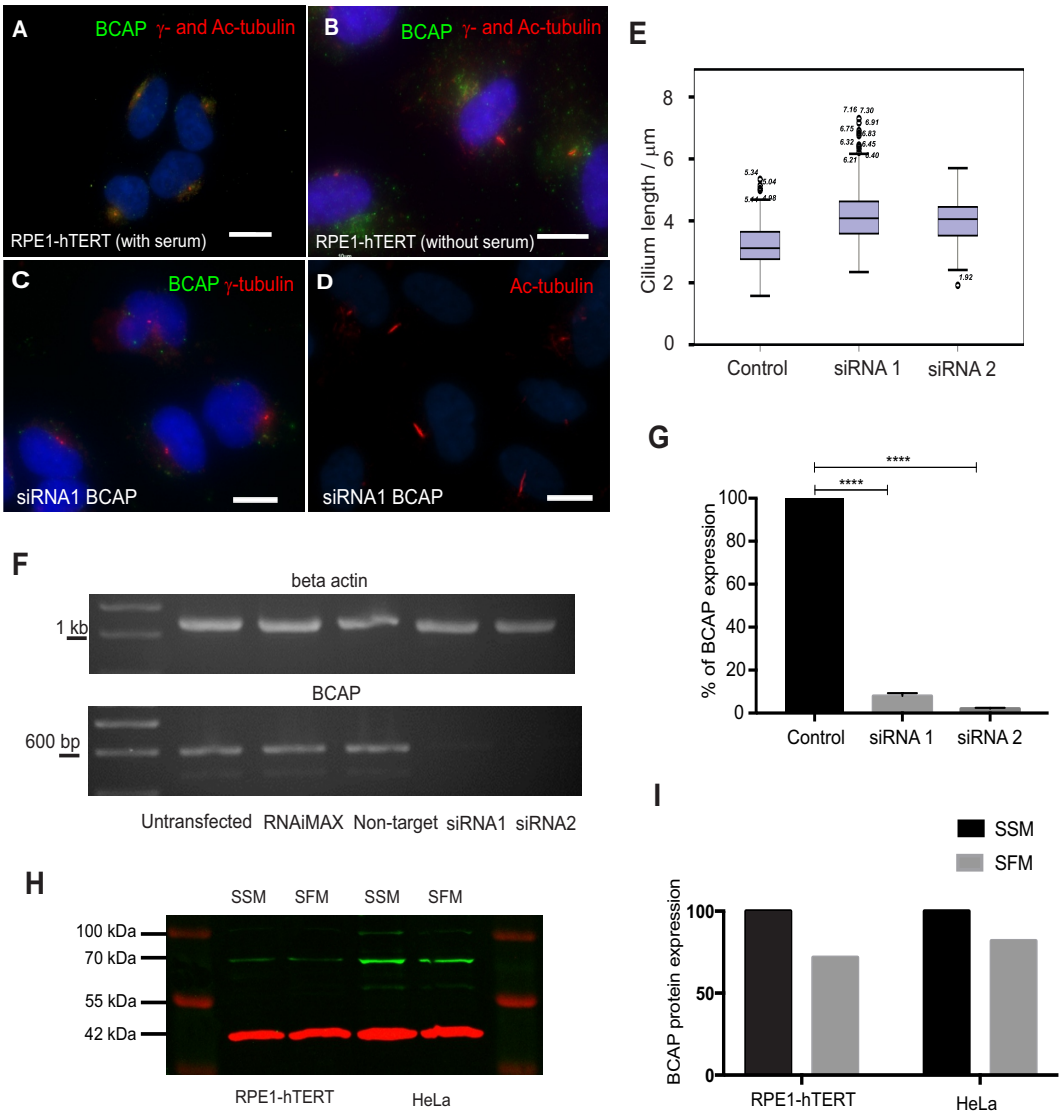

Figure 6. 1 B BCAP depletion promotes ciliogenesis. A) Cycling RPE1-hTERT cells stained with anti-BCAP (Proteintech), anti-γ-tubulin and anti-acetylated tubulin antibody in serum supplemented media. BCAP appears satellite-like around the centrosome visualised by -γ-tubulin. B) in serum-free media (SFM), cells at presumably different stages of ciliogenesis can be observed. BCAP is seen at the base of the cilium (green) or clustered away from it. C-D) two different siRNA duplexes both effectively deplete BCAP, by immunofluorescence, BCAP signal disappears in siRNA treated cells (C), D) a large proportion of these cells in serum-supplemented medium now form cilia (acetylated tubulin in red). E) Cilium length also increases in serum-starved and BCAP depleted RPE1-hTERT cells from 3-4µm, P<0.001 by Student's t-test, 150 cilia were counted in each sample. F-G) RT-PCR shows siRNAs effectively deplete BCAP: a 600bp fragment of BCAP is amplified by RT-PCR in various control samples (untransfected, lipofectamine and non-target siRNA) but is absent when proliferating RPE1-hTERT cells are treated with the siRNAs; beta actin is amplified to the same level in all samples (three independent experiments P<0.001 by one-way ANOVA). H-I) Anti-BCAP (Proteintech) antibody was used to probe cell extracts before and after ciliogenesis in RPE1-hTERT and HeLa cells, levels of this protein decrease slightly rather than disappearing, β-actin is stained in red quantified in E. Scale bars 10 µm. Data from de Saram et al. (2017)

6.2.2 BCAP localisation and levels change during ciliogenesis

We have shown BCAP expression changes from localising to the centrosome in proliferative cells to, at least, reduced levels in cells that have ciliated. We sought to observe the dynamics of BCAP expression and localisation as cells ciliate, to try to resolve the discrepancy between the two antibodies. Since we had an antibody but not a stable, fluorescent cell line, time-points were taken during the process of ciliogenesis, rather than using time-lapse microscopy. This experiment was initially carried out by PdS, which I then repeated. The data shown in this figure is my own. RPE1-hTERT cells were synchronised at G2/M transition phase by treating cells with 1.5 μM nocodazole for 24 hours. Cells were released from G2/M phase by placing them in media lacking serum and nocodazole. Cells were fixed at every hour and stained with anti-BCAP (Proteintech) and anti-γ-tubulin or anti-acetylated-tubulin antibodies. Through the course of ciliogenesis BCAP staining changed. Immediately after release from the nocodazole block BCAP, staining is mainly diffuse throughout the cytoplasm (Figure 6.2 C-C'' and D-D''). As time continues BCAP adopts a satellite-like staining pattern by two hours, which coincides with the centrosome (Figure 6.2 E-E''). By four hours, ciliogenesis has initiated, as small cilia can be observed (Figure 6.2 F-F''). At this point, BCAP staining has disappeared with only marginal fluorescence signal remaining (Figure 6.2 I). As ciliogenesis continues, cilia lengthen, and BCAP staining reappears near the base of the cilium, observed as centriolar satellite staining (Figure 6.2 G-G''). By 8 hours ciliogenesis is nears completion with BCAP continuing to appear in the satellites at the basal body (Figure 6.2 H-H''). BCAP expression is near 50% pre-ciliogenesis level (Figure 6.2 I). During the initial stages of ciliogenesis, BCAP disappears but then reappears as cilia are being formed.

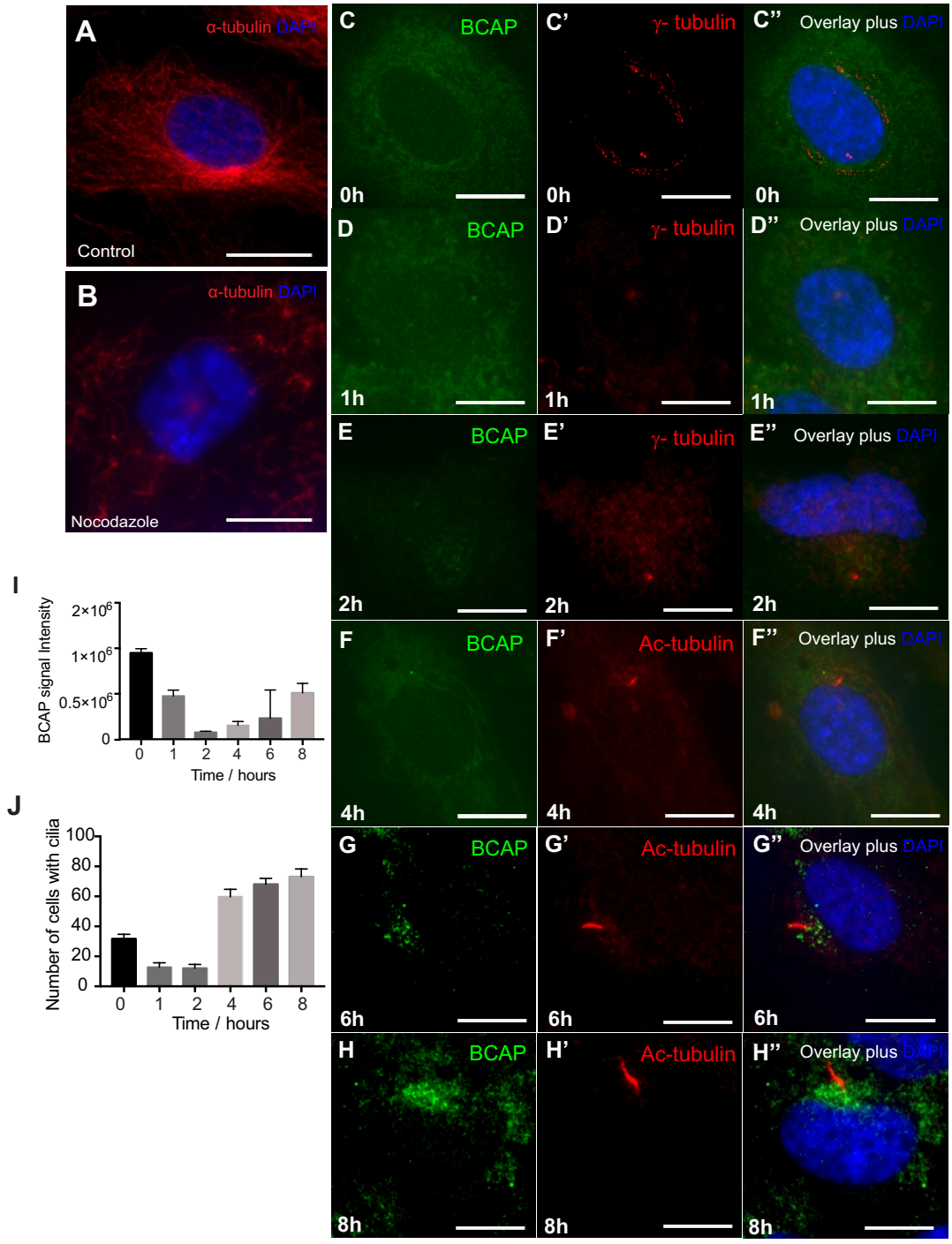

Figure 6. 2 BCAP levels and localisation change during ciliogenesis.

A) Untreated RPE1-hTERt cells are stained with anti-α-tubulin antibody and DAPi, α-tubulin (red) labels the microtubules seen extending across the cytoplasm. **B)** RPE1-hTERT cells are treated with nocodazole and stained with anti-α-tubulin antibody and DAPI, reduced microtubule staining is visible. **C-H'')** RPE1-Htert cells were synchronised by a nocodazole block followed by release. Samples were fixed at hourly intervals, with time-points at which key changes took place shown here. **D-D'')** After release at 1 h BCAP (green) is dispersed in the cytoplasm, as is the γ-tubulin signal (red). **E-F'')** While the γ-tubulin signal rearranges into recognisable centrosomes between 2-4 h, BCAP signal disappears. At 6 h cilia are visible and BCAP signal is returning. By 8 h, ciliogenesis appears complete and strong BCAP signal is visible at the base of the cilia. **I)** Signal intensity of BCAP was measured at each stage. BCAP is highly expressed at the first time-point and then gradually decreases. By 8 h BCAP expression has increased again to 50% of its pre-ciliation value. **J)** Number of cilia at each time-point was measured, with 60% of cells showing cilia by 8 h. This represent 3 independent experiments. Scale bars 10 μm.

6.2.3 BCAP localisation changes when PCM-1 is depleted in RPE1-hTERT cells

PCM-1 is the prototypical satellite protein. Previously, we showed that PCM-1 co-localises with BCAP. Depletion of PCM-1 by RNA interference (RNAi) in mammalian cells results in loss of centriolar satellites and reduced centrosomal localisation of some centriolar satellite-associated proteins (Stowe et al. 2012). Similarly, to strengthen the evidence that BCAP is a satellite protein, I tested if BCAP localisation is affected when PCM-1 is depleted. RPE1-hTERT cells were transfected with either control siRNA or siRNAs targeting PCM-1. After 48 hours, cells were fixed and stained with anti-PCM-1, anti-γ-tubulin or anti-BCAP antibody. In control cells, PCM-1 appears as granular specks around the centrosome, visualised by γ-tubulin (Figure 6.3 A-C). When PCM-1 is depleted, PCM1 staining is no longer visible, while centrosomal staining with gamma tubulin is unaffected (Figure 6.3 D-F). However, PCM-1 depletion changes BCAP localisation, with it now observed as a diffuse, non-punctate cytoplasmic staining (Figure 6.3 G-I). This supports BCAP being a centriolar satellite protein.

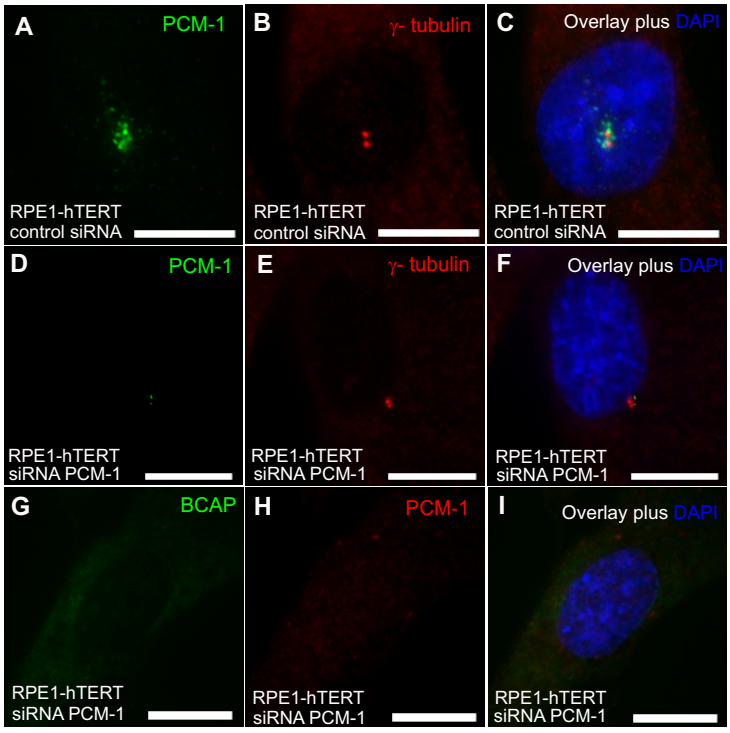

Figure 6.3 Removal of PCM-1 disperses BCAP.
A-C) RPE1-hTERT cells are transfected with control siRNAs and stained with anti-PCM1 (green) and anti-γ-tubulin (red) antibodies. PCM-1 is seen clustered around the centrosome visualised by γ-tubulin, they are unaffected in control siRNA cells. **D-F)** PCM-1 is depleted in RPE1-hTERT cells by RNAi using an siRNA targeting PCM-1, as PCM-1 staining disappears (D) while γ-tubulin is unaffected (E). **G-I)** siRNA depletion of PCM-1 results (H, PCM-1 in red) in BCAP no longer localising at the satellites (G BCAP in green). Instead a diffuse, non-punctate cytoplasmic staining is observed, Scale bars: 10 μm

6.2.4 Rescue of depleted BCAP inhibits ciliogenesis in RPE1-hTERT cells

When ciliogenesis is induced by serum-starvation, BCAP levels drop to below detection, suggesting BCAP is an inhibitor of ciliogenesis. We predict that BCAP depletion by RNAi would cause cells to ciliate under conditions in which they normally do not ciliate. RPE1-hTERT cells were therefore transfected with either control siRNA or siRNAs targeting BCAP (all isoforms) in serum-supplemented conditions. Following 48 hours post-transfection, cells were fixed and stained with anti-BCAP (Proteintech) and anti-acetylated-tubulin antibodies to stain cilia. In control transfected cells, BCAP localises to the centrioles/basal bodies (Figure 6.4 A-C). While in cells transfected with siRNAs targeting BCAP this staining is not seen (Figure 6.4 D-I). In serum-supplemented conditions, 5% of cells ciliate, whereas over 70% of cells ciliate when BCAP is depleted (Figure 6.4 M). I next tested the specificity of the siRNAs targeting BCAP. As the coding sequence of mouse BCAP is not completely identical with human BCAP at the target sites of the two siRNAs used, RPE1-hTERT cells were co-transfected with siRNAs targeting BCAP (all isoforms) and the expression construct for mouse BCAP. After 48 hours post transfection cells were fixed and stained with anti-Ac-tubulin antibody. In cells depleted of human BCAP but expressing GFP-mBCAP, only 20% of cells formed a cilium while over 60% of cells were able to ciliate in the absence of overexpressed GFP-mBCAP (Figure 6.4 J-K and L). This shows that mBCAP is able to restore BCAP levels and prevent cilia formation in cycling cells.

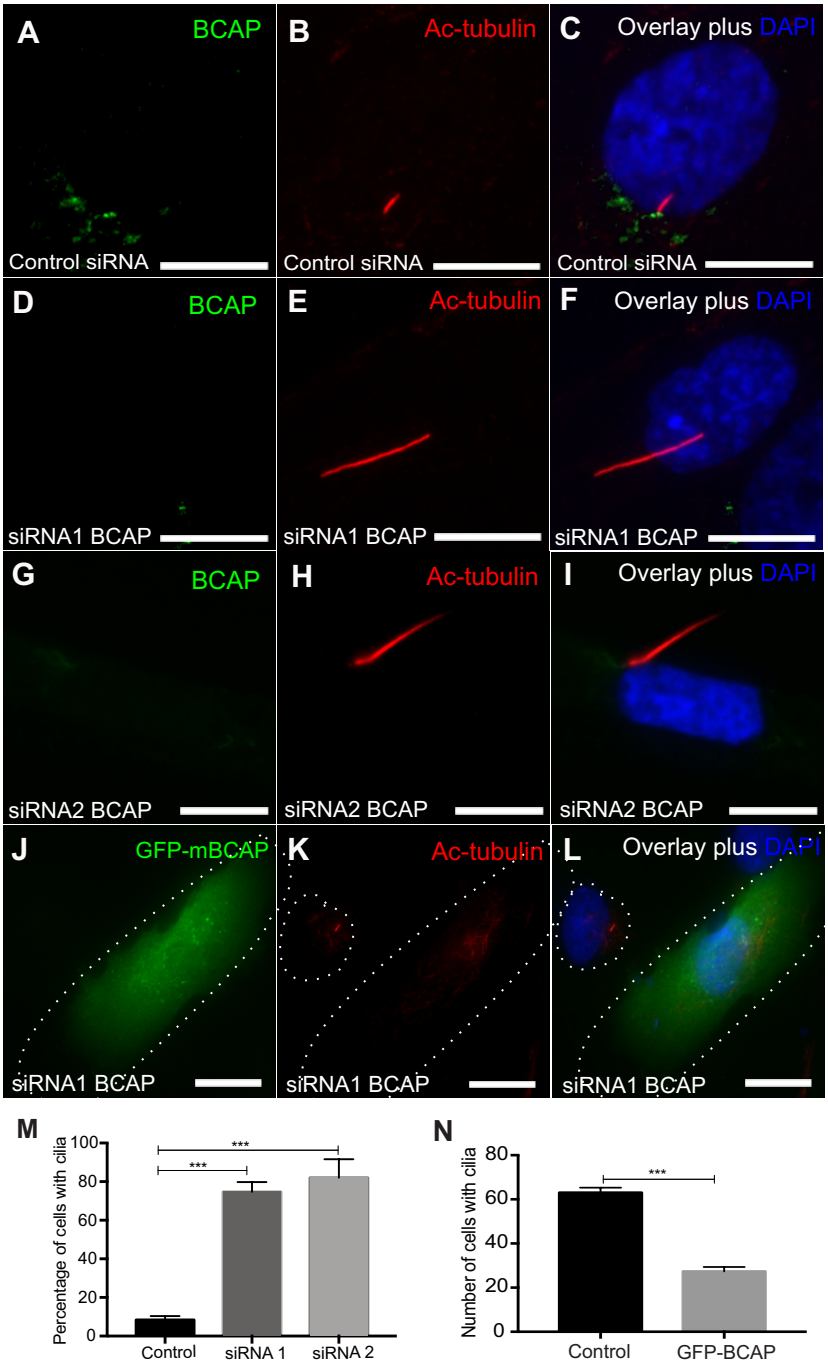

Figure 6. 4 Rescue of depleted BCAP inhibits ciliogenesis in RPE1-hTERT cells.
A-C) RPE1-hTERT cells are transfected with control siRNA and stained with anti-BCAP (Proteintech) and anti-acetylated tubulin antibodies, BCAP is seen at the base of the cilia visualised by acetylated tubulin, example of control cilia **D-I)** When BCAP is depleted in RPE1-hTERT cells by two different siRNA duplexes cilia length increases, example of longer cilia observed while BCAP staining is no longer seen**. J-L)** Mouse BCAP will rescue RNAi depletion, with transfected cells not making cilia, shown separately in K and with DAPI and GFP-mBCAP together in L (N, P<0.001: Student's t-test, 100 cells were counted in three independent experiments **M)** only 7% of control cells form cilia but 79% of cells treated with siRNAs ciliate; a total of 100 cells were counted, P<0.001 by chi-squared test. These data are from are from 3 independent experiments. Scale bars; 10 μm.

6.2.5 BCAP depletion does not affect localisation of a centriolar satellite protein or centriolar appendage proteins in RPE1-hTERT cells.

I have shown PCM-1 depletion results in diffuse BCAP staining. I next tested whether BCAP depletion could similarly change the localisation of other centriolar satellite proteins or of other centrosomal proteins. RPE1-hTERT cells were either transfected with control siRNA or siRNA1 targeting BCAP. Following 48 hours post-transfection cells were fixed and co-stained with anti-BCAP and anti-γ-tubulin or anti-PCM-1 or anti-ODF2 antibody. In control cells, BCAP staining is seen as small granular punctate at the centrosome, visualised by γ-tubulin and ODF2 which is a centriolar appendage protein (Figure 6.5 A-F). BCAP is also seen to co-localise with the centriolar satellite protein PCM-1 (Figure 6.5 G-I). In treated cells where BCAP is depleted, minimal BCAP staining is seen while neither γ-tubulin, ODF2 nor PCM-1 staining is affected (Figure 6.5 J-R). The characteristic punctae of the two centrioles are visible and the speckled, centriolar satellite staining of PCM-1 is observed.

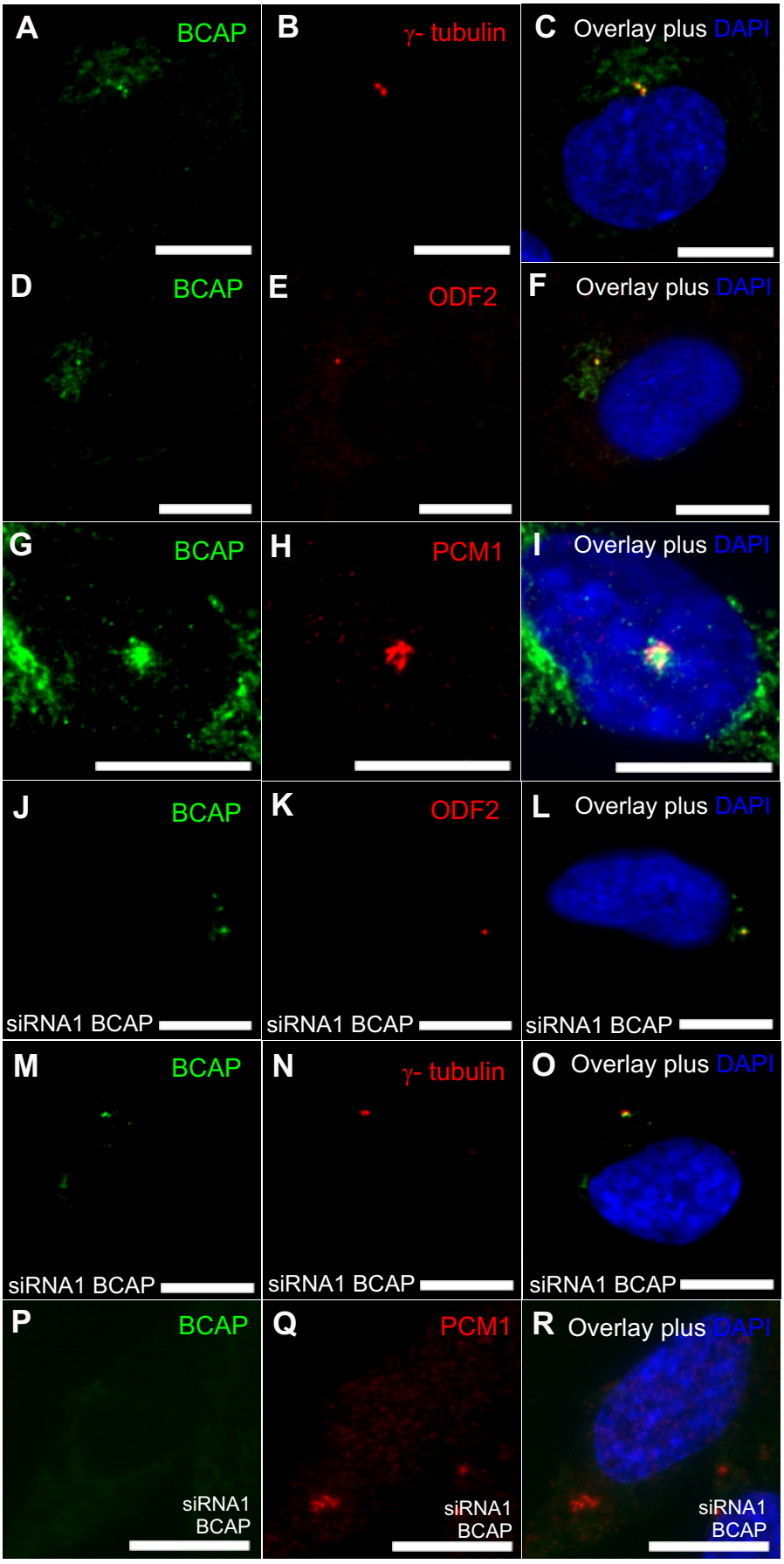
A
BCAP
B
γ- tubulin
C
Overlay plus DAPI
D
BCAP
E
ODF2
F
Overlay plus DAPI
G
BCAP
H
PCM1
I
Overlay plus DAPI
J
BCAP
siRNA1 BCAP
K
ODF2
siRNA1 BCAP
L
Overlay plus DAPI
siRNA1 BCAP
M
BCAP
siRNA1 BCAP
N
γ- tubulin
siRNA1 BCAP
O
Overlay plus DAPI
siRNA1 BCAP
P
BCAP
siRNA1
BCAP
Q
PCM1
siRNA1
BCAP
R
Overlay plus DAPI
siRNA1
BCAP

Figure 6.5 BCAP depletion does not affect localisation of centrosomal proteins in RPE1-hTERT cells. **A-C)** Proliferating RPE1-hTERT cells are stained with anti-BCAP (Proteintech) and anti-γ-tubulin antibodies. BCAP (green) appears as satellite staining around the centrosome with some overlap with the γ-tubulin signal (red). **D-F)** Cells stained with anti-BCAP (Proteintech) and anti-ODF2 antibodies show a single punctum for ODF2 signal (red) with minimal overlap with BCAP. **G-I)** RPE1-hTERT cells are stained with anti-PCM-1 and anti-BCAP (Proteintech) antibodies, PCM-1 (red) staining co-localises with that of BCAP (green). **J-R)** RPE1-hTERT cells were transfected with siRNAs targeting BCAP and stained with anti-BCAP (Proteintech) antibody and co-stained with anti- γ-tubulin, anti-PCM-1 or anti-ODF2 antibodies. BCAP staining is much reduced with minimal staining observed. However, ODF2 (K), γ-tubulin (N) and PCM-1 (Q) staining is unaffected. Scale bars: 10 μm.

6.2.6 RPE1-hTERT cells express BCAP isoforms

I have demonstrated BCAP is a centriolar satellite protein and an inhibitor of ciliogenesis. When validating these results with another BCAP antibody subtle differences were observed. In brief, initial experiments were carried out with the only commercially BCAP antibody available at the time Biorbyt orb31049 (anti-BCAP (Biorbyt)), where BCAP showed centriolar satellite staining around the centrosome in proliferating cells. When ciliation was induced this staining, pattern was no longer visible around the basal body/ centrioles. BCAP also disappeared from the cells, as assayed by Western blotting. When these experiments were repeated with anti-BCAP (Proteintech), proliferating cells showed centriolar satellite staining but BCAP remained after ciliogenesis, although at reduced levels, shown by Western blotting data, and was absent mid-ciliogenesis (Figure 6.2). Similarly, immunofluorescence data showed in a mixed population of RPE1-hTERT cells at different stages of ciliogenesis a portion of cells showed no BCAP staining while another showed satellite staining around the basal bodies. This partially resolves the differences observed between the two antibodies as both go at some point during ciliogenesis. One way to completely resolve this is by proposing there are two or more isoforms, one of which returns, which led us to think BCAP may have different isoforms Therefore, I set out to determine how many isoforms are present in RPE1-hTERT cells.

I next sought to determine whether BCAP has multiple isoforms in RPE1-hTERT cells. This might explain why one antibody shows that BCAP disappears when cells ciliate, while another antibody shows that BCAP levels reduce but does not fully disappear. The NCBI database predicts four BCAP isoforms as a, b, c and d while a previous study by Ponsard and colleagues identified five: three long and two short isoforms with a naming scheme (S/L-BCAP del x). To avoid confusion, we have named them as $\alpha,\beta,\gamma,\delta$ corresponding to

a, b, c and d of the NCBI numbering. Figure 6.6 A is a schematic of the four predicted isoforms on NCBI database and the ones identified by Ponsard et al. (2007)

I decided to test for these isoforms by RT-PCR. Primers were designed to enable amplification of exons 9-11 and exons 12-15. The predicted isoforms of α and δ do not contain exon 10, while isoforms β and γ do. RT-PCR using primers to amplify exons 9-11 results in a single band corresponding to skipping of exon 10 and presence of isoform α and δ, suggesting isoforms β and γ do not exist (Figure 6.6 B). Primers deigned to amplify exons 12-15, would determine the differences at the C-terminus as predicted isoforms α and β are thought to have contain exon 13, while it is predicted to be spliced out of isoforms γ and δ. The first set of RT-PCR results suggest isoforms β and γ do not exist, which then leaves isoforms isoform α and δ. If this is the case the second set of primers amplifying exons 12-15 would give us two bands, one at 416 bp and the second at 218 bp. The RT-PCR with primers to amplify exons 12-15 formed two bands (Figure 6.6 B). RT-PCR results confirm RPE1-hTERT cells have two BCAP isoforms (BCAPα and BCAPδ). I then designed primers to amplify full length BCAPα and BCAPδ. For both only one band is observed (Figure 6.6 C). This supports previous RT-PCR results as the presence of isoforms β or γ would result in two bands when either α and δ where amplified respectively.

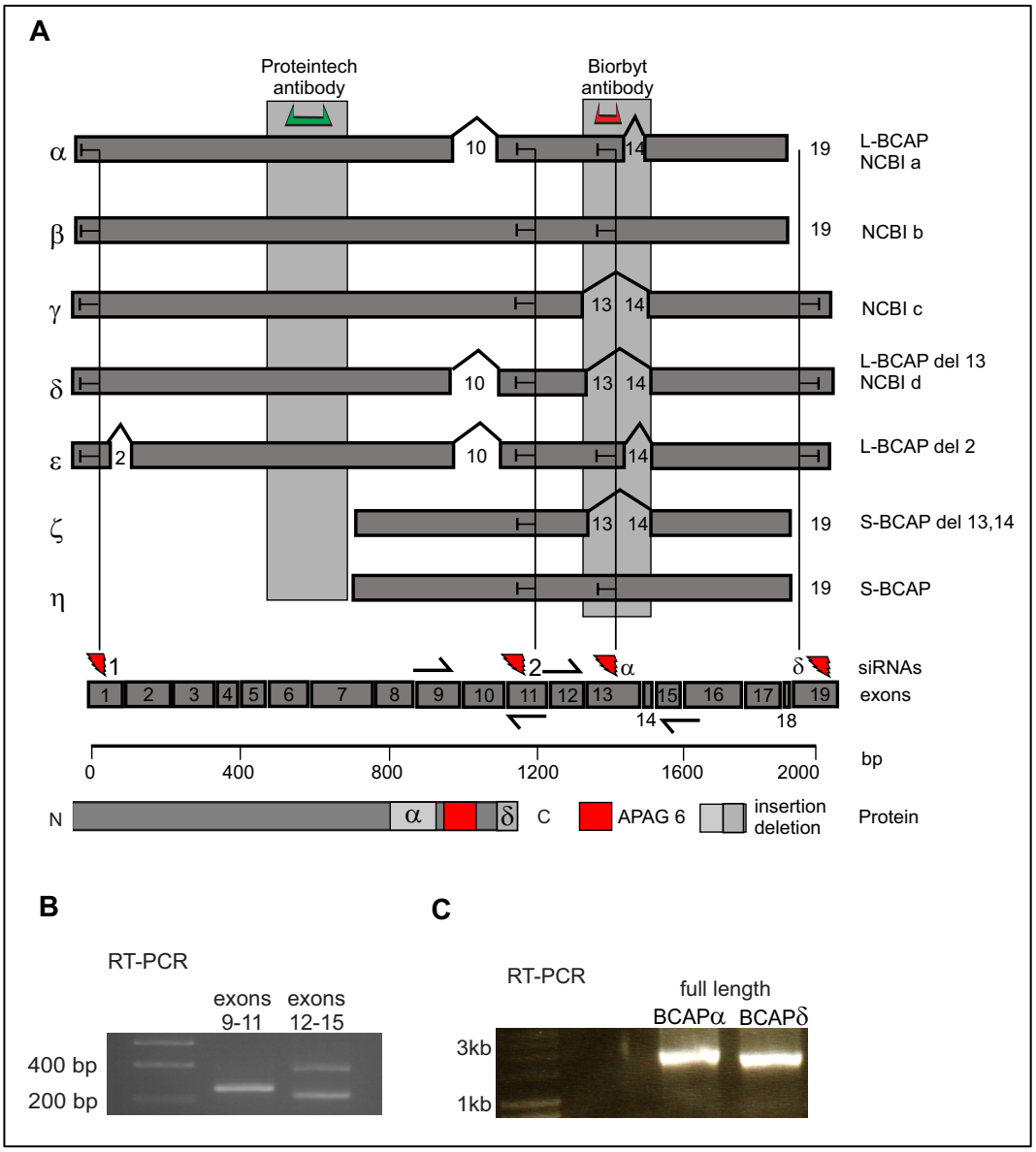

Figure 6.6 Gene structure of BCAP and RT-PCR detecting two BCAP isoforms in RPE1-hTERT cells.
A) Schematic of BCAP gene and BCAP isoforms. The NCBI database The NCBI database and Ponsard et al. have predicted/observed several transcripts and isoforms. These are summarised here. We have named them α–η to combine while avoiding confusion. NCBI numbering (a-d) and Ponsard et al. naming schemes (S/L-BCAP del x) are also shown for completeness. In isoforms where exons are skipped, the number of the exon skipped is in the gap between the two exons that are incorporated. Single-headed arrows show the binding sites for primers used to determine which variants were present. Target sites for the siRNAs used in this study are shown in red at the base of the diagram, lines with blunt arrowheads showing which isoforms would be targeted. The α and δ protein isoforms differ in the C-terminus, with BCAPα having a 50 amino acid insertion by inclusion of exon 13 compared to BCAPδ, which possesses an additional 20 amino acids in the tail due to inclusion of exon 19 instead of exon 18. The anti-BCAP (Biorbyt) antibody was raised to the C-terminus of BCAP whereas the anti-BCAP (Proteintech) antibody binds the N-terminus of BCAP and so will detect both BCAPα and BCAPδ. The APAG6 domain is coloured red in the protein schematic, with the inserted/deleted sequences of the α/β isoforms in grey shades. Diagram taken from de Saram et al. (2017) **B)** RT-PCR using primers to amplify axons 9-11 forms 1 band, result of skipping of exon 10. RT-PCR with primers to amplify exons 12-15 results in two bands, result of inclusion or skipping of exon 13. **C)** Full-length BCAPα and BCAPδ are present in RREP1-hTERT cells.

6.2.7 Isoform-specific depletion of BCAP

RT-PCR results reveal RPE1-hTERT cells have two isoforms of BCAP. To test the role of BCAPα and BCAPδ individually, I designed siRNAs targeting exons 13 and 19 targeting BCAPα and BCAPδ respectively. I first checked by RT-PCR if the siRNAs were isoform specific. RPE1-hTERT cells were transfected with control siRNA or siRNAs targeting BCAPα and BCAPδ. After 48 hours of transfection, RNA was harvested from each treatment, followed by cDNA synthesis. Primers used previously to detect the two isoforms by amplifying exons 9-11 and exons 12-15, were used to check depletion of individual BCAP isoform. Cells treated with siRNA targeting BCAPα show successful depletion as only a very faint band at 400bp can be seen with over 89 % reduction (corresponding to exons 12, 13 and 15) (Figure 6.7 A and B). Similarly, siRNA targeting BCAPδ show isoform specific depletion although this was not as efficient as siRNA targeting BCAPα. The band at 200bp (corresponding to exons 12 and 15) is fainter than in the controls and cells treated with BCAPα, with over 80 % depletion (Figure 6.7 A and B). β-actin was used as a control, which did not change in any of the treatments (Figure 6.7 A).

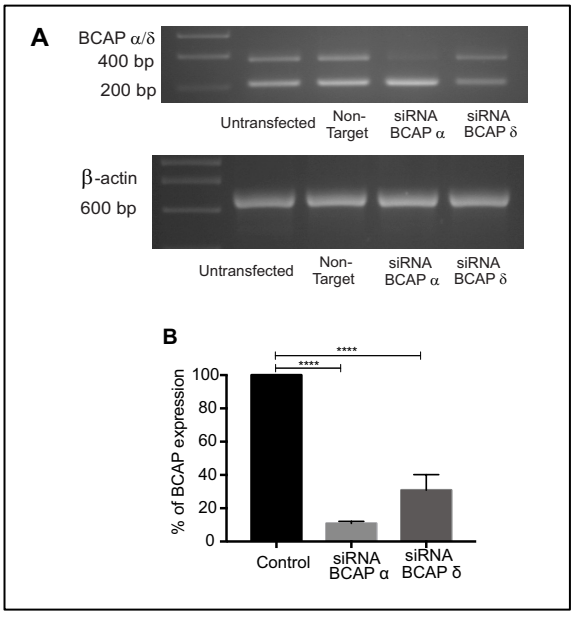

Figure 6.7 Isoform specific depletion of BCAP.
A) RPE1-hTERT cells were transfected siRNAs targeting BCAPα and BCAPδ. RT-PCR shows two bands; band at 200bp corresponds to BCAPα while the band at 400bp is for BCAPδ. siRNAs targeting either variant was successfully depleted while various control samples are unaffected. Beta actin is amplified to the same level in all samples. **B)** The amount of depletion of each isoform was assessed quantitatively by RT-PCR, with more than 70% depletion of either isoform ($P<0.001$; one-way ANOVA, three independent experiments).

6.2.8 Cilia length regulated by isoform specific depletion of BCAP

Having established the means to target BCAPα and BCAPδ individually, confirmed by RT-PCR, I next checked how BCAP staining changes when each isoform is depleted independently. RPE1-hTERT cells were either transfected with control siRNA or siRNAs targeting BCAPα and BCAPδ respectively in serum-supplemented media. After 48 hours of transfection, cells were fixed and stained with anti-BCAP and anti-γ-tubulin antibody. In control cells, BCAP staining is seen as centriolar satellite staining, small granular specks surrounding the centrosome (Figure 6.8 A-C). When either BCAPα or BCAPδ was targeted, BCAP staining decreased but was not eliminated (Figure 6.8 D-F and G-I). Reduced satellite staining is observed supporting the idea that anti-BCAP (Proteintech) binds to both isoforms. Since depletion of both BCAP isoforms simultaneously (siRNAs 1 and 2) causes the formation of cilia, cells treated with isoform specific siRNAs were also stained with anti-Ac-tubulin antibody to check if one or both isoforms are responsible for inhibiting ciliogenesis. Depletion of either isoform resulted in ciliogenesis where 30% and 20% of cells now formed cilia when either BCAPα or BCAPδ were depleted, respectively (Figure 6.8 K-M). It was notable that cilium length increased in BCAPδ depleted cells but not in those depleted of BCAPα (Figure 6.8 N).

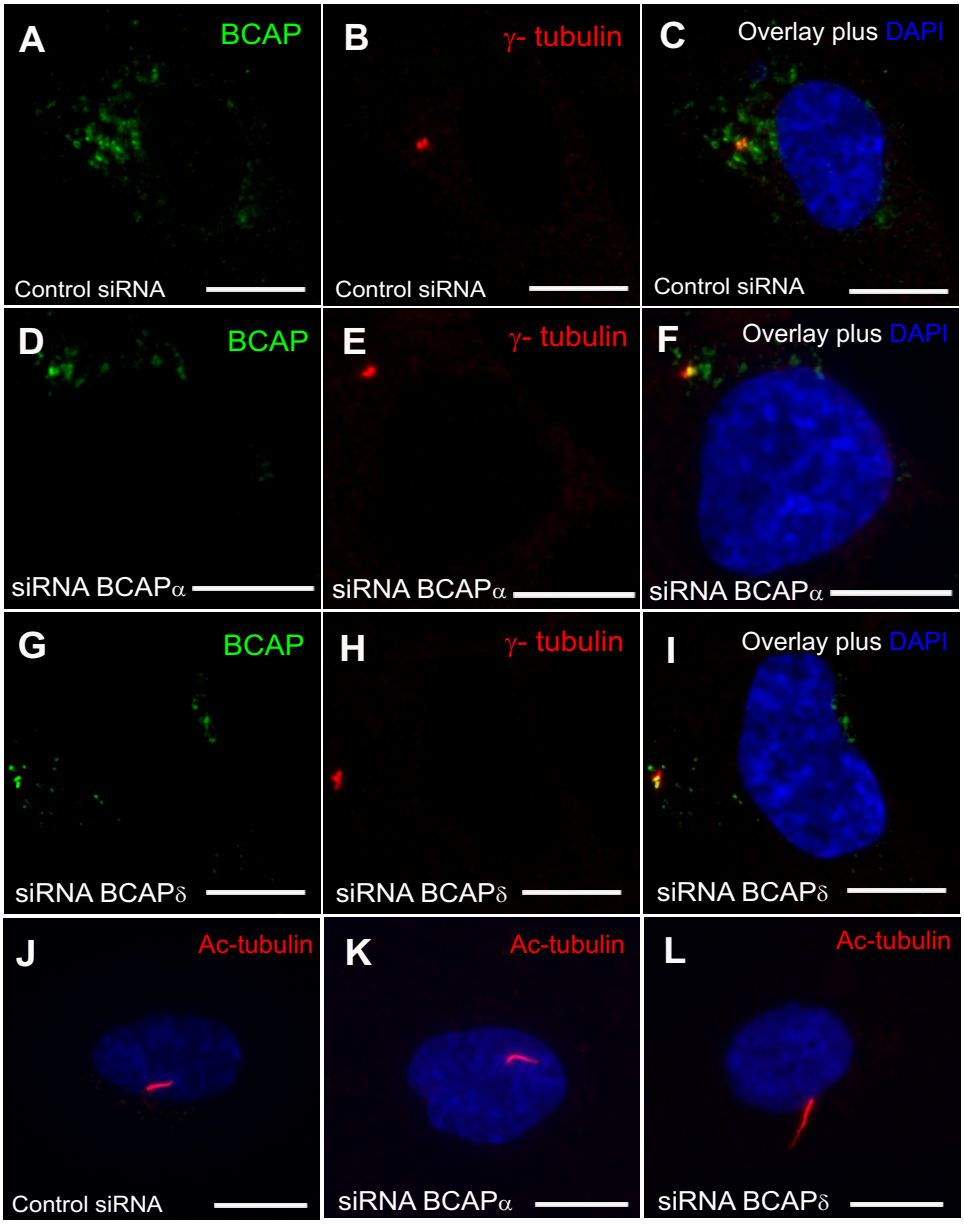
A
BCAP
Control siRNA
B
γ- tubulin
Control siRNA
C
Overlay plus DAPI
Control siRNA
D
BCAP
siRNA BCAPα
E
γ- tubulin
siRNA BCAPα
F
Overlay plus DAPI
siRNA BCAPα
G
BCAP
siRNA BCAPδ
H
γ- tubulin
siRNA BCAPδ
I
Overlay plus DAPI
siRNA BCAPδ
J
Ac-tubulin
Control siRNA
K
Ac-tubulin
siRNA BCAPα
L
Ac-tubulin
siRNA BCAPδ

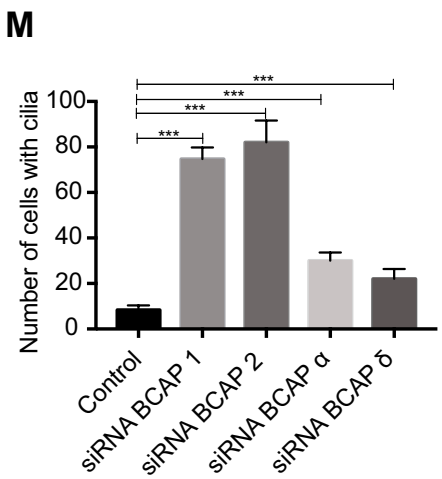
M
Number of cells with cilia
100
80
60
40
20
0
***
***
***
***
Control
siRNA BCAP 1
siRNA BCAP 2
siRNA BCAP α
siRNA BCAP δ

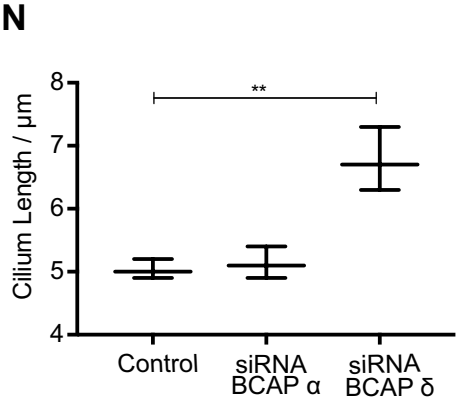
N
Cilium Length / µm
8
7
6
5
4
**
Control
siRNA BCAP α
siRNA BCAP δ

Figure 6.8 Cilia length is regulated by isoform specific depletion of BCAP.
A-C) RPE1-hTERT cells were transfected with control siRNAs and stained with anti-BCAP (Proteintech) and anti-γ-tubulin antibodies. BCAP (green) is observed as satellite-like staining appearing as granular punctate around the centrosome, visualised by γ-tubulin (red). There is some overlap with BCAP and γ-tubulin at the centrioles, the staining is unaffected with control siRNAs. **D-I)** When cells are transfected with siRNAs targeting isoform specific BCAP, reduced BCAP (green) (Proteintech) staining is observed around the centrosome (γ-tubulin in red). **J-M)** RPE1-hTERT cells were either control transfected or isoform specific siRNAs targeting BCAPα/δ, they are stained with anti-acetylated tubulin antibody and DAPI. Depletion of either isoform resulted in cilia formation in serum supplemented media, quantified in M ($P<0.001$; one-way ANOVA, 100 cells counted, three independent experiments. **N)** Cilia length; in control treated cells (J) and cells when BCAPα is depleted similar cilia length is observed however, when BCAPδ is depleted longer cilia are observed with an average length of 5μm in control while 6.7μm in BCAPδ depleted cells, quantified in N ($P<0.001$; one-way ANOVA, 100 cells counted, three independent repeats). Scale bars 10 μm.

6.2.9 Localisation of BCAPα

I have shown that depletion of either variant, BCAPα and BCAPδ , promotes ciliogenesis, while depletion of BCAPδ also increases cilium length. I next tested if they have similar or different localisation pattern by overexpressing GFP expression constructs of each isoform. Both variants of BCAP were amplified from RPE1-hTERT cells and cloned into GFP expression constructs. RPE1-hTERT cells were transfected with GFP-BCAPα. After 24 hours cells were fixed and stained with either anti-PCM-1, anti-γ-tubulin or anti-ODF2 antibodies. When GFP-BCAPα is overexpressed, it shows satellite-like staining which co-localises with PCM-1 (Figure 6.9 A-C). GFP-BCAPα signal is around but not overlapping γ-tubulin (Figure 6.9 D-F). Similarly, GFP-BCAPα appears as granular specks around ODF2, an appendage protein, which appears as a single punctum (Figure 6.9 G-I).

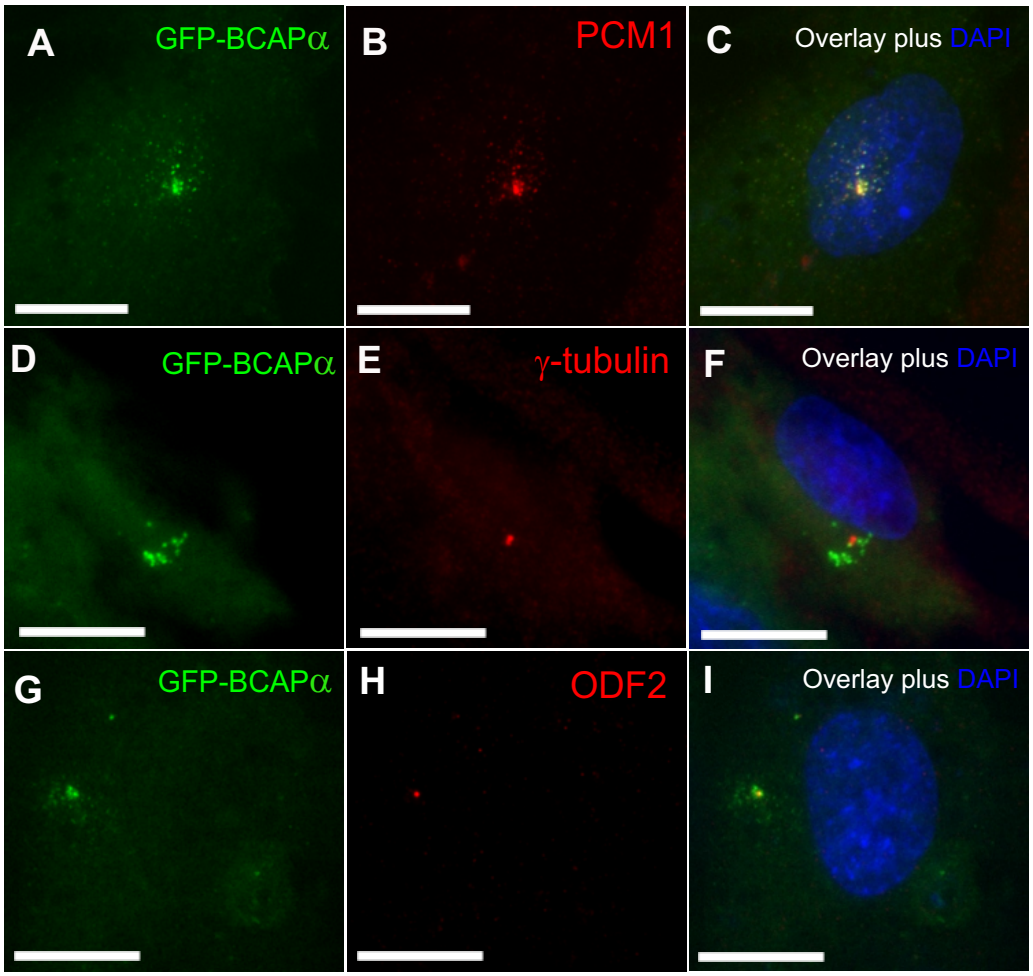

Figure 6.9 Localisation of BCAPα.

A-I) RPE1-hTERT cells are transfected with GFP-BCAPα expression constructs and stained with either anti-PCM-1, anti-γ-tubulin or anti-ODF2 antibodies and DAPi. **A, D, G)** GFP-BCAPα is observed as satellite-like staining appearing as small granular specks. GFP-BCAPα co-localises with PCM-1 a known centriolar satellite protein. **D-F)** GFP-BCAPα granular specks surround the centrosome characteristic of centriolar satellite proteins. **G-H)** Similarly GFP-BCAPα surrounds the single punctum of ODF2 staining. The staining pattern is consistently observed as satellite-like staining. Scale bars 10 μm.

6.2.10 Localisation of BCAPδ

I have shown when GFP-BCAPα is overexpressed it appears as satellite-like staining that co-localises with PCM-1, and that surrounds both centrosome markers γ-tubulin and ODF2. Similarly, RPE1-hTERT cells were transfected with GFP-BCAPδ expression construct, after 24 hours cells were fixed and stained with anti-γ-tubulin and anti-PCM-1 antibodies. GFP-BCAPδ shows a pericentriolar/ centriolar- like staining that overlaps with γ-tubulin (Figure 6.10 A-C), it also shows a satellite-like staining where it also co-localises with PCM-1 (Figure 6.10 D-F). Though both localisation patterns are observed, GFP-BCAPδ appears as centriolar-like staining 80% of the time.

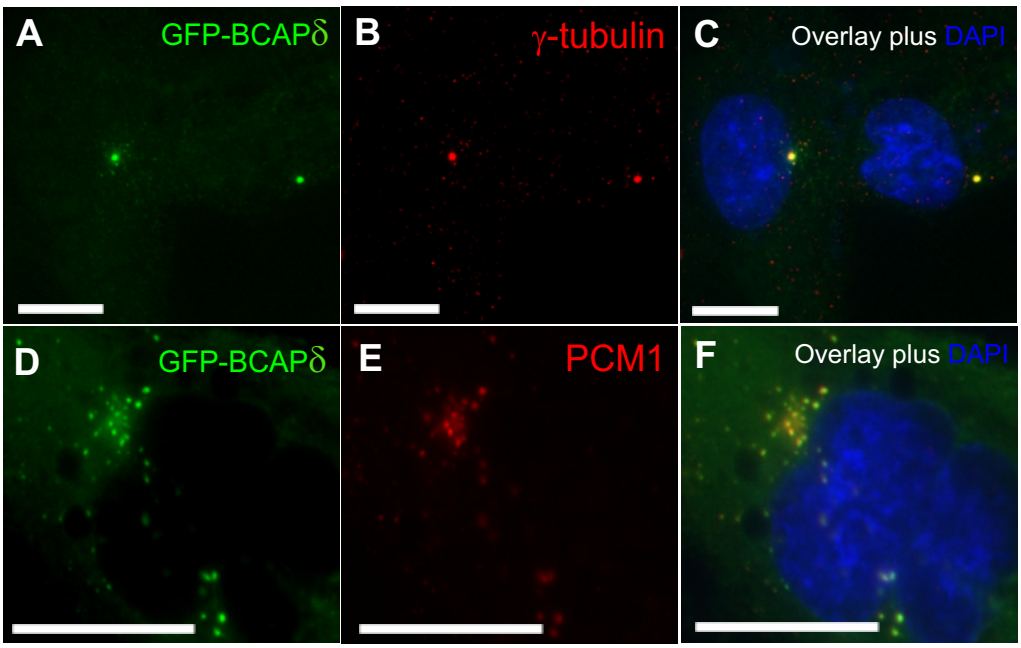

Figure 6.10 Localisation of BCAPδ.
A-F) RPE1-hTERT cells were transfected with GFP-BCAPδ expression constructs, cells were stained with either anti-γ-tubulin or anti-PCM-1 antibodies and DAPI. **A-C)** GFP-BCAPδ (green) expression appears as centriolar-like as small punctae that overlap with γ-tubulin (red), this staining pattern was observed 80% of times when GFP-BCAPδ is overexpressed. **D-F)** 20% of times GFP-BCAPδ (green) also appears as satellite-staining observed as small granular specks that overlaps with PCM-1 (red), a centriolar satellite protein. Scale bars 10 μm.

6.2.11 Overexpression of either BCAP variant inhibits cilia formation in RPE1-hTERT cells

I have shown that when BCAP (all isoforms) is removed, cells form a cilium, while overexpressing GFP-mBCAP inhibited cilia formation. I next tested whether inhibition of ciliogenesis by BCAP was isoform dependent. RPE1-hTERT cells were transfected with either GFP-BCAPα or GFP-BCAPδ in serum supplemented media. After 24 hours media was replaced without serum for a further 24 hours. Cells were fixed and stained with anti-acetylated-tubulin. When either isoform is overexpressed, ciliogenesis is inhibited (Figure 11 A-C and D-F). In both treatments ciliogenesis is inhibited in over 80% of the cells (Figure 6.11 G). I have shown that depletion of either BCAP isoform results in ciliation while overexpression inhibits ciliogenesis. I next tested if the two isoforms were functionally redundant with respect to inhibition of ciliogenesis. I depleted one isoform and overexpressed the other and then assayed whether cells could ciliate. RPE1-hTERT cells were simultaneously transfected with either a GFP-BCAPα expression plasmid and an siRNA targeting BCAPδ or with GFP-BCAPδ and siRNA targeting BCAPα in media containing serum. Media was replaced after 24 hours without serum, cells were fixed and stained with anti-acetylated-tubulin antibody. In both treatment conditions, overexpression of one isoform while the other is depleted inhibited ciliogenesis as cilia was only observed in 30% of transfected cells (Figure 6.11 H-J, K-M and N). This compares to 70% of cell ciliating when all isoforms of BCAP were depleted and 90% of cells ciliating under serum-starvation.

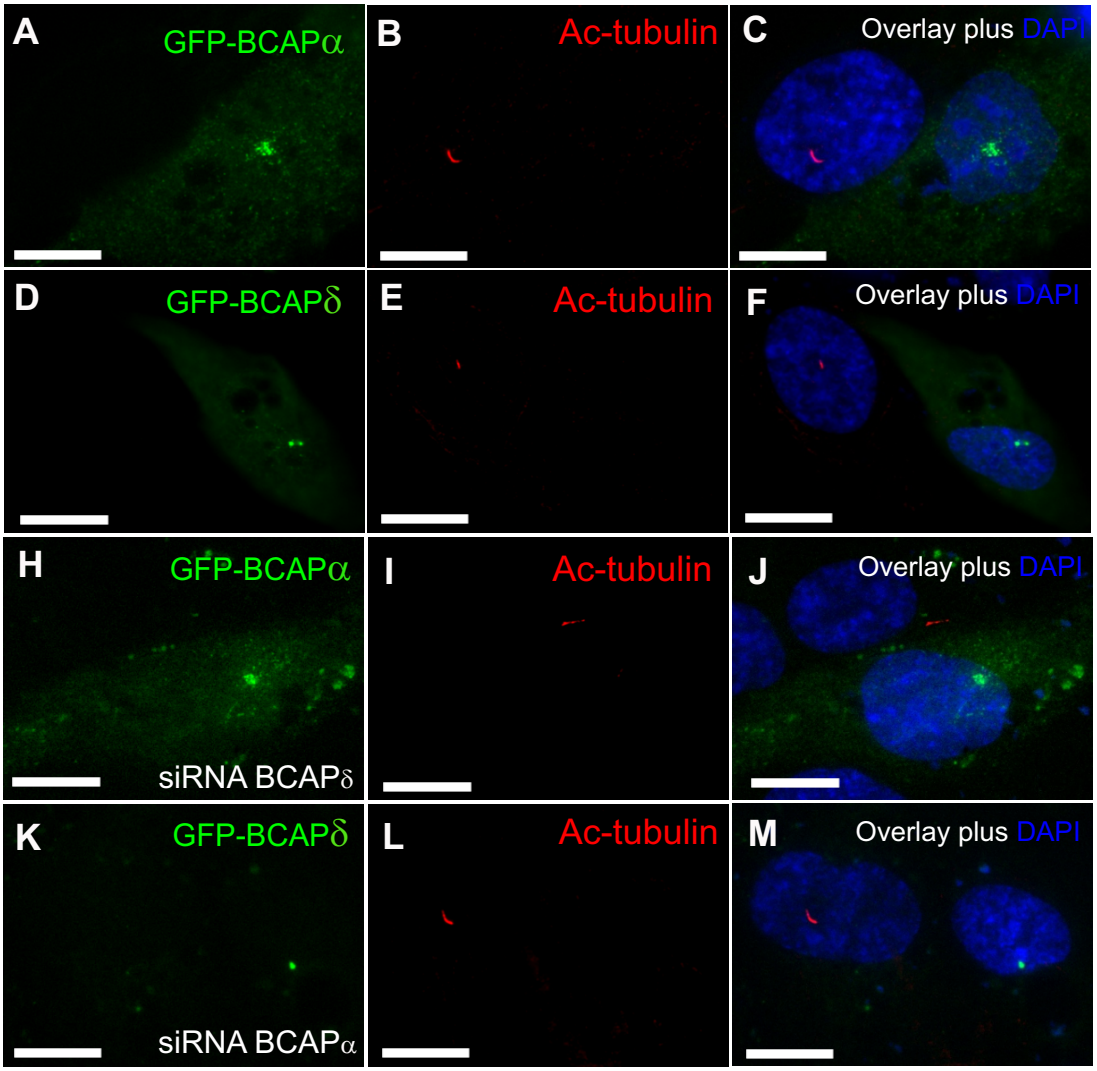
A
GFP-BCAPα
B
Ac-tubulin
C
Overlay plus DAPI
D
GFP-BCAPδ
E
Ac-tubulin
F
Overlay plus DAPI
H
GFP-BCAPα
siRNA BCAPδ
I
Ac-tubulin
J
Overlay plus DAPI
K
GFP-BCAPδ
siRNA BCAPα
L
Ac-tubulin
M
Overlay plus DAPI

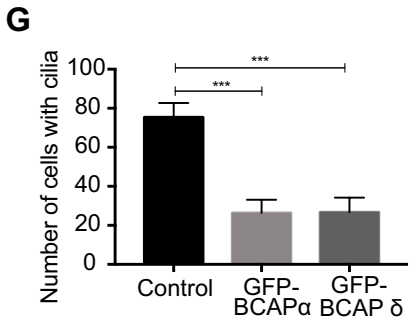
G
Number of cells with cilia
100
80
60
40
20
0
***
***
Control
GFP-BCAPα
GFP-BCAP δ

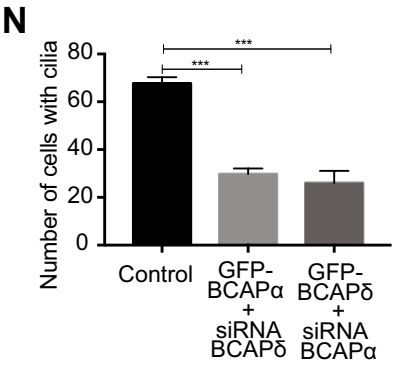
N
Number of cells with cilia
80
60
40
20
0
***
***
Control
GFP-BCAPα + siRNA BCAPδ
GFP-BCAPδ + siRNA BCAPα

Figure 6.11 Overexpression of either BCAP isoform inhibits ciliogenesis.
A-C) RPE1-hTERT cells were transfected with GFP-BCAPα in serum-free media (SFM) and stained with anti-acetylated tubulin antibody and DAPI. GFP-BCAPα appears as satellite staining, as a cloud of small granular specks are observed, cilia is not observed when GFP-BCAPα is overexpressed while cilia can be seen at the untransfected cell. **D-F)** Similarly, when GFP-BCAPδ is overexpressed it appears as two punctae, characteristic of centriole staining. Cilia is not seen when cells are overexpressing GFP-BCAPδ as the untransfected cell is able to ciliate, quantified in G ($P<0.001$; one-way ANOVA, 100 cells counted, three independent experiments. **H-M)** RPE1-hTERT cells were simultaneously transfected with either GFP-BCAPα and siRNA targeting BCAPδ or GFP-BCAPδ and siRNA targeting BCAPα in serum-supplemented media (SSM). Cells were stained with anti-acetylated tubulin and DAPI. **H-J)** As before, GFP-BCAPα appears as satellite-like staining, acetylated tubulin detects cilia in cells that does not overexpress GFP-BCAPα but presuming cells that BCAPδ is removed. K-L) Similarly, when GFP-BCAPδ is overexpressed it centriolar-like staining is observed, cilia are seen in cells that do not overexpress GFP-BCAPδ but BCAPα is depleted, quantified in N ($P<0.001$; one-way ANOVA, 100 cells counted, three independent experiments) Scale bars 10 μm.

6.3 Discussion

Centriolar satellite proteins support a number of centrosomal processes including centrosome biogenesis, cytokinesis and ciliogenesis. BCAP staining in mammalian cell lines shows satellite-like pattern in proliferative cells, which co-localises with the pro-typical centriolar satellite protein PCM-1. Since PCM-1 is considered as a scaffold for centriolar satellite proteins, removal of PCM-1 should result in the dispersal of any centriolar satellites protein. This was observed with BCAP staining as it appeared diffuse throughout the cytoplasm. When ciliogenesis was induced by serum starvation, BCAP expression diminishes as BCAP staining is no longer observed at the basal bodies. Overexpression of BCAP inhibited ciliogenesis. When BCAP was depleted by RNAi in serum supplemented media, cells formed cilia. Cilium length also increased by a quarter from 3.1 μm to 4.1 μm. When repeating some of these experiments with another BCAP antibody, subtle differences were observed. Although, satellite staining is apparent, the reduction of BCAP when cells ciliate was marginal which led us to think BCAP could exist as multiple isoforms.

I first analysed the dynamics of BCAP localisation in ciliogenesis, as BCAP localisation changes from when cells are proliferating to when they have a cilium. Change in BCAP localisation during the ciliogenesis was followed. Cells were synchronised by nocodazole block, followed by release, where samples were fixed at hourly intervals. BCAP staining changed through the time course, initially, BCAP is dispersed throughout the cytoplasm, the staining becomes more pronounced eventually adopting a more satellite-like appearance. When cells start to ciliate, BCAP staining disappeared. Only when the cilia are extending further BCAP staining at the basal bodies is seen. Since one of the BCAP (Biorbyt) antibodies disappears when cells ciliate, and the dynamics of BCAP assay stained with a different BCAP (Proteintech) antibody shows BCAP levels deplete before ciliogenesis is initiated but reappear as cilia form also suggested BCAP could have multiple isoforms. Overall the staining with BCAP- Biorbyt was eliminated in ciliating cells, while staining with BCAP- Proteintech shows staining disappears as ciliogenesis initiates by the time-lapse of BCAP dynamics. This solves the discrepancy between the two

antibodies. All BCAP has to be removed for ciliogenesis to occur, but some of it comes back. For this to be true at least two or more BCAP isoforms must exist.

I show, by RT-PCR, that BCAP has two isoforms in RPE1-hTERT cells: BCAPα and BCAPδ. These isoforms were targeted individually by RNAi, where depletion resulted in cilia formation. The anti-BCAP (Proteintech) antibody binds to the N-terminus of BCAP therefore will detect both BCAPα and BCAPδ whereas anti-BCAP (Biorbyt) binds to the C-terminus BCAPα, so this antibody will only bind to BCAPα in RPE1-hTERT cells. The anti-BCAP antibody raised by Ponsard et al. (2007) detected all BCAP isoform, using a mixture of peptide sequences encoded by exons 13 and 15. While exon 15 is present in all isoforms but exon 13 is present in two of the long isoforms (L-BCAP/α and L-BCAP del 2/ε), and one short isoform (S-BCAP/η). Additionally, they stained multi-ciliated epithelial cells. As the peptide against which the antibody was raised and different cell line stained, may explain the centrosome/centriole staining they observe. It resembles the staining I observe when GFP- BCAPδ is overexpressed.

Depletion of both BCAP isoforms result in ciliogenesis under serum-supplemented conditions. 70% of cells form cilia when BCAP is depleted, compared to 30 % of cells that form cilia when either BCAPα and BCAPδ was depleted, suggesting there is partial redundancy of both isoforms, maybe an even contribution to ciliogenesis. This is consistent with the two BCAP isoforms acting together. Additionally, when both BCAP isoforms were depleted increase in cilia length was observed. However, when the isoforms were depleted individually, depletion of BCAPδ alone increased cilia length.

We show BCAP depletion promotes ciliogenesis, through observing change in BCAP localisation and depletion by RNAi. BCAP disappears when the cilium is being formed but reappears when cilia is elongating. Both BCAP isoforms need to be removed for ciliogenesis to start as evidenced by the staining from the BCAP antibody (Biorbyt), that detects the α variant, which disappears after ciliogenesis. The BCAP (Proteintech) antibody that detects both variants, the staining disappears during a short period during the process. However, BCAP (Proteintech) staining reappears once ciliogenesis has initiated. As depletion of BCAPδ resulted in longer cilia, it is possible BCAPδ has an additional role in regulating cilia length, which could explain why BCAP reappears when

cilia are elongating. Cilia length is determined by the assembly and disassembly of the microtubule axoneme which is regulated by intraflagellar transport (IFT). The assembly rate of cilium mediated via IFT gradually decreases as the cilium elongates and eventually is balanced by the constant rate of disassembly. Once ciliation has been initiated BCAP reappears at the basal bodies as the cilia are elongating, as observed during the time-course after cell synchronisation. This is most likely the BCAPδ variant that reappears to possibly regulate cilia length. As longer cilia are observed when BCAP δ variant is removed, it is possible BCAP is involved in IFT. In brief, the IFT system is composed of two protein complexes IFT-A and IFT-B, IFT-B is associated with anterograde transport, mutants of IFT-B are shown to have defective or eliminated cilia while IFT-A is associated with retrograde transport. It has been shown increased activity of anterograde IFT complex leads to further elongation of cilia, whereas decrease in activity result in shorter cilia.

Since one isoform is shown to regulate cilia length it was possible they could have different localisation in the cell. Human BCAPα and BCAPδ were cloned into GFP expression constructs that were overexpressed to observe cellular localisation. Subtle differences in localisation is observed between the two isoforms. GFP-BCAPα appeared as centriolar satellite-like staining that overlapped with PCM-1, this staining also surrounded the centrioles marked by γ-tubulin and ODF2. Similarly, GFP-BCAPδ was overexpressed, while it too showed satellite staining that overlapped with PCM-1, pericentriolar/centriolar localisation was also observed. GFP-BCAPδ centriolar localisation overlapped with γ-tubulin, this pattern of localisation was observed in 80% of cells. Ciliogenesis is inhibited when GFP-mBCAP is overexpressed or either of the human BCAP variants. When cells were co-transfected with GFP-BCAPα and siRNA targeting BCAPδ or GFP-BCAPδ and siRNA targeting BCAPα, ciliogenesis was inhibited suggesting inhibition of ciliogenesis is not isoform specific.

Ciliogenesis is regulated by many proteins, centrosomal proteins including satellite proteins. Like BCAP, OFD1 is a centrosomal protein that is distributed between the centrosome and centriolar satellites, where the satellite pool of OFD1 is removed for ciliogenesis to occur (Tang et al. 2013). We show that BCAP also localises between the centriolar satellite and centrioles, while BCAPα is only seen at the satellites, BCAPδ is

observed at both but predominantly at the centrioles. Similarly, like OFD1, it is clear removal of BCAP localising at the satellites is required for ciliogenesis to occur. As cells ciliate when either BCAPα or BCAPδ are depleted, and as BCAP staining is no longer seen at the basal body when cells ciliate in serum free conditions. Since OFD1 is a negative regulator of ciliogenesis and behaves in a similar fashion to BCAP it could be possible both OFD1 and BCAP are involved in the same regulatory pathway of ciliogenesis whether they are acting upstream or downstream of one another. One of the ways this could be tested is by the removal of either one affects the presence and localisation of the other. Additionally, removal of OFD1 from the satellites is regulated by autophagy. Since BCAP is predicted to have an APG6 domain a region which is similar to that of yeast autophagy protein, and acts similar to OFD1, suggests BCAP could also be removed via autophagy. CP110 is another inhibitor of ciliogenesis, it localises at the tips of centrioles preventing centriole elongation. CPP10 is displaced from the mother centriole by tau tubulin kinase 2 TTBK2 and microtubule affinity regulating kinase 4 (MARK4) (Kuhns et al. 2013).

Autophagy is also known as a regulator of ciliogenesis, where both pathways are activated upon serum starvation. Autophagy is tightly coordinated at different stages of ciliogenesis, at the early stages of ciliogenesis, OFD1 is removed via autophagy for ciliogenesis to proceed at this stage autophagy is regarded as a positive regulator of ciliogenesis. When full-length cilia have been made, autophagy is directed towards limiting cilium length, where reduced autophagy result in longer cilia (Pampliega et al. 2013). Similarly, IFT20 is targeted by autophagy before ciliogenesis but is required for cargo transport inside the cilium, an inhibitory role of autophagy in ciliogenesis. It is possible BCAP levels are also regulated by autophagy, or BCAP assists in the autophagy of other proteins.

We have shown that BCAP is a centriolar satellite protein and an inhibitor of ciliogenesis. Further investigation could advance our understanding of BCAP and its role in ciliogenesis. Initial ideas would be to look at the autophagy pathway. Firstly, to check if BCAP is degraded via autophagy. This could be achieved by using autophagy-deficient cells, similar to the experimental design in Tang et al. (2013). If BCAP levels are regulated by autophagy to check whether it is in the same regulatory pathway to OFD1. Another pathway that could be looked at is the CP110-Cep97 pathway, as depletion of Cep97 led

to the disappearance of CP110 at the centrosome. Depletion of both centriolar proteins supress ciliation (Spektor et al. 2007). Similarly, Cep97 can be depleted by siRNA, and stained for BCAP localisation, if staining disappears it would suggest BCAP is involved in this regulator pathway of ciliogenesis. I have shown that BCAP has two isoforms in RPE1-hTERT cell. This cell line is known to form a primary cilium. It would be interesting to see the expression and localisation of BCAP in other cell lines, particularly cells that possess multiple cilia. Whether the number of isoforms expressed would change in cells that structurally different cilia, as described by Ponsard et al. (2007). It would seem possible BCAP exerts its affect via autophagy. Autophagy is important in regulating ciliogenesis. This work relates to the previous chapter as autophagic disruption results in the accumulation of toxic proteins, that form protein inclusions. I have shown that aggresomes inhibit ciliogenesis. The next step would be to assess if aggresomes disrupt autophagy and therefore ciliogenesis.

7. Discussion

In this thesis, I investigated the effect of aggresomes on centrosome function. Protein inclusions are a pathological hallmark for many neurodegenerative diseases, such as the Lewy bodies found in the dopaminergic neurons of Parkinson's patients (Spillantini et al. 1997). Increasing evidence supports the idea that Lewy bodies are derived from aggresomes as they share many biochemical properties (Olanow et al. 2004). Aggresomes are protein inclusions formed next to the nucleus, at the centre of the microtubule network. In many cells, the microtubule organising centre is the centrosome. The centrosome is an organelle with diverse roles, it is the main microtubule organising centre of animal cells, and the centrioles of the centrosome become the basal body from which the microtubule axoneme extends. The centrosome nucleates the microtubules by which the aggregated protein is transported across via dynein motors where it forms the aggresome. Centrosome dysfunction could partially explain the molecular pathological features observed in Parkinson's yet, the role of centrosomes in the pathogenesis of Parkinson's has been rarely investigated. Most research on Parkinson's currently focuses on the mitochondria and autophagy pathways. It is possible the protein inclusions could affect the centrosome which could contribute to the pathogenesis of Parkinson's.

This work shows for the first time aggresomes disrupt multiple functions of the centrosome. The three centrosomal functions assessed in the presence of aggresomes showed either total inhibition or the function to be severely compromised . Table 5 summarises the results from chapter 3, 4 and 5. One possible explanation on how these aggresomes are able to disrupt all three functions is through steric hinderance. If the aggresome can act as a barrier it could explain why the centrosome is compromised in discharging its function. The steric hinderance could also limit other factors that are required to facilitate the centrosome function. For example, if a substantial amount of the free tubulin is incorporated at the aggresome, microtubule nucleation and polymerisation is limited due to the reduce supply of free tubulin.

Microtubule stability has been widely researched as axonal degeneration is a feature observed in Parkinson's. Microtubules are important in regulating long distant axonal transport and forming specialised functional compartments. Post-translational modifications of tubulin correlate with microtubule stability. More stable microtubules

display a longer half-life and are accumulated during neuronal differentiation or in specific neuronal compartments, reflecting the importance of microtubules in neuronal function. Additionally, some of the associated genetic risk factors of Parkinson's have shown to be implicated in microtubule stability including α-synuclein. By showing aggresomes limit microtubule nucleation and prevent the cell from maintaining the microtubule network strengthens the association of microtubules in the pathogenesis of Parkinson's.

Cilia dysfunction has also been reported in number of neurodegenerative diseases including Parkinson's, Alzheimer's and Huntington's disease. Primary cilia assembly is regulated by a number of pathways, including autophagy and the ubiquitin proteasome pathway, that are also implicated in the pathogenesis of neurodegenerative diseases including Parkinson's. One of the early pre-clinical symptoms of Parkinson's and other neurodegenerative diseases is the loss of smell. Reduced ability in the sense of smell is also regarded as an age-related symptom, while it is not as advanced compared to patients with a neurodegenerative disorder (Boyce & Shone 2006; Katotomichelakis et al. 2007). From a clinical perspective, tests to assess olfaction have been developed, including sniff tests. However, these tests have many limitations, including that the data accumulated is in a qualitative format and it is not a definitive test. I have shown aggresomes affect cilia formation and maintenance. If the olfactory cilia from the nasal tissue could be accessible to routine screening, cilium numbers can be quantifiable and maybe used as an early diagnostic tool for Parkinson's.

The key findings of this thesis contribute to the current research associated with Parkinson's by exploring a unique association between the aggresome and the centrosome. The overall findings contribute to the current pathways involved in the pathogenesis of Parkinson's.

Table 5 Summary of results

Centrosome Function	In the presence of aggresomes
Microtubule nucleation	Microtubule nucleation is severely reduced , microtubule network failed to re-establish itself.
Cell polarity and migration	Rate of cell migration reduced with fewer cells able to orientate the Golgi.
Ciliogenesis	Cilia formation and maintenance inhibited , shorter olfactory cilia observed in zebrafish larvae.

8. Bibliography

Abal, M. et al., 2002. Microtubule release from the centrosome in migrating cells. *The Journal of cell biology*, 159(5), pp.731–7.

Adams, J., 2003. The proteasome: structure, function, and role in the cell. *Cancer Treatment Reviews*, 29, pp.3–9.

Ahmad, F.J. et al., 1999. An essential role for katanin in severing microtubules in the neuron. *The Journal of cell biology*, 145(2), pp.305–15.

Ahmad, F.J. et al., 1998. Cytoplasmic Dynein and Dynactin Are Required for the Transport of Microtubules into the Axon. *The Journal of Cell Biology*, 140(2).

Ahn, M. et al., 2006. Chaperone-like activities of α-synuclein: α-Synuclein assists enzyme activities of esterases. *Biochemical and Biophysical Research Communications*, 346(4), pp.1142–1149.

Akhshi, T.K., Wernike, D. & Piekny, A., 2014. Microtubules and actin crosstalk in cell migration and division. *Cytoskeleton*, 71(1), pp.1–23.

Akutsu, M., Dikic, I. & Bremm, A., 2016. Ubiquitin chain diversity at a glance. *Journal of cell science*, 129(5), pp.875–80.

Alexopoulou, Z. et al., 2016. Deubiquitinase Usp8 regulates α-synuclein clearance and modifies its toxicity in Lewy body disease. *Proceedings of the National Academy of Sciences of the United States of America*, 113(32), pp.E4688-97.

Alim, M.A. et al., 2004. Demonstration of a role for α-synuclein as a functional microtubule-associated protein. *Journal of Alzheimer's Disease*, 6(4), pp.435–442.

Alim, M.A. et al., 2002. Tubulin seeds alpha-synuclein fibril formation. *The Journal of biological chemistry*, 277(3), pp.2112–7.

Alves-Cruzeiro, J.M. da C., Nogales-Cadenas, R. & Pascual-Montano, A.D., 2014. CentrosomeDB: a new generation of the centrosomal proteins database for *Human* and *Drosophila melanogaster*. *Nucleic Acids Research*, 42(D1), pp.D430–D436.

de Anda, F.C. et al., 2005. Centrosome localization determines neuronal polarity. *Nature*, 436(7051), pp.704–708.

de Anda, F.C. et al., 2010. Centrosome motility is essential for initial axon formation in the neocortex. *The Journal of neuroscience : the official journal of the Society for Neuroscience*, 30(31), pp.10391–406.

Andersen, E.F. & Halloran, M.C., 2012. Centrosome movements in vivo correlate with specific neurite formation downstream of LIM homeodomain transcription factor activity. *Development (Cambridge, England)*, 139(19), pp.3590–9.

Anderson, R.G. & Brenner, R.M., 1971. The formation of basal bodies (centrioles) in the Rhesus monkey oviduct. *The Journal of cell biology*, 50(1), pp.10–34.

Ansley, S.J. et al., 2003. Basal body dysfunction is a likely cause of pleiotropic Bardet–Biedl syndrome. *Nature*, 425(6958), pp.628–633.

Aplin, A. et al., 1992. Cytoskeletal elements are required for the formation and maturation of autophagic vacuoles. *Journal of Cellular Physiology*, 152(3), pp.458–466.

Appel-Cresswell, S. et al., 2013. Alpha-synuclein p.H50Q, a novel pathogenic mutation for Parkinson's disease. *Movement Disorders*, 28(6), pp.811–813.

Ardley, H.C. et al., 2004. UCH-L1 aggresome formation in response to proteasome impairment indicates a role in inclusion formation in Parkinson's disease. *Journal of Neurochemistry*, 90(2), pp.379–391.

Ardley, H.C. & Robinson, P.A., 2005. E3 ubiquitin ligases. *Essays in Biochemistry*, 41(1), p.15.

Arias-Carrión, O. et al., 2010. Dopaminergic reward system: a short integrative review. *International archives of medicine*, 3, p.24.

Armato, U. et al., 2011. Is Alzheimer's Disease at Least Partly a Ciliopathy? *Journal of Alzheimer's Disease & Parkinsonism*, 1(1), pp.1–3.

Asher, G., Reuven, N. & Shaul, Y., 2006. 20S proteasomes and protein degradation "by default." *BioEssays*, 28(8), pp.844–849.

Baas, P.W. et al., 1988. Polarity orientation of microtubules in hippocampal neurons: uniformity in the axon and nonuniformity in the dendrite. *Proceedings of the National Academy of Sciences of the United States of America*, 85(21), pp.8335–9.

Baba, Y. et al., 2006. Phenotypic Commonalities in Familial and Sporadic Parkinson Disease. *Archives of Neurology*, 63(4), p.579.

Bäckman, C. et al., 1996. Systemic administration of a nerve growth factor conjugate reverses age-related cognitive dysfunction and prevents cholinergic neuron atrophy. *The Journal of neuroscience : the official journal of the Society for Neuroscience*, 16(17), pp.5437–42.

De Baets, G. et al., 2015. Increased Aggregation Is More Frequently Associated to Human Disease-Associated Mutations Than to Neutral Polymorphisms. *PLoS computational biology*, 11(9), p.e1004374.

Baird, D.H. et al., 2004. Distribution of the microtubule-related protein ninein in developing neurons. *Neuropharmacology*, 47(5), pp.677–683.

Bancher, C. et al., 1993. Neuropathological staging of Alzheimer lesions and intellectual status in Alzheimer's and Parkinson's disease patients. *Neuroscience Letters*, 162(1–2), pp.179–182.

Bang, Y. et al., 2016. LRRK2 interferes with aggresome formation for autophagic clearance. *Molecular and Cellular Neuroscience*, 75, pp.71–80.

Barbour, R. et al., 2008. Red Blood Cells Are the Major Source of Alpha-Synuclein in Blood. *Neurodegenerative Diseases*, 5(2), pp.55–59.

Bartels, T., Choi, J.G. & Selkoe, D.J., 2011. α-Synuclein occurs physiologically as a helically folded tetramer that resists aggregation. *Nature*, 477(7362), pp.107–110.

Bartles, J.R., 2000. Parallel actin bundles and their multiple actin-bundling proteins. *Current opinion in cell biology*, 12(1), pp.72–8.

Basto, R. et al., 2006. Flies without Centrioles. *Cell*, 125(7), pp.1375–1386.

Bauer, N.G. & Richter-Landsberg, C., 2006. The Dynamic Instability of Microtubules Is Required for Aggresome Formation in Oligodendroglial Cells After Proteolytic Stress. *Journal of Molecular Neuroscience*, 29(2), pp.153–168.

Bauso, D.J. et al., 2012. Incidence and prevalence of Parkinson's disease in Buenos Aires City, Argentina. *European Journal of Neurology*, 19(8), pp.1108–1113.

Beaulieu, J.-M. & Gainetdinov, R.R., 2011. The physiology, signaling, and pharmacology of dopamine receptors. *Pharmacological reviews*, 63(1), pp.182–217.

Benamer, H.T.S., 2014. The Frequency of Neurological Disorders in the Arab World. In *Neurological Disorders in the Arab World*. Cham: Springer International Publishing, pp. 25–73.

Bence, N.F., Sampat, R.M. & Kopito, R.R., 2001. Impairment of the ubiquitin-proteasome system by protein aggregation. *Science (New York, N.Y.)*, 292(5521), pp.1552–5.

Bergen, L.G. & Borisy, G.G., 1980. Head-to-tail polymerization of microtubules in vitro. Electron microscope analysis of seeded assembly. *The Journal of cell biology*,

84(1), pp.141–50.
Bernhardt, R. & Matus, A., 1984. Light and electron microscopic studies of the distribution of microtubule-associated protein 2 in rat brain: A difference between dendritic and axonal cytoskeletons. *The Journal of Comparative Neurology*, 226(2), pp.203–221.
Bertler, Å. & Rosengren, E., 1959. Occurrence and distribution of dopamine in brain and other tissues. *Experientia*, 15(1), pp.10–11.
Bertoncini, C.W. et al., 2005. Familial mutants of alpha-synuclein with increased neurotoxicity have a destabilized conformation. *The Journal of biological chemistry*, 280(35), pp.30649–52.
Betarbet, R. et al., 2006. Intersecting pathways to neurodegeneration in Parkinson's disease: Effects of the pesticide rotenone on DJ-1, α-synuclein, and the ubiquitin–proteasome system. *Neurobiology of Disease*, 22(2), pp.404–420.
Bettencourt-Dias, M. et al., 2011. Centrosomes and cilia in human disease. *Trends in genetics : TIG*, 27(8), pp.307–15.
Beyer, K., Domingo-Sàbat, M. & Ariza, A., 2009. Molecular pathology of Lewy body diseases. *International journal of molecular sciences*, 10(3), pp.724–45.
Binder, L.I., Frankfurter, A. & Rebhun, L.I., 1985. The distribution of tau in the mammalian central nervous system. *The Journal of cell biology*, 101(4), pp.1371–8.
Björklund, A. et al., 1973. The organization of tubero-hypophyseal and reticulo-infundibular catecholamine neuron systems in the rat brain. *Brain Research*, 51, pp.171–191.
Björklund, A. & Dunnett, S.B., 2007. Dopamine neuron systems in the brain: an update. *Trends in Neurosciences*, 30(5), pp.194–202.
Boeddrich, A., Lurz, R. & Wanker, E.E., 2003. Huntingtin Fragments Form Aggresome-Like Inclusion Bodies in Mammalian Cells. In *Protein Misfolding and Disease*. New Jersey: Humana Press, pp. 217–230.
Bogerts, B., Häntsch, J. & Herzer, M., 1983. A morphometric study of the dopamine-containing cell groups in the mesencephalon of normals, Parkinson patients, and schizophrenics. *Biological psychiatry*, 18(9), pp.951–69.
Boltshauser, E. & Isler, W., 1977. Joubert Syndrome: Episodic Hyperpnea, Abnormal Eye Movements, Retardation and Ataxia, Associated with Dysplasia of the Cerebellar Vermis. *Neuropediatrics*, 8(1), pp.57–66.
Bornens, M., 2002. Centrosome composition and microtubule anchoring mechanisms. *Current Opinion in Cell Biology*, 14(1), pp.25–34.
Bosco, D.A. et al., 2006. Elevated levels of oxidized cholesterol metabolites in Lewy body disease brains accelerate α-synuclein fibrilization. *Nature Chemical Biology*, 2(5), pp.249–253.
Boyce, J.M. & Shone, G.R., 2006. Effects of ageing on smell and taste. *Postgraduate medical journal*, 82(966), pp.239–41.
Braak, H. et al., 2003. Staging of brain pathology related to sporadic Parkinson's disease. *Neurobiology of Aging*, 24(2), pp.197–211.
Braak, H. et al., 2002. Staging of the intracerebral inclusion body pathology associated with idiopathic Parkinson's disease (preclinical and clinical stages). *Journal of neurology*, 249 Suppl 3, p.III/1-5.
Brabander, M. De et al., 1986. Microtubule Dynamics during the Cell Cycle: The Effects of Taxol and Nocodazole on the Microtubule System of Pt K2 Cells at Different Stages of the Mitotic Cycle. *International Review of Cytology*, 101, pp.215–274.

Brangwynne, C.P. et al., 2006. Microtubules can bear enhanced compressive loads in living cells because of lateral reinforcement. *The Journal of cell biology*, 173(5), pp.733–41.
Breslow, D.K. et al., 2013. An in vitro assay for entry into cilia reveals unique properties of the soluble diffusion barrier. *The Journal of cell biology*, 203(1), pp.129–47.
Brooks, E.R. & Wallingford, J.B., 2014. Multiciliated cells. *Current biology : CB*, 24(19), pp.R973-82.
Buetow, L. & Huang, D.T., 2016. Structural insights into the catalysis and regulation of E3 ubiquitin ligases. *Nature Reviews Molecular Cell Biology*, 17(10), pp.626–642.
Burre, J. et al., 2010. -Synuclein Promotes SNARE-Complex Assembly in Vivo and in Vitro. *Science*, 329(5999), pp.1663–1667.
Burré, J., 2015. The Synaptic Function of α-Synuclein. *Journal of Parkinson's disease*, 5(4), pp.699–713.
Burré, J., Sharma, M. & Südhof, T.C., 2015. Definition of a molecular pathway mediating α-synuclein neurotoxicity. *The Journal of neuroscience : the official journal of the Society for Neuroscience*, 35(13), pp.5221–32.
Bussell, R. & Eliezer, D., 2003. A structural and functional role for 11-mer repeats in alpha-synuclein and other exchangeable lipid binding proteins. *Journal of molecular biology*, 329(4), pp.763–78.
Calo, L. et al., 2016. Synaptic failure and α-synuclein. *Movement Disorders*, 31(2), pp.169–177.
Cambray-Deakin, M.A. & Burgoyne, R.D., 1987. Posttranslational modifications of alpha-tubulin: acetylated and detyrosinated forms in axons of rat cerebellum. *The Journal of cell biology*, 104(6), pp.1569–74.
von Campenhausen, S. et al., 2005. Prevalence and incidence of Parkinson's disease in Europe. *European Neuropsychopharmacology*, 15(4), pp.473–490.
Campenot, R.B., 1982. Development of sympathetic neurons in compartmentalized cultures: II. Local control of neurite survival by nerve growth factor. *Developmental Biology*, 93(1), pp.13–21.
Cappelletti, G. et al., 2001. MICROTUBULE ASSEMBLY IS DIRECTLY AFFECTED BY MPP+IN VITRO. *Cell Biology International*, 25(10), pp.981–984.
Carlsson, A. et al., 1958. On the presence of 3-hydroxytyramine in brain. *Science (New York, N.Y.)*, 127(3296), p.471.
Cartelli, D. et al., 2012. Microtubule Destabilization Is Shared by Genetic and Idiopathic Parkinson's Disease Patient Fibroblasts S. Salinas, ed. *PLoS ONE*, 7(5), p.e37467.
Cartelli, D. et al., 2010. Microtubule dysfunction precedes transport impairment and mitochondria damage in MPP+-induced neurodegeneration. *Journal of Neurochemistry*, 115(1), pp.247–258.
Cartelli, D. et al., 2016. α-Synuclein is a Novel Microtubule Dynamase. *Scientific Reports*, 6, p.33289.
Chakravarthy, B. et al., 2012. Reduction of the immunostainable length of the hippocampal dentate granule cells' primary cilia in 3xAD-transgenic mice producing human Aβ1-42 and tau. *Biochemical and Biophysical Research Communications*, 427(1), pp.218–222.
Chang, L. et al., 2009. The dynamic properties of intermediate filaments during organelle transport. *Journal of cell science*, 122(Pt 16), pp.2914–23.
Chau, V. et al., 1989. A multiubiquitin chain is confined to specific lysine in a targeted short-lived protein. *Science (New York, N.Y.)*, 243(4898), pp.1576–83.
Chen, J.-J., Lin, F. & Qin, Z.-H., 2008. The roles of the proteasome pathway in signal

transduction and neurodegenerative diseases. *Neuroscience bulletin*, 24(3), pp.183–94.
Chen, L. et al., 2007. Oligomeric α-synuclein inhibits tubulin polymerization. *Biochemical and Biophysical Research Communications*, 356(3), pp.548–553.
Chen, S. et al., 2016. Structural basis for dynamic regulation of the human 26S proteasome. *Proceedings of the National Academy of Sciences*, 113(46), pp.12991–12996.
Chen, S. et al., 2005. The RING finger ATPase Rad5p of Saccharomyces cerevisiae contributes to DNA double-strand break repair in a ubiquitin-independent manner. *Nucleic Acids Research*, 33(18), pp.5878–5886.
Cheng, H.-C., Ulane, C.M. & Burke, R.E., 2010. Clinical progression in Parkinson disease and the neurobiology of axons. *Annals of neurology*, 67(6), pp.715–25.
Chesselet, M.-F., 2008. In vivo alpha-synuclein overexpression in rodents: A useful model of Parkinson's disease? *Experimental Neurology*, 209(1), pp.22–27.
Chiba-Falek, O. et al., 2005. Regulation of alpha-synuclein expression by poly (ADP ribose) polymerase-1 (PARP-1) binding to the NACP-Rep1 polymorphic site upstream of the SNCA gene. *American journal of human genetics*, 76(3), pp.478–92.
Chiba, S. et al., 2013. NDR2-mediated Rabin8 phosphorylation is crucial for ciliogenesis by switching binding specificity from phosphatidylserine to Sec15. *The EMBO journal*, 32(6), pp.874–85.
Chin, L.-S., Olzmann, J.A. & Li, L., 2010. Parkin-mediated ubiquitin signalling in aggresome formation and autophagy. *Biochemical Society transactions*, 38(Pt 1), pp.144–9.
Chinta, S.J. & Andersen, J.K., 2005. Dopaminergic neurons. *The International Journal of Biochemistry & Cell Biology*, 37(5), pp.942–946.
Chiodo, L.A., 1988. Dopamine-containing neurons in the mammalian central nervous system: electrophysiology and pharmacology. *Neuroscience and biobehavioral reviews*, 12(1), pp.49–91.
Choi, Y.-K. et al., 2010. CDK5RAP2 stimulates microtubule nucleation by the gamma-tubulin ring complex. *The Journal of cell biology*, 191(6), pp.1089–95.
Ciechanover, A. & Brundin, P., 2003. The Ubiquitin Proteasome System in Neurodegenerative Diseases: Sometimes the Chicken, Sometimes the Egg. *Neuron*, 40(2), pp.427–446.
Ciechanover, A., Finley, D. & Varshavsky, A., 1984. Ubiquitin dependence of selective protein degradation demonstrated in the mammalian cell cycle mutant ts85. *Cell*, 37(1), pp.57–66.
Clark, A.B. et al., 1995. Regulation of ciliated cell differentiation in cultures of rat tracheal epithelial cells. *American Journal of Respiratory Cell and Molecular Biology*, 12(3), pp.329–338.
Cohen, R.S., Chung, S.K. & Pfaff, D.W., 1985. Immunocytochemical localization of actin in dendritic spines of the cerebral cortex using colloidal gold as a probe. *Cellular and Molecular Neurobiology*, 5(3), pp.271–284.
Cole, D.G. et al., 1998. Chlamydomonas kinesin-II-dependent intraflagellar transport (IFT): IFT particles contain proteins required for ciliary assembly in Caenorhabditis elegans sensory neurons. *The Journal of cell biology*, 141(4), pp.993–1008.
Conway, K.A. et al., 2000. Acceleration of oligomerization, not fibrillization, is a shared property of both alpha-synuclein mutations linked to early-onset Parkinson's disease: implications for pathogenesis and therapy. *Proceedings of the National*

Academy of Sciences of the United States of America, 97(2), pp.571–6.
Cuervo, A.M. et al., 2004. Impaired degradation of mutant alpha-synuclein by chaperone-mediated autophagy. *Science (New York, N.Y.)*, 305(5688), pp.1292–5.
Daubner, S.C., Le, T. & Wang, S., 2011. Tyrosine hydroxylase and regulation of dopamine synthesis. *Archives of biochemistry and biophysics*, 508(1), pp.1–12.
Daum, R.F. et al., 2000. [Olfactory testing with "sniffin' sticks" for clinical diagnosis of Parkinson disease]. *Der Nervenarzt*, 71(8), pp.643–50.
Dawe, H.R. et al., 2007. The Meckel–Gruber Syndrome proteins MKS1 and meckelin interact and are required for primary cilium formation. *Human Molecular Genetics*, 16(2), pp.173–186.
Dawson, T.M. & Dawson, V.L., 2003. Molecular pathways of neurodegeneration in Parkinson's disease. *Science (New York, N.Y.)*, 302(5646), pp.819–22.
Deane, J.A. et al., 2001. Localization of intraflagellar transport protein IFT52 identifies basal body transitional fibers as the docking site for IFT particles. *Current Biology*, 11(20), pp.1586–1590.
Delgehyr, N. et al., 2005. Microtubule nucleation and anchoring at the centrosome are independent processes linked by ninein function. *Journal of cell science*, 118(Pt 8), pp.1565–75.
DeMaagd, G. & Philip, A., 2015. Parkinson's Disease and Its Management: Part 3: Nondopaminergic and Nonpharmacological Treatment Options. *P & T : a peer-reviewed journal for formulary management*, 40(10), pp.668–79.
Deniau, J.M., Thierry, A.M. & Feger, J., 1980. Electrophysiological identification of mesencephalic ventromedial tegmental (VMT) neurons projecting to the frontal cortex, septum and nucleus accumbens. *Brain research*, 189(2), pp.315–26.
Denker, A. & Rizzoli, S.O., 2010. Synaptic vesicle pools: an update. *Frontiers in synaptic neuroscience*, 2, p.135.
Diaz-Corrales, F.J. et al., 2005. Rotenone induces aggregation of γ-tubulin protein and subsequent disorganization of the centrosome: Relevance to formation of inclusion bodies and neurodegeneration. *Neuroscience*, 133(1), pp.117–135.
Dickson, D.W. et al., 2008. Evidence that incidental Lewy body disease is pre-symptomatic Parkinson's disease. *Acta Neuropathologica*, 115(4), pp.437–444.
Dikiy, I. & Eliezer, D., 2014. N-terminal acetylation stabilizes N-terminal helicity in lipid- and micelle-bound α-synuclein and increases its affinity for physiological membranes. *The Journal of biological chemistry*, 289(6), pp.3652–65.
Dominguez, R. & Holmes, K.C., 2011. Actin Structure and Function. *Annual Review of Biophysics*, 40(1), pp.169–186.
Domire, J.S. et al., 2011. Dopamine receptor 1 localizes to neuronal cilia in a dynamic process that requires the Bardet-Biedl syndrome proteins. *Cellular and molecular life sciences : CMLS*, 68(17), pp.2951–60.
Donaldson, K.M. et al., 2003. Ubiquitin Signals Protein Trafficking via Interaction with a Novel Ubiquitin Binding Domain in the Membrane Fusion Regulator, Vps9p. *Current Biology*, 13(3), pp.258–262.
Doty, R.L., Deems, D.A. & Stellar, S., 1988. Olfactory dysfunction in parkinsonism: a general deficit unrelated to neurologic signs, disease stage, or disease duration. *Neurology*, 38(8), pp.1237–44.
Doty, Deems, D.A. & Stellar, S., 1988. Olfactory dysfunction in parkinsonism: A general deficit unrelated to neurologic signs, disease stage, or disease duration. *Neurology*, 38(8), pp.1237–1237.
Dragicevic, E., Schiemann, J. & Liss, B., 2015. Dopamine midbrain neurons in health

and Parkinson's disease: Emerging roles of voltage-gated calcium channels and ATP-sensitive potassium channels. *Neuroscience*, 284, pp.798–814.
Dubey, J., Ratnakaran, N. & Koushika, S.P., 2015. Neurodegeneration and microtubule dynamics: death by a thousand cuts. *Frontiers in cellular neuroscience*, 9, p.343.
Ducas, V.C. & Rhoades, E., 2014. Investigation of Intramolecular Dynamics and Conformations of α-, β- and γ-Synuclein D. R. Borchelt, ed. *PLoS ONE*, 9(1), p.e86983.
Dwane, S., Durack, E. & Kiely, P.A., 2013. Optimising parameters for the differentiation of SH-SY5Y cells to study cell adhesion and cell migration. *BMC research notes*, 6, p.366.
Eddé, B. et al., 1990. Posttranslational glutamylation of alpha-tubulin. *Science (New York, N.Y.)*, 247(4938), pp.83–5.
Van Den Eeden, S.K. et al., 2003. Incidence of Parkinson's disease: variation by age, gender, and race/ethnicity. *American journal of epidemiology*, 157(11), pp.1015–22.
Ehlinger, A. & Walters, K.J., 2013. Structural insights into proteasome activation by the 19S regulatory particle. *Biochemistry*, 52(21), pp.3618–28.
Emamzadeh, F.N., 2016. Alpha-synuclein structure, functions, and interactions. *Journal of research in medical sciences : the official journal of Isfahan University of Medical Sciences*, 21, p.29.
Emmanouilidou, E., Stefanis, L. & Vekrellis, K., 2010. Cell-produced α-synuclein oligomers are targeted to, and impair, the 26S proteasome. *Neurobiology of Aging*, 31(6), pp.953–968.
Esteves, A.R. et al., 2010. Microtubule depolymerization potentiates alpha-synuclein oligomerization. *Frontiers in aging neuroscience*, 1, p.5.
Etlinger, J.D. & Goldberg, A.L., 1977. A soluble ATP-dependent proteolytic system responsible for the degradation of abnormal proteins in reticulocytes. *Proceedings of the National Academy of Sciences of the United States of America*, 74(1), pp.54–8.
Fahn & S., 1987. Recent developments in Parkinson's disease. *Macmillan health care information*, 2, pp.293–304.
Falk, N. et al., 2015. Specialized Cilia in Mammalian Sensory Systems. *Cells*, 4(3), pp.500–19.
Farrer, M. et al., 2004. Comparison of kindreds with parkinsonism and ?-synuclein genomic multiplications. *Annals of Neurology*, 55(2), pp.174–179.
Fiorino, D.F. et al., 1993. Electrical stimulation of reward sites in the ventral tegmental area increases dopamine transmission in the nucleus accumbens of the rat. *Behavioural brain research*, 55(2), pp.131–41.
Fleming, S.M. et al., 2008. Olfactory deficits in mice overexpressing human wildtype alpha-synuclein. *The European journal of neuroscience*, 28(2), pp.247–56.
Fliegner, K.H. et al., 1994. Expression of the gene for the neuronal intermediate filament protein ?-internexin coincides with the onset of neuronal differentiation in the developing rat nervous system. *The Journal of Comparative Neurology*, 342(2), pp.161–173.
Fong, K.-W. et al., 2008. CDK5RAP2 Is a Pericentriolar Protein That Functions in Centrosomal Attachment of the γ-Tubulin Ring Complex S. Doxsey, ed. *Molecular Biology of the Cell*, 19(1), pp.115–125.
Footer, M.J. et al., 2007. Direct measurement of force generation by actin filament polymerization using an optical trap. *Proceedings of the National Academy of*

Sciences of the United States of America, 104(7), pp.2181–6.
Forno, L.S., 1996. Neuropathology of Parkinson's disease. *Journal of neuropathology and experimental neurology*, 55(3), pp.259–72.
Fox, S.H., 2013. Non-dopaminergic Treatments for Motor Control in Parkinson's Disease. *Drugs*, 73(13), pp.1405–1415.
Franke, W.W. et al., 1978. Different intermediate-sized filaments distinguished by immunofluorescence microscopy. *Proceedings of the National Academy of Sciences of the United States of America*, 75(10), pp.5034–8.
Franke, W.W. et al., 1979. Widespread occurrence of intermediate-sized filaments of the vimentin-type in cultured cells from diverse vertebrates. *Experimental Cell Research*, 123(1), pp.25–46.
Franke, W.W., Hergt, M. & Grund, C., 1987. Rearrangement of the vimentin cytoskeleton during adipose conversion: formation of an intermediate filament cage around lipid globules. *Cell*, 49(1), pp.131–41.
Frigerio, R. et al., 2011. Incidental Lewy body disease: do some cases represent a preclinical stage of dementia with Lewy bodies? *Neurobiology of aging*, 32(5), pp.857–63.
Fu, W. et al., 2014. Primary cilia control hedgehog signaling during muscle differentiation and are deregulated in rhabdomyosarcoma. *Proceedings of the National Academy of Sciences of the United States of America*, 111(25), pp.9151–6.
Fuchs, J. et al., 2007. Phenotypic variation in a large Swedish pedigree due to SNCA duplication and triplication. *Neurology*, 68(12), pp.916–22.
Fujiwara, Y., Wada, K. & Kabuta, T., 2016. Lysosomal degradation of intracellular nucleic acids—multiple autophagic pathways. *Journal of Biochemistry*, 161(2), p.mvw085.
Fuxe, K., 1965. Evidence for the existence of monoamine neurons in the central nervous system. *Zeitschrift f□r Zellforschung und Mikroskopische Anatomie*, 65(4), pp.573–596.
Gall, J.G., 1966. Microtubule fine structure. *The Journal of cell biology*, 31(3), pp.639–43.
Galloway, P.G., Mulvihill, P. & Perry, G., 1992. Filaments of Lewy bodies contain insoluble cytoskeletal elements. *The American journal of pathology*, 140(4), pp.809–22.
Ganguly, A. et al., 2015. A dynamic formin-dependent deep F-actin network in axons. *The Journal of cell biology*, 210(3), pp.401–17.
García-Mata, R. et al., 1999. Characterization and dynamics of aggresome formation by a cytosolic GFP-chimera. *The Journal of cell biology*, 146(6), pp.1239–54.
Garcia-Reitboeck, P. et al., 2013. Endogenous alpha-synuclein influences the number of dopaminergic neurons in mouse substantia nigra. *Experimental neurology*, 248, pp.541–5.
Gardel, M.L. et al., 2010. Mechanical integration of actin and adhesion dynamics in cell migration. *Annual review of cell and developmental biology*, 26, pp.315–33.
Giasson, B.I. et al., 2001. A hydrophobic stretch of 12 amino acid residues in the middle of alpha-synuclein is essential for filament assembly. *The Journal of biological chemistry*, 276(4), pp.2380–6.
Glickman, M.H. et al., 1999. Functional analysis of the proteasome regulatory particle. *Molecular biology reports*, 26(1–2), pp.21–8.
Gloeckner, C.J. et al., 2006. The Parkinson disease causing LRRK2 mutation I2020T is

associated with increased kinase activity. *Human Molecular Genetics*, 15(2), pp.223–232.
Godena, V.K. et al., 2014. Increasing microtubule acetylation rescues axonal transport and locomotor deficits caused by LRRK2 Roc-COR domain mutations. *Nature Communications*, 5(1), p.5245.
Goetz, C.G. et al., 2004. *Movement* Disorder Society Task Force report on the Hoehn and Yahr staging scale: Status and recommendations The *Movement* Disorder Society Task Force on rating scales for Parkinson's disease. *Movement Disorders*, 19(9), pp.1020–1028.
Goetz, S.C. & Anderson, K. V., 2010. The primary cilium: a signalling centre during vertebrate development. *Nature Reviews Genetics*, 11(5), pp.331–344.
Goetz, S.C., Liem, K.F. & Anderson, K.V., 2012. The Spinocerebellar Ataxia-Associated Gene Tau Tubulin Kinase 2 Controls the Initiation of Ciliogenesis. *Cell*, 151(4), pp.847–858.
Goldman, J.E. et al., 1983. Lewy bodies of Parkinson's disease contain neurofilament antigens. *Science (New York, N.Y.)*, 221(4615), pp.1082–4.
Goodenough, U.W. & Heuser, J.E., 1985. Outer and inner dynein arms of cilia and flagella. *Cell*, 41(2), pp.341–2.
Gotlieb, A.I. et al., 1981. Distribution of microtubule organizing centers in migrating sheets of endothelial cells. *The Journal of cell biology*, 91(2 Pt 1), pp.589–94.
Gould, R.R. & Borisy, G.G., 1977. The pericentriolar material in Chinese hamster ovary cells nucleates microtubule formation. *The Journal of cell biology*, 73(3), pp.601–15.
Graziadei, P.P.C. & Graziadei, G.A.M., 1979. Neurogenesis and neuron regeneration in the olfactory system of mammals. I. Morphological aspects of differentiation and structural organization of the olfactory sensory neurons. *Journal of Neurocytology*, 8(1), pp.1–18.
Green, J.A. & Mykytyn, K., 2014. Neuronal primary cilia: an underappreciated signaling and sensory organelle in the brain. *Neuropsychopharmacology : official publication of the American College of Neuropsychopharmacology*, 39(1), pp.244–5.
Greffard, S. et al., 2010. A stable proportion of Lewy body bearing neurons in the substantia nigra suggests a model in which the Lewy body causes neuronal death. *Neurobiology of Aging*, 31(1), pp.99–103.
Grundke-Iqbal, I. et al., 1986. Abnormal phosphorylation of the microtubule-associated protein tau (tau) in Alzheimer cytoskeletal pathology. *Proceedings of the National Academy of Sciences of the United States of America*, 83(13), pp.4913–7.
Guemez-Gamboa, A., Coufal, N.G. & Gleeson, J.G., 2014. Primary cilia in the developing and mature brain. *Neuron*, 82(3), pp.511–21.
Gunawardane, R.N. et al., 2000. Characterization and reconstitution of Drosophila gamma-tubulin ring complex subunits. *The Journal of cell biology*, 151(7), pp.1513–24.
Haehner, A., Hummel, T. & Reichmann, H., 2014. A clinical approach towards smell loss in Parkinson's disease. *Journal of Parkinson's disease*, 4(2), pp.189–95.
Halliwell, B. & Jenner, P., 1998. Impaired clearance of oxidised proteins in neurodegenerative diseases. *The Lancet*, 351(9114), p.1510.
Hamilton, R.L., 2006. Lewy Bodies in Alzheimer's Disease: A Neuropathological Review of 145 Cases Using α-Synuclein Immunohistochemistry. *Brain Pathology*, 10(3),

pp.378–384.
Han, Y.H. et al., 2009. The effect of MG132, a proteasome inhibitor on HeLa cells in relation to cell growth, reactive oxygen species and GSH. *Oncology Reports*, 22(1), pp.215–221.
Hancock, D.B. et al., 2007. Smoking, Caffeine, and Nonsteroidal Anti-inflammatory Drugs in Families With Parkinson Disease. *Archives of Neurology*, 64(4), p.576.
Hansson, O. et al., 2014. Levels of cerebrospinal fluid α-synuclein oligomers are increased in Parkinson's disease with dementia and dementia with Lewy bodies compared to Alzheimer's disease. *Alzheimer's research & therapy*, 6(3), p.25.
Hao, L. et al., 2011. Intraflagellar transport delivers tubulin isotypes to sensory cilium middle and distal segments. *Nature Cell Biology*, 13(7), pp.790–798.
Hao, R. et al., 2013. Proteasomes activate aggresome disassembly and clearance by producing unanchored ubiquitin chains. *Molecular cell*, 51(6), pp.819–28.
Hara, T. et al., 2006. Suppression of basal autophagy in neural cells causes neurodegenerative disease in mice. *Nature*, 441(7095), pp.885–889.
Harada, A. et al., 1994. Altered microtubule organization in small-calibre axons of mice lacking tau protein. *Nature*, 369(6480), pp.488–491.
Haren, L. et al., 2006. NEDD1-dependent recruitment of the γ-tubulin ring complex to the centrosome is necessary for centriole duplication and spindle assembly. *The Journal of Cell Biology*, 172(4), pp.505–515.
Hashimoto, M. & Masliah, E., 1999. Alpha-synuclein in Lewy body disease and Alzheimer's disease. *Brain pathology (Zurich, Switzerland)*, 9(4), pp.707–20.
Heinemeyer, W. et al., 1997. The active sites of the eukaryotic 20 S proteasome and their involvement in subunit precursor processing. *The Journal of biological chemistry*, 272(40), pp.25200–9.
Hendricks, A.G. et al., 2010. Motor Coordination via a Tug-of-War Mechanism Drives Bidirectional Vesicle Transport. *Current Biology*, 20(8), pp.697–702.
Herculano-Houzel, S., 2009. The human brain in numbers: a linearly scaled-up primate brain. *Frontiers in human neuroscience*, 3, p.31.
Hill-Burns, E.M. et al., 2016. Identification of genetic modifiers of age-at-onset for familial Parkinson's disease. *Human Molecular Genetics*, 25(17), pp.3849–3862.
Hoehn, M.M. & Yahr, M.D., 1967. Parkinsonism: onset, progression, and mortality. *Neurology*, 17(5), pp.427–427.
Hollenbeck, P.J., 1996. The pattern and mechanism of mitochondrial transport in axons. *Frontiers in bioscience : a journal and virtual library*, 1, pp.d91-102.
Hong, E., Jayachandran, P. & Brewster, R., 2010. The polarity protein Pard3 is required for centrosome positioning during neurulation. *Developmental Biology*, 341(2), pp.335–345.
Hoyer, W. et al., 2002. Dependence of alpha-synuclein aggregate morphology on solution conditions. *Journal of molecular biology*, 322(2), pp.383–93.
Huber, F. et al., 2015. Cytoskeletal crosstalk: when three different personalities team up. *Current Opinion in Cell Biology*, 32, pp.39–47.
Huisman, E., Uylings, H.B.M. & Hoogland, P. V., 2004. A 100% increase of dopaminergic cells in the olfactory bulb may explain hyposmia in Parkinson's disease. *Movement Disorders*, 19(6), pp.687–692.
Hunn, B.H.M. et al., 2015. Impaired intracellular trafficking defines early Parkinson's disease. *Trends in Neurosciences*, 38(3), pp.178–88.
Ibi, M. et al., 2011. Trichoplein controls microtubule anchoring at the centrosome by binding to Odf2 and ninein. *Journal of cell science*, 124(Pt 6), pp.857–64.

Ishikawa, H. et al., 2005. Odf2-deficient mother centrioles lack distal/subdistal appendages and the ability to generate primary cilia. *Nature Cell Biology*, 7(5), pp.517–524.
Iwata, A. et al., 2005. Increased susceptibility of cytoplasmic over nuclear polyglutamine aggregates to autophagic degradation. *Proceedings of the National Academy of Sciences of the United States of America*, 102(37), pp.13135–40.
Jakes, R., Spillantini, M.G. & Goedert, M., 1994. Identification of two distinct synucleins from human brain. *FEBS Letters*, 345(1), pp.27–32.
Jellinger, K.A., 2004. Lewy body-related ?-synucleinopathy in the aged human brain. *Journal of Neural Transmission*, 111(10–11), pp.1219–1235.
Jenkins, P.M., McEwen, D.P. & Martens, J.R., 2009. Olfactory cilia: linking sensory cilia function and human disease. *Chemical senses*, 34(5), pp.451–64.
Ji, H. et al., 1997. Identification of a breast cancer-specific gene, BCSG1, by direct differential cDNA sequencing. *Cancer research*, 57(4), pp.759–64.
Jin, J. et al., 2007. Dual E1 activation systems for ubiquitin differentially regulate E2 enzyme charging. *Nature*, 447(7148), pp.1135–1138.
Johnston, J.A., Illing, M.E. & Kopito, R.R., 2002. Cytoplasmic dynein/dynactin mediates the assembly of aggresomes. *Cell Motility and the Cytoskeleton*, 53(1), pp.26–38.
Johnston, J.A., Ward, C.L. & Kopito, R.R., 1998. Aggresomes: a cellular response to misfolded proteins. *The Journal of cell biology*, 143(7), pp.1883–98.
Joshi, H.C. et al., 1992. γ-Tubulin is a centrosomal protein required for cell cycle-dependent microtubule nucleation. *Nature*, 356(6364), pp.80–83.
Junn, E. et al., 2002. Parkin accumulation in aggresomes due to proteasome impairment. *The Journal of biological chemistry*, 277(49), pp.47870–7.
Kalia, L. V & Lang, A.E., 2015. Parkinson's disease. *The Lancet*, 386(9996), pp.896–912.
Kaliszewski, M., Knott, A.B. & Bossy-Wetzel, E., 2015. Primary cilia and autophagic dysfunction in Huntington's disease. *Cell Death & Differentiation*, 22(9), pp.1413–1424.
Kang, L. et al., 2012. N-terminal acetylation of α-synuclein induces increased transient helical propensity and decreased aggregation rates in the intrinsically disordered monomer. *Protein science : a publication of the Protein Society*, 21(7), pp.911–7.
Kapitein, L.C. & Hoogenraad, C.C., 2015. Building the Neuronal Microtubule Cytoskeleton. *Neuron*, 87(3), pp.492–506.
Kapitein, L.C. & Hoogenraad, C.C., 2011. Which way to go? Cytoskeletal organization and polarized transport in neurons. *Molecular and Cellular Neuroscience*, 46(1), pp.9–20.
Kasahara, K. et al., 2014. Ubiquitin-proteasome system controls ciliogenesis at the initial step of axoneme extension. *Nature communications*, 5, p.5081.
Kasten, M. & Klein, C., 2013. The many faces of alpha-synuclein mutations. *Movement Disorders*, 28(6), pp.697–701.
Katotomichelakis, M. et al., 2007. The effect of smoking on the olfactory function. *Rhinology*, 45(4), pp.273–80.
Keating, T.J. & Borisy, G.G., 2000. Immunostructural evidence for the template mechanism of microtubule nucleation. *Nature Cell Biology*, 2(6), pp.352–357.
Keefe, K.A. & Gerfen, C.R., 1995. D1–D2 dopamine receptor synergy in striatum: effects of intrastriatal infusions of dopamine agonists and antagonists on immediate early gene expression. *Neuroscience*, 66(4), pp.903–913.
Keller, A. & Malaspina, D., 2013. Hidden consequences of olfactory dysfunction: a patient report series. *BMC Ear, Nose and Throat Disorders*, 13(1), p.8.

Keryer, G. et al., 2011. Ciliogenesis is regulated by a huntingtin-HAP1-PCM1 pathway and is altered in Huntington disease. *The Journal of clinical investigation*, 121(11), pp.4372–82.

Khwanraj, K. et al., 2015. Differential Expression of Tyrosine Hydroxylase Protein and Apoptosis-Related Genes in Differentiated and Undifferentiated SH-SY5Y Neuroblastoma Cells Treated with MPP +. *Neurology Research International*, 2015, pp.1–11.

Kiely, A.P. et al., 2013. α-Synucleinopathy associated with G51D SNCA mutation: a link between Parkinson's disease and multiple system atrophy? *Acta Neuropathologica*, 125(5), pp.753–769.

Kim, H. et al., 2014. Ciliary membrane proteins traffic through the Golgi via a Rabep1/GGA1/Arl3-dependent mechanism. *Nature Communications*, 5(1), p.5482.

Kim, J. et al., 2015. Actin remodelling factors control ciliogenesis by regulating YAP/TAZ activity and vesicle trafficking. *Nature Communications*, 6(1), p.6781.

Kim, J. et al., 2010. Functional genomic screen for modulators of ciliogenesis and cilium length. *Nature*, 464(7291), pp.1048–1051.

Kimura, S., Noda, T. & Yoshimori, T., 2008. Dynein-dependent movement of autophagosomes mediates efficient encounters with lysosomes. *Cell structure and function*, 33(1), pp.109–22.

Klein, C. & Westenberger, A., 2012. Genetics of Parkinson's disease. *Cold Spring Harbor perspectives in medicine*, 2(1), p.a008888.

Knödler, A. et al., 2010. Coordination of Rab8 and Rab11 in primary ciliogenesis. *Proceedings of the National Academy of Sciences of the United States of America*, 107(14), pp.6346–51.

Köchl, R. et al., 2006. Microtubules Facilitate Autophagosome Formation and Fusion of Autophagosomes with Endosomes. *Traffic*, 7(2), pp.129–145.

Koonce, M.P., Cloney, R.A. & Berns, M.W., 1984. Laser irradiation of centrosomes in newt eosinophils: evidence of centriole role in motility. *The Journal of cell biology*, 98(6), pp.1999–2010.

Kopito, R.R., 2000. Aggresomes, inclusion bodies and protein aggregation. *Trends in Cell Biology*, 10(12), pp.524–530.

Korecka, J.A. et al., 2013. Phenotypic Characterization of Retinoic Acid Differentiated SH-SY5Y Cells by Transcriptional Profiling K.-L. Lim, ed. *PLoS ONE*, 8(5), p.e63862.

Korn, E.D., Carlier, M.F. & Pantaloni, D., 1987. Actin polymerization and ATP hydrolysis. *Science (New York, N.Y.)*, 238(4827), pp.638–44.

Kozminski, K.G. et al., 1993. A motility in the eukaryotic flagellum unrelated to flagellar beating. *Proceedings of the National Academy of Sciences of the United States of America*, 90(12), pp.5519–23.

Krüger, R. et al., 1998. Ala30Pro mutation in the gene encoding α-synuclein in Parkinson's disease. *Nature Genetics*, 18(2), pp.106–108.

Krüger, R. et al., 1999. Increased susceptibility to sporadic Parkinson's disease by a certain combined alpha-synuclein/apolipoprotein E genotype. *Annals of neurology*, 45(5), pp.611–7.

Kuhns, S. et al., 2013. The microtubule affinity regulating kinase MARK4 promotes axoneme extension during early ciliogenesis. *The Journal of cell biology*, 200(4), pp.505–22.

Kuusisto, E., Parkkinen, L. & Alafuzoff, I., 2003. Morphogenesis of Lewy bodies: dissimilar incorporation of alpha-synuclein, ubiquitin, and p62. *Journal of*

neuropathology and experimental neurology, 62(12), pp.1241–53.
Kuzuhara, S. et al., 1988. Lewy bodies are ubiquitinated. A light and electron microscopic immunocytochemical study. *Acta neuropathologica*, 75(4), pp.345–53.
L'Hernault, S.W. & Rosenbaum, J.L., 1985. Chlamydomonas .alpha.-tubulin is posttranslationally modified by acetylation on the .epsilon.-amino group of a lysine. *Biochemistry*, 24(2), pp.473–478.
Labandeira-Garcia, J.L. et al., 2017. Brain Renin-Angiotensin System and Microglial Polarization: Implications for Aging and Neurodegeneration. *Frontiers in Aging Neuroscience*, 9, p.129.
Lambert, M.P. et al., 1998. Diffusible, nonfibrillar ligands derived from Abeta1-42 are potent central nervous system neurotoxins. *Proceedings of the National Academy of Sciences of the United States of America*, 95(11), pp.6448–53.
Lashuel, H.A. et al., 2013. The many faces of α-synuclein: from structure and toxicity to therapeutic target. *Nature reviews. Neuroscience*, 14(1), pp.38–48.
de Lau, L.M. & Breteler, M.M., 2006. Epidemiology of Parkinson's disease. *The Lancet Neurology*, 5(6), pp.525–535.
Lautenschläger, J. et al., 2018. C-terminal calcium binding of α-synuclein modulates synaptic vesicle interaction. *Nature Communications*, 9(1), p.712.
Lavedan, C. et al., 2002. A mutation in the human neurofilament M gene in Parkinson's disease that suggests a role for the cytoskeleton in neuronal degeneration. *Neuroscience Letters*, 322(1), pp.57–61.
Lavedan, C. et al., 1998. Identification, localization and characterization of the human gamma-synuclein gene. *Human genetics*, 103(1), pp.106–12.
Law, B.M.H. et al., 2014. A Direct Interaction between Leucine-rich Repeat Kinase 2 and Specific β-Tubulin Isoforms Regulates Tubulin Acetylation. *Journal of Biological Chemistry*, 289(2), pp.895–908.
Lazarus, J.E. et al., 2013. Dynactin Subunit p150Glued Is a Neuron-Specific Anti-Catastrophe Factor D. Pellman, ed. *PLoS Biology*, 11(7), p.e1001611.
Lechtreck, K.F., 2015. IFT-Cargo Interactions and Protein Transport in Cilia. *Trends in biochemical sciences*, 40(12), pp.765–778.
Lee, H.-J. et al., 2004. Clearance of -Synuclein Oligomeric Intermediates via the Lysosomal Degradation Pathway. *Journal of Neuroscience*, 24(8), pp.1888–1896.
Lee, H.-J., Choi, C. & Lee, S.-J., 2002. Membrane-bound alpha-synuclein has a high aggregation propensity and the ability to seed the aggregation of the cytosolic form. *The Journal of biological chemistry*, 277(1), pp.671–8.
Lee, J., Giordano, S. & Zhang, J., 2012. Autophagy, mitochondria and oxidative stress: cross-talk and redox signalling. *The Biochemical journal*, 441(2), pp.523–40.
Lee, J.W. et al., 2006. Editing-defective tRNA synthetase causes protein misfolding and neurodegeneration. *Nature*, 443(7107), pp.50–55.
Lee, S.-J., Jeon, H. & Kandror, K. V, 2008. Alpha-synuclein is localized in a subpopulation of rat brain synaptic vesicles. *Acta neurobiologiae experimentalis*, 68(4), pp.509–15.
Lemasters, J.J., 2005. Selective Mitochondrial Autophagy, or Mitophagy, as a Targeted Defense Against Oxidative Stress, Mitochondrial Dysfunction, and Aging. *Rejuvenation Research*, 8(1), pp.3–5.
Leroy, E. et al., 1998. The ubiquitin pathway in Parkinson's disease. *Nature*, 395(6701), pp.451–452.
Lewy & FH, 1912. Paralysis agitans. I. Pathologische Anatomie. *Handbuch der*

Neurologie, 3, pp.920–958.
Li, W. et al., 2017. Centriole translocation and degeneration during ciliogenesis in Caenorhabditis elegans neurons. *The EMBO journal*, 36(17), pp.2553–2566.
Li, W., Li, J. & Bao, J., 2012. Microautophagy: lesser-known self-eating. *Cellular and Molecular Life Sciences*, 69(7), pp.1125–1136.
Li, Y. et al., 2009. Mutant LRRK2 R1441G BAC transgenic mice recapitulate cardinal features of Parkinson's disease. *Nature Neuroscience*, 12(7), pp.826–828.
Lilienbaum, A., 2013. Relationship between the proteasomal system and autophagy. *International journal of biochemistry and molecular biology*, 4(1), pp.1–26.
Lindersson, E. et al., 2004. Proteasomal inhibition by alpha-synuclein filaments and oligomers. *The Journal of biological chemistry*, 279(13), pp.12924–34.
Litwack, G. & Litwack, G., 2018. Metabolism of Amino Acids. *Human Biochemistry*, pp.359–394.
Liu, C.-W. et al., 2005. A precipitating role for truncated alpha-synuclein and the proteasome in alpha-synuclein aggregation: implications for pathogenesis of Parkinson disease. *The Journal of biological chemistry*, 280(24), pp.22670–8.
Liu, C.-W. & Jacobson, A.D., 2013. Functions of the 19S complex in proteasomal degradation. *Trends in biochemical sciences*, 38(2), pp.103–10.
Liu, J.-P. & Zeitlin, S.O., 2011. The long and the short of aberrant ciliogenesis in Huntington disease. *The Journal of clinical investigation*, 121(11), pp.4237–41.
Liu, P., Choi, Y.-K. & Qi, R.Z., 2014. NME7 is a functional component of the γ-tubulin ring complex. *Molecular biology of the cell*, 25(13), pp.2017–25.
Liu, Z., Steward, R. & Luo, L., 2000. Drosophila Lis1 is required for neuroblast proliferation, dendritic elaboration and axonal transport. *Nature Cell Biology*, 2(11), pp.776–783.
Loopuijt, L.D. & Sebens, J.B., 1990. Loss of dopamine receptors in the olfactory bulb of patients with Alzheimer's disease. *Brain Research*, 529(1–2), pp.239–244.
Lopes, F.M. et al., 2010. Comparison between proliferative and neuron-like SH-SY5Y cells as an in vitro model for Parkinson disease studies. *Brain Research*, 1337, pp.85–94.
Lowe, J. et al., 1988. Ubiquitin is a common factor in intermediate filament inclusion bodies of diverse type in man, including those of Parkinson's disease, Pick's disease, and Alzheimer's disease, as well as Rosenthal fibres in cerebellar astrocytomas, cytoplasmic bodies in m. *The Journal of Pathology*, 155(1), pp.9–15.
Lowery, J. et al., 2015. Intermediate Filaments Play a Pivotal Role in Regulating Cell Architecture and Function. *The Journal of biological chemistry*, 290(28), pp.17145–53.
Ltic, S. et al., 2004. Alpha-synuclein is expressed in different tissues during human fetal development. *Journal of molecular neuroscience : MN*, 22(3), pp.199–204.
Lu, Q. et al., 2015. Early steps in primary cilium assembly require EHD1/EHD3-dependent ciliary vesicle formation. *Nature Cell Biology*, 17(3), pp.228–240.
Lücking, C.B. & Brice, A., 2000. Alpha-synuclein and Parkinson's disease. *Cellular and Molecular Life Sciences*, 57(13), pp.1894–1908.
Lyser, K.M., 1968. An electron-microscope study of centrioles in differentiating motor neuroblasts. *Development*, 20(3).
Ma, X., Peterson, R. & Turnbull, J., 2011. Adenylyl cyclase type 3, a marker of primary cilia, is reduced in primary cell culture and in lumbar spinal cord in situ in G93A SOD1 mice. *BMC neuroscience*, 12, p.71.

Madero-Pérez, J. et al., 2018. Parkinson disease-associated mutations in LRRK2 cause centrosomal defects via Rab8a phosphorylation. *Molecular Neurodegeneration*, 13(1), p.3.
Mahjoub, M.R., 2013. The importance of a single primary cilium. *Organogenesis*, 9(2), pp.61–69.
Majeski, A.E. & Fred Dice, J., 2004. Mechanisms of chaperone-mediated autophagy. *The International Journal of Biochemistry & Cell Biology*, 36(12), pp.2435–2444.
Mallavarapu, A. & Mitchison, T., 1999. Regulated actin cytoskeleton assembly at filopodium tips controls their extension and retraction. *The Journal of cell biology*, 146(5), pp.1097–106.
Mann, S.S. & Hammarback, J.A., 1994. Molecular characterization of light chain 3. A microtubule binding subunit of MAP1A and MAP1B. *The Journal of biological chemistry*, 269(15), pp.11492–7.
Maraganore, D.M. et al., 2004. UCHL1 is a Parkinson's disease susceptibility gene. *Annals of Neurology*, 55(4), pp.512–521.
Margiotta, A. & Bucci, C., 2016. Role of Intermediate Filaments in Vesicular Traffic. *Cells*, 5(2), p.20.
Marley, A. & von Zastrow, M., 2010. DISC1 Regulates Primary Cilia That Display Specific Dopamine Receptors A. I. Bush, ed. *PLoS ONE*, 5(5), p.e10902.
Maroteaux, L., Campanelli, J. & Scheller, R., 1988. Synuclein: a neuron-specific protein localized to the nucleus and presynaptic nerve terminal. *Journal of Neuroscience*, 8(8).
Marshall, L.E. & Himes, R.H., 1978. Rotenone inhibition of tubulin self-assembly. *Biochimica et biophysica acta*, 543(4), pp.590–4.
Marshall, W.F., 2001. Centrioles take center stage. *Current biology : CB*, 11(12), pp.R487-96.
Martinez-Vicente, M. et al., 2008. Dopamine-modified α-synuclein blocks chaperone-mediated autophagy. *Journal of Clinical Investigation*, 118(2), pp.777–88.
Matsuda, N. et al., 2010. PINK1 stabilized by mitochondrial depolarization recruits Parkin to damaged mitochondria and activates latent Parkin for mitophagy. *The Journal of cell biology*, 189(2), pp.211–21.
Mayer, R.J. et al., 1989. Intermediate filament-ubiquitin diseases: implications for cell sanitization. *Biochemical Society symposium*, 55, pp.193–201.
McLean, P.., Kawamata, H. & Hyman, B.., 2001. α-Synuclein–enhanced green fluorescent protein fusion proteins form proteasome sensitive inclusions in primary neurons. *Neuroscience*, 104(3), pp.901–912.
McLean, P.J. et al., 2000. Membrane association and protein conformation of alpha-synuclein in intact neurons. Effect of Parkinson's disease-linked mutations. *The Journal of biological chemistry*, 275(12), pp.8812–6.
McNaught, Shashidharan, P., et al., 2002. Aggresome-related biogenesis of Lewy bodies. *European Journal of Neuroscience*, 16(11), pp.2136–2148.
McNaught, Belizaire, R., et al., 2002. Selective loss of 20S proteasome α-subunits in the substantia nigra pars compacta in Parkinson's disease. *Neuroscience Letters*, 326(3), pp.155–158.
McNaught, . & Olanow, C.W., 2003. Proteolytic stress: A unifying concept for the etiopathogenesis of Parkinson's disease. *Annals of Neurology*, 53(S3), pp.S73–S86.
McNaught, K.S.. & Jenner, P., 2001. Proteasomal function is impaired in substantia nigra in Parkinson's disease. *Neuroscience Letters*, 297(3), pp.191–194.

Menzies, F.M. et al., 2017. Autophagy and Neurodegeneration: Pathogenic Mechanisms and Therapeutic Opportunities. *Neuron*, 93(5), pp.1015–1034.
Mitchison, H.M. & Valente, E.M., 2017. Motile and non-motile cilia in human pathology: from function to phenotypes. *The Journal of Pathology*, 241(2), pp.294–309.
Mitchison, T. & Kirschner, M., 1984a. Dynamic instability of microtubule growth. *Nature*, 312(5991), pp.237–42.
Mitchison, T. & Kirschner, M., 1984b. Microtubule assembly nucleated by isolated centrosomes. *Nature*, 312(5991), pp.232–7.
Miyoshi, K. et al., 2014. Lack of dopaminergic inputs elongates the primary cilia of striatal neurons. *PloS one*, 9(5), p.e97918.
Molinoff, P.B. & Axelrod, J., 1971. Biochemistry of Catecholamines. *Annual Review of Biochemistry*, 40(1), pp.465–500.
Molla-Herman, A. et al., 2010. The ciliary pocket: an endocytic membrane domain at the base of primary and motile cilia. *Journal of cell science*, 123(Pt 10), pp.1785–95.
Mollenhauer, B. et al., 2013. Früherkennung der Parkinson-Krankheit. *Der Nervenarzt*, 84(8), pp.918–926.
Muangpaisan, W., Hori, H. & Brayne, C., 2009. Systematic review of the prevalence and incidence of Parkinson's disease in Asia. *Journal of epidemiology*, 19(6), pp.281–93.
Mueller, J.C. et al., 2005. Multiple regions of α-synuclein are associated with Parkinson's disease. *Annals of Neurology*, 57(4), pp.535–541.
Murphy, S.M. et al., 2001. GCP5 and GCP6: two new members of the human gamma-tubulin complex. *Molecular biology of the cell*, 12(11), pp.3340–52.
Murphy, S.M., Urbani, L. & Stearns, T., 1998. The mammalian gamma-tubulin complex contains homologues of the yeast spindle pole body components spc97p and spc98p. *The Journal of cell biology*, 141(3), pp.663–74.
Nakajo, S. et al., 1990. Purification and Characterization of a Novel Brain-Specific 14-kDa Protein. *Journal of Neurochemistry*, 55(6), pp.2031–2038.
Narendra, D. et al., 2008. Parkin is recruited selectively to impaired mitochondria and promotes their autophagy. *The Journal of Cell Biology*, 183(5), pp.795–803.
Nigg, E.A. & Raff, J.W., 2009. Centrioles, Centrosomes, and Cilia in Health and Disease. *Cell*, 139(4), pp.663–678.
Niimura, Y. & Nei, M., 2003. Evolution of olfactory receptor genes in the human genome. *Proceedings of the National Academy of Sciences of the United States of America*, 100(21), pp.12235–40.
Nishioka, K. et al., 2006. Clinical heterogeneity of α-synuclein gene duplication in Parkinson's disease. *Annals of Neurology*, 59(2), pp.298–309.
Nobes, C.D. & Hall, A., 1995. Rho, Rac, and Cdc42 GTPases regulate the assembly of multimolecular focal complexes associated with actin stress fibers, lamellipodia, and filopodia. *Cell*, 81(1), pp.53–62.
Nobes, C.D. & Hall, A., 1999. Rho GTPases control polarity, protrusion, and adhesion during cell movement. *The Journal of cell biology*, 144(6), pp.1235–44.
Novorol, C. et al., 2013. Microcephaly models in the developing zebrafish retinal neuroepithelium point to an underlying defect in metaphase progression. *Open biology*, 3(10), p.130065.
Noyce, A.J. et al., 2012. Meta-analysis of early nonmotor features and risk factors for Parkinson disease. *Annals of Neurology*, 72(6), pp.893–901.

Oakley, B.R. et al., 1990. γ-tubulin is a component of the spindle pole body that is essential for microtubule function in Aspergillus nidulans. *Cell*, 61(7), pp.1289–1301.
Obadiah, J. et al., 1999. Adenylyl cyclase interaction with the D2 dopamine receptor family; differential coupling to Gi, Gz, and Gs. *Cellular and molecular neurobiology*, 19(5), pp.653–64.
Okubadejo, N.U. et al., 2006. Parkinson's disease in Africa: A systematic review of epidemiologic and genetic studies. *Movement Disorders*, 21(12), pp.2150–2156.
Olanow, C.W. et al., 2004. Lewy-body formation is an aggresome-related process: a hypothesis. *The Lancet. Neurology*, 3(8), pp.496–503.
Olzmann, J.A., Li, L. & Chin, L.S., 2008. Aggresome formation and neurodegenerative diseases: therapeutic implications. *Current medicinal chemistry*, 15(1), pp.47–60.
Orlowski, M. & Wilk, S., 2000. Catalytic Activities of the 20 S Proteasome, a Multicatalytic Proteinase Complex. *Archives of Biochemistry and Biophysics*, 383(1), pp.1–16.
Osborn, M. & Weber, K., 1976. Cytoplasmic microtubules in tissue culture cells appear to grow from an organizing structure towards the plasma membrane. *Proceedings of the National Academy of Sciences of the United States of America*, 73(3), pp.867–71.
St. P. McNaught, K. et al., 2003. Altered Proteasomal Function in Sporadic Parkinson's Disease. *Experimental Neurology*, 179(1), pp.38–46.
Pampliega, O. et al., 2013. Functional interaction between autophagy and ciliogenesis. *Nature*, 502(7470), pp.194–200.
Pampliega, O. & Cuervo, A.M., 2016. Autophagy and primary cilia: dual interplay. *Current opinion in cell biology*, 39, pp.1–7.
Pantaloni, D. & Carlier, M.F., 1993. How profilin promotes actin filament assembly in the presence of thymosin beta 4. *Cell*, 75(5), pp.1007–14.
Papandréou, M.-J. & Leterrier, C., 2018. The functional architecture of axonal actin. *Molecular and Cellular Neuroscience*, 91, pp.151–159.
Papapetropoulos, S. et al., 2007. A Prospective Study of Familial versus Sporadic Parkinson's Disease. *Neurodegenerative Diseases*, 4(6), pp.424–427.
Parkinson, J., 1817. An essay on the shaking palsy. *The Journal of neuropsychiatry and clinical neurosciences*, pp.223–36. Available at: https://archive.org/details/essayonshakingpa00parkuoft/page/n4 [Accessed June 14, 2019].
Pasanen, P. et al., 2014. A novel α-synuclein mutation A53E associated with atypical multiple system atrophy and Parkinson's disease-type pathology. *Neurobiology of Aging*, 35(9), p.2180.e1-2180.e5.
Paul, S., 2008. Dysfunction of the ubiquitin-proteasome system in multiple disease conditions: therapeutic approaches. *BioEssays*, 30(11–12), pp.1172–1184.
Pazour, G.J., Wilkerson, C.G. & Witman, G.B., 1998. A dynein light chain is essential for the retrograde particle movement of intraflagellar transport (IFT). *The Journal of cell biology*, 141(4), pp.979–92.
Pearce, J.M., 1989. Aspects of the history of Parkinson's disease. *Journal of neurology, neurosurgery, and psychiatry*, Suppl(Suppl), pp.6–10.
Pearce, R.K.B., Hawkes, C.H. & Daniel, S.E., 1995. The anterior olfactory nucleus in Parkinson's disease. *Movement Disorders*, 10(3), pp.283–287.
Peng, J. et al., 2003. A proteomics approach to understanding protein ubiquitination. *Nature Biotechnology*, 21(8), pp.921–926.

Peris, L. et al., 2006. Tubulin tyrosination is a major factor affecting the recruitment of CAP-Gly proteins at microtubule plus ends. *The Journal of cell biology*, 174(6), pp.839–49.
Perrot, R. et al., 2008. Review of the Multiple Aspects of Neurofilament Functions, and their Possible Contribution to Neurodegeneration. *Molecular Neurobiology*, 38(1), pp.27–65.
Piel, M. et al., 2000. The respective contributions of the mother and daughter centrioles to centrosome activity and behavior in vertebrate cells. *The Journal of cell biology*, 149(2), pp.317–30.
Pinto, J.M., 2011. Olfaction. *Proceedings of the American Thoracic Society*, 8(1), pp.46–52.
Pissadaki, E.K. & Bolam, J.P., 2013. The energy cost of action potential propagation in dopamine neurons: clues to susceptibility in Parkinson's disease. *Frontiers in computational neuroscience*, 7, p.13.
Pitaval, A. et al., 2017. Microtubule stabilization drives 3D centrosome migration to initiate primary ciliogenesis. *The Journal of cell biology*, 216(11), pp.3713–3728.
Plotnikova, O. V, Pugacheva, E.N. & Golemis, E.A., 2009. Primary cilia and the cell cycle. *Methods in cell biology*, 94, pp.137–60.
Plouvier, A.O.A. et al., 2014. Prodromal symptoms and early detection of Parkinson's disease in general practice: a nested case-control study. *Family Practice*, 31(4), pp.373–378.
Plowey, E.D. et al., 2008. Role of autophagy in G2019S-LRRK2-associated neurite shortening in differentiated SH-SY5Y cells. *Journal of Neurochemistry*, 105(3), pp.1048–1056.
Polymeropoulos, M.H. et al., 1997. Mutation in the alpha-synuclein gene identified in families with Parkinson's disease. *Science (New York, N.Y.)*, 276(5321), pp.2045–7.
Ponsard, C. et al., 2007. Identification of BCAP, a new protein associated with basal bodies and centrioles. *Frontiers in bioscience : a journal and virtual library*, 12, pp.3683–93.
Premchandar, A. et al., 2016. Structural Dynamics of the Vimentin Coiled-coil Contact Regions Involved in Filament Assembly as Revealed by Hydrogen-Deuterium Exchange. *The Journal of biological chemistry*, 291(48), pp.24931–24950.
Prensa, L. et al., 2009. The nigrostriatal pathway: axonal collateralization and compartmental specificity. *Journal of neural transmission. Supplementum*, (73), pp.49–58.
Pringsheim, T. et al., 2014. The prevalence of Parkinson's disease: A systematic review and meta-analysis. *Movement Disorders*, 29(13), pp.1583–1590.
Prots, I. et al., 2013. α-Synuclein oligomers impair neuronal microtubule-kinesin interplay. *The Journal of biological chemistry*, 288(30), pp.21742–54.
Quintyne, N.J. et al., 1999. Dynactin is required for microtubule anchoring at centrosomes. *The Journal of cell biology*, 147(2), pp.321–34.
Ravikumar, B. et al., 2009. Mammalian macroautophagy at a glance. *Journal of cell science*, 122(Pt 11), pp.1707–11.
Ravikumar, B., Duden, R. & Rubinsztein, D.C., 2002. Aggregate-prone proteins with polyglutamine and polyalanine expansions are degraded by autophagy. *Human Molecular Genetics*, 11(9), pp.1107–1117.
Reiter, J.F., Blacque, O.E. & Leroux, M.R., 2012. The base of the cilium: roles for transition fibres and the transition zone in ciliary formation, maintenance and compartmentalization. *EMBO reports*, 13(7), pp.608–18.

Ren, Y. et al., 2015. Parkin mutations reduce the complexity of neuronal processes in iPSC-derived human neurons. *Stem cells (Dayton, Ohio)*, 33(1), pp.68–78.
Ren, Y., Zhao, J. & Feng, J., 2003. Parkin binds to alpha/beta tubulin and increases their ubiquitination and degradation. *The Journal of neuroscience : the official journal of the Society for Neuroscience*, 23(8), pp.3316–24.
Reyes-Turcu, F.E. & Wilkinson, K.D., 2009. Polyubiquitin binding and disassembly by deubiquitinating enzymes. *Chemical reviews*, 109(4), pp.1495–508.
Rhee, S. et al., 2016. Depletion of primary cilia from mature dentate granule cells impairs hippocampus-dependent contextual memory. *Scientific reports*, 6, p.34370.
Rich, T. et al., 1999. Disassembly of nuclear inclusions in the dividing cell--a novel insight into neurodegeneration. *Human molecular genetics*, 8(13), pp.2451–9.
Robbins, E., Jentzsch, G. & Micali, A., 1968. The centriole cycle in synchronized HeLa cells. *The Journal of cell biology*, 36(2), pp.329–39.
Rochet, J.-C. et al., 2004. Interactions among alpha-synuclein, dopamine, and biomembranes: some clues for understanding neurodegeneration in Parkinson's disease. *Journal of molecular neuroscience : MN*, 23(1–2), pp.23–34.
Rock, K.L. et al., 1994. Inhibitors of the proteasome block the degradation of most cell proteins and the generation of peptides presented on MHC class I molecules. *Cell*, 78(5), pp.761–71.
Rodríguez-Martín, T. et al., 2013. Tau phosphorylation affects its axonal transport and degradation. *Neurobiology of aging*, 34(9), pp.2146–57.
Rosenbaum, J.L. & Child, F.M., 1967. Flagellar regeneration in protozoan flagellates. *The Journal of cell biology*, 34(1), pp.345–64.
Ross, C.A. & Poirier, M.A., 2004. Protein aggregation and neurodegenerative disease. *Nature Medicine*, 10(7), pp.S10–S17.
Roychowdhury, S. et al., 1999. G protein alpha subunits activate tubulin GTPase and modulate microtubule polymerization dynamics. *The Journal of biological chemistry*, 274(19), pp.13485–90.
Saeki, H. et al., 1984. Immotile cilia syndrome associated with polycystic kidney. *The Journal of urology*, 132(6), pp.1165–6.
Saez, I. & Vilchez, D., 2014. The Mechanistic Links Between Proteasome Activity, Aging and Age-related Diseases. *Current genomics*, 15(1), pp.38–51.
Saha, A.R. et al., 2004. Parkinson's disease alpha-synuclein mutations exhibit defective axonal transport in cultured neurons. *Journal of cell science*, 117(Pt 7), pp.1017–24.
Sang, L. et al., 2011. Mapping the NPHP-JBTS-MKS Protein Network Reveals Ciliopathy Disease Genes and Pathways. *Cell*, 145(4), pp.513–528.
de Saram, P. et al., 2017. BCAP is a centriolar satellite protein and inhibitor of ciliogenesis. *Journal of cell science*, 130(19), pp.3360–3373.
Sarkar, S. et al., 2007. Trehalose, a novel mTOR-independent autophagy enhancer, accelerates the clearance of mutant huntingtin and alpha-synuclein. *The Journal of biological chemistry*, 282(8), pp.5641–52.
Satir, P. & Christensen, S.T., 2008. Structure and function of mammalian cilia. *Histochemistry and cell biology*, 129(6), pp.687–93.
Satir, P., Pedersen, L.B. & Christensen, S.T., 2010. The primary cilium at a glance. *Journal of cell science*, 123(Pt 4), pp.499–503.
Savica, R. et al., 2013. Incidence of dementia with Lewy bodies and Parkinson disease dementia. *JAMA neurology*, 70(11), pp.1396–402.

Schou, K.B., Pedersen, L.B. & Christensen, S.T., 2015. Ins and outs of GPCR signaling in primary cilia. *EMBO reports*, 16(9), pp.1099–113.
Schrag, A., Ben-Shlomo, Y. & Quinn, N.P., 2000. Cross sectional prevalence survey of idiopathic Parkinson's disease and Parkinsonism in London. *BMJ (Clinical research ed.)*, 321(7252), pp.21–2.
Schubert, U. et al., 2000. Rapid degradation of a large fraction of newly synthesized proteins by proteasomes. *Nature*, 404(6779), pp.770–774.
Schulze, E. & Kirschner, M., 1986. Microtubule dynamics in interphase cells. *The Journal of cell biology*, 102(3), pp.1020–31.
Shah, A.S. et al., 2009. Motile Cilia of Human Airway Epithelia Are Chemosensory. *Science*, 325(5944), pp.1131–1134.
Sharma, N. et al., 2011. Soluble levels of cytosolic tubulin regulate ciliary length control. *Molecular biology of the cell*, 22(6), pp.806–16.
Shavali, S., Combs, C.K. & Ebadi, M., 2006. Reactive Macrophages Increase Oxidative Stress and Alpha-Synuclein Nitration During Death of Dopaminergic Neuronal Cells in Co-Culture: Relevance to Parkinson's Disease. *Neurochemical Research*, 31(1), pp.85–94.
Shaw, G. & Weber, K., 1982. Differential expression of neurofilament triplet proteins in brain development. *Nature*, 298(5871), pp.277–279.
Shemesh, O.A. et al., 2008. Tau-Induced Traffic Jams Reflect Organelles Accumulation at Points of Microtubule Polar Mismatching. *Traffic*, 9(4), pp.458–471.
Shimizu, N. et al., 1998. Mutations in the parkin gene cause autosomal recessive juvenile parkinsonism. *Nature*, 392(6676), pp.605–608.
Shimura, H. et al., 2000. Familial Parkinson disease gene product, parkin, is a ubiquitin-protein ligase. *Nature Genetics*, 25(3), pp.302–305.
Shimura, H. et al., 1999. Immunohistochemical and subcellular localization of parkin protein: Absence of protein in autosomal recessive juvenile parkinsonism patients. *Annals of Neurology*, 45(5), pp.668–672.
Si, X., Pu, J. & Zhang, B., 2017. Structure, Distribution, and Genetic Profile of α-Synuclein and Their Potential Clinical Application in Parkinson's Disease. *Journal of movement disorders*, 10(2), pp.69–79.
Sode, K. et al., 2006. Effect of reparation of repeat sequences in the human alpha-synuclein on fibrillation ability. *International journal of biological sciences*, 3(1), pp.1–7.
Sonsalla, P.K. & Heikkila, R.E., 1986. The influence of dose and dosing interval on MPTP-induced dopaminergic neurotoxicity in mice. *European journal of pharmacology*, 129(3), pp.339–45.
Sorokin, S.P., 1968. Reconstructions of centriole formation and ciliogenesis in mammalian lungs. *Journal of cell science*, 3(2), pp.207–30.
Spektor, A. et al., 2007. Cep97 and CP110 Suppress a Cilia Assembly Program. *Cell*, 130(4), pp.678–690.
Spillane, M. et al., 2011. The actin nucleating Arp2/3 complex contributes to the formation of axonal filopodia and branches through the regulation of actin patch precursors to filopodia. *Developmental Neurobiology*, 71(9), pp.747–758.
Spillantini, M.G. et al., 1998. alpha-Synuclein in filamentous inclusions of Lewy bodies from Parkinson's disease and dementia with lewy bodies. *Proceedings of the National Academy of Sciences of the United States of America*, 95(11), pp.6469–73.
Spillantini, M.G. et al., 1997. α-Synuclein in Lewy bodies. *Nature*, 388(6645), pp.839–

840.
Spudich, J.A., Huxley, H.E. & Finch, J.T., 1972. Regulation of skeletal muscle contraction: II. Structural studies of the interaction of the tropomyosin-troponin complex with actin. *Journal of Molecular Biology*, 72(3), pp.619–632.
Stearns, T., Evans, L. & Kirschner, M., 1991. γ-Tubulin is a highly conserved component of the centrosome. *Cell*, 65(5), pp.825–836.
Stefanis, L. et al., 2001. Expression of A53T mutant but not wild-type alpha-synuclein in PC12 cells induces alterations of the ubiquitin-dependent degradation system, loss of dopamine release, and autophagic cell death. *The Journal of neuroscience : the official journal of the Society for Neuroscience*, 21(24), pp.9549–60.
Steinert, P.M. & Parry, D.A.D., 1985. Intermediate Filaments: Conformity and Diversity of Expression and Structure. *Annual Review of Cell Biology*, 1(1), pp.41–65.
Stowe, T.R. et al., 2012. The centriolar satellite proteins Cep72 and Cep290 interact and are required for recruitment of BBS proteins to the cilium. *Molecular biology of the cell*, 23(17), pp.3322–35.
Strickland, D. & Bertoni, J.M., 2004. Parkinson's prevalence estimated by a state registry. *Movement Disorders*, 19(3), pp.318–323.
Sulimenko, V. et al., 2017. Regulation of microtubule nucleation mediated by γ-tubulin complexes. *Protoplasma*, 254(3), pp.1187–1199.
Sun, X.-M. et al., 2004. Caspase activation inhibits proteasome function during apoptosis. *Molecular cell*, 14(1), pp.81–93.
Sveinbjornsdottir, S., 2016. The clinical symptoms of Parkinson's disease. *Journal of Neurochemistry*, 139(S1), pp.318–324.
Swatek, K.N. & Komander, D., 2016. Ubiquitin modifications. *Cell research*, 26(4), pp.399–422.
Szeverenyi, I. et al., 2008. The Human Intermediate Filament Database: comprehensive information on a gene family involved in many human diseases. *Human Mutation*, 29(3), pp.351–360.
Takeda, T. et al., 2014. Olfactory dysfunction related to TDP-43 pathology in amyotrophic lateral sclerosis. *Clinical Neuropathology*, 33(1), pp.65–67.
Takemura, R. et al., 1992. Increased microtubule stability and alpha tubulin acetylation in cells transfected with microtubule-associated proteins MAP1B, MAP2 or tau. *Journal of cell science*, 103 (Pt 4), pp.953–64.
Tan, E.-K. & Skipper, L.M., 2007. Pathogenic mutations in Parkinson disease. *Human Mutation*, 28(7), pp.641–653.
Tanaka, K. et al., 2004. Ubiquitin, proteasome and parkin. *Biochimica et Biophysica Acta (BBA) - Molecular Cell Research*, 1695(1–3), pp.235–247.
Tang, Z. et al., 2013. Autophagy promotes primary ciliogenesis by removing OFD1 from centriolar satellites. *Nature*, 502(7470), pp.254–257.
Tanos, B.E. et al., 2013. Centriole distal appendages promote membrane docking, leading to cilia initiation. *Genes & development*, 27(2), pp.163–8.
Taylor, J.P. et al., 2003. Aggresomes protect cells by enhancing the degradation of toxic polyglutamine-containing protein. *Human Molecular Genetics*, 12(7), pp.749–757.
Taylor, K.A., Taylor, D.W. & Schachat, F., 2000. Isoforms of alpha-actinin from cardiac, smooth, and skeletal muscle form polar arrays of actin filaments. *The Journal of cell biology*, 149(3), pp.635–46.
Theillet, F.-X. et al., 2016. Structural disorder of monomeric α-synuclein persists in mammalian cells. *Nature*, 530(7588), pp.45–50.

Thomas, B. & Beal, M.F., 2007. Parkinson's disease. *Human Molecular Genetics*, 16(R2), pp.R183–R194.
Tilney, L.G., 1971. How microtubule patterns are generated. The relative importance of nucleation and bridging of microtubules in the formation of the axoneme of Raphidiophrys. *The Journal of cell biology*, 51(3), pp.837–54.
Titeux, M. et al., 2001. Human synemin gene generates splice variants encoding two distinct intermediate filament proteins. *European journal of biochemistry*, 268(24), pp.6435–49.
Tobin, J.E. et al., 2008. Haplotypes and gene expression implicate the MAPT region for Parkinson disease: the GenePD Study. *Neurology*, 71(1), pp.28–34.
Tofaris, G.K. et al., 2003. Ubiquitination of alpha-synuclein in Lewy bodies is a pathological event not associated with impairment of proteasome function. *The Journal of biological chemistry*, 278(45), pp.44405–11.
Tompkins, M.M. & Hill, W.D., 1997. Contribution of somal Lewy bodies to neuronal death. *Brain research*, 775(1–2), pp.24–9.
Totterdell, S., Hanger, D. & Meredith, G.E., 2004. The ultrastructural distribution of alpha-synuclein-like protein in normal mouse brain. *Brain Research*, 1004(1–2), pp.61–72.
Trétiakoff, C., 1919. *Contribution a l'etude l'anatomie pathologique du locus Niger de soemmering: avec quelques d{é}ductions relatives {à} la pathog{é}nie des troubles du tonus musculaire et de la maladie de Parkinson*, Jouve.
Trojanowski, J.Q. et al., 1998. Fatal attractions: abnormal protein aggregation and neuron death in Parkinson's disease and Lewy body dementia. *Cell Death and Differentiation*, 5(10), pp.832–837.
Troy, C.M. et al., 1990. Ontogeny of the neuronal intermediate filament protein, peripherin, in the mouse embryo. *Neuroscience*, 36(1), pp.217–237.
Tsigelny, I.F. et al., 2012. Role of α-synuclein penetration into the membrane in the mechanisms of oligomer pore formation. *The FEBS journal*, 279(6), pp.1000–13.
Tucker, R.P., 1990. The roles of microtubule-associated proteins in brain morphogenesis: a review. *Brain Research Reviews*, 15(2), pp.101–120.
Uéda, K. et al., 1993. Molecular cloning of cDNA encoding an unrecognized component of amyloid in Alzheimer disease. *Proceedings of the National Academy of Sciences of the United States of America*, 90(23), pp.11282–6.
Ungerstedt, U., 1971. Stereotaxic Mapping of the Monoamine Pathways in the Rat Brain*. *Acta Physiologica Scandinavica*, 82(S367), pp.1–48.
Unno, M. et al., 2002. The Structure of the Mammalian 20S Proteasome at 2.75 Å Resolution. *Structure*, 10(5), pp.609–618.
Urushitani, M. et al., 2002. Proteasomal inhibition by misfolded mutant superoxide dismutase 1 induces selective motor neuron death in familial amyotrophic lateral sclerosis. *Journal of Neurochemistry*, 83(5), pp.1030–1042.
Utton, M.A. et al., 2005. Molecular motors implicated in the axonal transport of tau and alpha-synuclein. *Journal of cell science*, 118(Pt 20), pp.4645–54.
Valente, E.M. et al., 2001. Localization of a novel locus for autosomal recessive early-onset parkinsonism, PARK6, on human chromosome 1p35-p36. *American journal of human genetics*, 68(4), pp.895–900.
Vamvaca, K. et al., 2009. The first N-terminal amino acids of alpha-synuclein are essential for alpha-helical structure formation in vitro and membrane binding in yeast. *Journal of molecular biology*, 389(2), pp.413–24.
Varshavsky, A., 2001. Ubiquitin. In *Encyclopedia of Genetics*. Elsevier, pp. 2091–2093.

Vinzenz, M. et al., 2012. Actin branching in the initiation and maintenance of lamellipodia. *Journal of Cell Science*, 125(11), pp.2775–2785.
Vogiatzi, T. et al., 2008. Wild type alpha-synuclein is degraded by chaperone-mediated autophagy and macroautophagy in neuronal cells. *The Journal of biological chemistry*, 283(35), pp.23542–56.
Vora, S.M. & Phillips, B.T., 2016. The benefits of local depletion: The centrosome as a scaffold for ubiquitin-proteasome-mediated degradation. *Cell cycle (Georgetown, Tex.)*, 15(16), pp.2124–2134.
Wakabayashi, K. et al., 2007. The Lewy body in Parkinson's disease: Molecules implicated in the formation and degradation of α-synuclein aggregates. *Neuropathology*, 27(5), pp.494–506.
Waters, A.M. & Beales, P.L., 2011. Ciliopathies: an expanding disease spectrum. *Pediatric nephrology (Berlin, Germany)*, 26(7), pp.1039–56.
Waudby, C.A. et al., 2013. In-Cell NMR Characterization of the Secondary Structure Populations of a Disordered Conformation of α-Synuclein within E. coli Cells P. A. Temussi, ed. *PLoS ONE*, 8(8), p.e72286.
Westlake, C.J. et al., 2011. Primary cilia membrane assembly is initiated by Rab11 and transport protein particle II (TRAPPII) complex-dependent trafficking of Rabin8 to the centrosome. *Proceedings of the National Academy of Sciences of the United States of America*, 108(7), pp.2759–64.
Wheway, G. et al., 2015. An siRNA-based functional genomics screen for the identification of regulators of ciliogenesis and ciliopathy genes. *Nature cell biology*, 17(8), pp.1074–87.
Whitfield, J.F. et al., 2015. The Possible Roles of the Dentate Granule Cell's Leptin and Other Ciliary Receptors in Alzheimer's Neuropathology. *Cells*, 4(3), pp.253–74.
Wiese, C. & Zheng, Y., 2000. A new function for the γ -tubulin ring complex as a microtubule minus-end cap. *Nature Cell Biology*, 2(6), pp.358–364.
Winner, B. et al., 2011. In vivo demonstration that -synuclein oligomers are toxic. *Proceedings of the National Academy of Sciences*, 108(10), pp.4194–4199.
Withers, G.S. et al., 1997. Delayed localization of synelfin (synuclein, NACP) to presynaptic terminals in cultured rat hippocampal neurons. *Developmental Brain Research*, 99(1), pp.87–94.
Woerner, A.C. et al., 2016. Cytoplasmic protein aggregates interfere with nucleocytoplasmic transport of protein and RNA. *Science (New York, N.Y.)*, 351(6269), pp.173–6.
Wong, E.S.P. et al., 2008. Autophagy-mediated clearance of aggresomes is not a universal phenomenon. *Human molecular genetics*, 17(16), pp.2570–82.
Wu, C.-T., Chen, H.-Y. & Tang, T.K., 2018. Myosin-Va is required for preciliary vesicle transportation to the mother centriole during ciliogenesis. *Nature Cell Biology*, 20(2), pp.175–185.
Xie, Y. & Varshavsky, A., 2000. Physical association of ubiquitin ligases and the 26S proteasome. *Proceedings of the National Academy of Sciences*, 97(6), pp.2497–2502.
Xilouri, M. et al., 2009. Abberant α-Synuclein Confers Toxicity to Neurons in Part through Inhibition of Chaperone-Mediated Autophagy H. E. Gendelman, ed. *PLoS ONE*, 4(5), p.e5515.
Xu, K., Zhong, G. & Zhuang, X., 2013. Actin, Spectrin, and Associated Proteins Form a Periodic Cytoskeletal Structure in Axons. *Science*, 339(6118), pp.452–456.
Yamaguchi, T. et al., 2011. Mesocorticolimbic glutamatergic pathway. *The Journal of*

neuroscience : the official journal of the Society for Neuroscience, 31(23), pp.8476–90.

Yang, F. et al., 2005. Parkin stabilizes microtubules through strong binding mediated by three independent domains. *The Journal of biological chemistry*, 280(17), pp.17154–62.

Yanishevsky, R.M. & Stein, G.H., 1981. Regulation of the cell cycle in eukaryotic cells. *International review of cytology*, 69, pp.223–59.

Yazdani, U. et al., 2006. Rat model of Parkinson's disease: Chronic central delivery of 1-methyl-4-phenylpyridinium (MPP+). *Experimental Neurology*, 200(1), pp.172–183.

Yoshimura, S.-I. et al., 2007. Functional dissection of Rab GTPases involved in primary cilium formation. *The Journal of cell biology*, 178(3), pp.363–9.

Yu, W. et al., 1993. Microtubule nucleation and release from the neuronal centrosome. *The Journal of cell biology*, 122(2), pp.349–59.

Zaarur, N. et al., 2014. Proteasome failure promotes positioning of lysosomes around the aggresome via local block of microtubule-dependent transport. *Molecular and cellular biology*, 34(7), pp.1336–48.

Zabrocki, P. et al., 2008. Phosphorylation, lipid raft interaction and traffic of α-synuclein in a yeast model for Parkinson. *Biochimica et Biophysica Acta (BBA) - Molecular Cell Research*, 1783(10), pp.1767–1780.

Zarranz, J.J. et al., 2004. The new mutation, E46K, of α-synuclein causes parkinson and Lewy body dementia. *Annals of Neurology*, 55(2), pp.164–173.

Zeng, B.-Y. et al., 2006. MPTP treatment of common marmosets impairs proteasomal enzyme activity and decreases expression of structural and regulatory elements of the 26S proteasome. *European Journal of Neuroscience*, 23(7), pp.1766–1774.

Zhang, W. & Benson, D.L., 2001. Stages of synapse development defined by dependence on F-actin. *The Journal of neuroscience : the official journal of the Society for Neuroscience*, 21(14), pp.5169–81.

Zhao, J. et al., 2003. Parkin is recruited to the centrosome in response to inhibition of proteasomes. *Journal of cell science*, 116(Pt 19), pp.4011–9.

Zheng, Y. et al., 2008. Dynein is required for polarized dendritic transport and uniform microtubule orientation in axons. *Nature Cell Biology*, 10(10), pp.1172–1180.

Zheng, Y. et al., 1995. Nucleation of microtubule assembly by a γ-tubulin-containing ring complex. *Nature*, 378(6557), pp.578–583.

Zhou, Z. et al., 2011. Rho GTPase regulation of α-synuclein and VMAT2: Implications for pathogenesis of Parkinson's disease. *Molecular and Cellular Neuroscience*, 48(1), pp.29–37.

Zhu, M. & Fink, A.L., 2003. Lipid Binding Inhibits α-Synuclein Fibril Formation. *Journal of Biological Chemistry*, 278(19), pp.16873–16877.

Zhu, Q., Couillard-Després, S. & Julien, J.-P., 1997. Delayed Maturation of Regenerating Myelinated Axons in Mice Lacking Neurofilaments. *Experimental Neurology*, 148(1), pp.299–316.